Measurement-Based Evaluation of Non-Composite Steel Girder Bridges

by

David Villegas Jáuregui, B.S., M.S.

Dissertation

Presented to the Faculty of the Graduate School of

The University of Texas at Austin

in Partial Fulfillment

of the Requirements

for the Degree of

Doctor of Philosophy

The University of Texas at Austin

August, 1999

Measurement-Based Evaluation of Non-Composite
Steel Girder Bridges

Approved by
Dissertation Committee:

Joseph A. Yura, Supervisor

Karl H. Frank

Sharon L. Wood

James O. Jirsa

Kenneth M. Liechti

Dedication

To Gabriela and Camila

For their love and inspiration

Acknowledgements

I am deeply thankful to my parents for their faith in me and for teaching me never to give up on my dreams no matter what the cost. I also wish to thank the Aguilar family for their support. A special thanks goes to my wife, Gabriela, for her unending encouragement, patience, and love throughout my graduate education. None of my accomplishments would have been possible without the many sacrifices she made. I am also grateful to her for our daughter, Camila, who inspires me to achieve all I can.

Measurement-Based Evaluation of Non-Composite
Steel Girder Bridges

David Villegas Jáuregui, Ph.D.

The University of Texas at Austin, 1999

Supervisor: Joseph A. Yura

The results from an experimental study into the behavior of non-composite slab-on-steel girder bridges are presented. A load rating technique was developed that uses site-specific measurements to estimate the capacity of a suspect bridge. Two bridge units were tested under increasing static loads beyond first yield of the girders with a flatbed trailer loaded with concrete barriers. Both units were originally four-span continuous but were altered to three spans to increase the maximum span length. The load tests were unique in that dump trucks were applied between trailer load cycles to monitor the effect of overloads on the bridge response. Measured deformations included strain, vertical deflection, and girder-slab slip.

Lateral load distribution was evaluated experimentally by expressing the bending moment in each girder section (derived from the measured strains) as a

percentage of the total bridge moment. The strain derived bridge moment was lower than the statical bridge moment due in part to bearing restraint and deck stiffness. Measured distribution factors compared well with finite element analysis but were below empirical factors from AASHTO Standard (1996) and LRFD (1998) Specifications. There was more agreement with the LRFD-based values. Partial composite action was examined by comparing the measured section properties (i.e., moment of inertia, neutral axis position, section modulus) of the girders with those for a non-composite and full composite section. Due in part to the flexural participation of the curb, the exterior girder exhibited more composite action than interior girders. As a result, a higher percentage of the applied load was distributed to the exterior girder. The heavy trailer loads had no significant impact on the load distribution and partial composite action of the girders. More significant changes occurred between different transverse load positions of the dump truck.

The proposed experimental bridge rating process consists of a hierarchy of steps of increasing complexity and effort, some of which do not require load testing. The process terminates once a satisfactory rating is achieved. Procedures for using measured distribution factors and section moduli for the girders to improve the AASHTO Allowable Stress and Load Factor ratings are given.

Table of Contents

List of Tables

List of Figures

xviii

xix

CHAPTER 1

INTRODUCTION

1.1 BACKGROUND

An experimental and analytical investigation into the behavior of non-composite slab-on-steel girder bridges was conducted. The objective of the study was to develop a technique that is based on the measurements collected during a load test to assess the strength of an existing bridge. In particular, the unintended partial composite action between the non-composite girders and the bridge deck, the flexural participation of the deck and curbs, and the effects of bearing restraint are examined. Although not considered in the design, these attributes of behavior have been observed in numerous load tests to favorably influence the load distribution and strength of existing non-composite steel bridges (Burdette and Goodpasture 1988). Standard rating procedures specified in the AASHTO (American Association of State Highway and Transportation Officials) *Manual for the Condition Evaluation of Bridges* (1994) employ concepts and assumptions similar to those used in design. Although appropriate for design, these same conservative procedures, when applied in the rating of an existing bridge, often underestimate its load capacity. Consequently, some bridges are unnecessarily posted with load restrictions or in some cases completely closed to traffic awaiting rehabilitation or replacement.

1

Because of the economic impact associated with closing, rehabilitating, or replacing a bridge, many state highway departments have adopted non-destructive testing procedures to obtain a more accurate prediction of a bridge's capacity. Starting in the early 1980's, the New York Department of Transportation (DOT) has occasionally used load testing to determine the safe load levels for a bridge (Kissane et al., 1980). Over the last decade, load-testing activity has expanded to other state DOTs including Alabama (Conner, 1997) and Florida (Shahawy, 1995). In states without in-house testing capabilities, universities and private consultants have provided services to bridge owners when the strength of a particular bridge or set of bridges was in question. A study to standardize non-destructive load testing procedures for bridge assessment was carried out under Project 12-28(13) of the National Cooperative for Highway Research Program (NCHRP) by Pinjarkar et al. (1990) and Lichtenstein (1993). Outside the United States, both Canada and Switzerland have long records of experience from testing both old and new bridges (Pinjarkar et al., 1990 and Lichtenstein, 1993).

The research reported herein represents one part of a bridge-testing project conducted for the Texas Department of Transportation (TxDOT). The overall purpose of the project was to develop experimental procedures to more accurately load rate Texas bridges that are currently being posted or closed based on the traditional rating methods given by AASHTO. Along with reinforced concrete slab bridges, the project addressed beam-slab bridge types with steel, reinforced concrete, and prestressed concrete girders. TxDOT identified these bridge types of short and medium-span length as potential candidates for load testing since

2

many of them were designed for loads less than current design load levels. As shown in Table 1.1, this set of bridges comprises over 16,000 structures; about half of the total inventory of state-owned bridges.

Table 1.1 Inventory of Candidate Bridges in Texas by Type.

Bridge Type	Number of Bridges
Reinforced Concrete Slab	2,700
Steel Girder	2,930
Reinforced Concrete Pan-Girder	3,907
Prestressed Concrete Girder	6,600
Total	16,137

As part of the TxDOT project, service load studies were performed on the four bridge types listed in Table 1.1, the results of which are reported in Bussell (1997), Schonwetter (1999), Velazquez (1998), and Matsis (1999).

1.2   BRIDGE RATING USING AASHTO

Starting with the *Manual for Maintenance Inspection of Bridges* (1983), the American Association of State Highway and Transportation Officials (AASHTO) has regulated the process of bridge appraisal. This tradition has continued with the release of the *Guide Specifications for the Strength Evaluation of Existing Steel and Concrete Bridges* (1989) and more recently the *Manual for Condition Evaluation of Bridges* (1994). In this set of guidelines, three methods for load rating are provided including the Allowable Stress (AS) method, the Load Factor (LF) method, and the Load and Resistance Factor (LRF) method. In the state of Texas, highway bridges are load rated according to the LF method.

The rating of a bridge, RT, represents the product between a rating factor, RF, and the weight of the rating vehicle, W:

$$RT = RF \ x \ W \qquad (1.1)$$

The following basic equation is used to determine the rating factor

$$RF = \frac{R_n - \gamma_D D}{\gamma_L L(1+I)} \qquad (1.2)$$

where RF = rating factor, R_n = nominal resistance, γ_D = dead load factor, D = nominal dead load effect, γ_L = live load factor, L = nominal live load effect caused by rating vehicle, and I = live load impact factor. The rating factor represents the multiple of rating vehicles that the bridge can safely carry. If less than one, the live load effects caused by the rating vehicle exceed the capacity minus the dead load effects. Separate factors are computed for the different load effects (i.e., moment, shear, etc.), with the smaller value controlling the rating.

In the AS and LF methods, highway bridges are load rated at an inventory and operating rating level. The inventory rating is the smaller of the two rating levels and corresponds to the heaviest load that can safely utilize a bridge on a continual basis. The operating rating is the absolute maximum permissible load that a bridge may be subjected to but on a less frequent basis. These two ratings are reported in terms of the rating vehicle that was used to compute the live load effects. For example, a rating analysis giving inventory and operating rating factors of 1.05 and 1.76, respectively, for an HS-20 vehicle would be reported as HS-21.0 and HS-35.2.

4

In the AS method, the dead load and live load factors are taken as unity while the nominal capacity is determined based on the rating level. The nominal capacity is determined based on an allowable stress. For steel bridge members, the inventory and operating ratings are determined based on allowable stresses of 55% and 75% of the yield stress, respectively. In the LF method, the dead load factor is taken as 1.3 whereas the live load factor is taken as 1.3 and 2.17 for operating and inventory ratings, respectively. The nominal capacity remains the same regardless of the rating level and is computed according to AASHTO design specifications.

Unlike the previous two methods, the LRF method has only a single load rating level at the strength limit state. The selection of load and resistance factors is based on an on-site condition appraisal of the bridge and a review of past inspection reports. Prior experience in bridge inspection is beneficial for the selection of proper load and resistance factors. Due to the subjective nature of selecting these factors, inconsistencies in load ratings may occur. In a paper comparing the LF and LRF methods by Barker (1997), several advantages and disadvantages of the LRF approach were noted which are listed in Table 1.2.

Table 1.2 Advantages / Disadvantages of LRF Method (Barker 1997).

Advantages	Disadvantages
1. Implicitly recognizes difference between design and evaluation. 2. Provides consistent level of safety for all bridges. 3. Uses site-specific load and resistance characteristics. 4. Incorporates engineering judgment in the rating process. 5. Uses form similar to LF method. 6. Permits potential improvements in ratings through extra efforts in inspection and maintenance. 7. Encourages better inspection and maintenance programs. 8. Eliminates much of the variation in state posting practices.	1. Load, impact, and resistance factors are subjective. 2. Terms such as "careful", "estimated", "vigorous", and "intermittent" are subjective. 3. States may choose to categorically use conservative factors, defeating the purpose of the STRENGTH method. 4. Additional inspection information is required. 5. It changes established bridge rating programs.

In Equation 1.2, a reduction factor Φ ranging from 0.55 to 0.95 is applied to the nominal resistance to account for the effects of deterioration, the level of redundancy, and inspection / maintenance activity. The dead load factor is taken as 1.2 with an additional 20% on overlay thickness to account for the uncertainties of the actual asphalt thickness. The live load factor depends on the Average Daily Truck Traffic (ADTT) and the level of surveillance for trucks exceeding the legal limit. Additional correction to the live load factor is needed if alternative analysis techniques and/or field measurements are used instead of the AASHTO approach for load distribution. The impact factor is based on a subjective judgment of the wearing surface and ranges from 0.1 for a smooth surface to 0.3 for a severely irregular pavement.

Figure 1.1 shows the legal vehicles adopted by AASHTO for rating purposes. These vehicle configurations are based on a U. S. truck survey and are considered to better represent normal traffic than the H or HS vehicle used in bridge design (Moses and Verma 1987). The axle configuration for an H-20 and HS-20 design truck are given in Figure 1.2. Load ratings must also be done for other legal loads if expected to cause more severe load effects than the AASHTO design and rating vehicles. In Texas, ratings are also performed under other legal loads specific to the state, two of which are shown in Figure 1.3.

(a) TYPE 3: Unit Weight = 222.4 kN (50 kips)
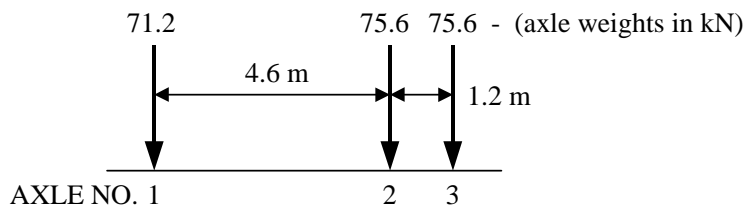
(b) TYPE 3S2: Unit Weight = 320.3 kN (72 kips)
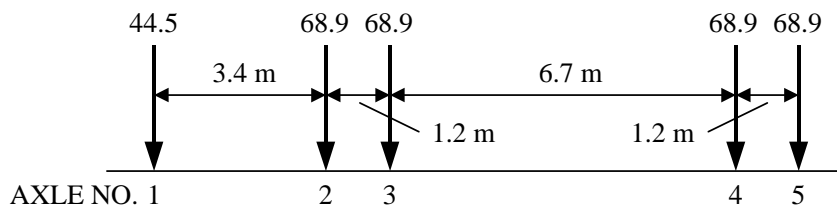
(c) TYPE 3-3: Unit Weight = 355.9 kN (80 kips)
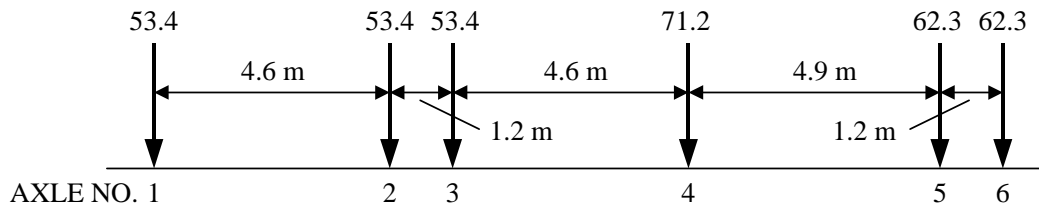
Figure 1.1 AASHTO Legal Loads (Moses and Verma 1987).

7

(a) H-20: Unit Weight = 177.9 kN (40 kips)

35.6   142.3 - (axle weights in kN)

4.3 m

AXLE NO. 1   2

(b) HS-20: Unit Weight = 320.3 kN (72 kips)

35.6   142.3   142.3

4.3 m   4.3 m to 9.1 m

AXLE NO. 1   2   3
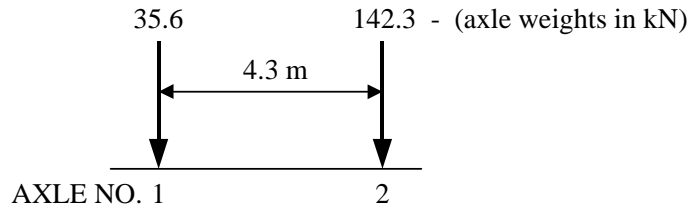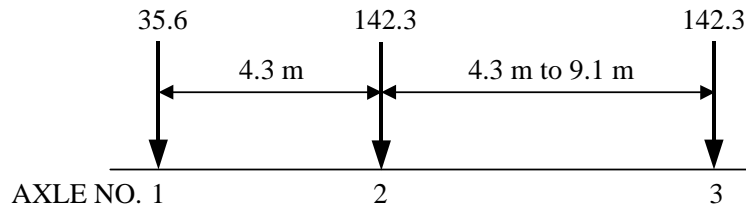
Figure 1.2 AASHTO Design Loads.

(a) Concrete Truck: Unit Weight = 306.9 kN (69 kips)

102.3   102.3 102.3 - (axle weights in kN)

4.3 m

1.2 m

AXLE NO. 1   2   3
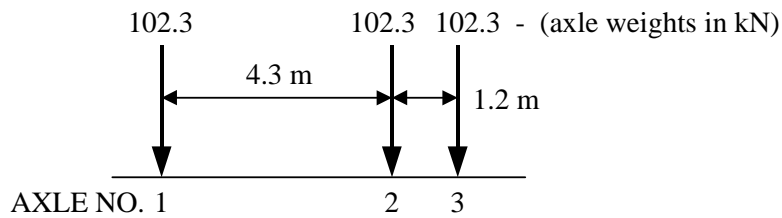
(b) 18-Wheeler: Unit Weight = 355.9 kN (80 kips)

53.4   75.6 75.6   75.6 75.6

4.6 m   8.5 m

1.2 m   1.2 m

AXLE NO. 1   2   3   4   5
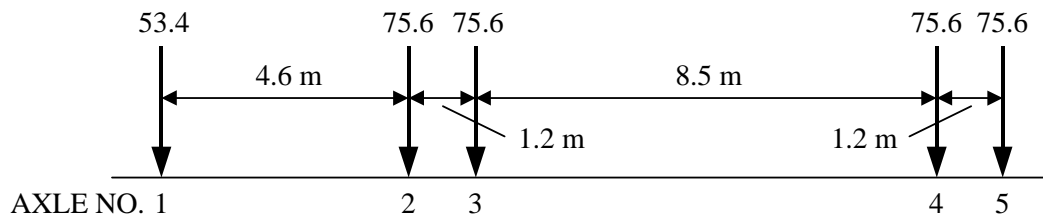
Figure 1.3 Texas Legal Loads.

In Figure 1.4, the maximum moment caused by the AASHTO and Texas legal loads are plotted as a percentage of the HS-20 design moment for simple span lengths of 3.0 m (10 ft) to 33.5 m (110 ft).
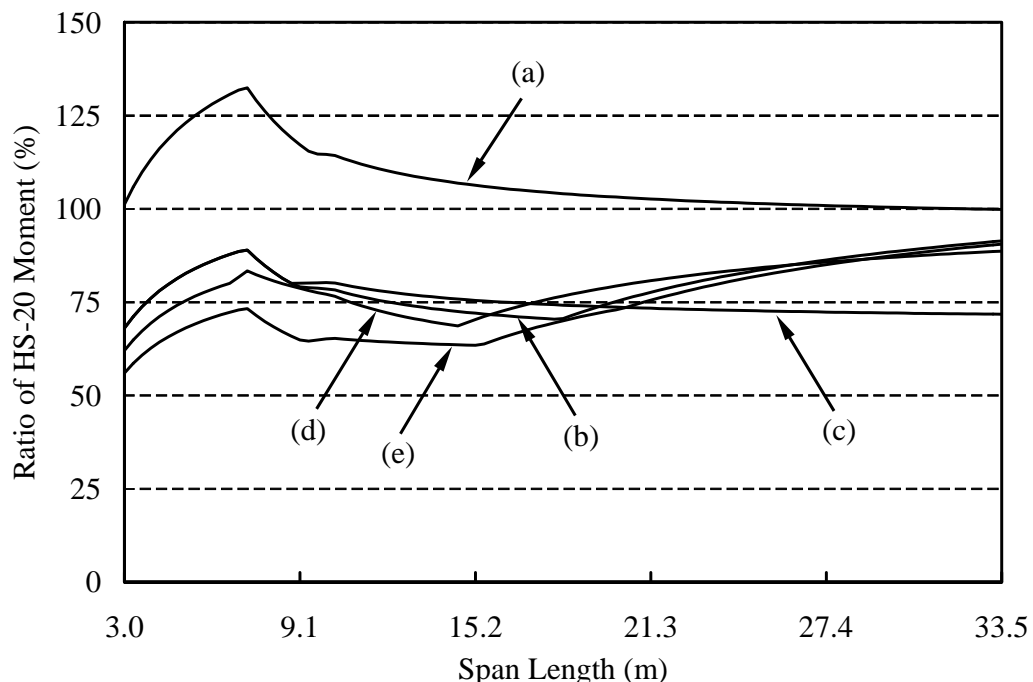
Figure 1.4 Moment Ratio between Legal Loads and HS-20 Vehicle; (a) Concrete Truck, (b) 18-Wheeler, (c) Type 3, (d) Type 3S2, and (e) Type 3-3.

For these span lengths, the maximum moment and thus rating is controlled by the axle configuration of the Texas concrete truck. Even for longer span lengths, the moment caused by the concrete truck exceeds that of heavier vehicles. The AASHTO Type 3-3 and Texas 18-Wheeler exceed the weight of the concrete truck by 16% but cause less severe load effects since the load is distributed over a longer axle base and to more axles. Just by weight alone, the concrete truck

9

exceeds the Type 3 and is just below the Type 3S2 of AASHTO. With respect to the HS-20 vehicle, the concrete truck reaches a peak ratio of 132% at 7.1 m (24 ft) and becomes asymptotic to 100% at larger span lengths. This simple comparison clearly illustrates the heavier loads that short- to medium-span bridges must carry compared to the load used for the original design. In addition, the significant load effects caused by the concrete truck make it a suitable choice for load testing.

1.3   BRIDGE TESTING TERMINOLOGY

The two types of non-destructive load tests commonly used to evaluate the response of an existing bridge are diagnostic and proof tests.   These two methods differ in terms of the level of load applied to the bridge, the quantity and significance of measurements taken, and the manner in which the experimental findings are used to
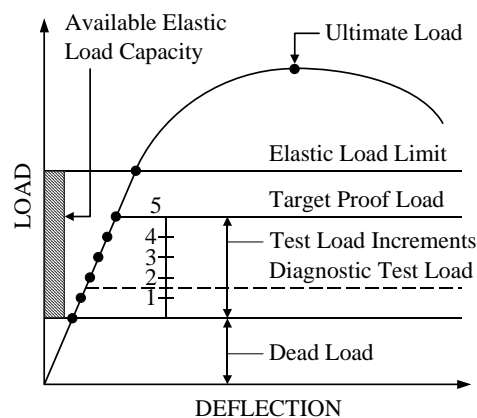
Figure 1.5 Hypothetical Load-Deflection Response of a Bridge (Pinjarkar et al. 1990).

determine the load rating. In a diagnostic test, a bridge is subjected to a known load below its elastic load limit as shown in Figure 1.5. Strain and deflection measurements are taken at strategic locations to determine the load distribution and stiffness characteristics of the bridge. Following the test, the experimental information is then used in combination with an analytical model to explain the

10

behavior of the bridge and estimate its capacity. In a proof test, increasing loads are applied to the bridge until a target load level is reached or non-linear behavior is observed. When either of these two events occurs, the load test is stopped. The maximum load carried by the bridge is then adjusted to determine the bridge rating. Typically, measurements are taken only at a few critical locations to monitor the condition of the bridge during the test.

Unlike a proof test approach where rating decisions may be made based on specific strains and/or deformations recorded during a test, diagnostic testing requires a more rigorous post-test analysis of the data. Additional details of these two methods are provided in the ensuing sections.

1.3.1   Diagnostic Testing

Diagnostic testing is usually employed when the original design plans of a bridge are available to create a representative analytical model (Pinjarkar et al. 1990). This type of testing has been used extensively for the evaluation of steel bridges because of the rather well defined behavior of this bridge type in the elastic region.

Ordinarily, the test vehicle used for diagnostic testing is a dump truck filled with asphalt or roadway base material. The truck and driver can be arranged through the local transportation agency making it a convenient form of load application should testing become a regular part of the bridge evaluation process. The test load can be applied in either a static or semi-static manner. In the former case, the test truck remains stationary at the load positions while

discrete readings are taken. In the latter case, continuous measurements are made as the test truck is driven longitudinally across the bridge at a slow speed along different transverse paths. In some cases, high-speed runs are also made to determine dynamic impact effects.

Following the test, the field measurements are compared with the results of an analytical bridge model. Typically, the measured strains and deflections are lower than the analytical results due to difficulties in accurately modeling the actual stiffness and boundary conditions of the structure. These differences are used to adjust and possibly improve the original bridge rating. Because of the low load level applied during a diagnostic test (see Figure 1.5), caution must be taken in extrapolating the measured response of the bridge to a higher rating load.

1.3.2 Proof Testing

A proof test is an attempt to experimentally prove that a bridge can safely carry a certain rating vehicle. In situations where an analytical model cannot be developed because of the lack of design drawings or when the bridge has suffered severe deterioration difficult to quantify, proof testing is preferred (Pinjarkar et al. 1990). This form of testing is also employed to evaluate bridge types that are difficult to analyze with linear models and/or are troublesome to instrument in the field.

Before a proof test is executed, a target proof load is determined which will produce the load effects of the rating vehicle times the live load and impact factors. To achieve this high load level, a variety of loading systems have been

employed including tractor-trailers loaded with concrete blocks and military tanks. Regardless of the loading system, the proof load should produce load effects similar to the effects caused by the factored rating load but below the elastic limit. Specific procedures for computing the proof load are provided by Lichtenstein (1993), Moses et al. (1994), and Fu and Tank (1995). The proof load can either be applied all at once or in stages. The first option can be completed faster but is more likely to cause damage to the bridge. The second option provides a more controlled load test since maximum strains and/or deflections can be monitored during each load increment to ensure that the load test proceeds as planned. After each increment of load, the amount of deflection and/or strain recovery is used as an indication of the condition of the bridge and is a deciding factor for continuing to the next level of load. The test is discontinued either when the target test load is reached or the response of the bridge becomes non-linear. The final load placed on the bridge is considered the factored capacity and is reduced by the impact and live load factors to obtain the bridge rating.

1.4   HISTORICAL FACTORS AFFECTING BRIDGE PERFORMANCE

Through a review of load tests conducted between 1929 and 1987, Burdette and Goodpasture (1988) extensively documented the various aspects of bridge behavior which are often revealed but go unaccounted for in the rating. This work was carried out under NCHRP Project 12-28(8) with the following two objectives: 1) to gather and review test data pertaining to the load-carrying capacity for different bridge types and 2) to identify and evaluate attributes of

13

behavior which exist in the field but are typically ignored when rating a bridge. A

summary of findings from this study is given in Table 1.3.

Table 1.3 Summary of Factors Affecting Bridge Performance (Burdette and
Goodpasture 1987).

Variable / Bridge Type	Beam and Slab	Slab	Truss	Box Girder
Unintended Composite Action	P, I/T	N/A	S, I/T	P, I/T
Participation of Edge Members	P, A	P, A	N/A	P, A
Actual vs. Assumed Material Properties	S, I/T	S, I/T	S, I/T	S, I/T
Participation of Bracing and Secondary Members	S	N/A	S	S
Two-Way Slab Action	N/A	S	N/A	N/A
End Restraint and Unintended Continuity	S, I/T	S, I/T	S, I/T	S, I/T
Participation of Floor Beams with Chords of Trusses	N/A	N/A	S, I/T	N/A
Load Distribution Effects	P, A	P, A	P, A	P, A
Effects of Skew	S, A	P *	N/A	S, A

P: Primary Factor
S: Secondary Factor
A: Include in Conventional Analysis
I/T: Inspection and/or Testing Needed to Verify
N/A: Not Applicable
* Short Span Bridges Only (S for Longer Span Bridges)

As shown in the table, unintended composite action will require some form of

load testing while skew effects may only require a more complex analytical

model. Load distribution effects and the participation of edge members such as

parapets and curbs may call for both an experimental and analytical effort. In

addition to the work of Burdette and Goodpasture (1987), further discussion of

these and other factors that can influence the load carrying capacity of a bridge

can be found in Bakht and Jaeger (1990), Tharmabala (1990), Pinjarkar et al.

(1990), Lichtenstein (1993), and Edberg (1994). Brief descriptions of the factors pertinent to beam-and-slab bridges are given in the following sections.

1.4.1   Unintended Composite Action

A potential source of increased stiffness for non-composite beam-and-slab bridges is unintended composite action. Regardless of the absence of mechanical shear connectors at the girder-slab interface, several tests have shown evidence of interaction between the girders and slab (Suetoh et al. 1990). Two factors that contribute to this behavior are natural or chemical bonding between the steel and concrete and friction at the steel-concrete interface caused by the slab bearing down on the girder top flange under its own weight and under live load (Suetoh et al. 1990). Both of these elements restrain the slab from sliding freely relative to the girder thus causing either partial or full composite action. As shown in Figure 1.6, a strain discontinuity at the girder-slab interface distinguishes partial composite from complete interaction. Under full composite action, the neutral axis may lie in either the girder or the slab.
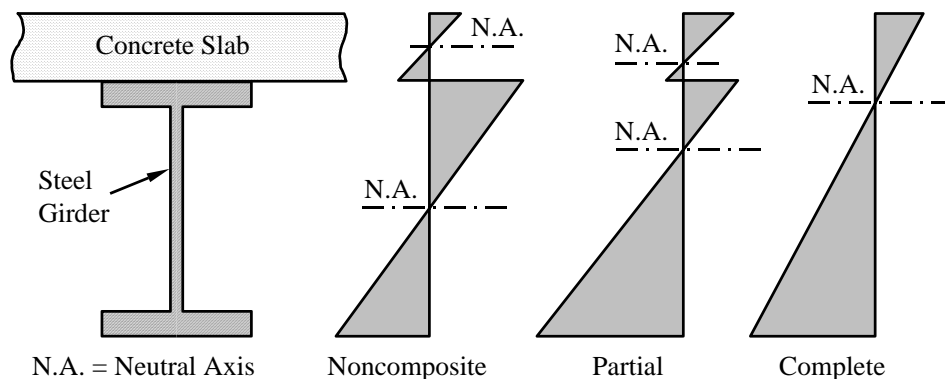
Figure 1.6 Strain Distribution for Various Levels of Composite Action.

The degree of composite action experienced by the girders depends on the strength of the undesigned girder-slab connection. Some researchers suggest that the natural or chemical bond provides the stronger restraint to girder-slab slippage, especially when the top flange is embedded into the bottom of the slab, but is unreliable and virtually unrecoverable if ever broken (Suetoh et al. 1990, Lichtenstein 1993). Lichtenstein (1993) suggests that composite action may be assumed if the horizontal shear between the slab and top flange does not exceed 0.106 times the square root of the concrete compressive strength (in units of MPa) when the flanges are not embedded into the bottom of the slab. The coefficient increases to 0.151 for the case when the flanges are embedded into the slab. For a concrete strength of 20.7 MPa (3000 psi), the shear stress limits come out to 0.483 MPa (70 psi) and 0.689 MPa (100 psi) for embedded and nonembedded top flanges, respectively.

1.4.2 Participation of Non-Structural Components

Typically, non-structural components such as the parapets, the curbs and railings, and the asphalt-wearing surface are considered in bridge rating only to determine the dead load effects on the main load-carrying members. However, a statistical analysis of deflection data from over 200 load tests in Switzerland demonstrated that these elements effectively increase the bending stiffness of the superstructure (Favre et al. 1992; Hassan et al. 1995). The degree of participation from the border members (i.e., parapets, curbs, and railings) depends on the connection with the slab, the longitudinal continuity and size of the member, and

16

its relative position in the cross-section. Aside from its thickness, the influence of the asphalt overlay depends strongly on the surrounding temperature; it is most effective under low temperatures when the modulus of elasticity is highest (Favre et al. 1992; Hassan et al. 1995).

1.4.3   Load Distribution Effects

In a beam-and-slab bridge, the distribution of load in the superstructure is directly related to the relative stiffness of the girders. Edge members can stiffen the exterior girders causing more load to be distributed to these members and less to the interior girders (Smith and Mikelsteins 1988; Mabsout et al. 1997). Moreover, in non-composite bridges, the degree of interaction between the girder and slab is uncertain and may vary from beam to beam causing an irregular distribution of girder stiffness through the cross-section.

A constructed bridge rarely exhibits the simple-support behavior assumed in design due to the effects of unintended continuity and bearing restraint. Both these factors can prohibit free rotation and translation at the end(s) of a "simple-supported" bridge and subsequently alter the distribution of load along the length of the girders. Unintended continuity is caused when the concrete slab is cast continuous across the joint separating adjacent spans or when neighboring spans are placed end to end with little space between them. The former design detail is typical of prestressed concrete bridge construction. The latter detail is typical of reinforced concrete slab and pan-formed girder bridge construction. Debris

deposited from rainwater runoff may also build up in the expansion joint and further increase the continuity between the abutting spans.

The mechanics of bearing restraint are similar to those for unintended composite action. As shown in Figure 1.7, under live load forces, the girder bottom flange at the expansion bearing attempts to move outward relative to mid-span. Relative moment between the girder bottom flange and the bearing seat is partially restrained by friction

(a)

(b)

Figure 1.7 Beam Displacement Under (a) Live Load Forces and (b) Bearing Restraint Forces.

causing horizontal forces to develop at the interface (Bakht and Jaeger 1988). Corrosion at the bearings can further restrain the longitudinal movement of the girder.   An approximate measure of the frictional force can be taken as the support reaction (under dead load and live load) times the coefficient of friction between the bottom of the beam and the bearing seat. Because these forces act below the neutral axis of the girder, a moment restraint is produced at the supports equal to the bearing restraint force times the distance from the bottom of the girder to the neutral axis. Bakht and Jaeger (1988) showed that live load moments at mid-span can be reduced by up to 20% in simply supported slab-on-steel girder bridges.

18

1.4.4 Summary

In addition to the factors discussed in the preceding sections, there are other variables that can affect the response of a bridge. For one, the traffic history can play a significant role in the future performance of a bridge. Overloads can destroy sources of extra strength such as unintended composite action and/or end restraint that can subsequently alter the load distribution pattern and weaken the bridge. Material properties may also change during the service life of a bridge. Concrete may increase in strength and stiffness as it cures over long periods of time. Corrosion and/or deterioration of the main load carrying members may also alter the load distribution pattern as stiffer sections begin to relieve weaker sections. Spalling of concrete cover leads to corrosion of the rebar and ultimately section loss. Similarly, steel bridges can suffer section loss as a result of corrosion.

1.5 RESEARCH OBJECTIVES AND SCOPE

The objectives and scope of the research described herein are outlined below.

Develop Data Acquisition System for Field Use

A major difficulty faced in full-scale testing of bridges is the collection of reliable strain and/or deflection measurements. In the field, measurement signals are particularly vulnerable to electrical noise from sources such as AC power lines and generators. Reducing the effects of noise requires that the electrical hardware

be properly selected and grounded. In addition, the data acquisition system must be able to withstand the harsh treatment it will experience in the field. Significant amounts of time and money may be wasted should a load test have to be repeated because of noisy measurements or faulty equipment. Because of these problems, the first goal of this research is to develop a data acquisition system specifically for field use.

Evaluate Inadvertent Factors of Non-Composite Steel Bridge Behavior

While many bridges originally built as non-composite have been observed to exhibit partial composite action, there is minimal guidance available to measure the degree of girder-slab interaction. An effort is made in this study to quantify the two mechanisms of shear transfer (friction and mechanical interlock) that contribute to unintended interaction between the deck slab and the girders in the absence of mechanical shear connectors. Shear restraint due by adhesive steel-to-concrete bond was ignored. Other factors identified and evaluated for their effects on the bridge response include the participation of the curbs built integral with the bridge deck and bearing restraint at the supports. In addition to partial composite action, both these factors may affect the stiffness of the bridge members and thus, the load distribution pattern of the bridge.

Evaluate Effects of Overloads

Attention is given to evaluating changes in the lateral distribution of load to the girders and the level of partial composite action as the girders are loaded up

to and beyond initial yielding of the steel. A baseline service load, applied between load levels, serves to monitor the lateral load distribution and girder-slab interaction under normal traffic loads after experiencing the effects of overloads. In the evaluation of the load distribution pattern, comparisons are made with the empirical distribution factors given in the AASHTO Standard (1996) and LRFD (1998) Bridge Design Specifications.

Integrate Bridge Testing into Load Rating Process

A variety of instrumentation layouts and testing procedures are used in the load tests to determine the best strategy for evaluating the load capacity of non-composite steel girder bridges. As a result of the load tests, the ultimate goal of this study is to provide a procedure for adjusting the original AASHTO rating (1994) based on the experimental findings. The proposed technique takes into account the increase in bending stiffness and resistance of the girders due to partial composite action and the participation of the curbs as well as the field measured load distribution factors. It is appropriate for steel bridges in which the bending moment caused by vehicular loading controls the rating. Cases where the load rating is governed by shear in the girders were not addressed.

1.6 ORGANIZATION OF STUDY

This dissertation contains nine chapters and four appendices. Chapter 1 provides a comparative review of the AASHTO methods currently used in the United States for load rating of bridges along with a discussion of bridge testing

21

terminology. The chapter also describes the attributes of bridge behavior that have been observed in previous load tests but which minimal guidance is available for incorporating them in the rating process. The specific objectives and scope of the research are given in the final section of the chapter. Chapter 2 provides a review of experimental bridge rating activity in the U. S. and in other countries with emphasis on domestic practice. Chapter 3 covers the design of an instrumentation / data acquisition system for conducting full-scale bridge tests. In Chapter 4, a description of the non-composite slab-on-steel girder bridge units that were tested is provided including the design details and material properties of the bridge members. Chapter 5 describes the planning and execution of the field tests that were performed on the bridge units. The load-deformation response of the tested units under increasing load is presented in Chapter 6. Based on the test results given in Chapter 6, Chapter 7 examines the lateral distribution of load and partial composite action of the girders. The chapter also describes the post-processing of the test measurements to determine the experimental bending moments and section properties of the girders. Chapter 8 covers the procedures for integrating the experimental findings from a load test into the AASHTO rating process. Also, the effect of overloads on the service load response of the bridge units is presented. Chapter 9 contains the conclusions of the study and recommendations for further research. Appendix A contains a cost breakdown of the data acquisition system. Appendix B describes the field procedures for installing and operating the test equipment. A typical data collection program is listed in Appendix C. Appendix D contains the load-deformation curves for the girders.

CHAPTER 2

LITERATURE REVIEW

2.1   GENERAL

A review of the literature has been organized according to the agencies actively involved in experimental bridge rating in the U. S.   Although only domestic practice is described here, both Canada and Switzerland have long experience in testing bridges.   Much of the Canadian research was done by the Ontario Ministry of Transportation and has been reviewed in the reports from NCHRP Projects 12-18(8) and 12-28(13).   In Switzerland, most of the load tests performed are acceptance proof tests on new bridges before they are opened to traffic (Ladner 1985, Markey 1991).   Suggestions for extending the testing procedures and evaluation criteria of the Swiss approach to existing bridges are provided by Moses et al. (1994).

2.2   NCHRP STUDIES

Pinjarkar et al. (1990) and Lichtenstein (1993) carried out two separate but complementary studies under NCHRP Project 12-28(13). The aim of this project was to develop a set of guidelines and procedures for evaluating short and medium-span bridges through nondestructive load testing.   In summary, the project provided a description of the following issues related to bridge evaluation: 1) the different types of nondestructive load tests, 2) the various factors that affect

the actual response of a bridge, 3) the criteria for screening candidate bridges, 4) the conditions not suited for load testing, and 5) load testing procedures, test equipment, and measurement types. Throughout both reports, specific examples are given to illustrate the use of the diagnostic and proof testing methods for bridge rating.

Pinjarkar et al. (1990) provides an extensive review of worldwide activity in experimental bridge assessment. The particular countries investigated included the United States, Canada, the United Kingdom, Switzerland, New Zealand, Portugal, and Italy. Existing practice in these countries was illustrated through a review of completed load tests. The authors proposed a general strategy for bridge rating using nondestructive load testing through consideration of the associated benefits, costs, and risks. In the report by Lichtenstein (1993), a more explicit methodology for integrating load test results into the bridge rating process is provided. For diagnostic testing, the author proposed the following relationship between the design rating and load test rating

$$RF_r = RF_c \; x \; K \tag{2.1}$$

where RF_r = the adjusted bridge rating applying the load test results, RF_c = the original AASHTO bridge rating before applying load test results, and K = the adjustment factor applied to RF_c. The factor K accounts for discrepancy between the experimental and theoretical response and is computed as

$$K = 1 + K_a \; x \; K_b \tag{2.2}$$

24

The K_a factor is based on a direct comparison between the theoretical and measured strains. The K_b factor represents the product of three factors that separately consider 1) the magnitude of the test load compared to the rating load, 2) the frequency of inspection, and 3) fatigue and redundancy. Exact agreement between the theory and the load test corresponds to K equal to one. A K greater than unity indicates that the measured response is not as severe as predicted by analysis. That is, the bridge may carry loads larger than the capacity estimated strictly with analysis. If less than one, then the bridge capacity was originally overrated based on theory alone. This may occur when the bridge members have experienced severe section loss due to corrosion causing a decrease in stiffness and resistance of the girder sections. As a result, the measured deformations are larger than predicted and the original rating must be reduced.

2.3   SURVEY OF STATE HIGHWAY DEPARTMENTS

Starting in the early 1980's, the New York Department of Transportation (DOT) has occasionally used diagnostic load testing to determine the safe level of load for a bridge. In the last ten years, experimental bridge rating activity has expanded to the state transportation departments of Alabama, Delaware, Florida, and Michigan. A description of the instrumentation, testing procedures, test data analysis, and load rating methodology employed in these states is provided in the following sections. The review focuses on tests performed on slab and beam-slab bridge types with the primary goal of improving the rating.

2.3.1 Diagnostic Testing in New York

Kissane, Beal and Sanford (1980)

In what may represent the first attempt by a state highway department in the U. S. to apply nondestructive testing to bridge evaluation, the New York DOT performed a series of static and dynamic load tests on five simple-span bridges. The New York DOT did not have original design plans for the structures tested which included three reinforced concrete tee beam bridges, a reinforced concrete slab bridge, and a concrete encased I-beam bridge. Strain measurements were taken at mid-span of each bridge, first under a single vehicle and then with two vehicles positioned side-by-side to check the validity of superposition.

In all cases, the measured strains were significantly lower than the analytical values. For the multi-beam bridges, the fascia beams showed lower values of strain in the tension steel than the interior beams due to the inability of positioning the load directly over the beam and the participation of the curbs and parapets. In the dynamic tests, a single vehicle was driven at different speeds across the bridge to determine the maximum dynamic to static strain ratio (i.e., impact factor). With the exception of the slab bridge, the measured impact factors agreed well with the limiting value of 30 percent given in the AASHTO Standard Specifications.

The authors discussed the difficulties of load rating reinforced concrete bridges using diagnostic load test data. For an allowable stress rating, reliable information about concrete strength is required but difficult to obtain. For a load

factor rating, the non-linear relationship between moment and strain approaching ultimate does not permit a linear extrapolation of the test results.

Fu, Pezze and Alampalli (1994)

The authors of this study performed a diagnostic load test on a composite steel girder bridge to improve the rating of the fascia beams which were rated low following removal of their cover plates. The cross section of the 16.2-m (53-ft) bridge included six steel beams positioned at 2.1 m (6.9 ft) on center. Strain gages were installed on the web and bottom flange of each girder at mid-span and on the bottom flange of the fascia beams at both ends of the bridge. The bridge was loaded with four dump trucks in two loading configurations to maximize the response in each fascia beam. The applied load was equivalent to 88% of an HS20 vehicle plus impact.

Similar load distribution factors were measured for the two fascia beams, which were both less than the value computed in accordance with the AASHTO Standard Specifications. At one end of the bridge, both fascia beams experienced large negative strains on their bottom flanges. The ratio of these negative strains to the positive strains recorded at mid-span was greater than one indicating a high degree of support fixity under the applied loads. Using the test data, a new inventory rating was calculated for the fascia beams equal to two times the original rating. Although proof testing was recommended to confirm the reliability of support fixity at higher loads, the authors fail to mention the consequences an overload may have on the inventory rating. If not controlled, an

overload could destroy the fixity at the supports which would increase the load distributed to mid-span of the fascia beams and subsequently reduce the inventory rating, possibly to unacceptable levels.

2.3.2   Proof Testing in Florida and Michigan

Shahawy (1995); Shahawy and Garcia (1990)

Starting in the early 1990s, the Florida DOT adopted a proof testing approach for bridge evaluation. To illustrate the program, proof load tests were conducted on two prestressed concrete girder bridges.   The loading system consisted of two specialized tractor-trailer vehicles, each equipped with an hydraulic crane for loading 9.6 kN (2.2 kips) concrete blocks. Each vehicle has the capacity to carry 72 concrete blocks for a gross weight of approximately 907 kN (204 kips).

During the static tests, each truck was initially loaded with 24 concrete blocks (i.e., 1/3 the total capacity) and positioned on the bridge at critical locations. Structural behavior during the tests was monitored with strain and deflection measurements taken at various positions along each girder primarily in areas of maximum response. Once sufficient strain and deflection data were collected, the trucks were moved off the bridge and the measurements were compared with theoretical estimates to evaluate the performance of the bridge. If the response of the bridge was linear elastic with no signs of distress, concrete blocks were added (in increments of 12) to each truck and the process was

repeated until the target load or stress limit was reached. In addition to static testing, dynamic testing was also performed to determine experimental impact factors and natural frequencies.

Saraf, Sokolik and Nowak (1996)

In the state of Michigan, proof load tests were performed on a 77-year old reinforced concrete tee-beam bridge with no available original design plans and a 69-year old non-composite steel girder bridge with severe corrosion in the bottom flanges. The bridges were loaded with flatbed trailers transporting 534 kN (60 ton) military tanks.

Both bridges were instrumented with strain and deflection gages at mid-span where preliminary calculations showed the bending moment to control the rating. The measured response of each structure remained linear under the target proof load. Consequently, original ratings were increased by about 15% for the concrete bridge and by over 200% for the steel bridge. The large increased stiffness for the steel bridge was attributed to unintended composite action in the girders.

2.3.3   Diagnostic / Proof Testing in Alabama

Stallings and Yoo (1993)

Results from the diagnostic testing (both static and dynamic) of three non-composite steel girder bridges in Alabama are presented. These tests were

performed with the purpose of investigating the load distribution characteristics, impact effects, and girder-slab interaction. Two of the bridges were built in 1930 with span lengths of 13.4 m (44 ft) and 23.5 m (77 ft). The third bridge of 14.9 m (49 ft) span length was built in 1953. Each bridge was simply supported with a cross-section of four non-composite steel girders and a reinforced concrete deck.

For the three bridges, the four girders were instrumented at mid-span with strain gages on the top and bottom flanges. Static measurements showed a high degree of composite action in all girders of the 13.4 m (44 ft) and 23.5 m (77 ft) spans and in the exterior girders of the 14.9 m (49 ft) span. An intermediate level of composite action was experienced in the interior girders of the 14.9 m (49 ft) span. Compared to analysis, the total measured moment at mid-span ranged from 20 to 40 percent lower. Similarly, girder strains calculated using measured wheel-load distribution factors overestimated the field strains. The authors credit these differences to end restraint, a factor not considered in the theoretical models. Based on these findings, it was demonstrated that analytical solutions cannot be improved solely by replacing the empirical distribution factors specified by AASHTO with their field-measured values; boundary conditions must also be accurately modeled.

Load ratings computed based on linear extrapolation of the test results showed no need for posting as rating factors exceeded unity by 75 to 95 percent. In spite of these improved ratings, the authors recommend that caution be taken when increasing the capacity to these levels due to the possibilities for loss of composite action and support fixity. Furthermore, the authors did not advise

using measured impact factors for load rating since the values represent only the effect under the specific test truck and not actual traffic conditions.

Conner, Stallings, McDuffie, Campbell, Fulton, Shelton, and Mullins (1997)

In this paper, the authors present the testing approach adopted by the Alabama DOT for rating steel girder bridges, a combination of proof and diagnostic testing. Similarly to Florida, the Alabama DOT has two trucks designed specifically for load testing, each with a crane for the loading and unloading of concrete test blocks. The weight of each truck can be adjusted between 178 kN (40 kips) to 445 kN (100 kips) using up to 32 blocks, each weighing 8.4 kN (1.9 kips).

Load test particulars such as instrument locations and target loads were determined using the BRUFEM (i.e., Bridge Rating using the Finite Element Method) program developed by the Florida DOT (Hays et al. 1994). During a typical static test, the test trucks were loaded from 10 to 15% above the required rating level (typically the legal load limit) and positioned side-by-side at critical positions. If the following conditions were met under the test load, the bridge was considered adequate to carry service loads:

1. No visible or audible signs of distress.

2. Maximum girder deflections are less than the span length over 800.

3. The maximum measured girder stress (increased by the AASHTO impact allowance) plus dead load stress is less than 75 percent of the yield strength.

In addition to static tests, dynamic runs are often performed to evaluate impact. The testing program has resulted in an increase or removal of posted load limits for 46 bridges in Alabama.

2.3.4   Diagnostic Testing in Delaware

<u>Chajes, Mertz and Commander (1997)</u>

In this study, the results of a diagnostic load rating of a reinforced concrete slab-on-steel girder bridge is presented. The Delaware bridge was built in 1940 with nine non-composite steel girders and three simple supported spans; two 7.0-m (23-ft) approach spans separated by a 19.5-m (64-ft) main span.   Various repairs had been made due to corrosion damage including one where the bottom flanges of the girders were welded to the bearing plates at the end supports. This particular repair, which restrained the girder from moving longitudinally relative to the bearing plates, produced restraint forces that transferred down to the pier caps causing them to crack.

The Delaware DOT conducted a rating analysis using the allowable stress method contained in the AASHTO Manual for Condition Evaluation of Bridges (1994) and assuming simple supports and non-composite action. In addition to the standard HS-20 vehicle, rating factors at the inventory and operating level were computed for six legal vehicles in Delaware. Posted ratings, taken as two-thirds the inventory rating plus one-third the operating rating, were less than one for three state vehicles and the HS-20 vehicle. As a result, certain load restrictions

were imposed on the bridge. In all cases, mid-span moment in the interior girders of the long span controlled the load rating.

Because of the posting restrictions, a diagnostic load test was performed to possibly improve the rating. Each of the nine steel girders of the main span was instrumented at mid-span with strain transducers on the top and bottom flanges. On selected girders, an intermediate point between mid-span and the end of the girder was also instrumented. Measured strains under service load levels showed evidence of composite girder behavior plus bearing restraint.

Using the field measurements, girder section properties and the rotational restraint stiffness at the supports were estimated and incorporated into a finite element model. In addition to this "field-fitted" model, two other models were created; one neglecting the effects of support restraint and the other neglecting the effects of both unintended composite action and support restraint. Due to the poor condition of the piers, the model that incorporated only composite action was used to determine the final posted ratings. Using this model all posted ratings exceeded one suggesting that load restrictions may be unnecessary. Based on a shear rating analysis of the girder-slab interface, the authors concluded that loss of composite action was unlikely under normal traffic loading but possible under overloads. The authors recommended frequent visual inspections and additional testing under normal traffic to continually monitor the girder-slab interaction.

2.4   PRIVATE CONSULTANTS

2.4.1   Specialized Bridge Evaluation Practice

In this section, the bridge assessment practice of Bridge Diagnostics, Inc. (BDI) is discussed. The basic concept of BDI is to use strain data collected during a semi-static diagnostic test to calibrate a finite element model to match the measured bridge response (Schulz et al. 1995). Measurements are taken using reusable strain transducers whose gage length can be lengthened to measure surface strain on concrete in tension. The extensions average the strain over a longer gage length to account for cracking. Certain parameters in the analytical model such as beam stiffness, boundary conditions, and material properties are optimized until the difference between test and theory is within 10%. Once this level of confidence is achieved, the refined model is then used to perform load ratings. The BDI technique has been used extensively in the evaluation of railroad bridges (Schulz and Commander 1995) and highway bridges with slab-on-steel girder, reinforced concrete slab, and other superstructures; a few of which are particularly noteworthy.

Commander and McMullen (1994)

In this paper, the bridge rating procedure of BDI was implemented on a steel structure built in 1969 and located in Eastern Colorado. Originally, the bridge had a 12.2 m (40 ft) span with a cross section of 15 non-composite steel stringers spaced at 610 mm (2 ft) on center supporting a corrugated steel deck.

To increase its load capacity, an exterior girder was added to both sides of the bridge to support a single floor beam placed below the existing stringers at mid-span. Prior to testing, the Colorado DOT performed a rating analysis assuming the floor beam as completely rigid and analyzing the interior stringers as two-span continuous beams. By neglecting the stiffness of the floor beam and exterior girders, this analysis produced misleading rating factors. Maximum positive moment in the stringers was underestimated causing a exceedingly high rating. In contrast, the load transferred to the floor beam and exterior girders was overestimated in which case an overly low rating factor was produced.

Because of its unusual structural configuration, the bridge was load tested to determine the distribution of load. A total of 12 strain transducers was used to instrument the floor beam, one exterior stringer, and two interior stringers. At each location, strain transducers were placed on the top and bottom flanges to evaluate flexural curvature and neutral axis position. A diagnostic test procedure was followed as the bridge was loaded with a 3-axle dump truck. Load test results showed 1) virtually no stiffness contribution from the deck to the girders, 2) signs of rotational and axial restraint, 3) interaction between the deck and the floor beam, and 4) minimal negative moment at mid-span of the interior stringers. Based on these observations, a finite element model of the bridge was developed and calibrated to fit the measured response to an accuracy of 3 percent. The calibrated model improved the rating for the floor beam and exterior girders but decreased the rating for the interior stringers. Furthermore, a more balanced rating between the stringers, floor beam, and girders was achieved.

<u>Commander and Schulz (1997)</u>

Diagnostic load tests were performed by BDI on a set of six reinforced concrete slab bridges designed according to the Illinois Bulletin 346 (Jensen et al. 1943) for the Kansas DOT. The typical instrumentation consisted of mounting surface transducers on the bottom face of the slab and at selected locations on the top of the slab. Additional transducers were mounted at different heights on the curbs. These installation schemes provided a direct evaluation of flexural curvature and neutral axis position. The slab bridges were modeled as a two-dimensional grid using specialized software and calibrated to an accuracy of 10%. Using the calibrated models, AASHTO ratings were determined. Negative moment at the pier locations controlled the ratings. Other significant findings included:

1. Positive and negative moment regions had essentially the same stiffness.

2. Gross section properties controlled the curb and slab stiffness.

3. The curbs contribute significantly to bending stiffness.

4. Rotational restraint existed at both the abutments and interior piers.

2.4.2 General Structural Engineering Consultants

<u>Craig, Gill, Everett, Vasquez, and Brooten (1994)</u>

This study presents the diagnostic load testing of 15 concrete encased I-beam bridges built between 1914 and 1928 in Chester County, Pennsylvania.

Field testing was performed by a bridge engineering firm with a subconsultant for the data acquisition and instrumentation. The main purpose of the load tests was to improve the posted capacity limits. With no mechanical shear connection between the concrete and steel, conventional rating guidelines required that the I-beams be assumed non-composite. Load was applied using water tank trucks allowing the truck weight to be adjusted to a safe level for each bridge test.

Experimental results showed strains lower than those predicted for a simple span structure with uncracked composite beams which the authors attribute to partial end restraint. Fascia beams showed smaller strains than the first interior beam due to the stiffening effect of the integral curb or parapet. Compared to the AASHTO Standard Specifications, measured distribution factors for the interior beams varied from 19% lower to 34% higher while the fascia beams averaged 59% higher. Together with the measured distribution factors, empirically derived section properties were used to compute new load rating factors. Of the 15 bridges, twelve received higher posting limits and three needed to be replaced as a result of the load testing.

2.5   OTHER ACTIVITY IN EXPERIMENTAL BRIDGE EVALUATION

While load testing may be common practice for the agencies cited in the preceding sections, there have been other notable applications of non-destructive load testing for bridge evaluation. Through diagnostic testing, Zhou (1996) was able to confirm unintended composite action and adjust the AASHTO distribution factor to increase the load rating of a non-composite steel plate girder bridge in

western Maryland by 50%. Azizinamini et al. (1994) conducted diagnostic load tests on a set of six three-span continuous slab bridges. Measured data were used to develop simple analytical procedures for predicting the response of these bridges at service load levels. A reliability-based rating procedure for reinforced concrete slab bridges integrating yield line and three-dimensional finite element analysis was proposed. Huria et al. (1994) performed a study comparing various analytical techniques for rating reinforced concrete slab bridges. In addition to the AASHTO rating procedures, linear and non-linear finite element analysis were examined. As part of the research reported herein, Bussell (1997) and Velazquez (1998) performed diagnostic load rating studies of reinforced concrete slab and pan-formed girder bridges, respectively. Matsis (1999) did a similar study applied to prestressed concrete girder bridges.

Instead of using diagnostic or proof testing, Ghosn et al. (1986) tested five bridges in Ohio with non-composite and composite steel girders under normal traffic loads to determine load distribution and dynamic impact factors. Axle weights and spacings of passing vehicles were obtained using weigh-in-motion technology. The aim of the study was to evaluate the potential for using field measurements taken under actual loading conditions for bridge rating. For four of the five bridges, rating factors increased by 23 to 50 percent when the field-measured distribution and impact factors were used instead of the AASHTO Standard values. Two other studies done related to assess girder distribution and impact factors from normal traffic loads have been performed by Fu et al. (1996) and Kim and Nowak (1997).

CHAPTER 3

BRIDGE TESTING SYSTEM

This chapter describes the design and implementation of a field testing system for full-scale bridge assessment. The chapter is divided into two sections beginning with a description of the testing equipment (including data acquisition and instrumentation hardware) followed by an explanation of the data collection software. The bridge testing system was designed to work with conventional strain gages and deflection transducers.

The development of the system was a major step of the research described herein since it was to be turned over to the Texas Department of Transportation (TxDOT) for performing routine load tests of suspect bridges. The procedures followed for using the system to load test steel girder bridges along with the post-processing routines for interpreting the collected measurements constitute the other major aspects of the research and are covered in Chapters 5 through 9.

3.1   DESCRIPTION OF TEST EQUIPMENT

The bridge testing system is divided into two types of equipment: instrumentation and data acquisition. Instrumentation refers to the sensors that are bonded or otherwise affixed to bridge members to measure their deformation under the application of load. Strain gages and displacement potentiometers are two such devices that operate electronically. Given a voltage input, these two

instruments will generate an output voltage signal proportional to the deformation of the component to which they are attached. Data acquisition refers to the network of electronic parts that collect and convert these electrical signals from analog to digital form for downloading to a computer. The major parts of the data acquisition system include a Campbell Scientific data logger, a laptop computer, and two 12-volt marine batteries.

The system can accommodate up to 55 simultaneous measurements by means of 11 junction boxes, each equipped with five sensor cables for connecting either conventional strain gages or deflection transducers. The system was assembled from off-the-shelf electronic items and designed to be able to adapt to various combinations of instruments as well as to different instrumentation layouts. An effort was made to limit the number of cables draping down from the instrumentation to the data acquisition system to provide a more efficient testing environment. All electronic components are housed in rugged enclosures and all cables are equipped with a teflon wrapping for weather protection. To facilitate equipment hookup, all cables and protective covers are equipped with bayonet-type connectors. A Windows driven software distributed by Campbell Scientific controls the collection, retrieval, and display of measurements.

3.1.1 Data Acquisition

The data collection system was assembled using BELDEN cable, ITT Cannon connectors, and BUD and NEMA type environmental enclosures. Part numbers and a cost breakdown of the system is provided in Appendix A. Listed below are the major parts of hardware shown in Figures 3.1 and 3.2. A detailed description of each piece of equipment follows.

(A)   Campbell Scientific CR9000C data logger in steel enclosure

(B)   166 MHz Pentium laptop computer

(C)   Campbell Scientific PLA-100 parallel port communication cable

(D)   Two 12V marine batteries in aluminum enclosures with cables

(E)   Routing cable

(F)   120-ohm full bridge completion boxes (for strain measurement)

(G)   Position indicator switch (for tracking load position)

(H)   Adapter cables (for deflection measurement)

(I)   Junction box with sensor cables
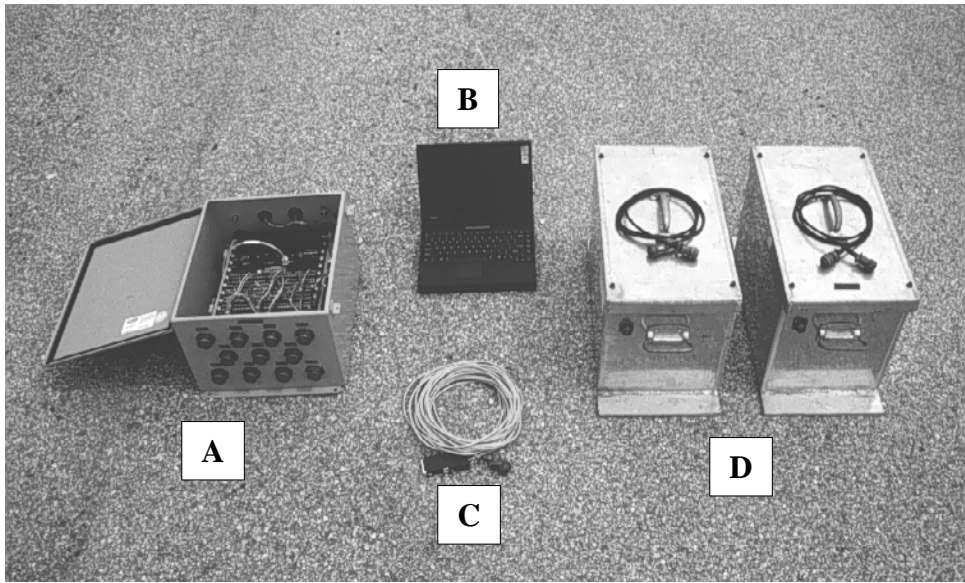
Figure 3.1 Major Components of Data Acquisition Equipment.
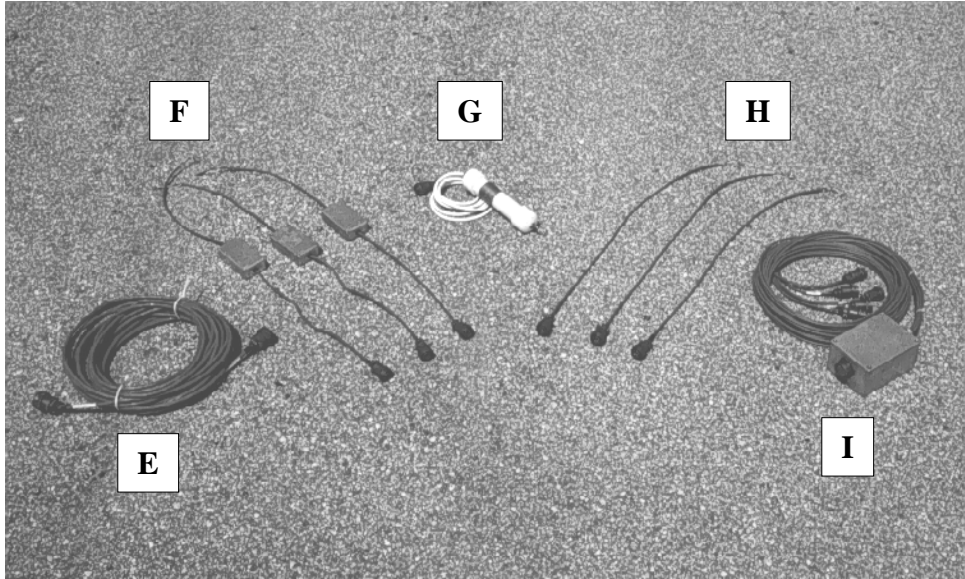
Figure 3.2 Major Components of Data Acquisition Equipment (cont.).

3.1.1.1 Data Logger and Enclosure

At the core of data acquisition is the Campbell Scientific CR9000C data logger. The logger is equipped with an aluminum enclosure, a grounding bus bar, a lead acid battery, and eight available slots for input/output and auxiliary modules. As shown in Figure 3.3, the three slots below the compartment for the internal lead acid battery contain a power supply module, a CPU module, and an A/D module. These three cards are essential for the logger to function and must be in place at all times. The five remaining peripherals are selected based on the application. For full-scale bridge testing, four analog input modules and a single excitation module were considered appropriate. Each input module has 14 differential or 28 single ended channels for measuring voltages up to ± 5 volts. The excitation module has sixteen outputs for providing voltages up to ± 5 volts at a maximum current of 50 mA each. The modules are secured in position with spring-loaded screws on both ends.
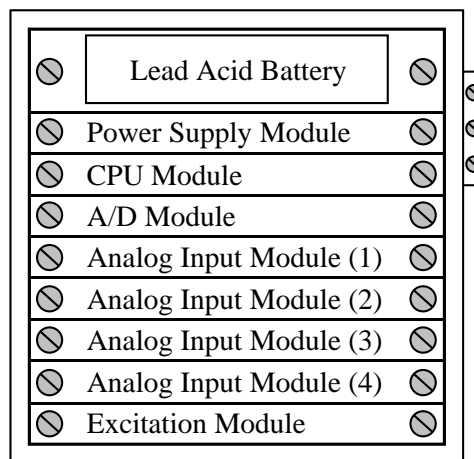
Figure 3.3 Module Layout of CR9000C Data Logger.

For protection in the field, the data logger is mounted on a steel panel inside a 410 mm x 360 mm x 250 mm (16 in x 14 in x 10 in) enclosure built from 14-gauge steel as shown in Figure 3.4. The enclosure has a hinged cover fitted

with a rubber gasket along its edges for shielding the logger from dust, dirt, and water intrusion. The cover is fastened to the enclosure with two steel clamps. Several packages of desiccant are also stored in the enclosure to further protect the logger modules from moisture damage. The aluminum lid of the logger is left off to facilitate the wiring inside the
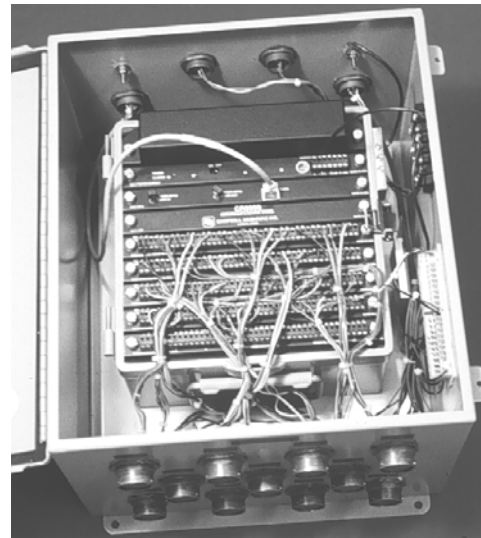
Figure 3.4 CR9000C Data Logger
in Steel Enclosure.

enclosure. A 5-volt, 4-amp power supply is positioned next to the data logger on the steel panel which provides voltage input for the measurements. Wire entry to the data logger is made through the two opposite and smaller sides of the steel enclosure. Figure 3.5 shows one side of the enclosure containing eleven 16-contact connectors labeled A through K for receiving voltage measurements. The connectors are sealed with rubber grommets to the enclosure and are sensibly spaced to provide adequate clearance during hook up. Figure 3.6 shows the other side of the enclosure which holds two 3-contact connectors for external batteries, a 12-contact connector for a laptop computer, and a 5-contact connector for a position indicator switch, all fitted with rubber gaskets. Grounding terminals are also installed which are tied to the grounding bus bar on the data logger. The logger should be properly grounded in the field for transient protection.
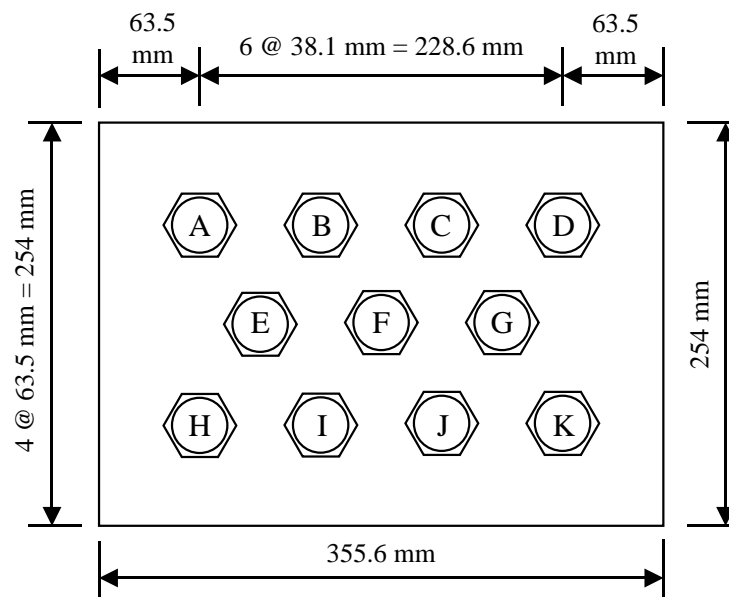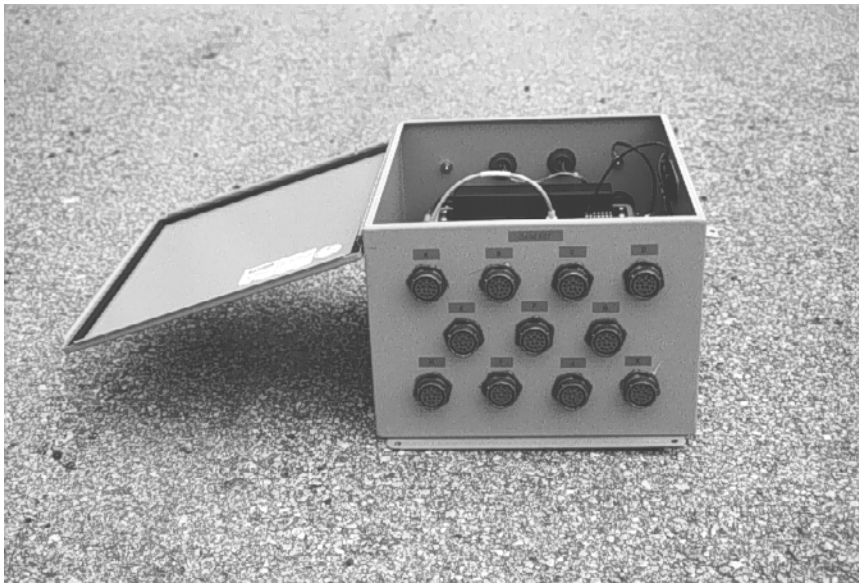
Figure 3.5 Side 1 of Data Logger Enclosure.
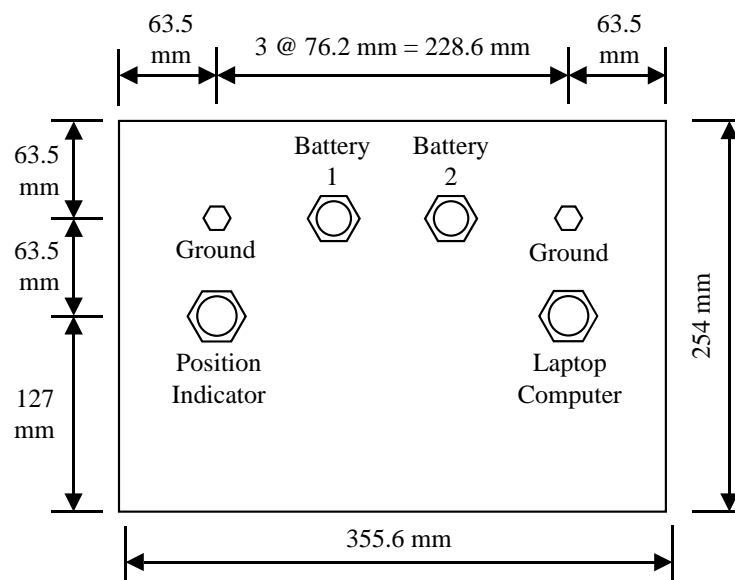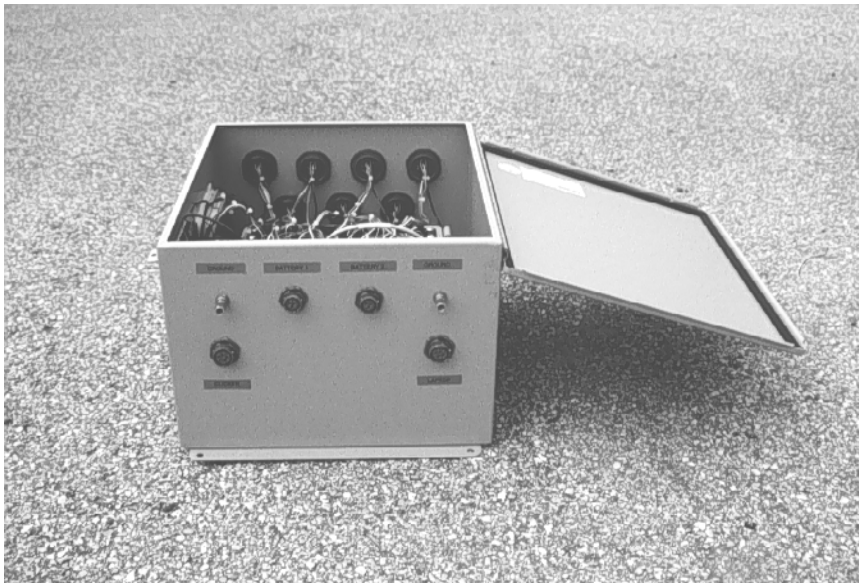
Figure 3.6 Side 2 of Data Logger Enclosure.

A schematic of the wiring layout inside the steel enclosure is provided in Figure 3.7. The laptop connects to a socket labeled TLINK in the CPU module. The incoming voltage from the 12V battery is collected at a manifold connector and distributed to the charging terminals on the logger's power supply module and the 5V power supply. The internal lead acid battery is removed so that the data logger receives power directly from the 12V battery. At the 5V power supply, the 12 volts from the marine battery is dropped down to 5 volts and is distributed to twelve outgoing excitation signals. Eleven of the signals are routed to the same number of junction boxes where the excitation is distributed to five bridge circuits. The twelfth signal is sent to a switch.

With four input modules, the data logger has a capacity of 56 differential input channels for voltage measurements. Each of the eleven lettered connectors on the data logger enclosure represents five channels of strain or deflection measurements. The channels are labeled with the letter on the junction box appended with the sensor number (i.e., A1 through A5, B1 through B5, C1 through C5, etc.). The last channel is used to record the bridge excitation voltage from the 5V power supply. This voltage signal is controlled by means of a mechanical switch that is installed at the end of a 30.5 m (100 ft) cable. When pressed, the switch interrupts the flow of electricity through the cable thus producing a zero voltage in the data record. The switch was built specifically to track the position of a load truck as it passes over a bridge during a test. The sequence in which these measurements were assigned to the differential input channels in the data logger is shown in Figure 3.7.

47

Laptop   Battery 1   Battery 2   Switch

Manifold

Power Supply Module

CPU Module

A/D Module

A1	A2	A3	A4	A5	B1	B2	B3	B4	B5	C1	C2	C3	C4

C5	D1	D2	D3	D4	D5	E1	E2	E3	E4	E5	F1	F2	F3

F4	F5	G1	G2	G3	G4	G5	H1	H2	H3	H4	H5	I1	I2

I3	I4	I5	J1	J2	J3	J4	J5	K1	K2	K3	K4	K5	PI

Analog Input Modules

5V Power Supply

Manifold

A   B   C   D   E   F   G   H   I   J   K

To Junction Boxes
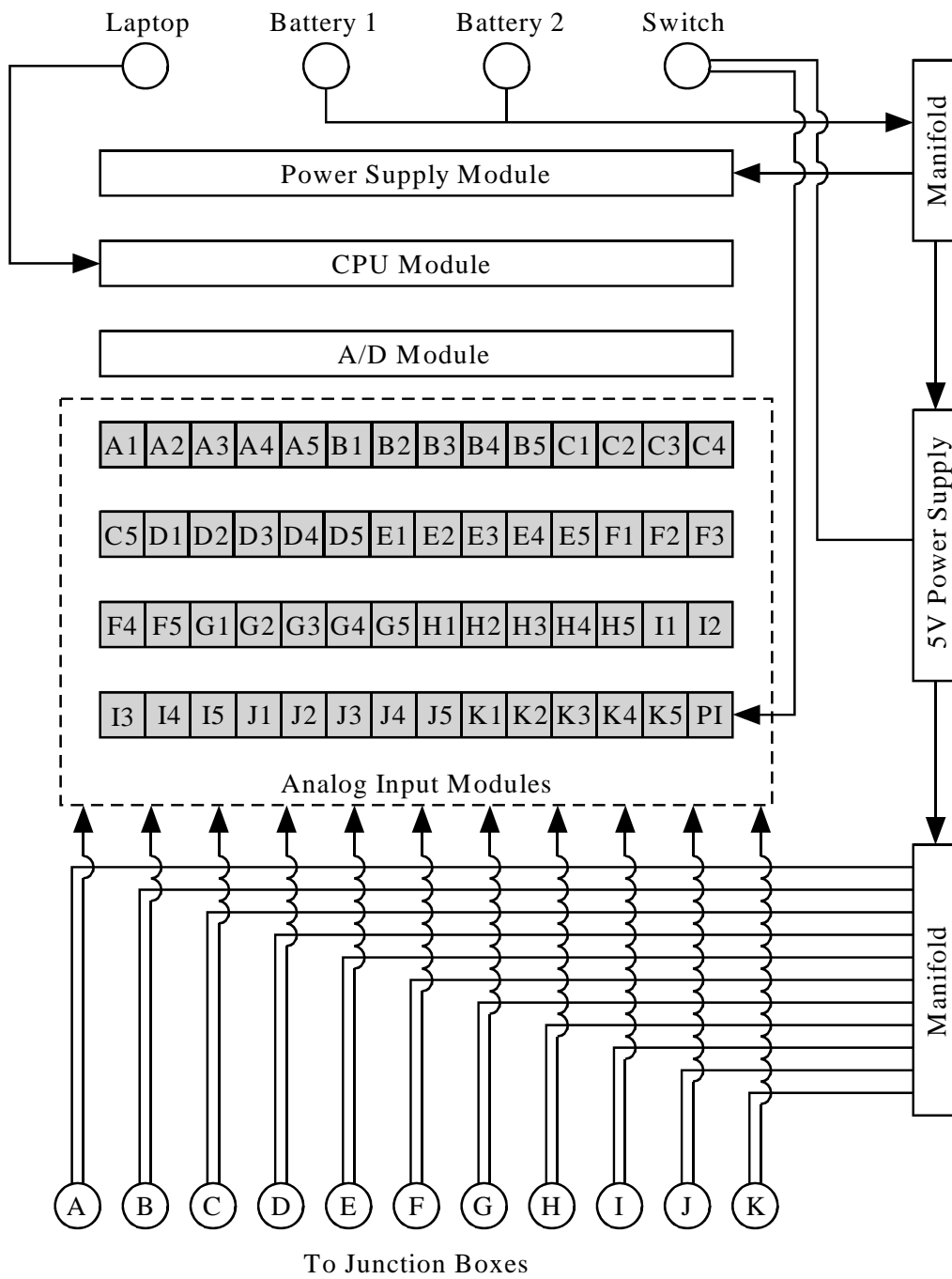
Figure 3.7 Wiring Layout Inside CR9000C Steel Enclosure.

48

With reference to Figure 3.3, analog input module 1 contains channels A1 through C4, module 2 contains channels C5 through F3, module 3 contains channels F4 through I2, and module 4 contains I3 through K5 plus the excitation channel.

3.1.1.2 System Control and Power Supply

A Windows PC9000 software is distributed with the data logger to control the collection, retrieval, and display of measurements. The software is installed on the laptop computer that operates under the Windows 95 operating system. Communication between the data logger and the computer is made through the parallel port with a 15.2 m (50 ft) PLA100-L cable supplied by Campbell Scientific. The computer has a 166 MHz Pentium processor, a 2.0 gigabyte hard drive, 40 megabytes of RAM, an active matrix display, and two removable lithium ion batteries. When fully charged, the internal batteries can power the computer for about 5 hours while operating the data logger. Alternatively, the computer can be run off of a 120V generator for longer periods of time. In the field, the generator should be properly grounded to protect the laptop.

Power to the data logger is provided externally from two 12V marine batteries, one at a time. The batteries are secured in aluminum boxes with plastic inserts for collecting battery acid in case of leakage. The two batteries are wired in parallel so that a low voltage battery can be replaced without losing power to the data logger. The wiring is interrupted with a 4-amp fuse for excessive current protection of the logger.

Due to the limited output current of 50 mA for the individual channels of the excitation card, an alternate voltage source was needed to provide excitation to the bridge circuits. Given 5 volts of excitation, a 120-ohm strain gage yields a current drain of 42 mA which is over 80% of the current capacity of the excitation channels. As a result, a separate excitation channel is needed to excite each 120-ohm strain gage circuit. Since only 16 output channels are available on the excitation card, additional excitation cards are needed for the 55 measurements required. With no available slots on the chassis of the data logger, input modules would have to be removed to accommodate extra excitation cards. This arrangement was considered unacceptable since fewer voltage measurements would be possible.

Instead, the excitation voltage is provided through a separate power supply connected in series with the 12V marine battery. The regulated power supply is rated at a voltage of 5 volts and a current of 4 amps. The critical state of the data logger is when all input channels are connected to strain gage circuits. In this condition, the current demand is about 3.3 amps. During operation, the logger modules consume about 1 amp of current while the strain gages require a current of 2.3 amps (i.e., 42 mA x 55 gages). With a current output of 4 amps, the power supply easily met the current demand for the worst case measurement situation.

3.1.1.3 Junction Boxes and Cables

The junction boxes are constructed from aluminum boxes with exterior dimensions of 80 mm x 110 mm x 150 mm (3 in x 4 in x 6 in). Five 4.6-m (15-ft) sensor cables exit the junction box through a hole protected with a watertight gasket. Each of the cables consists of 4 wires (22-gage) insulated with teflon and bundled in a red silicon jacket. A 5-contact plug is installed at the end of each cable that can be connected to either a strain gage or deflection transducer with the appropriate adapter. The exterior and interior configuration of a typical junction box is shown in Figure 3.8.
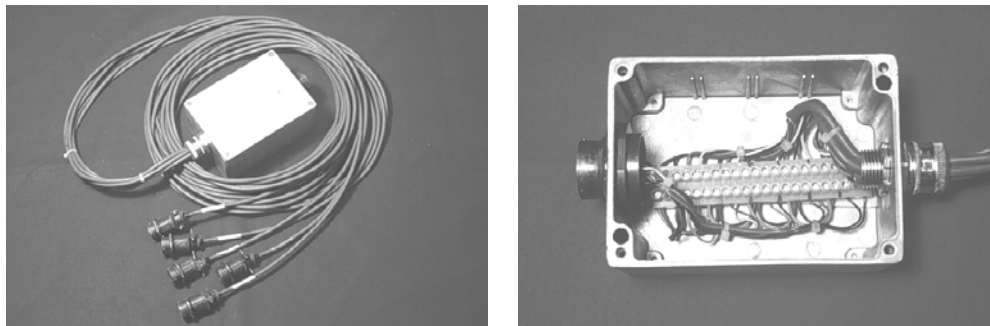
Figure 3.8 Junction Box and Sensor Cables.

A schematic of the junction box wiring is provided in Figure 3.9. Inside the junction box, the incoming excitation signal is distributed to the five sensor cables, each representing a separate measurement. Output signals from the strain gages or potentiometers are relayed back to the junction box where they are collected and distributed to a 16-contact connector placed on the opposite end of the junction box.
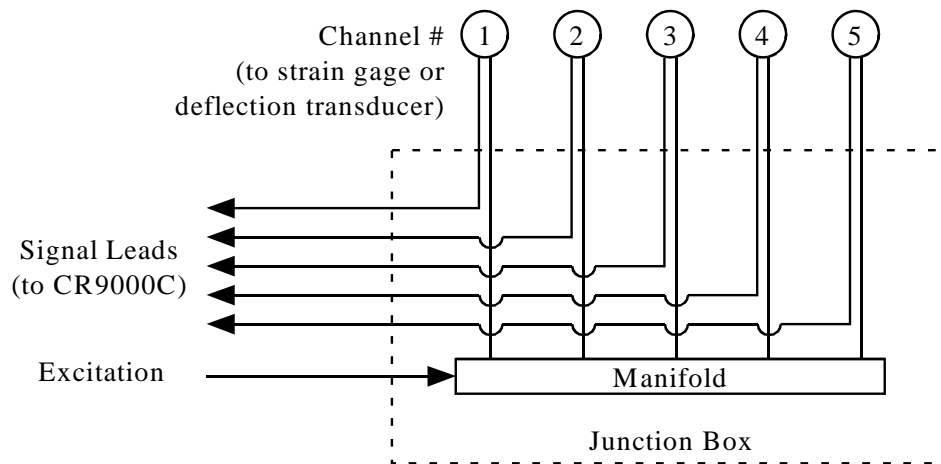
Figure 3.9 Junction Box Wiring Layout.

The junction boxes are labeled from letter A to K and are connected to their corresponding lettered connector on the data logger enclosure via routing cables. The routing cables were fabricated in lengths of 9.1 m (30 ft) and 15.2 m (50 ft) with twelve 16-gage conductors in a red teflon wrapping. Longer lengths can be obtained with extensions. Sixteen contact bayonet-type connectors are installed at either end of the routine cables and extensions. Large diameter wire was used to minimize signal attenuation over the length of the routing cable.

3.1.2   Instrumentation

3.1.2.1 Strain Measurement

The data acquisition system uses conventional 120-ohm resistance strain gages in a three-wire, quarter bridge arrangement for temperature compensation. Installation of an electrical resistance strain gage consists of five basic steps

52

which include: selection of the gage, preparation of the gage for field installation, preparation of the gage surface, attachment of the gage, and weatherproofing of the gage. Detailed procedures for carrying out each step are provided in Appendix B.

Electrical resistance strain gages distributed by Texas Measurements, Inc. were used to measure strain in both steel and concrete bridge components. For steel, the FLA-10 strain gage manufactured by Tokyo Sokki Kenkyojo, Inc. is used. This self-temperature compensating gage has a gage length of 10-mm (0.39 in), a resistance of 119.5 ohms (± 0.5), a gage factor of 2.11 ($\pm 1\%$), and is equipped with three lead wires. For concrete members, a two-lead wire 60-mm (2.36 in) foil gage is used. This gage (type PL-60) is also manufactured by Tokyo Sokki Kenkyujo with a resistance of 120.3 ohms (± 0.5) and a gage factor of 2.09 ($\pm 1.0\%$). Furthermore, the gage is self-temperature compensating but must be manually modified to a three-lead wire system.

To keep the lead wires short, the three completion resistors of the Wheatstone bridge circuit are housed in an aluminum box adjacent to the gage. The box has outer dimensions of 30 mm x 60 mm x 100 mm (1 in x 2 in x 4 in) with a 1.6 mm (1/16 in) thickness. The enclosure also has a 3-conductor cable for attaching a three lead-wire strain gage on one end and a 4-conductor cable (with a 5-contact plug) on the other end for attaching the sensor cable from the junction box. The cable cutouts are sealed with rubber grommets to protect the Wheatstone Bridge circuit. The configuration of a typical completion box is shown in Figure 3.10.

53
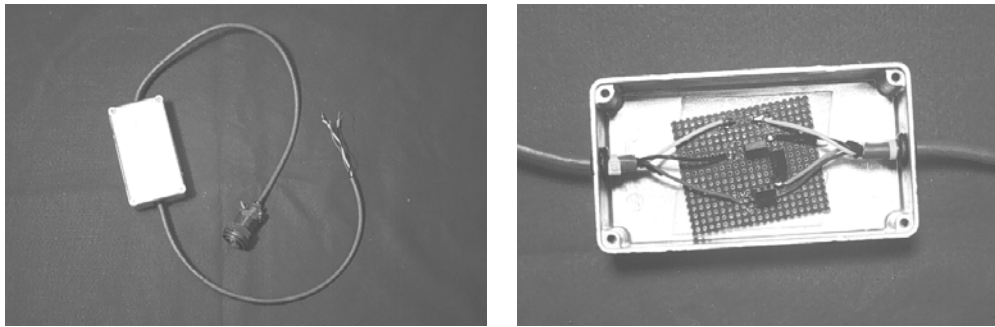
Figure 3.10 Strain Gage Completion Box.

Figure 3.11 shows a schematic of the bridge circuit inside the completion box. The dummy resistors are designated as R_1, R_2, and R_3 and are manufactured with a resistance of 120 ohms ($\pm$ 0.01%).
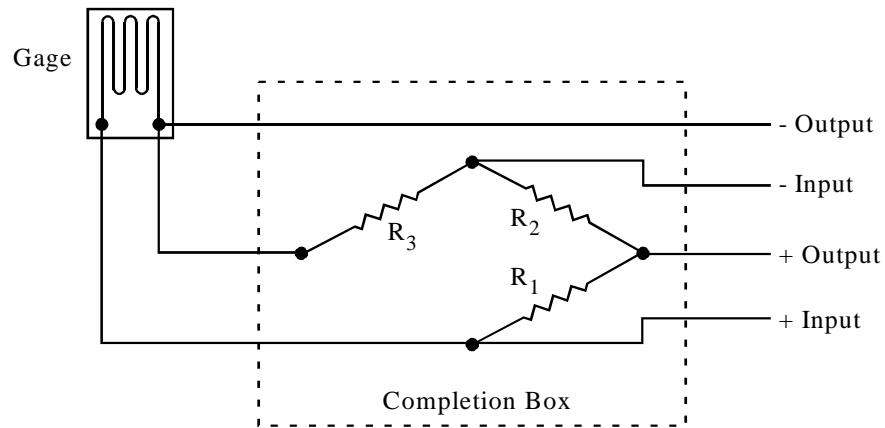
Figure 3.11 Wiring Layout for Three-Wire, Quarter Bridge Circuit.

With the strain gage in one active arm of the Wheatstone Bridge circuit, the equation relating strain to input / output voltage is given as

$$\frac{E_o}{E_I} = \frac{GF \; x \; \varepsilon}{4} \tag{3.1}$$

where E_o = output voltage, E_I = input voltage, GF = gage factor, and ε = strain.

3.1.2.2 Deflection Measurement

Using a DC input voltage, displacement measurements may be made with resistance potentiometers or a DC-DC displacement transducer. Potentiometers consist of a resistor with a movable contact (slide or wiper) on its surface and are available in a wound string or plunger assembly. The output voltage ranges from zero to the excitation voltage under full extension of the string or full depression of the plunger. The DC-DC transducer is a direct current version of the LVDT (linear variable differential transformer) and consists of a movable magnetic core and a hollow cylindrical transformer with a primary coil and two secondary coils. The unit has a voltage output of plus or minus the excitation voltage over the full range of motion of the magnetic core through the transformer. A null reading is produced at the midpoint of travel, where there is a voltage balance between the two secondary coils.

Each of the deflection instruments described above has its own adapter for connecting to the sensor cables of the junction box. With the proper setup, the instruments are capable of measuring vertical deflection, however, access is needed beneath the bridge. Installation procedures for this type of measurement are provided in Appendix B. The linear potentiometer can also be employed for measuring other actions of bridge behavior such as the relative slip between non-composite members. The voltage-displacement relationship of these instruments is obtained by calibration and is typically given in terms of millimeter (inch) of travel per volt of output.

3.2   DATA COLLECTION SOFTWARE

3.2.1   Overview of Program

There are five main features of the Campbell Scientific PC9000 software used to operate the data acquisition system: a program generator, a program editor, a real-time data display, a data retrieval utility, and a data graphing utility. The program generator and editor are both used to write the measurement instruction code for the data logger. These instructions are written in a native CRBASIC language and are downloaded to the data logger to specify the configuration of the modules, the measurement parameters for each input channel, the scanning rate for measurements, the functions of user-defined flags, and the format of the data output tables.

The real-time monitor is used for viewing measurements as they are being recorded and also for enabling / disabling user-defined flags. The data retrieval utility is used to download measurements stored in the data logger's CPU memory to the hard drive of the laptop computer. Downloaded data can be subsequently displayed using the data graphing utility. Complete instructions for the PC9000 software and the CRBASIC language can be found in the user manual and in the on-line help menus in the software.

Before conducting a test, the input file containing the measurement instructions must be prepared and given a .DLD extension. The program is downloaded to the logger from the laptop through the PLA100-L communication cable. A sample data collection program is listed in Appendix C that was created

for 40 strain gages, 15 deflection transducers, and the excitation voltage switch. These instructions must be modified directly with the program editor for other sensor combinations. If changes are made, however, they will not take effect until the new version of the program has been redownloaded. Input files are stored in Flash EEPROM (electrically erasable programmable read-only memory) located in the logger CPU module. As a result, the programs remain in memory after the system has been turned off. Several versions of the program can be stored in this memory.

Once in the logger memory, a program can be instructed manually to run or automatically upon activation of the logger. The program runs in the static RAM (random-access memory) buffer of the logger. Only one program can be run at one time. A step-by-step outline of the commands for using the program for a bridge test is given in Appendix B. Details of the program are reviewed in the following sections.

3.2.2 Channel Description and Scanning Interval

There are twelve voltage measurement blocks in the program. Voltage blocks 1 through 11 are used to set up the channels for junction boxes A through K while the twelfth block is used to set up the excitation voltage channel. Each voltage block is assigned four variables that determine the type of measurement to be made and the number of active channels. It is these variables which must be modified manually with the program editor to specify the instrumentation layout. The first variable is the voltage measurement range. The range can be set at ±50

mV, ±200 mV, ±1000 mV, or ±5000 mV but must be set higher than the level of voltage expected from the instrumentation. The second variable is the number of repetitions (i.e., active channels) in the voltage block. Repetitions for blocks 1 through 11 can be set from 1 to 5 depending on how many channels are being used in the junction box while a single repetition is specified in the twelfth block for the excitation voltage channel. The third and fourth variables are the delay and integration times. The delay period represents the amount of time allotted to the logger to switch to an input channel and wait for the voltage signal to stabilize. The default delay values for the measurement ranges of ±50 mV and ±5000 mV are 20 μs and 10 μs, respectively. Following the delay, the integration time represents the length of time over which measurements are taken every 10 μs and then averaged. For example, an integration time of 1000 μs will result in an average of 100 readings. This parameter is used for reducing noise in the measurements. The measurement range, delay time, and integration time are applied to all active channels in the voltage block.

The channels in voltage blocks 1 through 11 are labeled according to the junction box and sensor it is reading. Table 3.1 shows the channel arrangement in the twelve voltage blocks. Starting with voltage block 1, the channels are scanned at the rate specified in the scanning interval section of the program in the order given in the table below. Figure 3.7 shows the arrangement of these channels in the four analog input modules of the data logger.

Table 3.1 Channel Designation in Voltage Blocks.

Voltage Block	Measurement in Voltage Block				
	1st	2nd	3rd	4th	5th
1	A1	A2	A3	A4	A5
2	B1	B2	B3	B4	B5
3	C1	C2	C3	C4	C5
4	D1	D2	D3	D4	D5
5	E1	E2	E3	E4	E5
6	F1	F2	F3	F4	F5
7	G1	G2	G3	G4	G5
8	H1	H2	H3	H4	H5
9	I1	I2	I3	I4	I5
10	J1	J2	J3	J4	J5
11	K1	K2	K3	K4	K5
12	Excite				

In the program given in Appendix C, voltage blocks 1 through 8 are set up for strain gages and blocks 9 through 11 are set up for deflection transducers. Five repetitions are specified in each block, one for each channel in the junction box. For strain gages, the measurement range is set at ±50 mV with delay and integration times of 40 and 1000 µs, respectively. An integration time of 1000 µs was required to reduce the noise level to about ±0.005 mV or ±2 µε. Deflection transducers and the excitation voltage switch operate in the range of ± 5000 mV with a delay of 10 µs and an integration time of 400 µs. For these measurements, the noise level is about ±0.1 mV, which for a linear potentiometer with a 50.8 mm (2 in) stroke corresponds to a deflection less than ±0.003 mm (±0.0001 in). A shorter integration time could be used for these measurements due to the higher voltage range (i.e., higher signal-to-noise ratio). Changing the delay time had no significant effect on the noise level for either strain or deflection measurements.

59

Each input channel is equipped with a HI, LO, and ground slot. All channels are configured for dual differential voltage measurements meaning that a measurement is first made with the HI referenced to the LO input followed by a second measurement with the poles reversed. The appropriate delay and integration are applied in both measurements as shown in Figure 3.12. The final output is the average between the first reading and the negative value of the second reading.
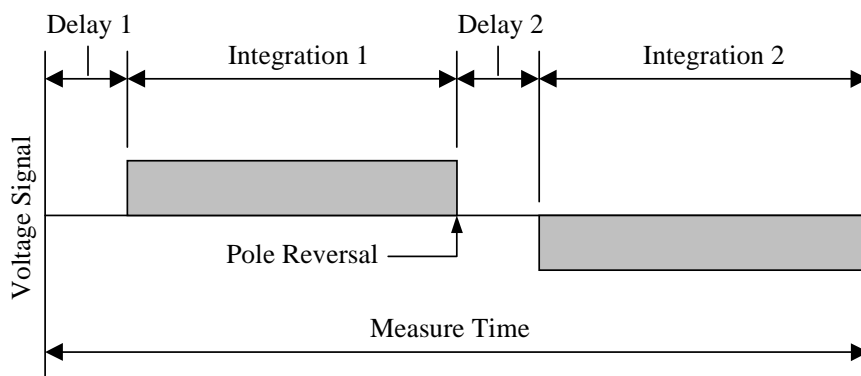
Figure 3.12 Measurement Sequence for a Single Channel.

As illustrated in Figure 3.12, the time required to carry out a dual differential measurement for a single channel is equal to two times the sum of the delay and integration times. For a series of K channels, the total measure time is approximated with the following summation formula:

$$Measure\,Time = 2 \sum_{i=1}^{K} (Delay\,Time + Integration\,Time) \qquad (3.2)$$

where i = the active channel.

60

The last variable that must be specified in the data collection program is the scan interval. The scan interval represents the time between scans of a single channel and must be set larger than the total measurement time and the maximum process time. Process time represents the total measurement time plus the time required for other tasks such as the A/D conversions of the data plus other mathematical operations and adjustment of the measurement range between voltage blocks. If the scan rate is lower than either the measure or process times, the logger will switch back to the first channel before completing the scan of all channels resulting in skipped scans.

For example, consider the program given in Appendix C developed for 40 strain channels, 15 deflection channels, and one excitation voltage channel. Using the relationship given earlier, the total measure time is approximately 95,910 μs (i.e., measure time = 2 x [40 x 1040 + 15 x 410 + 1 x 410]). In this case, the sampling rate is set at 10 Hz (i.e., one sample every 100,000 μs) to avoid skipping scans. To obtain faster measurements, the integration times must be reduced which will increase the noise level. Alternatively, the number of active channels must be reduced in order to keep the same integration times.

3.2.3 User-Defined Flags and Data Tables

The program has three flags to zero the data channels (Flag 1), to activate a continuous data collection mode (Flag 2), and to reset the data tables in the logger's CPU memory (Flag 3). These flags can be controlled from the real time

monitor once a program is downloaded and are discussed further in the following sections.

3.2.3.1 Flag 1: Zero Channels

Flag 1 activates a subroutine that takes an initial reading of all active channels in voltage blocks 1 through 11. An initial reading is not taken for the excitation voltage channel. During this process, the logger will take 100 readings at 10 Hz for each channel and output the average. These values are referred to as the zero readings and are stored in the logger's static RAM buffer in two tables named ZERO_1 and ZERO_2. Table ZERO_1 contains channels A1 through F5 while table ZERO_2 contains channels G1 through K5. Once the zeroing process is complete, the flag will disable itself.

Initially, all data channels are given default values of 1 and 0 for the multiplier and offset. As a result, measurements taken with *Flag 2* before the channels are zeroed represent the raw voltage from the instrumentation. A zero reading is needed so that all channels read close to null voltage before the application of load. Furthermore, zeroing allows measurements to be made over the full range of voltage specified in the voltage blocks.

3.2.3.2 Flag 2: Collect Continuous Data

Flag 2 instructs the data logger to collect voltage data continuously until the flag is disabled or the logger memory is full. During this mode, the logger will read the channels, subtract the initial readings taken with *Flag 1*, and output

the difference. Since no zero is taken for the excitation voltage channel, the output is always the raw voltage. Data are stored in binary format with 24-bit resolution in four tables named DATA_1, DATA_2, DATA_3, and DATA_4 located in RAM. As shown in Table 3.2, the first table contains channels A1 through C5, the second table contains channels D1 through F5, the third table contains channels G1 through I5, and the fourth table contains channels J1 through K5. The last data series in each table contains the excitation voltage.

Table 3.2 Channel Designation in Voltage Data Tables.

Data Series	Table Name			
	DATA_1	DATA_2	DATA_3	DATA_4
1	A1	D1	G1	J1
2	A2	D2	G2	J2
3	A3	D3	G3	J3
4	A4	D4	G4	J4
5	A5	D5	G5	J5
6	B1	E1	H1	K1
7	B2	E2	H2	K2
8	B3	E3	H3	K3
9	B4	E4	H4	K4
10	B5	E5	H5	K5
11	C1	F1	I1	Excitation
12	C2	F2	I2	
13	C3	F3	I3	
14	C4	F4	I4	
15	C5	F5	I5	
16	Excitation	Excitation	Excitation	

The data tables are specified as fill and stop, that is, once the tables are full, the data logger discontinues to collect data to avoid writing over previously taken data. Caution must be taken when using this type of memory for data storage since data are lost in the event of power outage to the logger.

Data are downloaded from the logger to the laptop's hard drive in ASCII format using the data retrieval utility in the PC9000 software. During download the status of the data transfer is displayed and includes the file name, the file length, the rate of data transfer, and the time record. By default, the software names the data files starting with the data table name followed by two digits and a .DAT extension. The numbering sequence of the data files begins at double zero and increments by 1 for each subsequent download of data. Thus, the first download of data will name the files DATA_100.DAT, DATA_200.DAT, DATA_300.DAT, and DATA_400.DAT. The next download produces files named DATA_101.DAT, DATA_201.DAT, and so forth. Once on the hard drive of the laptop, the data files can be read directly and plotted with the PC9000 graphing utility or imported into a spreadsheet for analysis.

3.2.3.3 Flag 3: Reset Data Tables

Flag 3 is used to reset the data tables in the logger buffer after the data have been downloaded to the laptop. Resetting the tables erases all data and sets all data records back to zero to begin another test. If the tables are reset or the logger loses power before the data are transferred to the laptop, the data are lost and cannot be recovered.

CHAPTER 4

BRIDGE DESCRIPTION

This chapter describes the non-composite steel girder bridge, designated as the Big Creek Relief Bridge, which was tested to failure. The decommissioned bridge was made available for testing purposes by the Texas Department of Transportation and is located adjacent to State Highway 6, about 4.8 km (3 miles) southeast of Marlin, Texas in Falls County. Main features of the bridge include a cast-in-place reinforced concrete deck (with monolithic curbs on both sides) and five non-composite steel girders that are continuous over four spans.

The description of the Big Creek Relief Bridge is divided into three parts. The first part discusses the history and basic layout of the bridge. The second part describes the design details of the bridge components. The third part reports on the mechanical properties of the bridge materials as determined from laboratory testing.

4.1   BRIDGE HISTORY AND GENERAL LAYOUT

Built in the late 1950's, the Big Creek Relief Bridge was designed for H20 truck loading in accordance with the A.A.S.H.O. Standard Specifications (1953) and T.H.D. Supplement No. 1 (1946). In November of 1996, the bridge was taken out of service due to a low condition rating for the superstructure, at which time Highway 6 was redirected over a new two-lane, prestressed concrete girder

65

bridge erected on the east side of the steel bridge. Before decommissioning, the bridge carried two lanes of traffic (one northbound, one southbound) on a 9.1-m (30-ft) roadway over the floodwater runoff from nearby Big Creek.

In elevation, the bridge is 158.5 m (520 ft) long having one 12.2 m (40 ft) unit continuous over two spans and four 36.6 m (120 ft) units, each continuous over four spans. The two-span unit has equal span lengths of 6.1 m (20 ft) and is situated on the north end of the bridge. The four-span continuous units make up the remaining 146.3 m (480 ft) of the bridge and each have exterior spans of 7.9 m (26 ft) and interior spans of 10.4 m (34 ft). Figures 4.1 and 4.2 show the north and south ends of the bridge in plan and elevation. There are two construction joints in the reinforced concrete deck of the four-span units, located 12.2 m (40 ft) from each end. Expansion joints (labeled as E) are located at the end of each unit to compensate for longitudinal movement caused by changes in temperature and live load. From visual inspection, these joints appeared functional since cracks had developed through the depth of the asphalt overlay. The bridge units have fixed bearings (labeled as F) at the three interior support locations, which restrict movement in the longitudinal direction.
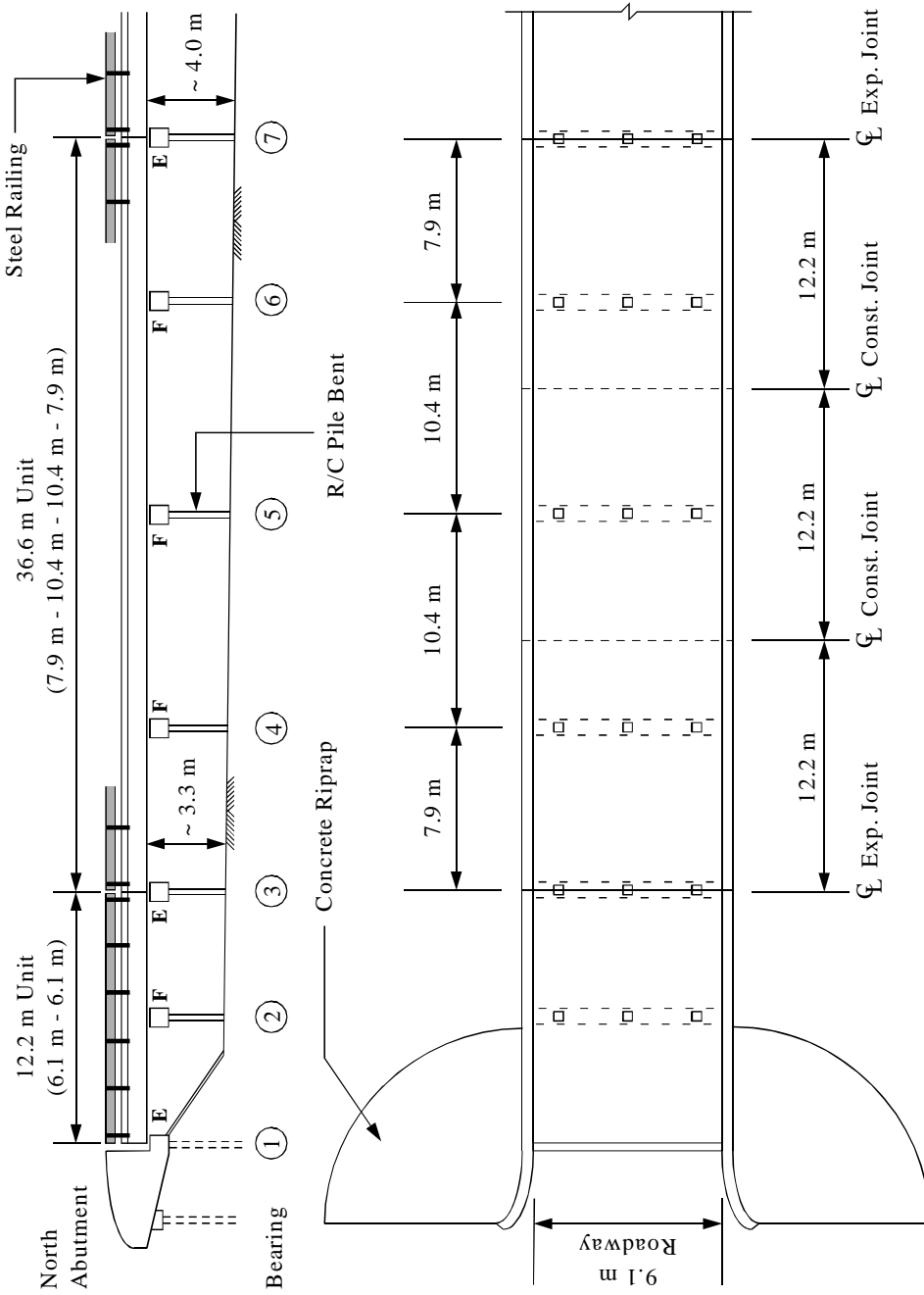
Figure 4.1 Elevation and Plan View of Bridge at North End.

67
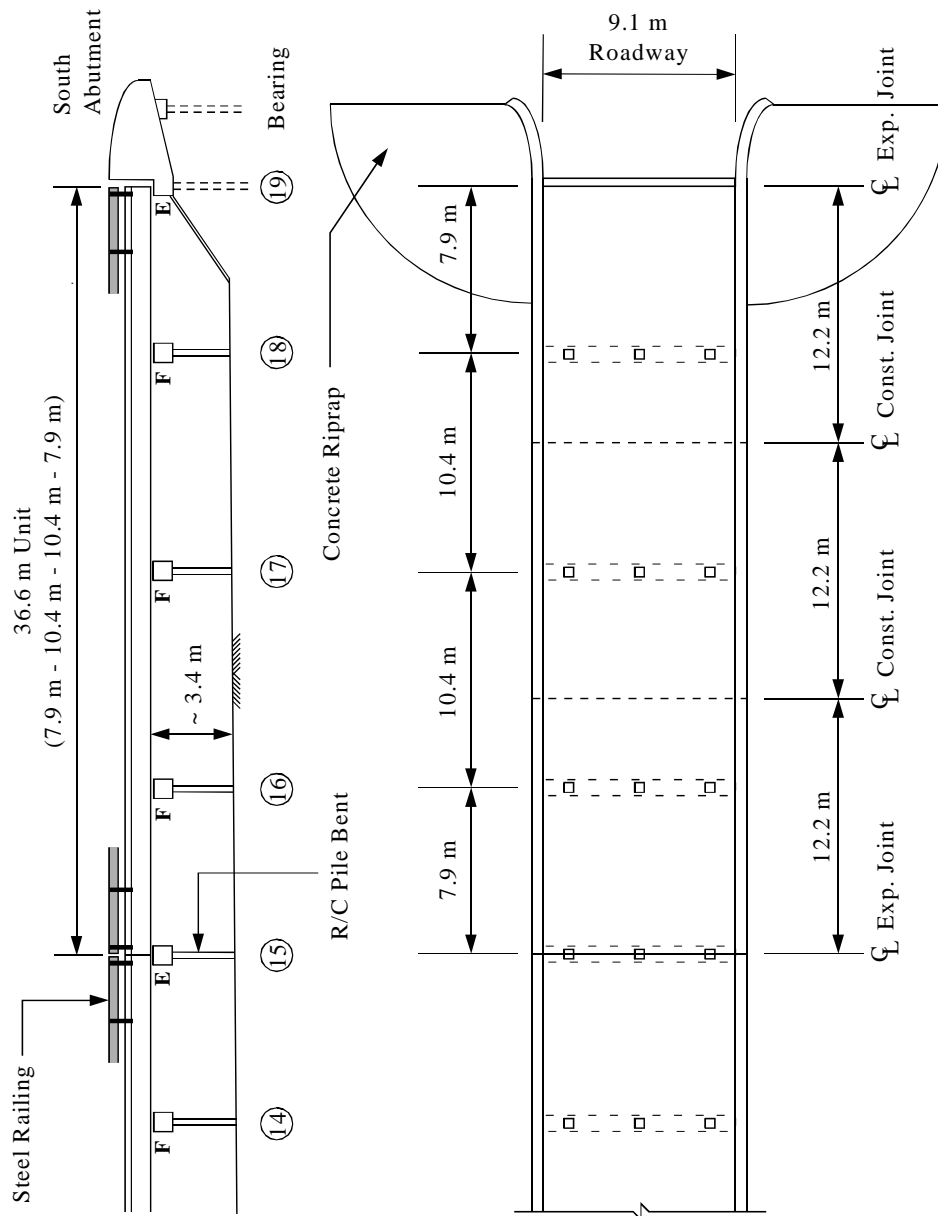
Figure 4.2 Plan and Elevation View of Bridge at South End.

Figure 4.3 shows a picture of the decommissioned steel bridge before it was tested. A reinforced concrete substructure consisting of cast-in-place bent caps on precast displacement piles supports the bridge. The bent caps are 760 mm x 760 mm (30 in x 30 in) in cross section and 9.1 m (30 ft) in length. Each cap is supported by three 410 mm (16 in) square piles driven approximately 10.7 m (35 ft) to point bearing in firm shale. The vertical clearance between the bottom of the steel girders and ground level varied from roughly 3.4 m (11 ft) at the north and south ends to 4.3 m (14 ft) towards the middle part of the bridge. Approach roadways were left in place at both ends of the bridge to provide easy access to the site.

Figure 4.3 View of Big Creek Relief Bridge from East Side.

4.2   BRIDGE COMPONENTS

In cross section, the superstructure consists of five steel girders equally spaced at 2.0 m (6 ft 6 in) on center supporting a 150 mm (6 in) cast-in-place reinforced concrete deck and a 60 mm (2.5 in) asphalt overlay. There are no mechanical shear connectors joining the girders and deck, however, the concrete slab was cast such that the top flanges of the girders were left embedded (through the flange thickness) into the underside of the bridge deck. The steel girders are constructed from a CB21x59 section (similar to a W21x62 wide flange section by current AISC standards) salvaged from a pre-existing bridge. The bridge deck has a 9.1 m (30 ft) roadway and integral curbs on both sides. At expansion and construction joint locations, 270 mm (10.5 in) deep by 230 mm (9 in) wide reinforced concrete diaphragms span between the girders. The diaphragms are reinforced with two #8 longitudinal bars (nominal diameter = 1.00 in = 25.4 mm, nominal cross-sectional area = 0.79 in^2 = 510 mm^2) and #4 transverse stirrups (diam. = 0.50 in = 12.7 mm, area = 0.20 in^2 = 129 mm^2) spaced at 250 mm (10 in).

The 150 mm (6 in) deck slab is reinforced with #5 bars (diam. = 0.625 in = 15.9 mm, area = 0.30 in^2 = 194 mm^2) in both the transverse and longitudinal directions. Longitudinally, the top and bottom steel is placed at an average center-to-center spacing of 480 mm (19 in) and 280 mm (11 in), respectively. Transversely, the spacing is 180 mm (7 in) for the tension steel (i.e., top steel above the girders and bottom steel between girders) and 360 mm (14 in) for the compression steel (i.e., bottom steel above the girders and top steel between

girders). The transverse reinforcing bars extend into the 460 mm x 180 mm (18 in x 7 in) curbs cast monolithically with the deck on both sides. The curbs overhang the exterior girder a length of 1.1 m (3 ft 7 in). The cross section of the superstructure, including the rebar layout in the deck, is shown in Figure 4.4. A steel railing, consisting of a single C12x20.7 rail and attached to WF5x16 posts, is connected to the outside face of the curbs. The posts are spaced at a distance of 2.6 m (8 ft 6 in) on center. Figure 4.5 shows the curb and railing detail.

In elevation, each 36.6 m (120 ft) continuous girder consists of three 12.2 m (40 ft) CB21x59 sections that are weld-spliced at locations coinciding with the construction joints in the slab. At the center of each 36.6 m (120 ft) girder, a 127 mm x 7.94 mm (5 in x 5/16 in) cover plate is welded on both the top and bottom flange. The plates extend 990 mm (3 ft 3 in) on either side of the support. Figure 4.6 shows a half elevation of a typical girder including the nominal girder sections and cover plate detail.
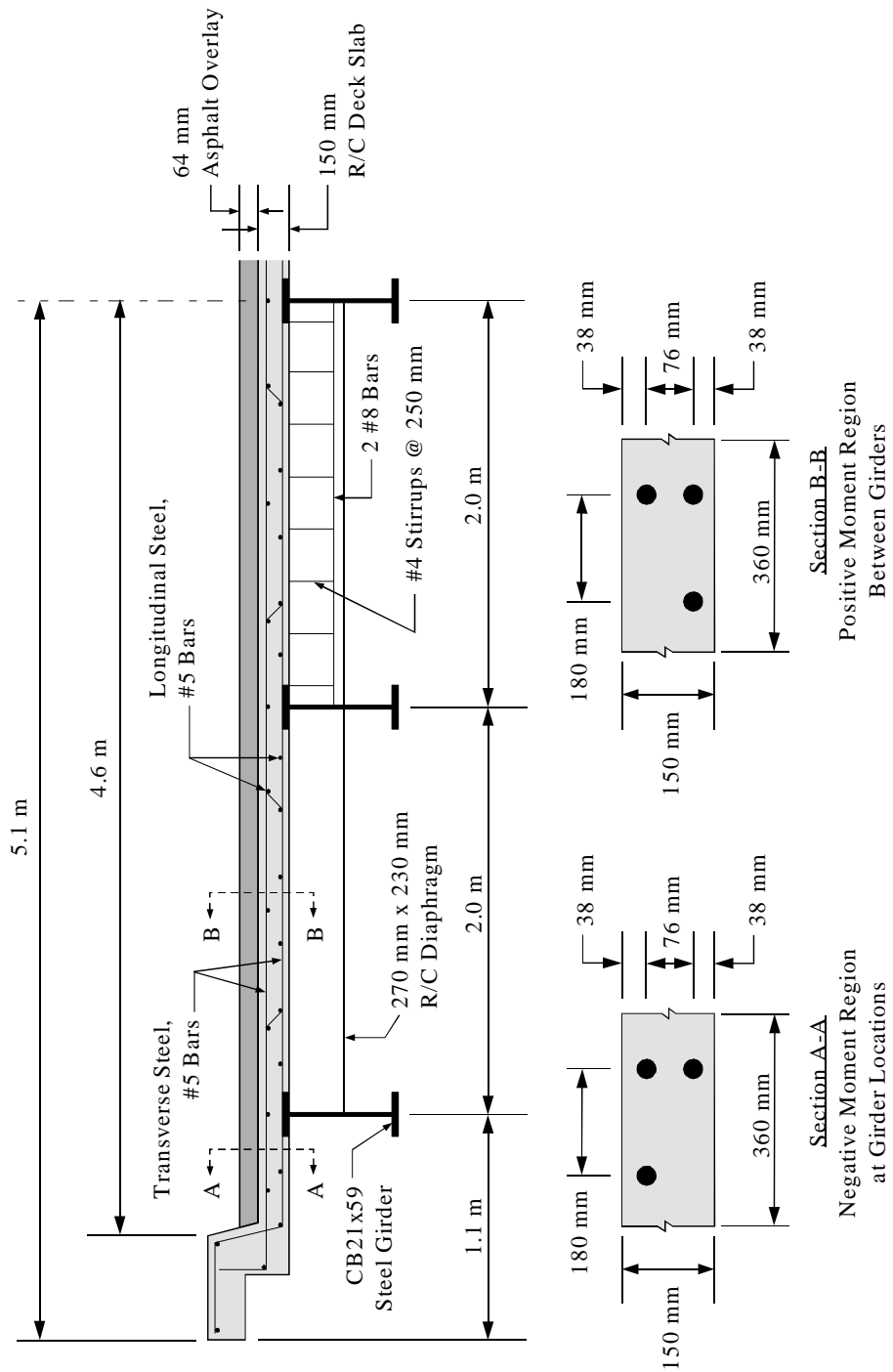
Figure 4.4 Cross-Section of Superstructure and Deck Reinforcement.

Post,
WF5x16

Rail,
C12x20.7

610 mm

360 mm

180 mm

22 mm (diam.) x 460 mm
Anchor Bolts

300 mm

480 mm

130 mm

610 mm

51 mm

230 mm

Drip Grooves

CB21x59
Steel Girder

#5 Bars

150 mm
R/C Deck Slab
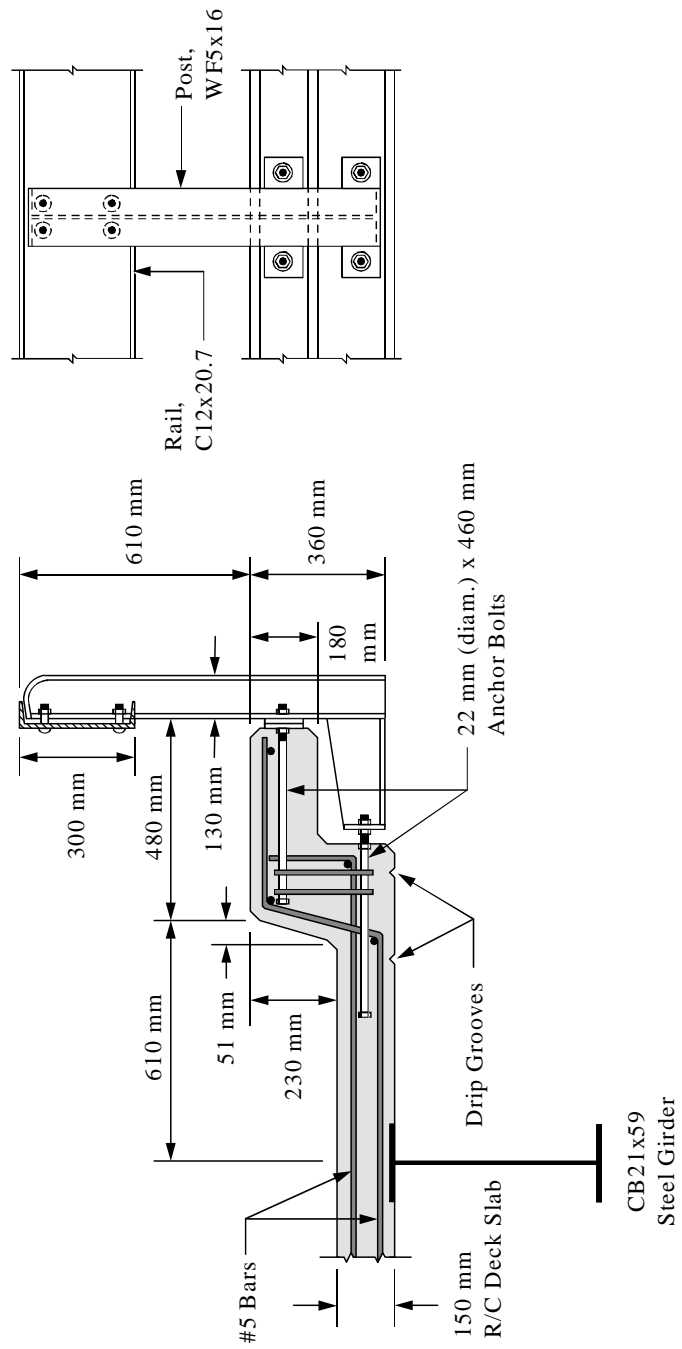
Figure 4.5 Curb and Railing Detail.

73
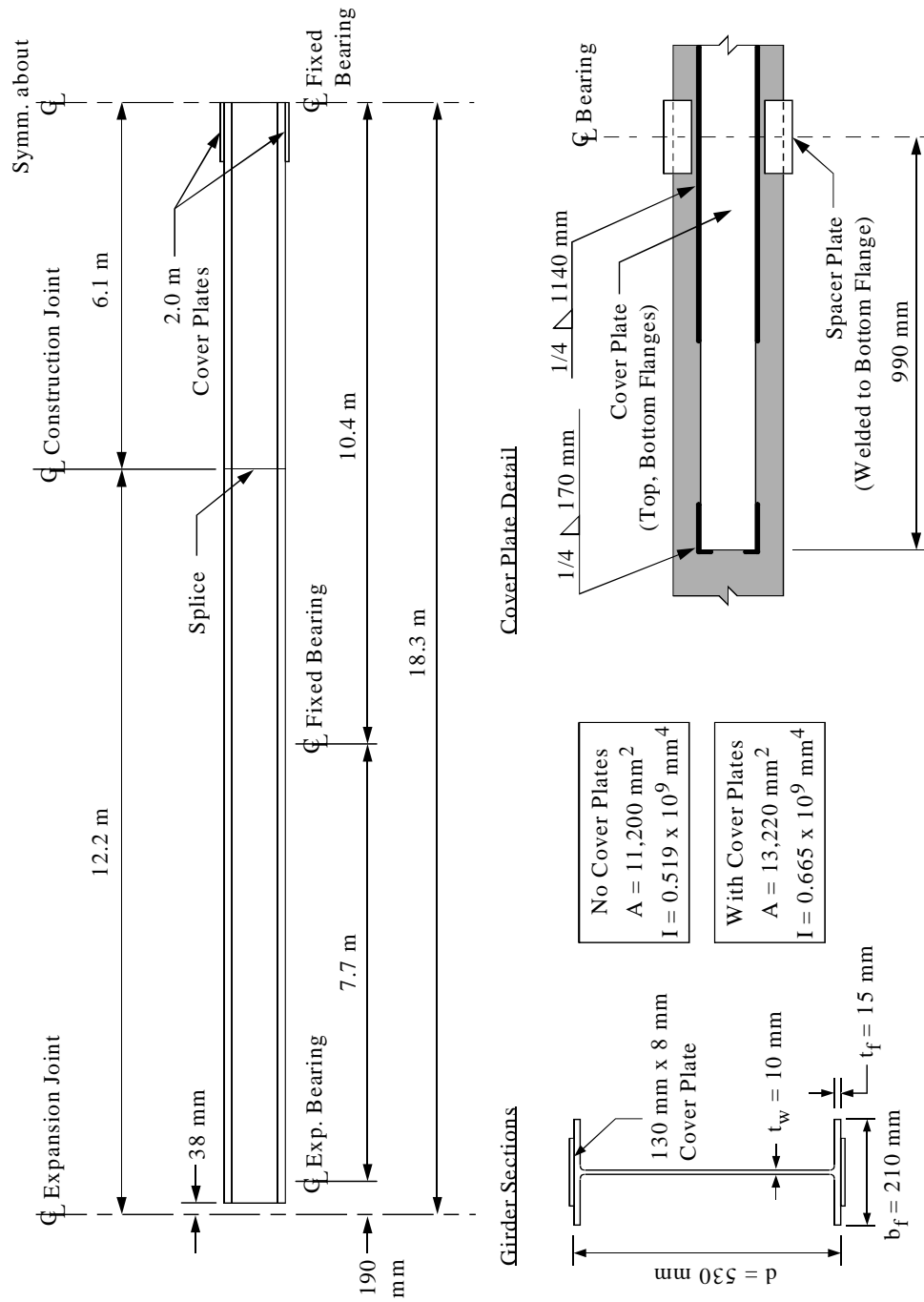
Figure 4.6 Half Elevation of Girder, Nominal Sections, and Cover Plate Detail.

74

The nominal properties and dimensions of the CB21x59 section given in Figure 4.6 were extracted from an AISC Catalog (1994) of rolled steel beams. To check these values, the bottom flange thickness, web thickness, and bottom flange width were field measured at three separate locations. Consequently, the cross-sectional area and moment of inertia were estimated assuming the top flange had the same measured dimensions as the bottom flange and using the nominal girder depth (Schonwetter, 1999). The comparison of the measured properties with the nominal values is given in Table 4.1. Since the difference was within 5% for the cross-sectional area and within 2% for the moment of inertia, the nominal values were considered to be representative of the girder properties.

Table 4.1 Measured Girder Dimensions and Properties.

| Section | Measured Dimensions | | | |
	t_w (mm)	t_{f1} (mm)	t_{f2} (mm)	b_f (mm)
1	8.94	14.4	15.2	211.0
2	9.47	15.0	15.2	213.5
3	9.04	14.9	14.8	210.7

| Section | Properties | | | |
	A (mm^2)	% Diff.	I ($10^9 mm^4$)	% Diff.
1	10,730	4.2	0.511	1.6
2	11,200	0.0	0.529	2.0
3	10,790	3.7	0.512	1.4
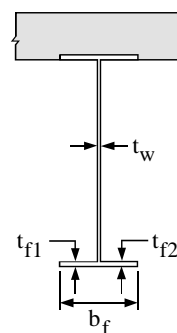
The girders bear on fixed shoes that restrict translation in the three orthogonal directions at the three interior supports. At the expansion joints, the girders rest on bearing shoes that permit translation in the longitudinal direction. Details of these two bearings are shown in Figures 4.7 and 4.8. Expansion joint details at the abutment and between adjacent spans are given in Figure 4.9.

75
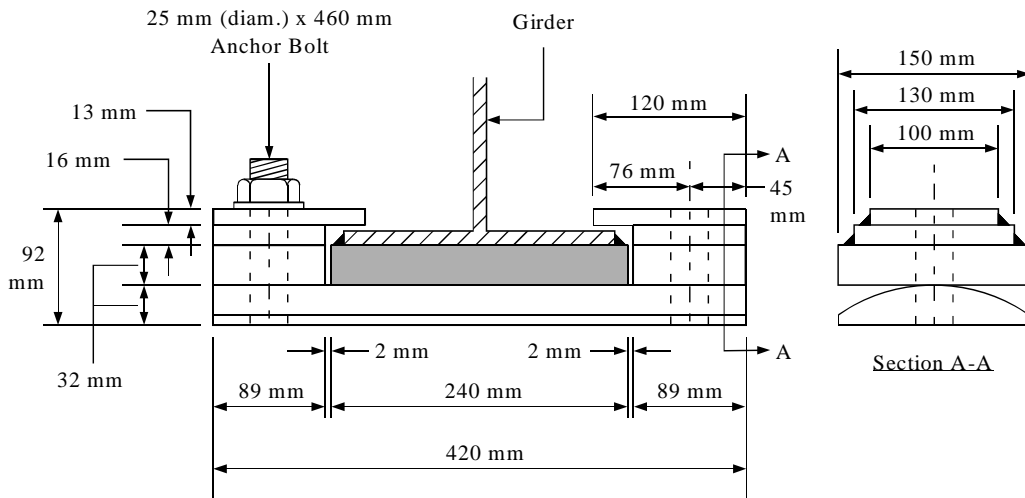
Figure 4.7 Expansion Bearing Detail.
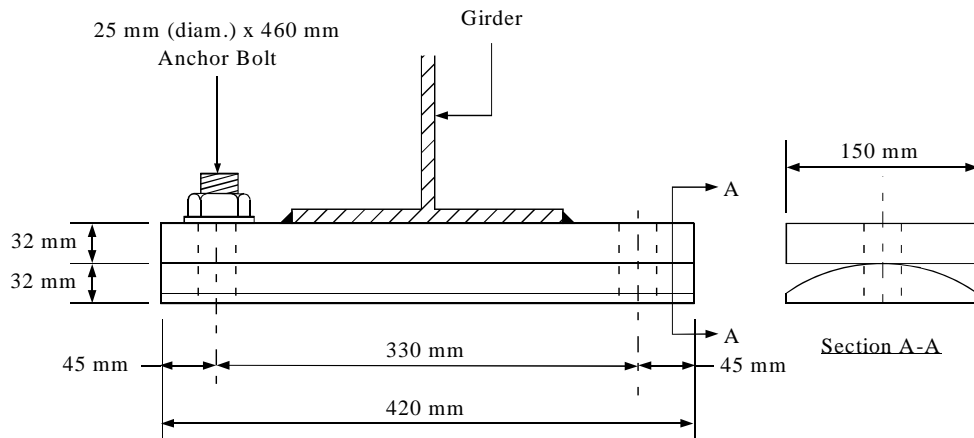
Figure 4.8 Fixed Bearing Detail.
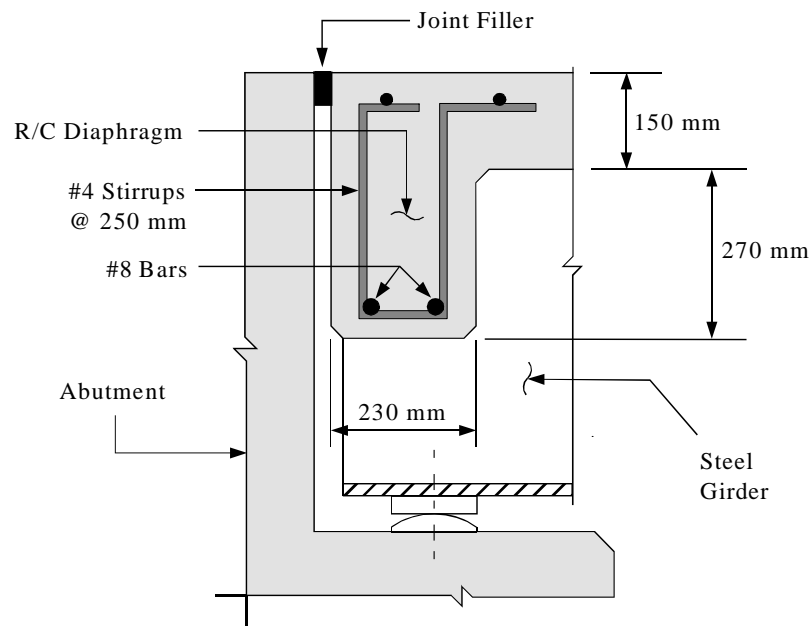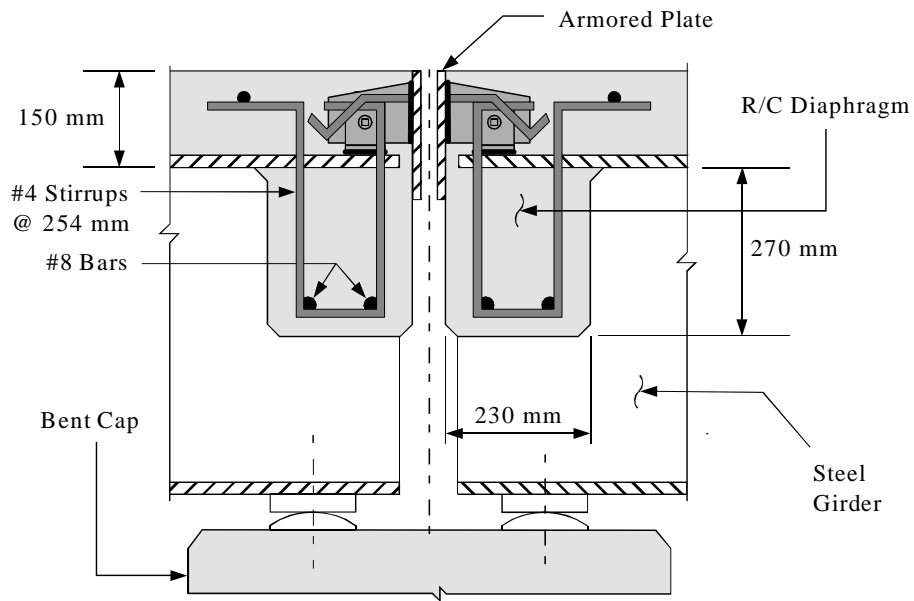
Figure 4.9 Expansion Joint Detail (a) At Abutment and (b) Between Units.

4.3   MATERIAL PROPERTIES

4.3.1   Structural Steel

There are two types of structural steel used in the Big Creek Relief Bridge. The cover and armored plates, bearing seats, and anchor bolts are specified as "new structural steel" in the design plans since the steel was manufactured at the time the bridge was built. For this structural steel, the A.A.S.H.O. Specifications (1953) specify a yield stress of 228 MPa (33 ksi). The same yield stress is also specified in the AISC Catalog (1954) for bridge steel dating after 1934.

The "old structural steel" corresponds to the steel of unknown age used to make the CB21x59 beams that were salvaged from the pre-existing bridge and re-used in the present Big Creek Relief Bridge. In the AISC Catalog (1954), the CB21x59 beam is listed as a standard shape once rolled by the Carnegie Brothers & Co. rolling mill. It is assumed that the CB21x59 section was discontinued in 1940, the last year in which the section was listed in a standard mill catalog (AISC, 1954). Under this assumption, the pre-existing structure could have been built as late as 1940, a few years after the yield stress for bridge steel changed to 228 MPa (33 ksi) from its previous value of 210 MPa (30 ksi) used prior to 1934 (AISC, 1954).

To determine the yield stress and approximate age of the "old structural steel", a tension coupon was torch cut from the bottom flange of an exterior CB21x59 girder on the north four-span unit. The coupon was removed from the end of the beam at its north end, milled to appropriate dimensions, and tested

according to ASTM Standard A370 (1995). The measured static yield stress was 210 MPa (30.5 ksi) which suggests that the CB21x59 beams were fabricated before 1934. Thus, the "old structural steel" was assumed to have a yield stress of 207 MPa (30 ksi) in future calculations.

4.3.2 Rail Steel, Reinforcing Steel and Concrete

The design plans for the Big Creek Relief Bridge specified the reinforcing steel as intermediate grade and the concrete as Class A. For intermediate grade reinforcing steel, the A.A.S.H.O. Specifications (1953) specify a yield stress of 276 MPa (40 ksi). The same specifications specify a yield capacity of 276 MPa (40 ksi) for the steel used to fabricate the traffic railings. Class A concrete is a TxDOT designation and thus is not included in the A.A.S.H.O Specifications (1953). The compressive strength for this type of concrete was found to be 21 MPa (3 ksi) in the TxDOT Standard Specifications (1951).

Compressive tests were conducted on six 100 mm (4 in) diameter cores removed from the bridge deck to obtain an experimental estimate of the concrete strength and for comparison with the values given in the specifications. A total of six concrete cores were removed; three from both the north and south four-span units. On each unit, the specimens were taken from three separate spots; one alongside the east curb, one alongside the west curb, and one towards the center of the roadway. Before each core, the general area of the deck to be drilled was scanned with a rebar locator to find the reinforcement. Because the scan needed to pass through the asphalt overlay, a clear image of the reinforcement pattern

could not be obtained which made it difficult to drill through the deck without hitting rebar. The close 180 mm (7 in) rebar spacing further complicated the removal of undisturbed samples. Figure 4.10 shows the coring rig and the 100 mm (4 in) drill bit used to remove the concrete samples.

Figure 4.10 Drilling of Concrete Core in Progress.

Physical examination of the cores showed an average concrete thickness of 150 mm (6 in), matching the design plans. The asphalt thickness, however, varied across the width of the roadway. Next to the curbs, the cores had an asphalt layer 64 mm (2.5 in) thick. The depth increased to 76 mm (3 in) on the cores taken from the middle region of the bridge deck. Two of the specimens had a rebar embedded near their bottom end. The cores were prepared for compressive testing according to ASTM Standards C42 (1994) and C617 (1994). First, the specimens were saw cut to remove the asphalt topping from the top end

and the harder, dried out concrete from the bottom end. The two cores with the embedded rebar were trimmed further on their bottom ends to eliminate the steel. After soaking 40 hours in lime-saturated water, the cores were capped with a sulfur mortar to obtain a level, smooth surface on both ends. The dimensions, length to diameter ratios, and cross-sectional areas of the capped concrete cores prior to testing are given in Table 4.2.

The cores were tested in moist conditions according to ASTM C39 (1994). Recorded data included the type of failure and the ultimate load. Four of the samples exhibited a cone type failure while two failed in a combination of cone and shear. In Table 4.2, the maximum load for the six samples is reported. The table also includes the strength correction factor, the maximum stress, and the compressive strength for each sample. Maximum stress values are simply the ultimate loads divided by the cross-section areas of the cores. To obtain the compressive strength, the maximum stress is multiplied by a strength correction factor and divided by a size factor. The factors account for size differences of the core with respect to the standard 150 mm x 300 mm (6 in x 12 in) concrete test cylinder. The strength reduction factor is applied to cores with length to diameter (L/D) ratios less than 1.94 to offset the gain in strength experienced by "stocky" samples (ASTM Standard C42, 1994). This factor varies from 0.87 to 0.98 for L/D ratios of 1.00 to 1.75, respectively (ASTM C42, 1994). The size factor (equal to 0.85) puts the results in terms of a standard 150 mm x 300 mm (6 in x 12 in) concrete cylinder.

Table 4.2 Core Properties and Compressive Strength.

(a) North Unit

Core	Height (mm)	Diameter (mm)	L / D Ratio	SCF*	Area (mm^2)	Max. Load (N)	Max. Stress (MPa)	Strength ** (MPa)
1	109.2	100.8	1.084	0.892	7,980	168,460	21.1	22.1
2	114.3	100.9	1.132	0.904	8,000	199,870	25.0	26.5
3	109.2	97.9	1.115	0.900	7,535	157,820	20.9	22.2
						Average		23.6
						Std. Deviation		2.55

(b) South Unit

Core	Height (mm)	Diameter (mm)	H / D Ratio	SCF*	Area (mm^2)	Max. Load (N)	Max. Stress (MPa)	Strength ** (MPa)
1	99.1	99.0	1.001	0.870	7,690	184,360	24.0	24.5
2	114.3	100.6	1.136	0.904	7,948	158,740	20.0	21.2
3	109.2	99.8	1.094	0.894	7,826	191,060	24.4	25.6
						Average		23.9
						Std. Deviation		2.28

* SCF: Strength Correction Factor
** Compressive Strength = SCF * Max. Stress / 0.85

   The measured strengths from the two sets of concrete cores were consistent, each averaging about 23.8 MPa (3450 psi) with a standard deviation of 2.41 MPa (350 psi). Hence, the standard deviation was about 10% of the average strength (i.e., coefficient of variation = 0.1). Given in terms of these experimental values, the concrete strength specified for design of 20.7 MPa (3000 psi) was approximately one standard deviation from the average measured strength. This good comparison indicated that the concrete had experienced only a slight increase in strength over the 40 years the bridge was in service. Nevertheless, the average measured strength from the concrete cores was considered to represent the compressive strength of the bridge deck concrete.

CHAPTER 5

TEST PROGRAM

As described in Chapter 4, the Big Creek Relief Bridge had one two-span continuous unit and four four-span continuous units. Two of the four-span units were tested in order to evaluate the repeatability in behavior between two similar units. Test objectives were to examine the interaction between the deck slab and the girders having no mechanical shear connection, to evaluate the participation of the curbs, and to investigate the effects of support restraint (i.e., bearing restraint and unintended continuity). Of particular importance was the influence of these inadvertent aspects of behavior on the load distribution pattern at different load levels.

Because of their close proximity to the abutments, the north four-span unit (hereafter referred to as Unit-N) and the south four-span unit (hereafter referred to as Unit-S) were selected for the load tests. The only apparent difference between the two units was that Unit-N was separated from the abutment by the 12.2 m (40 ft) approach span. Unit-N already had some instrumentation in place from service load tests conducted by Schonwetter (1999).

This chapter consists of three sections starting with a discussion of the preliminary actions taken to prepare the bridge units for testing. The second part describes the equipment used to apply incremental load to the test units and the vehicles used to simulate service loads. The third section describes the load tests performed on Unit-N and Unit-S. Included in this section is a description of the

instrumentation used to measure the response of the bridge units and the load testing procedures. A variety of instrumentation layouts and testing procedures were implemented for the two tests to determine the best strategy for evaluating the strength of non-composite steel girder bridges.

5.1   TEST PREPARATION

A bent cap separating an interior 10.4 m (34 ft) span and an exterior 7.9 m (26 ft) span was removed from each test unit in order to increase the span length and decrease the load required to yield the girders. The bent caps at bearing locations 4 and 18 (see Figures 4.1 and 4.2) were removed which increased the maximum span length from 10.4 m (34 ft) to 18.3 m (60 ft). Equipment used by the contractor for the removal consisted of an air-powered drilling hammer and a blowtorch.

The same procedure was followed in removing both bent caps. First, the 25.4 mm (1 in) diameter bolts attaching the fixed bearing plates to the top of the cap were torch cut at the five girder locations. By severing the bolts, the girders were no longer affixed to the bent cap. Next, the concrete at the top of the three 410 mm (16 in) square piles was chipped away below the base of the bent cap to expose the rebar as shown in Figure 5.1. The exposed reinforcement was then torch cut and the bent cap removed. At Unit-S, deflection measurements were made using a theodolite to determine the amount of girder deflection caused by the bent cap removal. At a distance of 9.1 m (30 ft) from the abutment (i.e., mid-span of the longest span), the girder displacement averaged 49.3 mm (1.94 in).

Figure 5.1 Removal of Bent Cap in Progress at Unit-N.

The relative slip between the top flanges of each of the girders and the deck slab was also measured at a distance of 610 mm (2 ft) from the abutment. Before the cap was taken out, a straight line was marked across the interface between the flanges and the deck slab. When the cap was removed, the line on the top flange was offset from the line on the deck. This offset (i.e., girder-slab slip) averaged 3.2 mm (1/8 in) for the five girders.

To estimate the level of interaction, a structural analysis was performed first assuming non-composite action and then full composite action between the girders and the slab. The dead load applied to the two models included the weight of the girders, the concrete slab, the asphalt overlay, and the steel railings. These analyses produced an average dead load deflection of 30.0 mm (1.18 in) for the composite case and 75.4 mm (2.97 in) for the non-composite case at the same

location where a deflection of 49.3 mm (1.94 in) was measured in the field. Averaging the two analytical deflections produced a value of 52.8 mm (2.08 in), about 7% higher than the measured deflection. This comparison indicates that the girders were acting neither fully composite nor totally independent of the deck in carrying the dead load. As a result, some level of unintended composite action was expected under live load.

Following removal of the bent caps, shoring was placed near the mid-span of the 18.3 m (60 ft) span as a safety precaution during testing and also for mounting instrumentation. Figure 5.2 shows the shoring in place under Unit-N. An 200 mm (8 in) clearance was left between the top of the I-beams and the bottom of the bridge girders.

Figure 5.2 Temporary Shoring in Place under Unit-N.

5.2   LOAD APPLICATION SYSTEMS

As an aid in developing the load application systems, the equipment and procedures employed in some other destructive bridge tests were reviewed. In an ultimate load test of a steel girder bridge performed by the Ontario Ministry of Transportation (Bakht and Jaeger, 1992), load was applied by placing concrete blocks directly on the deck with a crane situated off the bridge. With this system, a total load exceeding 1335 kN (300 kips) was applied by stacking the blocks in six vertical layers over a 4.9 m x 3.7 m (16 ft x 12 ft) area at midspan of the bridge. In a series of tests performed at the University of Tennessee (Burdette and Goodpasture, 1973), a hydraulic ram system was used to load four bridges to failure. The loading apparatus consisted of a series of 890 kN (100 ton) hydraulic rams reacting against high strength steel bars. The rams were situated at points on the bridge deck simulating the wheel loads of an HS-20 vehicle. The steel bars passed through cored holes in the deck and were anchored into concrete piles drilled in the terrain below the bridge. Loads exceeding 6672 kN (1500 kips) were applied with this system.

While the two loading systems discussed above both provided a relatively safe and controlled manner of applying a large amount of load to a bridge, neither system was considered appropriate for the testing to be performed in this project. The primary reason for rejecting these systems was that the concrete blocks or hydraulic ram hardware would block the roadway and thus not allow a service load vehicle to pass over the bridge between overload increments. The separate loading was essential in order to evaluate the service load behavior of the bridge

87

units after experiencing increasing levels of overloads. Therefore, a flatbed trailer, loaded with concrete traffic barriers and hauled with a tractor, was used to apply incremental loads. With the bent caps removed, this loading system provided the load necessary to yield the girders but just as important, could be moved on and off the deck, out of the way of the service vehicle. The portability of the tractor-trailer also served as a safety precaution since the load could be removed quickly from the bridge if signs of structural distress were observed. A description of the incremental loading system and the service load vehicles is provided in the following sections.

5.2.1   Incremental Loading System

The loading system used to apply incremental levels of load to the bridge consisted of a tractor-trailer, a loading crane, and a number of concrete barriers. The trailer was equipped with a 222 kN (50 kip) capacity tandem axle at its back end and was attached to the tractor at its front end. The flatbed of the trailer measured 12.2 m x 2.4 m (40 ft x 8 ft) and extended past the centerline of the back axle a distance of 910 mm (3 ft). A distance of 8.5 m (28 ft) separated the tandem axle of the tractor from the tandem axle of the trailer. The axle group spacing was 1.2 m (4 ft) and the wheel pairs were spaced at a transverse distance of 1.8 m (6 ft). A side view of the tractor-trailer and a schematic of the wheel and axle spacing are provided in Figure 5.3.
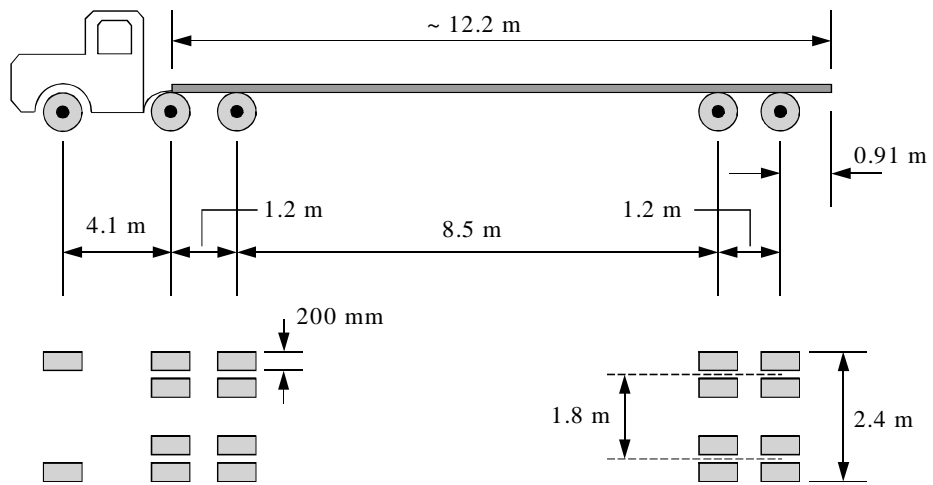
Figure 5.3 Tractor-Trailer provided by Contractor.

Three types of barriers were utilized for loading purposes; Jersey barriers, standard low-profile barriers, and tapered low-profile barriers. The 160 kN (18 ton) loading crane shown in Figure 5.4 was used to place the concrete barriers onto the flatbed of the trailer.

Figure 5.4 Loading Crane provided by Contractor.

The Jersey barriers were 9.1 m (30 ft) long and weighed about 70 kN (15.7 kips). These barriers required a special clamp to be lifted by the crane and were used only to test Unit-N. The Jersey barriers and the lifting clamp are shown in Figures 5.5 and 5.6, respectively. The standard and tapered low-profile barriers weighed 47 kN (10.5 kips) and 29 kN (6.5 kips), respectively, and both measured 6.1 m (20 ft) in length. Figure 5.7 shows the low-profile barriers with their measured dimensions. The center of gravity of the tapered barrier was computed to be about 4.0 m (13 ft) from its tapered end.

90

Figure 5.5 Jersey Barriers provided by Contractor.

Figure 5.6 Lifting Clamp for Jersey Barriers.
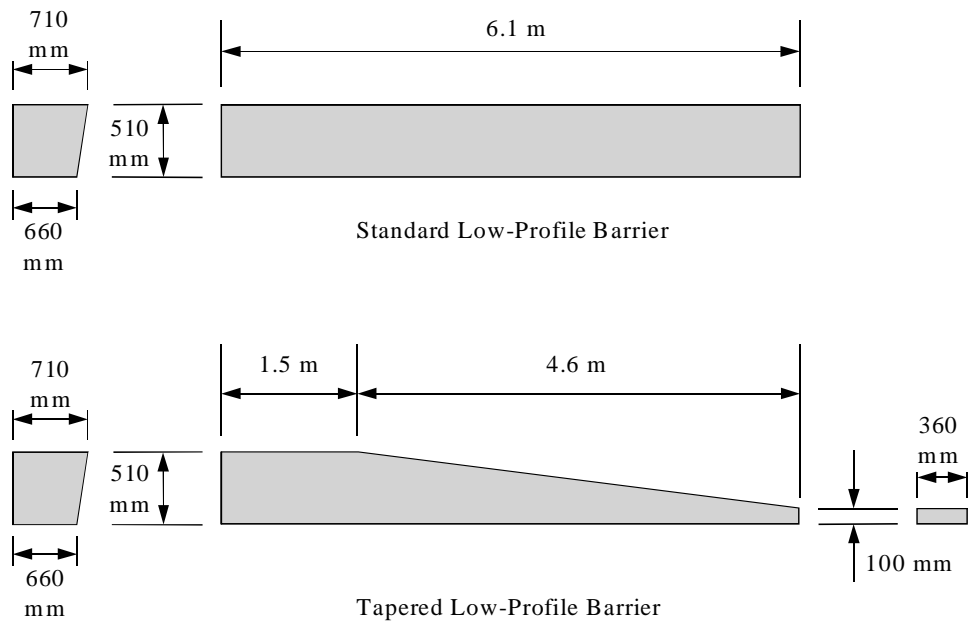
Figure 5.7 Low-Profile Barriers provided by TxDOT.

Compared with the Jersey-type barriers, the low-profile barriers were less difficult to handle with the crane because of their shorter lengths and lower weights. Figure 5.8 shows a standard low-profile barrier being placed onto the trailer bed.

Figure 5.8 Barrier Placement on Flatbed of Trailer.

In order to distribute their weight evenly to the 4 wheel pairs of the trailer, the barriers were placed longitudinally with their center of gravity in line with the centroid of the trailer's tandem axle. The barriers were also arranged symmetrically about the centerline of the trailer bed width in the transverse direction. Up to three barriers could be positioned side by side on the 2.4 m (8 ft) wide trailer bed. Vertically, the barriers were arranged in one or two layers, not to exceed six barriers at any one time. This limit was enforced in order to stay below the 222 kN (50 kip) capacity of the tandem axle and also to prevent the tires from bulging extensively and rubbing against each other.

Load was applied to the test units solely through the tandem axle of the trailer. The increment of axle loads was controlled by the arrangement of the concrete barriers on the flatbed of the trailer. At each stage of trailer loading, the 4 sets of wheel loads were measured simultaneously using portable weight scales. Each scale had a capacity of 89 kN (20 kips) and was accurate to within 445 N (100 lbs) based on laboratory calibration. When positioned on the scales, only one tire of each pair rested directly on the scale; the other tire remained suspended above the ground surface except at high load levels. When the tires on the scales started to bulge excessively, the other tires would remain in contact with the ground. For these cases, applied loads were approximated through superposition of the recorded weights from previous load levels.

Throughout the loading process, the axles of the tractor remained off the test units as the trailer was backed up to several positions along the 18.3 m (60 ft) span as shown in Figure 5.9. Transversely, the tandem axle of the trailer was positioned in the center of the loaded lane straddling the first interior girder. Load levels exceeding the capacity of the trailer axles were achieved by placing barriers directly on the deck. Timber platforms and elastomeric bearings were used to support these deck barriers at Unit-N and Unit-S, respectively. At both bridge units, the deck barriers were positioned with their centroids at midspan of the 18.3 m (60 ft) span and flush against the curb to allow the trailer load to remain centered in the loaded lane as shown in Figure 5.10.

Figure 5.9 Backing of Trailer into Position.

Figure 5.10 Trailer and Stationary Load.

95

The loading equipment was kept on the approach roadways on both sides of the bridge. These open areas provided a safe working zone with sufficient clearance for handling the concrete barriers with the crane. Furthermore, the tractor-trailer remained off the roadway as it was being prepared for the next load level, which allowed service load runs to be conducted without interruption.

5.2.2 Service Load Vehicles

Service loads were simulated with standard dump trucks having a ten-cubic yard capacity. The trucks were filled half full with asphalt to a total weight of about 160 kN (18 tons). To avoid the effects of impact, the dump trucks were driven over the test units along three transverse paths at a speed of approximately 2.2 meters per second (5 mph). On the first path, the outside wheel line of the tandem axle was 610 mm (2 ft) from the face of the curb as recommended by AASHTO specifications. The other two paths had the vehicle straddling the first interior girder and the middle girder. At load levels with barriers placed on the deck, the dump trucks traveled only in the latter two transverse positions.

The service load runs were made between overload stages as the trailer was being prepared for the next load level. These runs were not started until the load applied to the test units by the tandem axle of the trailer had exceeded the weight of the dump truck. The sequence of incremental loading and service runs during testing of Unit-N and Unit-S are discussed in detail in the next section. Figure 5.11 shows a typical service load run in progress and the measured configurations of the dump trucks used to test Unit-N and Unit-S.

Truck	Length (m)	
Dimension	Unit-N	Unit-S
A	3.8	3.9
B	1.4	1.4
C	2.0	2.0
D	1.9	1.8
Axle	Axle Weight (kN)	
Number	Unit-N	Unit-S
1	46	42
2	57	56
3	57	56
Total	160	153
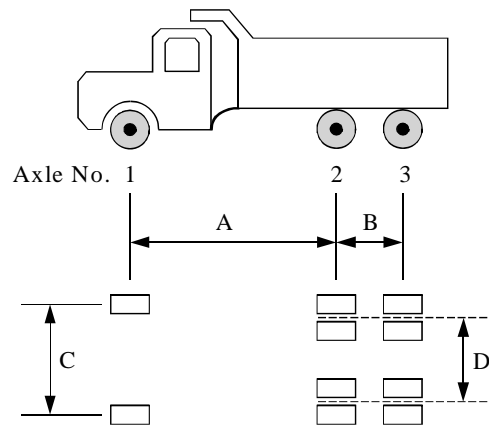
Figure 5.11 Service Load Run in Progress and Measured Vehicle Configurations.

5.3   LOAD TESTS

The test program started with the testing of Unit-N in November of 1997 and ended with the testing of Unit-S in April of 1998. In each test, a distinct instrumentation strategy and test procedure was implemented. Based on the

97

experience gained during the testing of Unit-N, adjustments were made to the test plan to improve the instrumentation and data quality in the load test of Unit-S.

The load tests were planned with the dual purpose of measuring the longitudinal and transverse distribution of load to the girders and the interaction between the girders and the deck slab. The two units were instrumented similarly to directly compare the test results. Unit-S, however, contained a more explicit arrangement of instruments to quantify the participation of the curbs, the relative slip between the girders and the slab, and the support restraint at the abutment.

The two types of instruments used to measure the behavior of the test units were uni-axial strain gages and linear potentiometers. Strain gages were installed according to the procedures outlined in Appendix B to measure the longitudinal strains in the girders and the curbs. Linear potentiometers were used to measure both the vertical deflections of the girders (hereafter referred to as deflection transducers) and the longitudinal slip between the girder top flanges and the bottom of the deck slab (hereafter referred to as slip transducers).

5.3.1   Test #1: Unit-N

5.3.1.1 Instrumentation Layout

As shown in Figure 5.12, Unit-N was instrumented at five cross-sections (designated as Sections a-a through e-e) along its length; three near the bearings and two towards the center of the 18.3 m (60 ft) span. Altogether, 44 strain gages, 5 slip transducers, and 5 deflection transducers were installed.

98
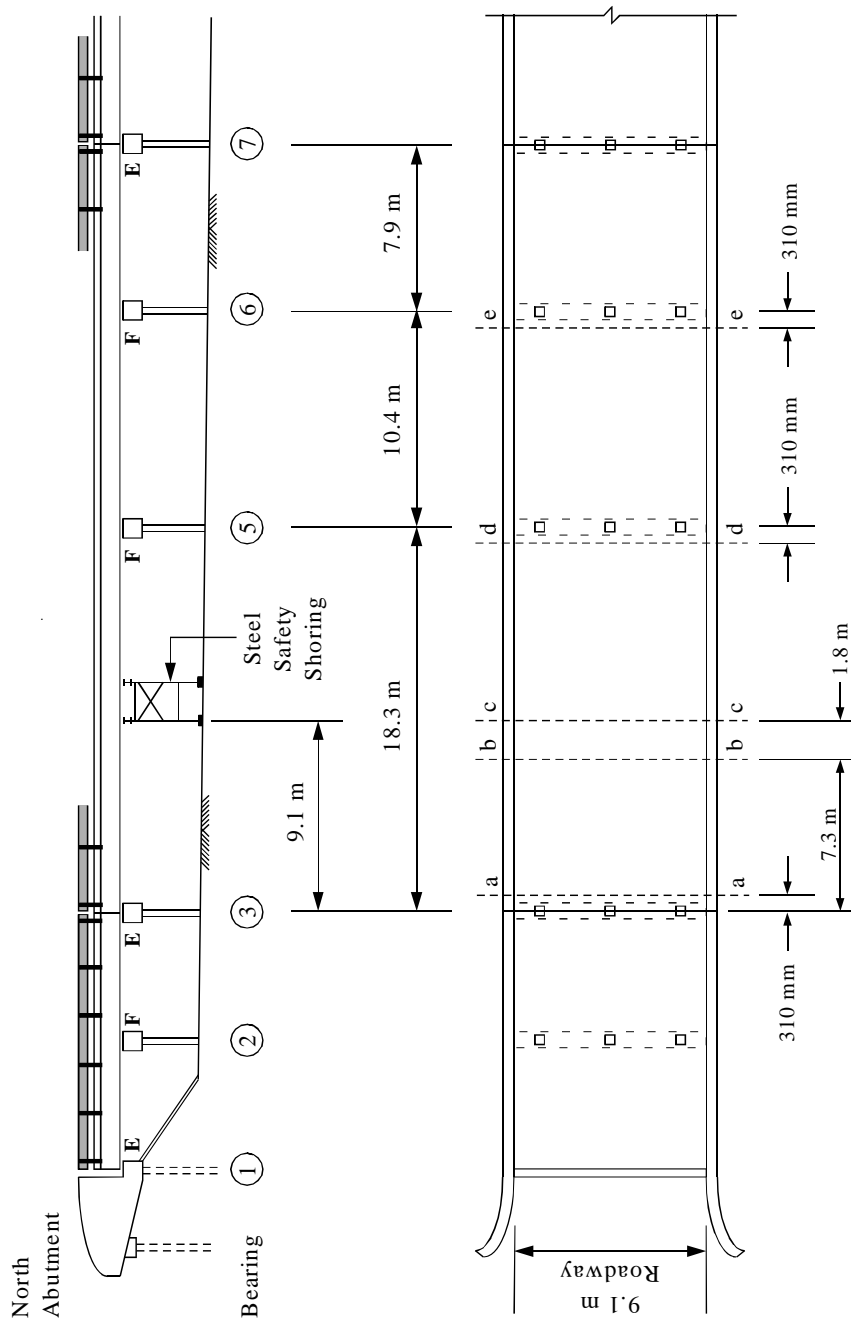
Figure 5.12 Instrumented Sections of Unit-N.

At Section a-a, slip transducers were installed on all five girders at the interface between the top flanges and the deck slab. Each slip transducer was mounted between a steel frame glued to the bottom of the slab and a piece of steel angle glued to the underside of the top flange as shown in Figure 5.13. The frame and angle were adhered in position using a two-part epoxy. Vertical deflections of all five girders were measured at Section c-c. Steel stands, attached to the steel shores with C-clamps, were used to mount the deflection transducers beneath the girders. The mounting assembly for a typical deflection transducer is shown in Figure 5.14. Positions and assigned labels of the slip and deflection transducers at Sections a-a and c-c are provided in Figure 5.15.

Longitudinal strains of the girders were measured at Sections b-b through e-e. No strain measurements were taken at Section a-a. At Section c-c, the most heavily instrumented section, strain gages were installed at three positions through the depth of each girder; one on the topside of the bottom flange, one on the web at mid-height of the girder, and one on the undersurface of the top flange. The second girder from the east side had strain gages installed on both sides of the web while the remaining girders were instrumented on only one side. At Sections d-d and e-e, all five girders were instrumented with strain gages on the interior face of their top and bottom flanges. Similar instrumentation was installed at Section b-b on three of the five girders; the middle girder and the two girders on the east side. Strain gage locations along with their assigned labels at Sections b-b through e-e are given in Figure 5.16.

Cross-Section

Linear Pot Stand

Elevation

Angle

50 mm

Linear
Pot
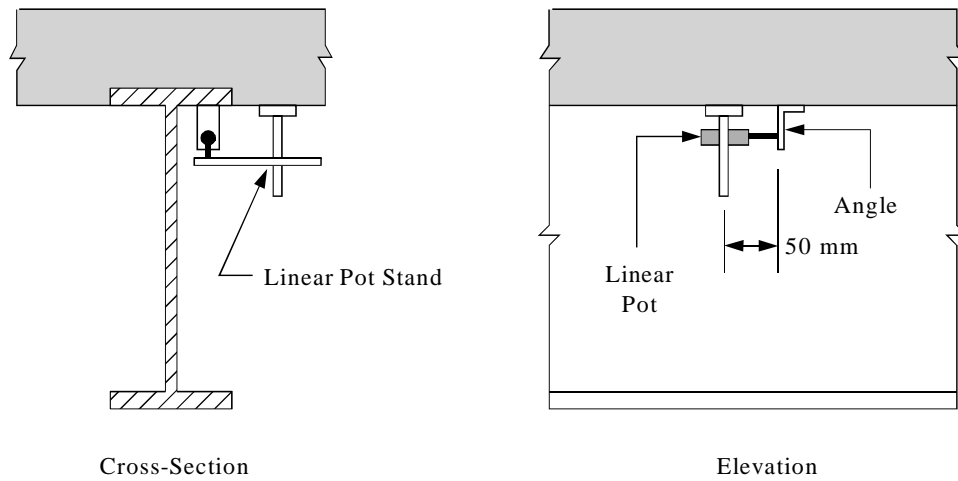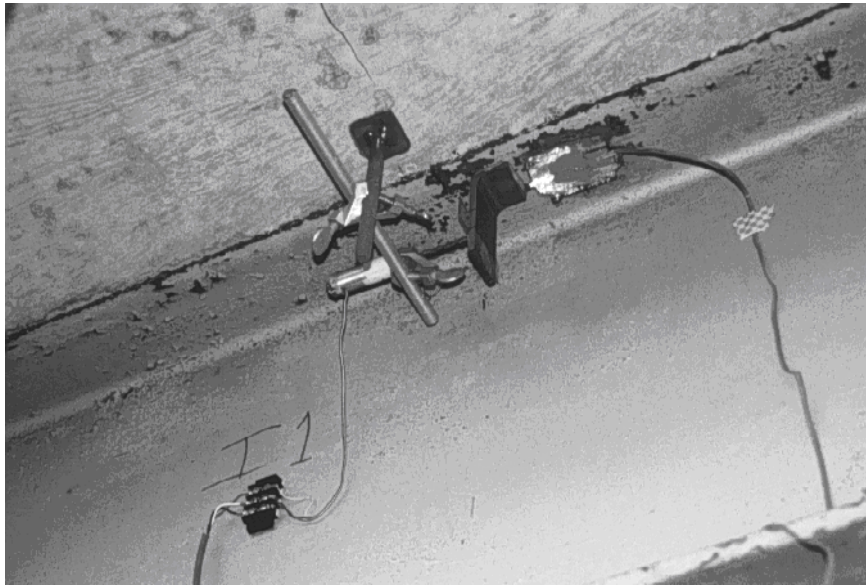
Figure 5.13 Mounting Assembly for Typical Slip Transducer.
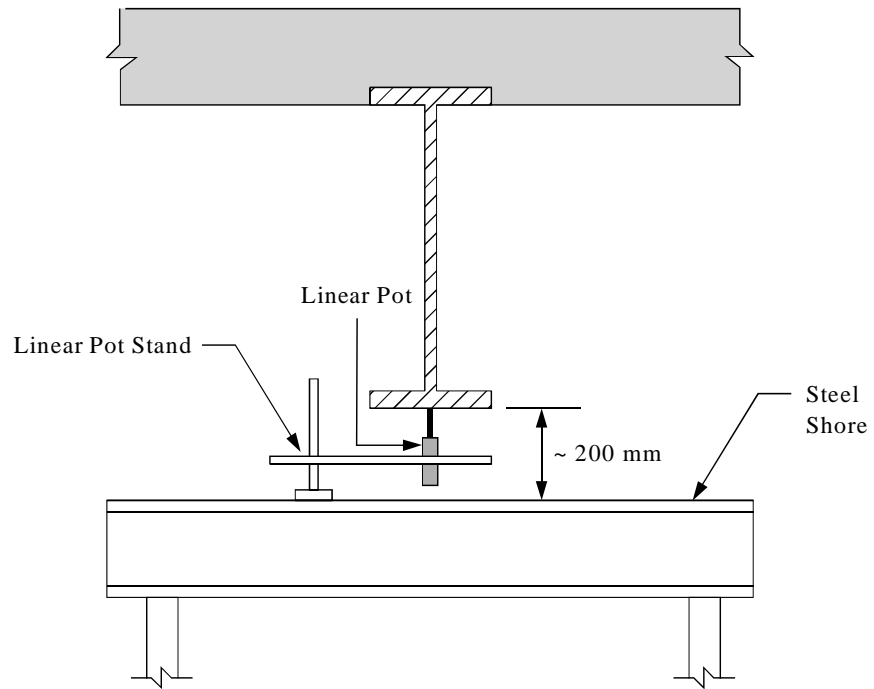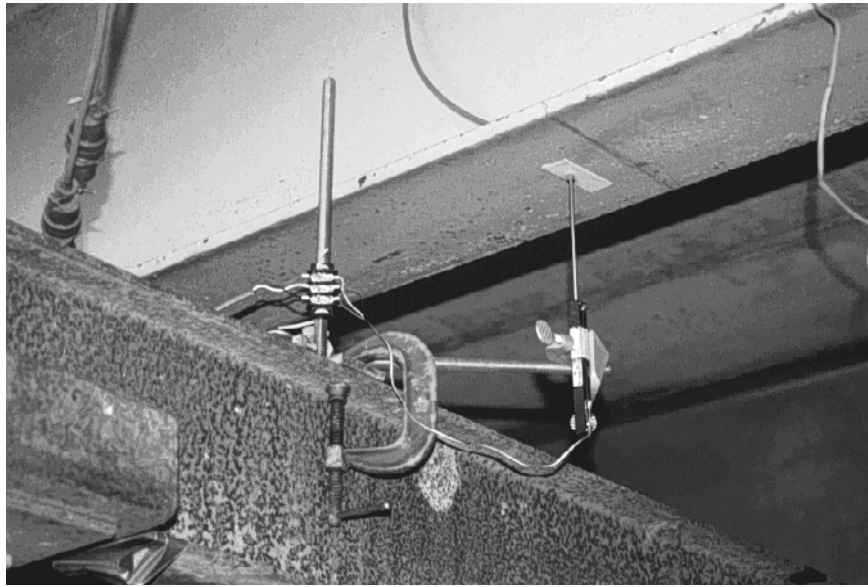
Figure 5.14 Mounting Assembly for Typical Deflection Transducer.
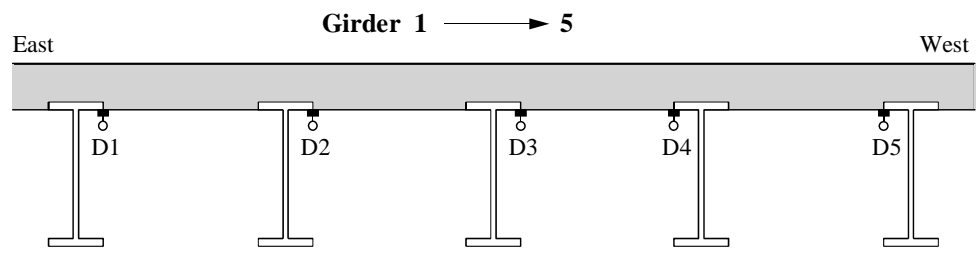
Section a-a: Slip Transducers Near Bearing 3
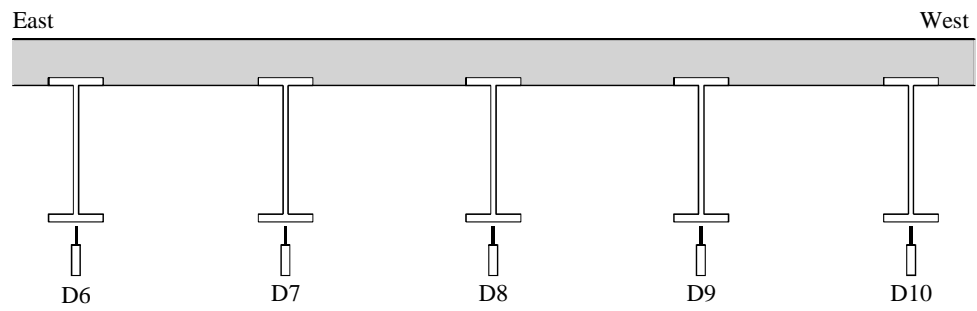
Section c-c: Deflection Transducers at Mid-Span of the 18.3 m Span

Figure 5.15 Layout of Slip and Deflection Transducers on Unit-N.

Girder 1 ⟶ 5

East   West

GT1   GT2 GT3   GT4   GT5   GT6
GM1   GM2 GM3   GM4   GM5   GB6
GB1   GB2 GB3   GB4   GB5   GB6

Section c-c: Strain Gages at Mid-span of the 18.3 m Span

East   West

GT7   GT8   GT9   GT10   GT11

GB7   GB8   GB9   GB10   GB11

Section d-d: Strain Gages Near Bearing 5

East   West

GT12   GT13   GT14   GT15   GT16

GB12   GB13   GB14   GB15   GB16

Section e-e: Strain Gages Near Bearing 6

East   West

GT17   GT18   GT19

GB17   GB18   GB19

Section b-b: Strain Gages at 1.8 m from Mid-span of the 18.3 m Span

Figure 5.16 Layout of Strain Gages on Unit-N.

5.3.1.2 Loading Procedure and Data Collection

The loading of Unit-N consisted of 20 load levels, which were completed in 3 phases. Service load runs were made in between load levels following the fifth level. An outline of the loading schedule for Unit-N is given in Table 5.1. At each load level, the total load applied consisted of two parts; a trailer load and a deck load. The trailer load represented the load applied by the tandem axle of the trailer with the barriers in place on the flatbed. The magnitude of the trailer load was taken as the sum of the measured weights of the four sets of tires. The deck load corresponded to the load applied by placing barriers directly on the deck. This load remained constant throughout each phase of loading. Table 5.1 lists the number of barriers on the trailer and on the deck for each load level.

In the first phase of loading, the first eleven load levels were applied entirely through the tandem axle of the trailer. There were no barriers on the deck (i.e., zero deck load) in this initial stage of loading. At the eleventh load level, the trailer load was measured to be 264 kN (59.3 kips) which included the self-weight of the trailer. The flatbed was loaded to its capacity of 3 tapered and 3 standard low-profile barriers. In the second phase of loading, a standard low-profile barrier was placed on the deck next to the east curb at midspan of the 18.3 m (60 ft) span. This barrier added a deck load of 47 kN (10.5 kips) to the load applied by the trailer. Load levels 12 and 13 were completed in this stage with trailer loads of 215 kN (48.3 kips) and 244 kN (54.8 kips), respectively. For these levels, the deck load represented about 20% of the total load.

Table 5.1 Loading Schedule for Unit-N.

Load Level	Number of Barriers on Flatbed			Trailer Load (kN)	Number of Barriers on Deck		Deck Load (kN)	Total Load (kN)
	Jersey	Tapered	Standard		Tapered	Standard		
1	0	1	0	66	0	0	0	66
2	0	2	0	95	0	0	0	95
3	0	3	0	124	0	0	0	124
4	0	2	1	142	0	0	0	142
5	0	1	2	159	0	0	0	159
Service Load Runs: Transverse Positions 1, 2, and 3								
6	0	0	3	177	0	0	0	177
Service Load Runs: Transverse Positions 1, 2, and 3								
7	0	2	2	188	0	0	0	188
Service Load Runs: Transverse Positions 1, 2, and 3								
8	0	1	3	206	0	0	0	206
Service Load Runs: Transverse Positions 1, 2, and 3								
9	0	3	2	217	0	0	0	217
Service Load Runs: Transverse Positions 1, 2, and 3								
10	0	2	3	235	0	0	0	235
Service Load Runs: Transverse Positions 1, 2, and 3								
11	0	3	3	264	0	0	0	264
Service Load Runs: Transverse Positions 1, 2, and 3								
12	1	1	2	215	0	1	47	262
13	1	2	2	244	0	1	47	291
Service Load Runs: Transverse Positions 2 and 3								
14	0	0	0	37	1	2	122	158
15	0	1	0	66	1	2	122	188
Service Load Runs: Transverse Positions 2 and 3								
16	1	0	0	93	1	2	122	215
Service Load Runs: Transverse Positions 2 and 3								
17	2	0	0	148	1	2	122	271
Service Load Runs: Transverse Positions 2 and 3								
18A	2	1	0	177	1	2	122	299
18B	2	1	0	177	1	2	122	299
18C	2	1	0	177	1	2	122	299
Service Load Runs: Transverse Positions 2 and 3								
19A	2	0	1	195	1	2	122	317
19B	2	0	1	195	1	2	122	317
Service Load Runs: Transverse Positions 2 and 3								
20A	3	0	0	204	1	2	122	326
20B	3	0	0	204	1	2	122	326
Service Load Runs: Transverse Positions 2 and 3								

In the third phase of loading, another standard and a tapered low-profile barrier were added to the deck, increasing the deck load to 122 kN (27.5 kips). These barriers were stacked on top of the standard barrier already in position on the deck. Load levels 14 through 20 were completed in this stage. Towards the end of the phase 3, the final three load levels were repeated to observe if there were significant increases in deformation under sustained loading. The final level of load placed on Unit-N was 326 kN (73.3 kips) with the trailer loaded with 3 Jersey barriers. At this level, the deck load was about 35% of the total load.

At the start of each load level, the four sets of tires of the trailer were placed on the portable scales and weighed. After an initial scan of all the gages, the trailer was backed up slowly along the centerline of the east lane (i.e., transverse position 2) onto the 18.3 m (60 ft) span until the tandem axle reached midspan. The axles of the tractor remained on the neighboring two-span unit. Before reaching midspan, the trailer was stopped at three intermediate positions when the tandem axle was 3.1 m (10 ft), 6.1 m (20 ft), and 7.6 m (25 ft) from bearing 3. The trailer was stopped at the same three positions as it was pulled off the span. Figure 5.17 shows the seven longitudinal positions of the trailer axles on the 18.3 m (60 ft) span. Trailer positions 1 through 4 represent the trailer backing up onto the span while trailer positions 5 through 7 represent the trailer moving off the span. The distance "x" was measured from the centerline of bearing 3 to the front axle of the trailer. At each longitudinal position, the trailer was held in place approximately 10 seconds to allow a representative sample of

107

data to be collected. Readings were taken at a rate of 10 Hz continuously as the trailer was moved into position on and off the span.

Since the trailer load straddled girder #2 and the deck load was placed directly over girder #1, there was an irregular pattern of load between the three phases of loading. In terms of the total load, the deck load comprised 0 percent in phase 1, 20% in phase 2, and 35% at the end of phase 3. These percentages show a shift in the applied load such that girders #1 and #2 were more uniformly loaded at later stages of loading. In spite of these irregularities in the loading pattern, the total applied load was assumed to be the sum of the deck load and the trailer load.

Following load level 5, service load runs were made between each load level with the dump truck traveling in the north direction. Throughout the first phase of loading, the truck passed in the three transverse positions shown in Figure 5.17. In the second and third phases of loading, transverse position 1 was omitted from the service load runs due to the deck load. At each transverse position, the dump truck was driven over the entire length of Unit-N starting at bearing 7. The test was ended when the back axle crossed over bearing 3. Longitudinal lines were drawn on the deck, with reference to the front left tire of the dump truck, as a guide to the truck driver. The location of the dump truck was monitored with the clicker switch described in Chapter 3. During these runs, readings were taken at a rate of 100 Hz after an initial scan had been made of all the gages.
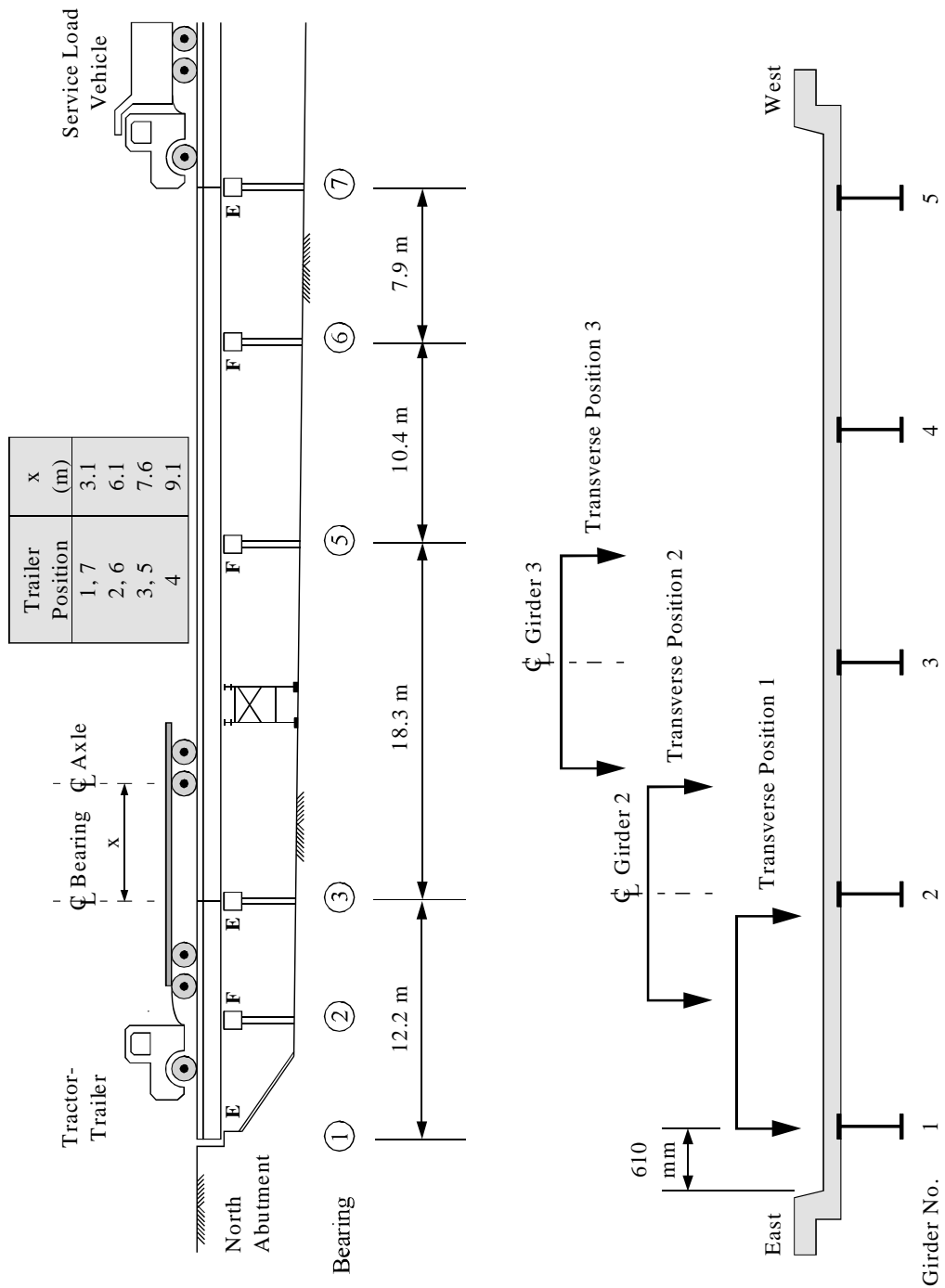
Figure 5.17 Longitudinal and Transverse Load Positions on Unit-N.

109

5.3.2   Test #2: Unit-S

5.3.2.1 Instrumentation Layout

Instrumentation was installed on Unit-S at four sections (designated as Sections a-a through d-d) along the length of its 18.3 m (60 ft) span. The region at bearing 16 was not instrumented to make room for extra slip measurements and strain gages for the integral curb. A plan and elevation view of Unit-S showing the instrumented sections and the steel shoring is given in Figure 5.18. In total, the instrumentation consisted of 40 strain gages, 9 slip transducers, and 5 deflection transducers.

At Section a-a, slip transducers were installed as described earlier on the middle girder and the two west girders (i.e., girders 1 through 3). On all five girders, strain gages were added to the inside face of the top and bottom flanges. At a distance of 4.6 m (15 ft) from bearing 19, Section b-b was instrumented with slip transducers on girders 1 through 3. No strain measurements were made at this section. At Section c-c, the strain gage layout on the girders remained the same as Unit-N with one exception; the mid-web gages were eliminated from girder 2. Vertical deflections of all five girders were measured with deflection transducers (see Figure 5.14). Strain gages were installed on the west curb at four locations and slip transducers installed at the girder-slab interface of girders 1 through 3. No changes were made to the instrumentation layout at Section d-d compared to Unit-N. Figures 5.19 and 5.20 show the layout and labels for the instrumentation of Unit-S.

110
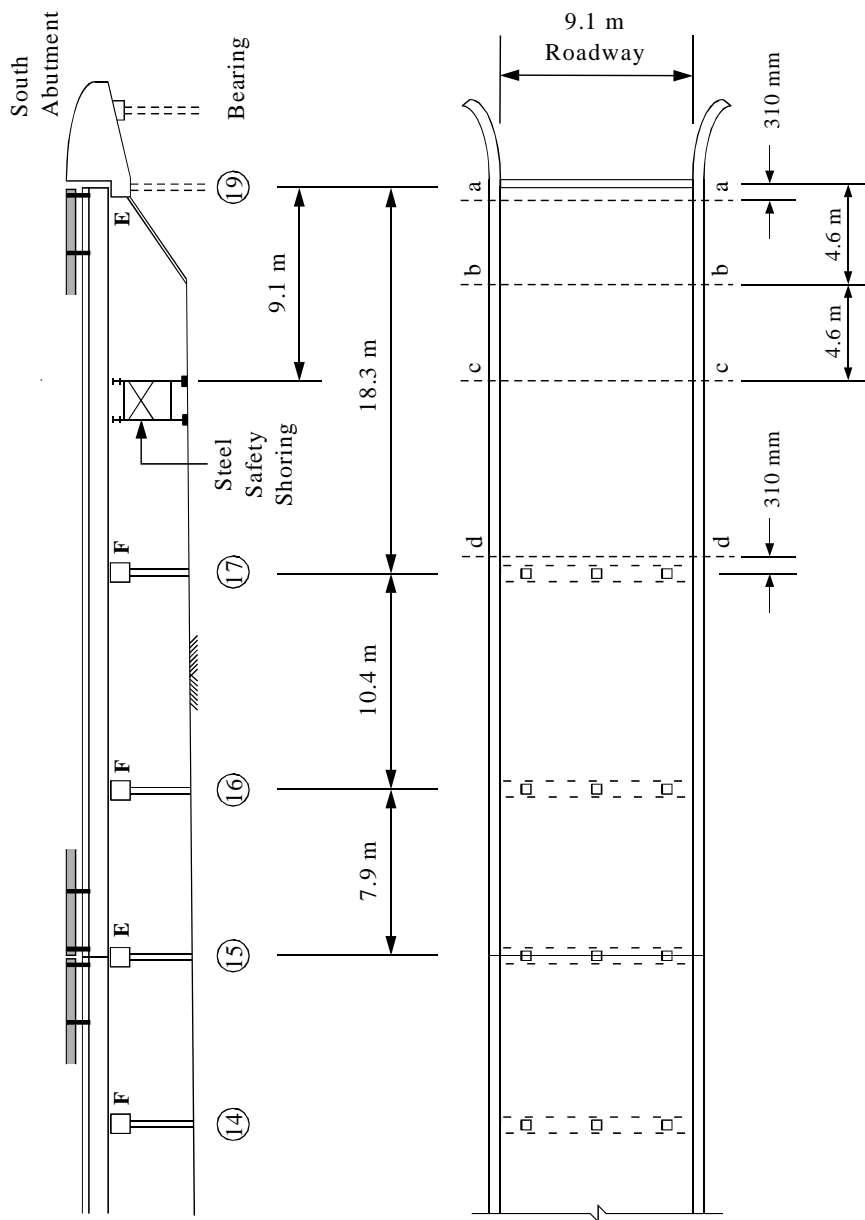
Figure 5.18 Instrumented Sections of Unit-S.

111
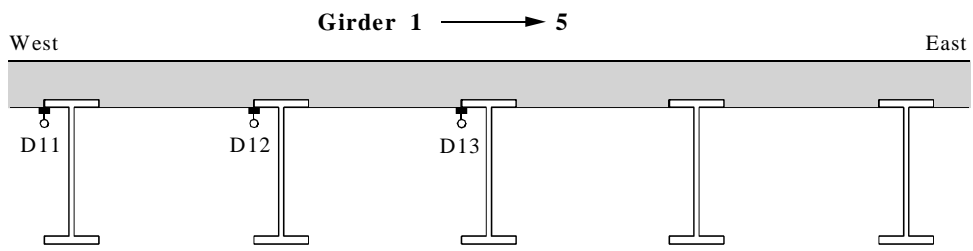
Section a-a: Slip Transducers Near Bearing 19
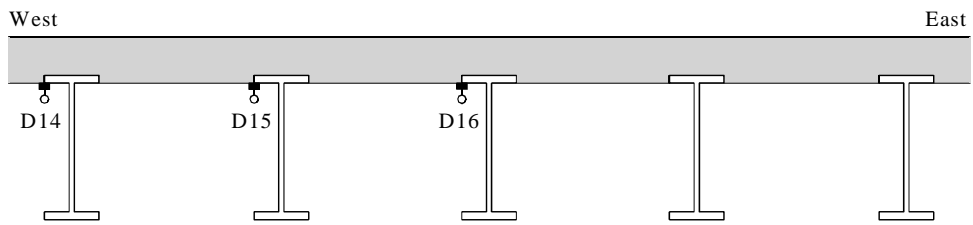
Section b-b: Slip Transducers at 4.6 m from Bearing 19
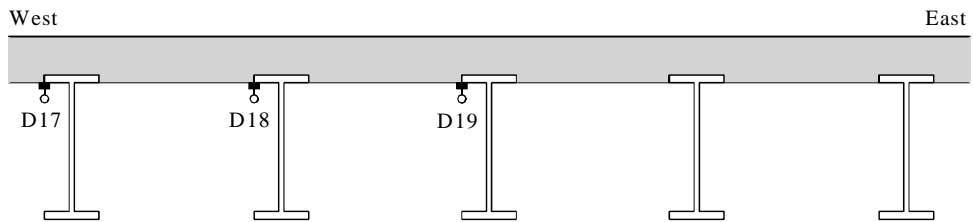
Section c-c: Slip Transducers at Mid-span of the 18.3 m Span
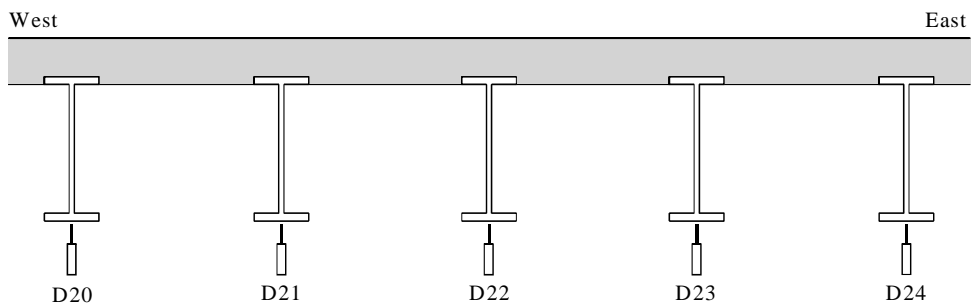
Section c-c: Deflection Transducers at Mid-span of the 18.3 m Span

Figure 5.19 Layout of Slip and Deflection Transducers on Unit-S.

Girder 1 ⟶ 5

West   East

GT20   GT21 GT22   GT23   GT24   GT25

GM20   • GM23   GM24   GB25

GB20   GB21 GB22   GB23   GB24   GB25

Section c-c: Strain Gages at Mid-span of the 18.3 m Span

West   East

GT26   GT27   GT28   GT29   GT30

GB26   GB27   GB28   GB29   GB30

Section a-a: Strain Gages Near Bearing 19

West   East

GT31   GT32   GT33   GT34   GT35

GB31   GB32   GB33   GB34   GB35

Section d-d: Strain Gages Near Bearing 17

254 mm   76 mm

West

C1

178 mm   C3   191 mm

                                                        152 mm

203 mm   C2

102 mm   C4

Section c-c: Strain Gages (on Western Curb) at Mid-Span of the 18.3 m Span

Figure 5.20 Layout of Strain Gages on Unit-S.

113

5.3.2.2 Loading Procedure and Data Collection

Having tested Unit-N, the load test of Unit-S was completed in less time with a significant improvement in the quality of data collected. The reduction in test time was due primarily to changes made in the loading schedule. As shown in Table 5.2, the loading of Unit-S consisted of 15 load levels, applied in two stages; 5 fewer load levels and one less loading stage compared to Unit-N. Jersey–type barriers were not used because of the difficulty in handling them.

Table 5.2 Loading Schedule for Unit-S.

Load Level	Number of Barriers on Trailer		Trailer Load (kN)	Number of Barriers on Deck		Deck Load (kN)	Total Load (kips)
	Tapered	Standard		Tapered	Standard		
1	0	0	37	0	0	0	37
2	1	0	66	0	0	0	66
3	3	0	124	0	0	0	124
4	1	2	159	0	0	0	159
Service Load Runs: Transverse Positions 1, 2, and 3							
5	2	2	188	0	0	0	188
Service Load Runs: Transverse Positions 1, 2, and 3							
6	3	2	217	0	0	0	217
Service Load Runs: Transverse Positions 1, 2, and 3							
7	2	3	235	0	0	0	235
Service Load Runs: Transverse Positions 1, 2, and 3							
8	1	1	113	1	2	122	235
Service Load Runs: Transverse Positions 2 and 3							
9	0	2	130	1	2	122	253
Service Load Runs: Transverse Positions 2 and 3							
10	1	2	159	1	2	122	282
Service Load Runs: Transverse Positions 2 and 3							
11	2	2	188	1	2	122	311
Service Load Runs: Transverse Positions 2 and 3							
12	1	3	206	1	2	122	328
Service Load Runs: Transverse Positions 2 and 3							
13	3	2	217	1	2	122	339
Service Load Runs: Transverse Positions 2 and 3							
14	2	3	235	1	2	122	357
Service Load Runs: Transverse Positions 2 and 3							
15	3	3	264	1	2	122	386
Service Load Runs: Transverse Positions 2 and 3							

Levels 1 through 7 were completed in the first stage of loading with no deck load. At the seventh load level, the applied load was measured to be 235 kN (52.8 kips), all of which consisted of trailer load. The second stage of loading included a deck load of one tapered and two standard low-profile barriers for a total weight of 122 kN (27.5 kips). In the eighth level of load, the total applied load matched the seventh load level, however, 50% consisted of deck load. The seventh and eighth load levels were arranged to have the same amount of load in order to evaluate the effects of the change in loading pattern. At the end of the second loading phase, the final level consisted of a trailer load of 264 kN (59.3 kips) and a deck load of 122 kN (27.5 kips), 32% of the total load. As with Unit-N, there was a gradual shift in the pattern of loading towards girder #1.

The loading arrangement of Unit-S was the mirror image of the test setup for Unit-N. The trailer was backed up along the center of the west lane (i.e., transverse position 2) while keeping the tractor axles on the south abutment. With respect to bearing 19, the trailer was stopped at the same longitudinal positions on the 18.3 m (60 ft) span. Starting after load level 4, service load runs were made with the dump truck traveling in the south direction along the three transverse positions shown in Figure 5.21. The runs started when the front axle crossed bearing 15 and ended when the back axle crossed bearing 19. As in the load testing of Unit-N, no runs were made along transverse position 1 once barriers were placed on the deck.

In the test of Unit-N, two separate data collection programs were used to take readings during the tractor-trailer loading and the service load runs. For the

test of Unit-S, the service load program was rewritten with a new data integration procedure, to reduce background noise observed in the data collected in the test of Unit-N. The modifications required the sampling rate to be reduced from 100 Hz to 10 Hz. The refined program is listed in Appendix C. This program was used to collect readings during both tractor-trailer loading and the service load runs. The gages were not zeroed before each individual test sequence as was done in the test of Unit-N. Re-zeroing required tedious data processing to determine the permanent deformations experienced by the bridge members in the test of Unit-N. Instead, a zero reading was taken only before load level 1 during the test of Unit-S. This approach also allowed a better examination of the deformation and stress recovery after each test sequence.

5.4   SUMMARY

A description of the load tests conducted on the Big Creek Relief Bridge has been provided. The tests were conducted on the north and south four-span units because of their favorable testing conditions compared to the middle two units. The dual tests allowed improvements to be made in the instrumentation, loading procedure, and the quality of collected data. The test procedure simulated a mix between a proof and diagnostic test. Proof loading was simulated using a tractor-trailer loaded with increasing levels of concrete barriers. The diagnostic aspect of the tests was done using a standard dump truck loaded with asphalt. The results of these two tests are presented in Chapter 6.
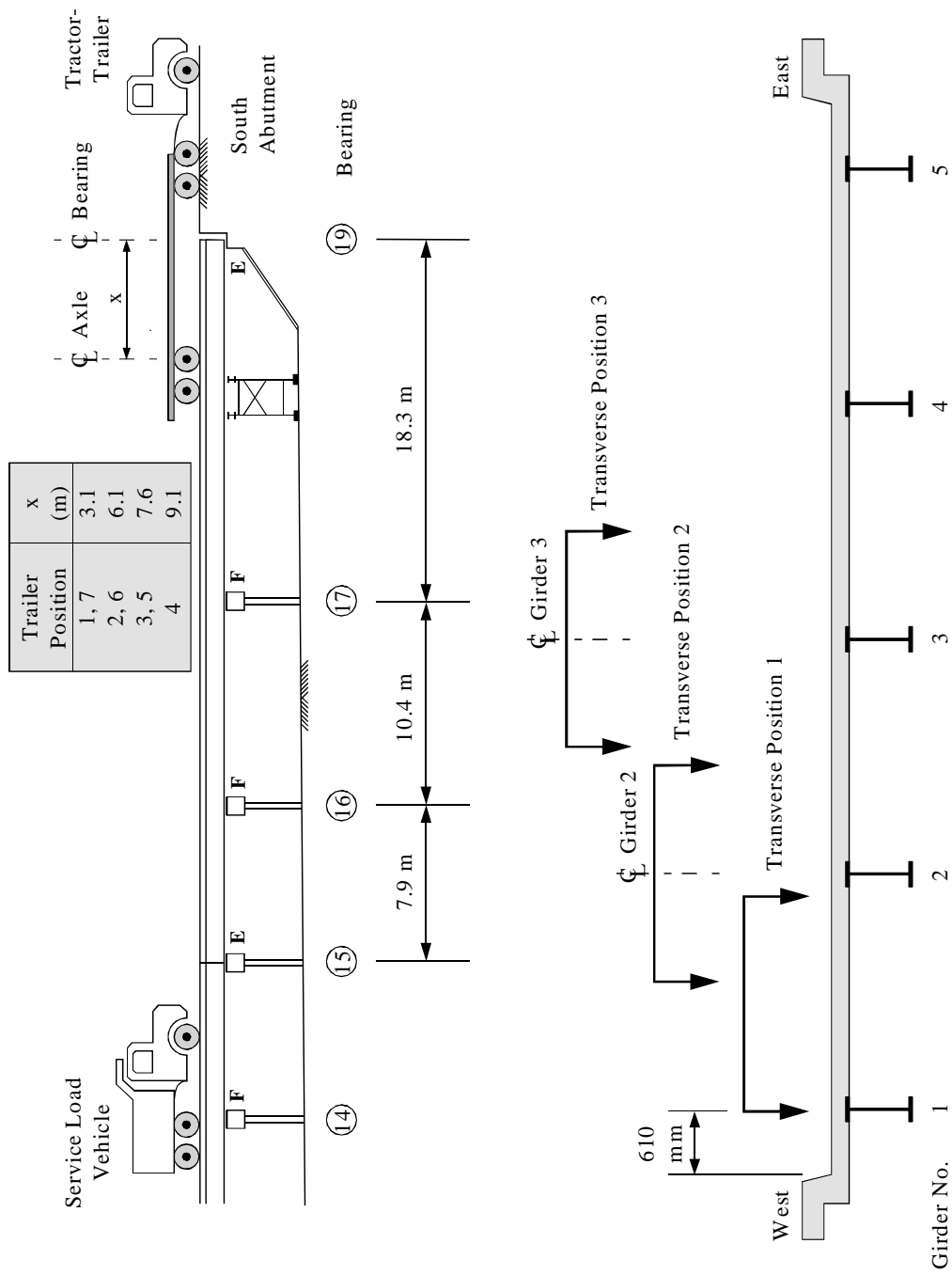
Figure 5.21 Loading Positions on Unit-S.

117

CHAPTER 6

LOAD-DEFORMATION RESPONSE OF BRIDGE UNITS

In this chapter, the load-deformation response of the bridge units under the increasing loads applied by the flatbed trailer-concrete barrier loading system is presented. The measured response is described at the sections instrumented in the loaded 18.3 m (60 ft) span with emphasis on the positive moment region (i.e., Section c-c) and negative moment region (i.e., Section d-d) of Unit-N and Unit-S as given in Figures 5.12 and 5.18, respectively. Whenever possible, an effort was made to compare the response of the two units.

There are three major sections in this chapter. The first section describes the steps taken to reduce the collected data to a form appropriate for interpreting the response of the bridge units. Because the two units were tested using different data logger programs and collection procedures, each one required its own set of data reduction routines. A few of the processing routines included: converting the raw voltage readings to units of strain and deflection; evaluating the reliability of the data through statistical analysis; reducing the trailer load data based on load position; and filtering the background noise from the service load data. Because of the rather complicated loading process, a description of the general load-deformation behavior of the girders is provided in the second section. The section also discusses the methodology for distinguishing between yielding and loss of partial composite action in the girders. In the third section, the measurements collected for Unit-N and Unit-S are presented in three parts according to the type

of measurement. The first and second parts cover the measured girder strains and deflections. Relative slip measured at the girder-slab interface is discussed in the third part. A summary of the response of both units concludes the chapter.

6.1   DATA REDUCTION

6.1.1   Data File Description and Unit Conversion

Table 6.1 shows a typical record of raw voltage readings (in its original format) after downloading from the data logger to the laptop computer.

Table 6.1 Typical Record of Measured Voltage Data.

TIMESTAMP (min:sec)	RECORD NUMBER	Gage A1 (mVolts)	Gage A2 (mVolts)	•	Gage K4 (mVolts)	Gage K5 (mVolts)	Excitation (mVolts)
18:03.6	0	-0.002	-0.001		0.055	-0.108	4996.1
18:03.7	1	0.002	-0.001	•	0.069	0.080	4996.1
18:03.8	2	-0.001	-0.002		-0.060	-0.059	4996.5
18:03.9	3	-0.002	-0.001	•	0.051	-0.093	4996.1
18:04.0	4	0.003	0.001		0.019	0.076	4996.2
18:04.1	5	-0.001	-0.001	•	-0.048	-0.053	4996.5
18:04.2	6	-0.002	-0.001		0.047	-0.063	4996.0
18:04.3	7	0.003	-0.001	•	0.001	0.064	4996.3
18:04.4	8	-0.002	-0.002		-0.056	-0.025	4996.5
18:04.5	9	-0.001	-0.002	•	0.035	-0.059	4996.0
18:04.6	10	0.003	-0.002		0.011	0.064	4996.3
•	•	•	•	•	•	•	•
•	•	•	•	•	•	•	•
20:30.4	1468	0.014	0.000		1.596	7.362	4996.1
20:30.5	1469	0.014	0.000	•	1.697	7.406	4996.1
20:30.6	1470	0.012	0.000		1.600	7.338	4996.2
20:30.7	1471	0.013	0.000	•	1.632	7.441	4996.0
20:30.8	1472	0.012	0.000		1.654	7.316	4996.2
20:30.9	1473	0.013	0.000	•	1.640	7.449	4996.1
20:31.0	1474	0.013	0.000		1.648	7.346	4996.2
20:31.1	1475	0.012	0.001	•	1.589	7.374	4996.1
20:31.2	1476	0.013	0.000		1.703	7.394	4996.1
20:31.3	1477	0.012	0.000	•	1.622	7.33 4	4996.2
20:31.4	1478	0.014	0.000		1.680	7.449	4996.1

The first column lists the times at which the readings were written to the table. In this case, the data was written at a resolution of 0.1 seconds (i.e., sampling frequency = 10 Hz) between 18 minutes 3.6 seconds and 20 minutes 31.4 seconds of the hour. Hence, the length of the data record was 2 minutes 27.8 seconds. The second column lists the record number for each reading in the data sample. In the example data sample given in Table 6.1, there were 1478 total records (not including the initial record). The next 55 columns of the table contain the output voltage signals (in millivolts) from the strain gages and deflection transducers that were connected to the 55 channels of the data acquisition system. As discussed in Chapter 3, the data channels were labeled with a letter-number combination as A1 through A5, B1 through B5, etc. up to K1 through K5. The last column contains the measured input (excitation) voltage from the power supply, which typically ranged between 4.49 and 5 volts.

Before the data could be used for evaluation, the raw voltage readings first needed to be converted to their appropriate units of strain and deflection. Both these conversions are functions of the ratio between the output and input voltages. Strains were computed using the equation for a quarter-bridge (Wheatstone bridge with one active arm) configuration given as

$$\varepsilon = \frac{4}{GF} \times \frac{E_o}{E_i} \tag{6.1}$$

where GF = the gage factor, E_i = the measured input voltage to the bridge circuit from the power supply (i.e., excitation voltage), and E_o = the measured output voltage from the bridge circuit (i.e., signal voltage). The gage factor is a constant

that relates the change in resistance of a strain gage to its change in length. Typical values range between 2.09 and 2.11 for strain gages used on steel and concrete components.

Similar to a strain gage, a deflection transducer produces an output voltage proportional to the deformation of the instrument. Accordingly, deflections were computed with the formula

$$\Delta = \frac{E_o}{E_i} \ x \ S \tag{6.2}$$

where S = the stroke of the deflection transducer. The ratio of S to the excitation voltage represents the calibration factor for the instrument. For example, if the excitation voltage is 5 volts, a deflection transducer with a 50 mm (2 in) stroke would yield a change in deflection of 10 mm (0.4 in) per volt of output. Thus, transducers with smaller strokes had a higher resolution.

6.1.2   Reduction of Trailer Load Data

As discussed in Chapter 5, the flatbed trailer axles were positioned at various longitudinal positions along the 18.3 m (60 ft) span of the test units. At each position, the trailer was stopped for approximately 10 seconds as data were recorded at a rate of 10 Hz. Figure 6.1 shows a typical strain history recorded on a girder flange as the trailer was moved on and then immediately off the bridge. The steep lines designate the response as the trailer was moved longitudinally from one load position to another. Plateaus in the strain record occurred when the trailer was at rest at a given load position. Immediately before each plateau, there was an abrupt fluctuation in strain as the brakes were applied to stop the trailer.

121

These sudden vibrations were short in duration and thus, were not considered in the evaluation of the data. Stopping the trailer provided a sample of readings at each load position, which were continuously checked for electrical noise and drift. The measurements were also examined for possible signs of girder yielding.
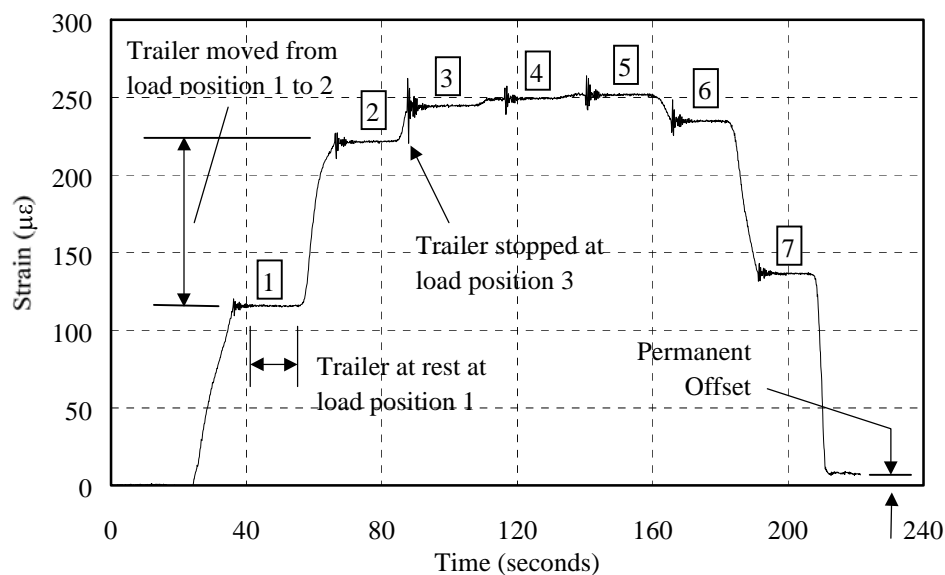
Figure 6.1 Typical Strain History during Trailer Load Sequence.

In the data logger program, the voltage range for strain measurements was set at 50 mV, which is the smallest it can be specified. Nevertheless, this limit was large compared with the small changes in voltage that were read from the strain gage circuits. For example, a change in strain of 500 $\mu\varepsilon$ (half the yield strain assuming 200 MPa steel) caused only a 1.319 mV change in voltage or 2.6% of the voltage range. Because the change in voltage is so small even for a substantial change in strain, the noise level needed to be kept low in order to maximize the signal-to-noise ratio.

To determine the reliability of the collected data, a statistical analysis was performed on the data samples with the trailer at rest at the seven load positions. Readings taken before and after loading with the trailer off the bridge were also evaluated. Table 6.2 lists the results (i.e., averages and standard deviations) of the analysis performed on the strain record displayed in Figure 6.1.

Table 6.2 Typical Strain Data Set for After Reduction.

	Before Load	Longitudinal Load Position							After Load
		1	2	3	4	5	6	7	
Average Strain (με) *	0	116	221	244	249	252	235	137	8
Standard Deviation (με) *	1	1	1	2	2	1	2	1	1

* The statistical analysis was performed on approximately 100 data points for each load position.

Strain readings were considered reliable if the standard deviation of the data sample did not exceed ±2 microstrain. This range of strain represented the normal noise level of the data acquisition system under laboratory conditions. In the field, however, the system was susceptible to more sources of noise such as improper grounding and bad wiring, which could lead to increased instability in the signals. As shown in Table 6.2, the standard deviation did not exceed 2 με indicating that the average readings were reliable and thus, could be used with confidence for interpreting the bridge behavior. Typically, a good signal-to-noise ratio target would be about 100. Noise was not as much a problem for the deflection readings since the measurements constituted a larger percentage of the instrument's full range of motion. Thus, a high signal-to-noise ratio was achieved since the voltage changes were significant.

Since the gage readings were continuously re-zeroed during the test of Unit-N, permanent deformations were not carried through between load cycles. Changes in deformation that occurred during a single load cycle were referred to as "incremental" readings. The "total" readings corresponded to the deformations over the entire course of loading. For Unit-N, the total deformations were determined by using the permanent deformations from a previous load cycle as the starting point for the present load cycle. This was not necessary for the test data of Unit-S since the gages were zeroed only once, at the beginning of the test. However, to obtain the incremental deformations, the data were shifted so that the readings before loading started at zero. This axis adjustment was also made to the service load data of Unit-S and is discussed in the next section.

6.1.3   Reduction of Service Load Data

During the test of Unit-N, measurements were written to the data tables at a rate of 100 Hz (every 0.01 seconds) for the service load runs carried out with the dump truck. Such a high rate was specified in order to evaluate the feasibility of the data acquisition system to record reliable data under dynamic loading (i.e., normal vehicular speed). However, because the data logger needed to scan through 55 data channels, the averaging of the voltage readings performed internally by the data logger was insufficient to reduce the noise to acceptable levels. As a result, the voltage signals were extremely noisy.

To restore the voltage signals, a digital filter was designed to remove all frequency components using the digital signal processing toolbox provided by the

MATLAB (1997, 1998) program. This particular toolbox offers several types of digital filters for reconstructing noisy signals, one being an nth order, lowpass Butterworth filter. Lowpass filters eliminate harmonics from a data signal that fall above a given cutoff frequency leaving only the lower frequency content. Figure 6.2 shows the frequency response of the fourth-order Butterworth filter used to remove noise from the data. The response is enlarged over the frequency range of 0 to 5 Hz to better illustrate the features of the filter. The Nyquist frequency corresponds to half the sampling rate.
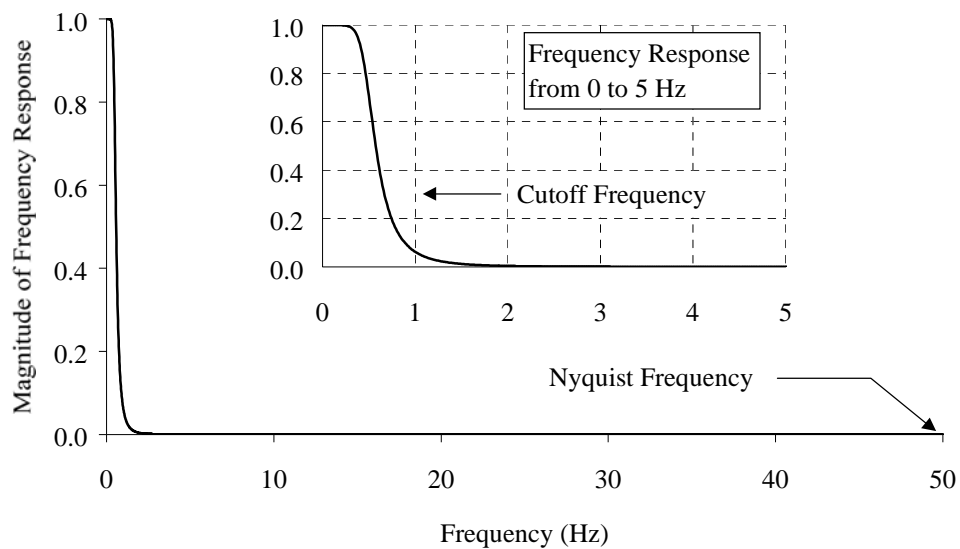
Figure 6.2 Frequency Response of Butterworth Filter.

As shown in the figure, the magnitude of the frequency response was unity over the range of 0 to approximately 0.5 Hz. The response then decreases rapidly to about 0.05 at the cutoff frequency of 1 Hz before becoming asymptotic to the

125

zero axis at 2 Hz. With such a steep drop-off rate, virtually no frequencies above 1 Hz remain in the signal after it is filtered.

There was some concern that such a low cutoff frequency would eliminate signals representative of the bridge's real behavior. The first natural frequency may be determined from a dynamic analysis of the bridge or alternatively, may be approximated with the simple relationship, $f_1 = 82L^{-0.9}$, developed by Paultre et al. (1992) where f_1 is the fundamental frequency (Hz) and L is the span length of the bridge (m). With this formula, the fundamental frequency comes out to 6 Hz using the length of the longest span of 18.3 m (60 ft). Vibration of the bridge at this frequency was not considered likely since the dump truck was driven over the bridge at a slow speed of less than 2.2 m/s (5 mph) without stopping. Thus, it was assumed that the bridge responded at its static frequency of 0.1 Hz, taken as one over the time required for the truck to cross over the length of the bridge, with higher frequency oscillations in the signals caused by noise.

According to the Nyquist criterion (MATLAB, 1998), noise frequencies up to 50 Hz were possible in the signals. This criterion states that in order to describe a signal completely, the sampling rate must be at least two times the frequency of the signal. Before the voltage signals were filtered, the number of samples in each record was first reduced to 4096 (i.e., 2^{12}). The filtering operation requires that the number of samples in the record be equal to some power of two (MATLAB, 1998).

Figure 6.3 shows a typical strain history recorded on a girder flange before the filter was applied. Strain values are plotted as a function of the location of the

126

front axle of the dump truck as it crossed over the bridge unit. As shown in the figure, the noise level was approximately $\pm 10 \mu\varepsilon$ before the filter was applied, which represented a maximum signal-to-noise ratio of only 20 for this particular record. Although the noise was effectively eliminated from the data for Unit-N as shown in Figure 6.4, the data collection programs were modified for the test of Unit-S to avoid having to use the MATLAB filter. In the new programs, the integration (i.e., averaging time) of the voltage signals performed internally by the data logger was increased. The changes made to the program reduced the noise level to about $2 \mu\varepsilon$, however, the sampling frequency needed to be reduced from 100 Hz to 10 Hz to provide more time to complete the averaging.
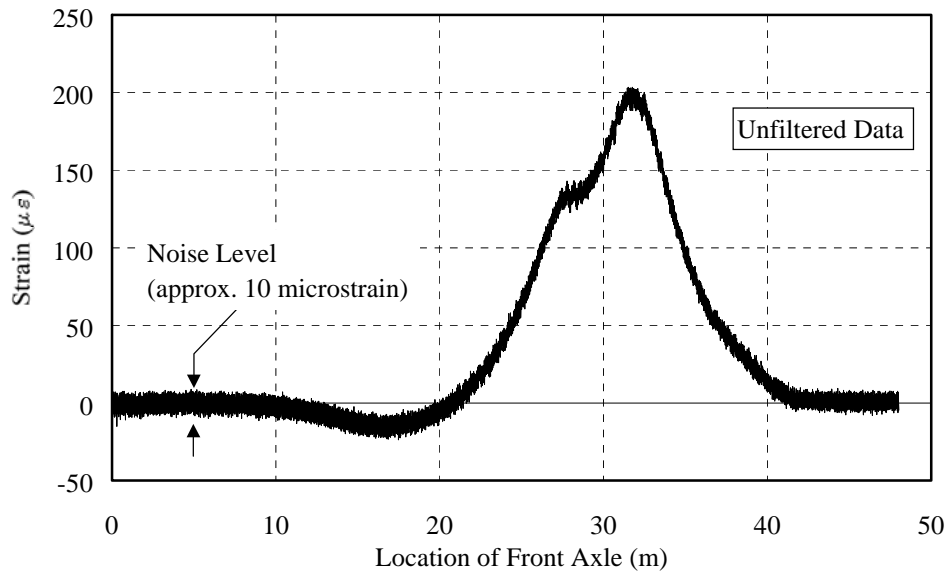
Figure 6.3 Typical Service Load Strain Record Before Filtering.
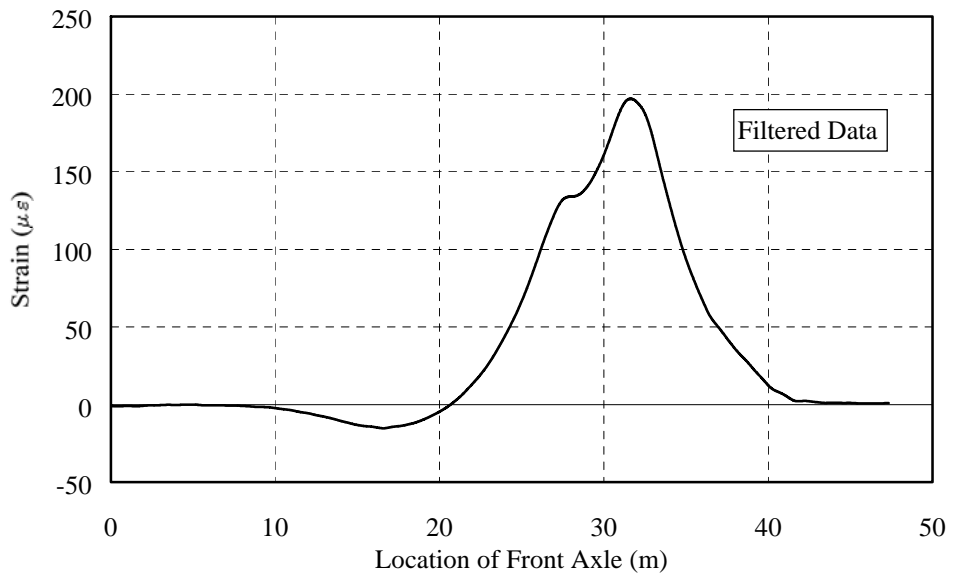
Figure 6.4 Typical Service Load Strain Record After Filtering.

128

In addition to reducing the noise, the program modifications improved the overall collection process in several ways. First, the reduction in the sampling rate significantly reduced the amount of information written to the tables. As a result, the data tables took up less memory in the data logger during the collection process and in the laptop computer after downloading. Smaller data files also reduced the download time from the data logger to the laptop computer and also the transfer time from the laptop to diskette. Since the data tables had a finite size, the lower rate also increased the range of time over which data could be taken. Finally, the same program could be used to collect data during the trailer loading and the dump truck loading avoiding the trouble of having to switch between programs during testing. The reduced sampling rate of 10 Hz was still fast enough to completely describe the signals under the moving dump truck.

Since the gages were zeroed only at the beginning of testing for Unit-S, the service load data needed to be shifted so that all readings began at zero. It was observed that the measurements did not return to zero after the bridge was subjected to the trailer loads. Because the service load runs were conducted between the trailer loading sequence, the service load data started at the final reading from the previous trailer load. The shifts were made by averaging the measurements before the dump truck entered the bridge (i.e., front axle position < 0) and subtracting the result from the remaining data points. Shifting the axes of the measurements isolated the response of the unit for each particular dump truck test. Figures 6.5 and 6.6 show the strain values recorded at the top flange, mid-web, and bottom flange of a girder before and after the shifts were made. For

example, the top flange data was adjusted by adding a strain of 68 $\mu\varepsilon$ to the entire record. These axis adjustments were not required for the service load data of Unit-N since the gages were zeroed before each separate run and thus, the response always began at zero.

As shown in the figures throughout this section, the response under the dump truck was plotted versus the position of the front axle. Thus, it seems only appropriate to provide a short description of the steps taken to convert to this scale. First, the driver of the dump truck was instructed to keep a constant speed of less than 2.2 m/s (5 mph) over the length of the bridge. As the dump truck was driven across the units, the mechanical switch connected to the excitation voltage channel (see description given in Chapter 3) was depressed when the front axle lined up with the bridge supports. Each time the switch was pushed, a zero value was written in the excitation voltage column of the data file identifying the times when the front axle crossed the supports.

Since the positions of the bearings were known, linear interpolation could then be used to determine the intermediate vehicle positions. For example, assuming it takes 6.5 seconds for the vehicle to cross two separate bearing locations separated a distance of 7.7 m (25.4 ft) the speed of the vehicle is 1.2 m/s (3.9 ft/s). If the data are written every 0.1 seconds, then the change in vehicle position from one record to the next is 120 mm (5 in). Subsequently, the vehicle position between bearings can then be determined by adding the increments to the bearing positions.
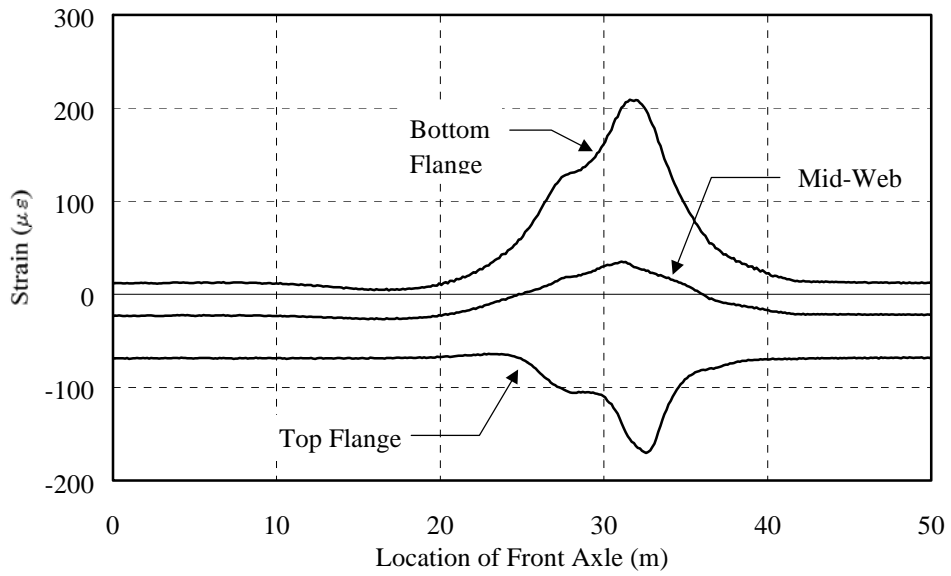
Figure 6.5 Typical Service Load Strains for Unit-S Before Adjustment.
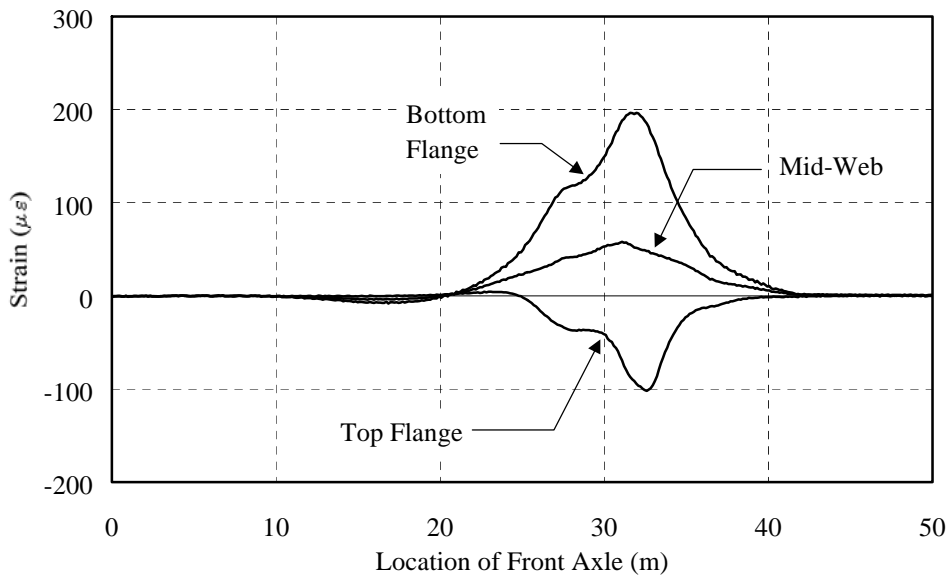
Figure 6.6 Typical Service Load Strains for Unit-S After Adjustment.

131

6.2   GENERAL DESCRIPTION OF LOAD-DEFORMATION RESPONSE

As described in Chapter 4, the bridge units were loaded in two separate stages (designated as loading Stage 1 and Stage 2). In both stages, the load was applied with the flatbed trailer loaded incrementally with concrete barriers. The main difference between the two stages was that in Stage 2, barriers were also placed directly on the deck in addition to the trailer load. The purpose of these barriers was to increase the initial stress in the girders before the trailer load sequence was continued. The extra weight on the bridge deck was needed in order to yield the girders. Thus, in Stage 2, the total load equaled the trailer load plus the deck load.

The deflections measured at girder 2 during the test of Unit-S are plotted in Figure 6.7 to illustrate the general deformation response of the girders versus load. At the top of the figure, a cross section of Unit-S is provided to show the transverse position of the trailer load and the deck load on the bridge deck. As shown, the trailer load was centered over girder 2 and the deck load was placed directly above girder 1. The deck load remained constant during Stage 2. The girders are numbered from 1 to 5 starting with the exterior girder on the "loaded lane". The "loaded lane" refers to the side of the bridge deck that was loaded (i.e., the west lane of Unit-S). The position of the trailer and deck loads on the cross-section of Unit-N was the mirror image of Unit-S with the loaded lane moved to the east side.

132
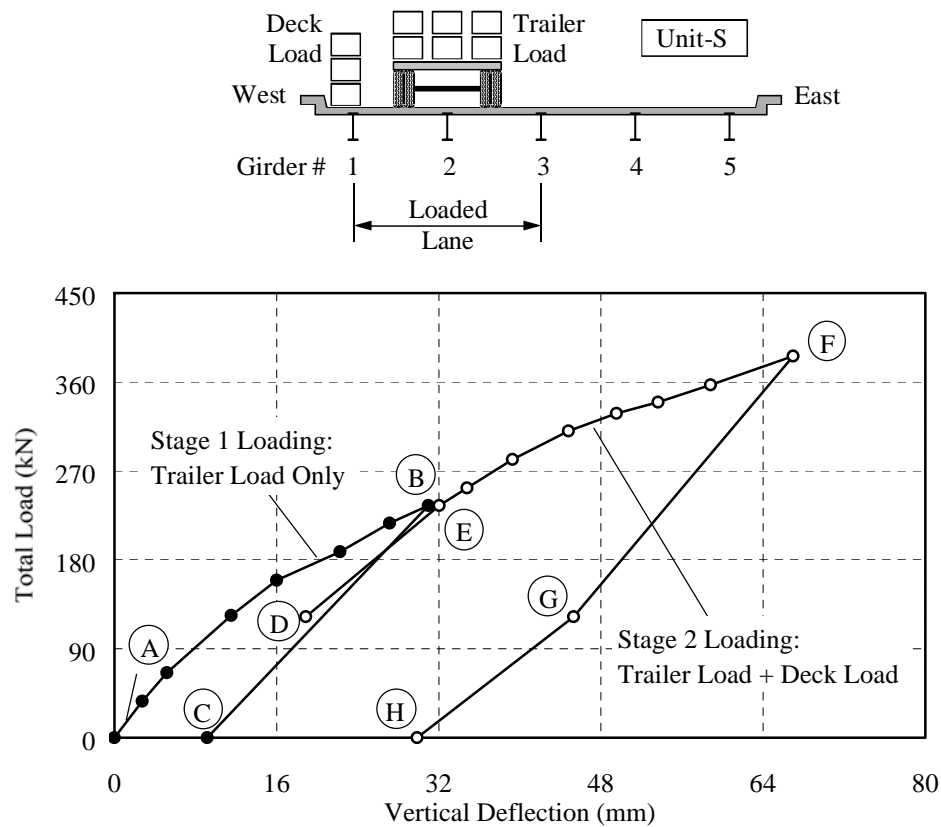
Figure 6.7 Vertical Deflection Response for Girder 2 of Unit-S.

As shown in Figure 6.7, the load-deflection curve followed a path along eight major points labeled A to H. Each of the eight points represented either a final or beginning step within a loading stage. Dark symbols are used to display the response during Stage 1 while open symbols are used for Stage 2. The horizontal axis represents the particular deformation being measured, which in this case is the vertical deflection of girder 2.

At points B and E, the total loads are approximately equal between Stage 1 and Stage 2. The discontinuity between points C and D marked the end of Stage

1 and the start of Stage 2. Points C and H are the permanent deformations remaining after Stages 1 and 2, respectively. For Unit-N, however, the response from point G to H was not recorded since the test was terminated before the deck load was removed from the bridge deck. A detailed description of the response path with the exact loads at the different points of loading is provided in Table 6.3. The table applies to all the load-deformation responses including the load-deflection, load-strain, and load-slip curves presented in Section 6.3.

Table 6.3 Description of Response Path.

Response	Description
Path AB	Stage 1 loading with trailer load only. No concrete barriers (i.e., deck load = 0) were placed on the bridge deck. At point B, the final loads were 235 kN (52.8 kips) for Unit-S and 264 kN (59.3 kips) for Unit-N.
Path BC	Unloading of trailer load at end of Stage 1. At point C, no load remained on either bridge unit.
Point D	Start of Stage 2 loading. Three barriers totaling a weight of 122 kN (27.5 kips) were placed directly on the deck next to the curb above girder 1 on the loaded lane of each unit.
Path DE	Stage 2 loading with trailer load plus deck load. At point E, the total load was approximately equal to the final load of Stage 1 (i.e., point B).
Path EF	Stage 2 loading continued. The deck load remained constant throughout this stage as the trailer load was increased. At point F, the final loads, including the deck load, were 326 kN (73.3 kips) and 386 kN (86.8 kips), respectively, for Unit-N and Unit-S.
Path FG	Unloading of trailer load at end of Stage 2. At point G, only the deck load remained on the bridge units.
Path GH	Removal of deck load at Unit-S only. At point H, no load remained on the unit. This response was not measured for Unit-N since the test was terminated before the removal of the deck load from the bridge deck. As a result, the girder response ended at a total load equal to the deck load for Unit-N.

In order to distinguish between girder yielding and deterioration of partial composite action as the source of non-linearity in the response, elastic strain limits were computed based on non-composite and composite action of the girders. The elastic limits were determined by subtracting the estimated dead load strains (assuming both non-composite and composite girder behavior) from a yield strain of 1035 $\mu\varepsilon$. As described in Chapter 4, the yield stress was determined experimentally from a tension coupon test to be 207 MPa (30 ksi). It was assumed that the girders of both bridge units were rolled from the same batch of steel and thus, had the same yield stress. In addition, the modulus of elasticity for the steel was assumed to be 200 GPa (29000 ksi).

Table 6.4 lists the estimated dead-load strains and elastic strain limits for the bottom flanges of the girders at the positive and negative moment regions, respectively, of the bridge units. Dead load includes the weight of the girders, the concrete slab and curbs, the steel railing, and the asphalt layer. In the case of non-composite action, the girders were assumed to carry all the dead load ignoring any flexural resistance from the concrete deck. This assumption resulted in the higher dead load strains and thus, established a lower bound for elastic behavior.

Table 6.4 Estimated Dead Load Strains and Elastic Limits on Girder Bottom
Flange at Section c-c and Section d-d.

Location	Non-Composite Action		Composite Action	
	Dead Load Strain ($\mu\varepsilon$)	Elastic Limit ($\mu\varepsilon$)	Dead Load Strain ($\mu\varepsilon$)	Elastic Limit ($\mu\varepsilon$)
Positive Moment	715	320	445	590
Negative Moment	-655	-380	-445	-590

Note: Elastic Limit = Yield Strain ($\pm$1035 $\mu\varepsilon$) - Dead Load Strain

135

Assuming the girders to resist the dead load as composite sections reduced the dead load strains by 38% and 32% at the positive and negative moment regions, respectively. As a result, there was a corresponding increase in the elastic limit therefore establishing an upper bound. Composite action of the girders under dead load is not unreasonable considering that the removal of the pier cap is analogous to the process of shored construction where the girders are temporarily supported along their length as the concrete deck is cast and allowed to cure. Although the Marlin bridges were built as non-composite, the start of inelastic behavior was expected to lie somewhere between the elastic strain limits because of partial composite action between the girders and the slab.

6.3   GIRDER DEFORMATIONS VERSUS LOAD

This section presents the girder deformations that were measured during testing of Unit-N and Unit-S under increasing loads. The deformations are divided into three groups that include: the strains on the cross-section of the girders, vertical girder deflections, and relative slip at the girder-slab interface. Measurements taken with the trailer at load position 4 (i.e., when the front axle was at mid-span of the 18.3 m (60 ft) span) were selected for evaluation. At this position, the trailer was at the critical longitudinal location for maximizing both the positive bending moment at Section c-c (i.e., mid-span of the loaded span) and negative moment at Section d-d (i.e., interior support of the loaded span). When the deck load was placed on the bridge deck, the center of gravity of the barrier group was aligned with the trailer's front axle. The slight offset between the

centroid of the barriers and the tandem axle of the trailer in the longitudinal direction was assumed to have a negligible affect on the load-deformation response of the girders.

In the sections that follow, the unloading portions of the load-deformation curves, as described in Figure 6.7 and Table 6.2, were omitted for clarity in comparing the behavior of the girders. In addition, only the deformations along Path AB of Stage 1 and Path EF of Stage 2 are plotted so that the response in Stage 2 started at the same load that ended Stage 1. Complete load-deformation (i.e., load-deflection, load-strain, etc.) curves for the girders, including the unloading paths, are given in Appendix D.

6.3.1 Girder Strains

Figures 6.8 and 6.9 show the strains measured on the bottom flange of girders 1 through 4 at Section c-c. Throughout this section, these two figures are referenced frequently to compare the behavior of the five girders and also of the two bridge units. On the horizontal axis of the figures, positive strains represent tension. Closed symbols are used to display the strain values for Stage 1 while open symbols are used for Stage 2. The shape of the symbol distinguishes the response of each girder. The two broken vertical lines represent the elastic strain limits for live load of 320 $\mu\varepsilon$ and 590 $\mu\varepsilon$ that were computed in the previous section at Section c-c. Measured strains for girder 5 were omitted from the plots because of their small magnitude relative to the other four girders. Essentially all the load was distributed to girders 1 through 4 because of the unsymmetrical loading pattern with respect to the bridge centerline.

137
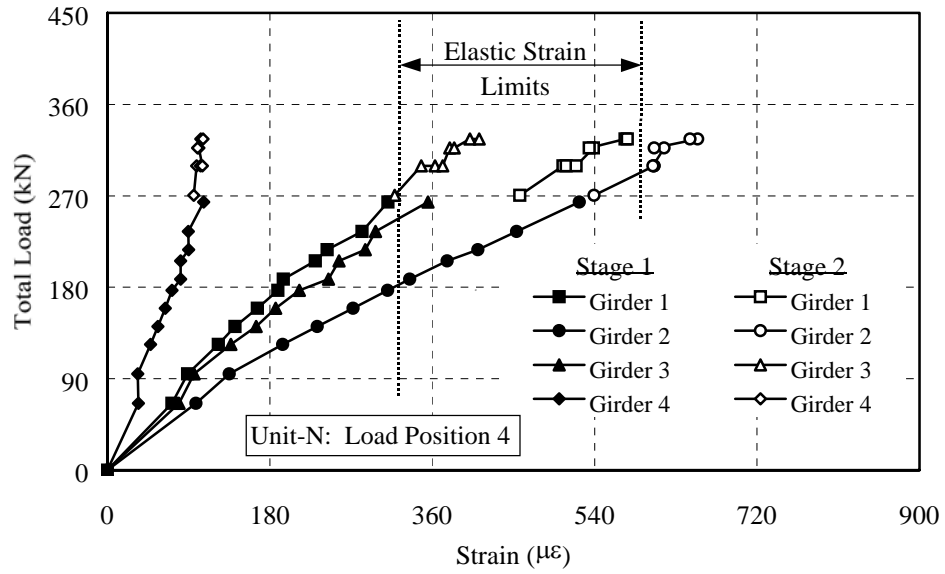
Figure 6.8 Bottom Flange Strain of Steel Girders at Section c-c of Unit-N.
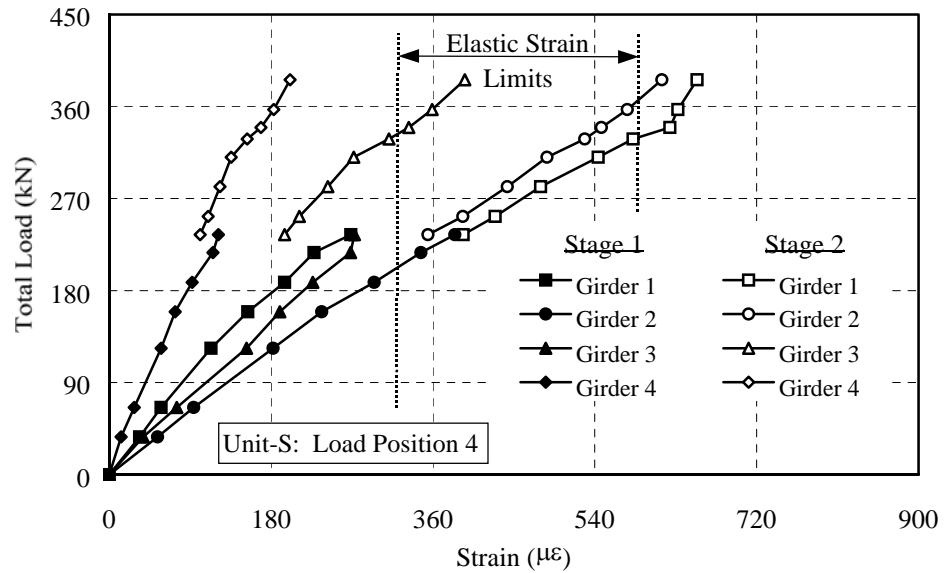
Figure 6.9 Bottom Flange Strain of Steel Girders at Section c-c of Unit-S.

138

As shown in Figure 6.8 and 6.9, the load-strain curves were discontinuous between load stages because the trailer and deck loads were positioned at two different transverse positions on the bridge deck. The longitudinal distribution of these loads was also slightly different. Recall that at the start of Stage 2, barriers were placed directly on the deck off to one side of the trailer load. The transverse offset between the two loads altered the load applied to the girders thus causing a shift in the strain response between the load stages. Under the trailer load, girder 2 was the most heavily loaded girder followed by the two adjacent girders, 1 and 3. Conversely, the majority of the deck load was carried by girder 1 followed sequentially by girders 2 through 4. In both cases, girder 4 carried the least amount of load since it was furthest from the load. Thus, the deck load caused a positive shift in the strain response for girder 1 and a negative shift for girders 2 through 4 at the start of Stage 2. Similar shifts occurred in the load-deflection and load-slip curves between load stages, which are shown in Sections 6.3.2 and 6.3.3.

The dead load strains in the girders at Section c-c were estimated as 715 and 445 microstrain (see Table 6.4), respectively, assuming non-composite and composite action. Adding these initial strain values to the final live load strains plotted in Figures 6.8 and 6.9 results in the total strains listed in Table 6.5.

Table 6.5 Total Strains on Bottom Flange of Girders 1 through 4 at Section c-c.

| Bridge Unit | Total Strains ($\mu\varepsilon$) | | | | | | | |
| | Non-Composite Action | | | | Composite Action | | | |
	Girder 1	Girder 2	Girder 3	Girder 4	Girder 1	Girder 2	Girder 3	Girder 4
Unit-N	1290	1370	1125	820	1020	1100	855	550
Unit-S	1370	1330	1110	915	1100	1060	840	645

As shown in the table, the final strains exceed the yield strain of 1035 microstrain for girders 1 through 3 assuming non-composite action and for girders 1 and 2 assuming composite action. The total strains show that girders 1 and 2 are likely inelastic and possibly girder 3 at the end of testing. A detailed discussion of the strain response of the girders of Unit-N and Unit-S are provided in the following sections.

Response of Unit-N

As shown in Figure 6.8, the response of girder 4 was essentially linear throughout the full range of loading while girders 1 through 3 exhibited non-linear behavior starting at small loads. The gradual decline in the slope of the load-strain curves indicated that girders 1 through 3 were losing stiffness at a slow but constant rate. However, since the loss of stiffness was moderate and the strains were still elastic, yielding was not considered a viable cause of the non-linearity during load Stage 1. Instead, the trends in the load-strain curves suggested that the unintended interaction between the girders and the deck was deteriorating. As will be discussed in Section 6.2.3, a non-recoverable and continual amount of slip was measured at the girder-slab interface throughout loading that further supported this hypothesis. Towards the end of Stage 1, the load-strain curve for girder 2 showed no noticeable signs of yielding even though the strains had surpassed the lower elastic limit by a margin of 200 $\mu\varepsilon$. At the same load, the measured strains of girders 1 and 3 had also just reached the lower elastic limit.

At Section d-d, the negative moment region, the bottom flange strains of girder 1 reached the lower elastic limit of -380 με at the final load of 264 kN (59.3 kips) applied during Stage 1 as shown in Figure 6.10. The figure shows the top and bottom flange strains (labeled as TF and BF, respectively) for girder 1 at Section d-d measured during the two loading stages. Solid symbols denote the response during Stage 1 while open symbols denote the response during Stage 2. In the second loading stage, the strains on the bottom flange of girder 1 continued to increase at a fast rate. Measured strains above the lower elastic limit were also detected in the top flange, however, the change in strain was not as large as the bottom flange. Throughout the loading increments, the top flange strain was about half of that on the bottom flange. This behavior indicated that girder 1 was acting as a partial composite section even as the girder became inelastic.
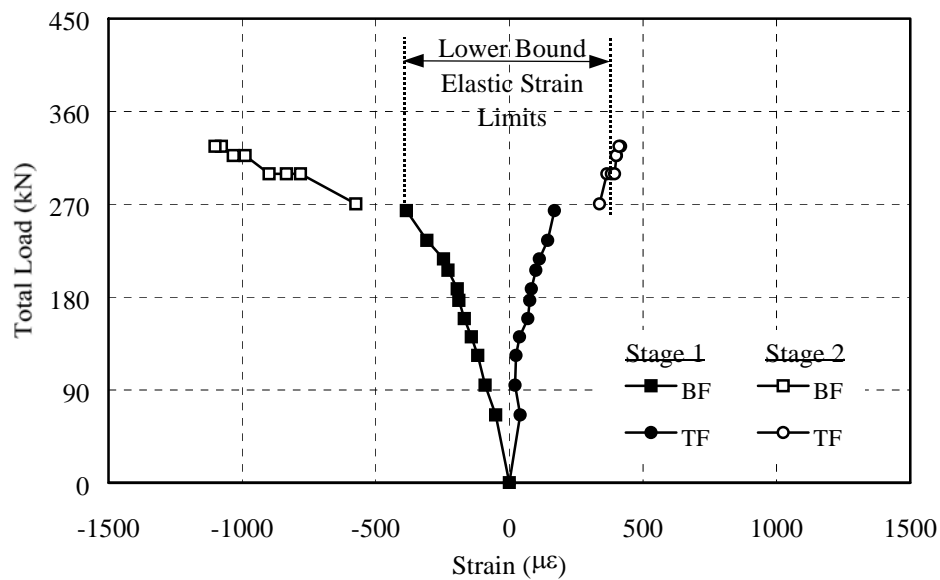
Figure 6.10 Measured Strains on Bottom Flange (BF) and Top Flange (TF) of Girder 1 at Section d-d of Unit-N.

141

As shown in the strain contours plotted in Figures 6.11 and 6.12, measured flange strains for girders 2 through 4 did not exceed 270 με, which indicated that the girders were still elastic at Section d-d. These figures show the strains measured during Stage 1 and Stage 2, respectively, on the top and bottom flanges of girders 1 through 4 across Section d-d, the negative moment region. The horizontal axis for each strain profile represents the girder number as shown in the sketch of the cross section provided at the top of the figure. At the end of Stage 2, the bottom flange strains for girder 1 greatly exceeded the lower elastic strain limit while the top flange strains were just above the lower bound.

Starting at a load of 188 kN (35.8 kips) in Stage 1, the bottom flange strain profile did not conform to the response at lower loads since the strains of girder 2 stopped increasing in proportion to the change in load. All the top flange strains, however, continued to increase with load rather consistently. For the interior girders 2 through 4, the measured strains on the top and bottom flange were about equal which showed that these girders were acting as non-composite sections.
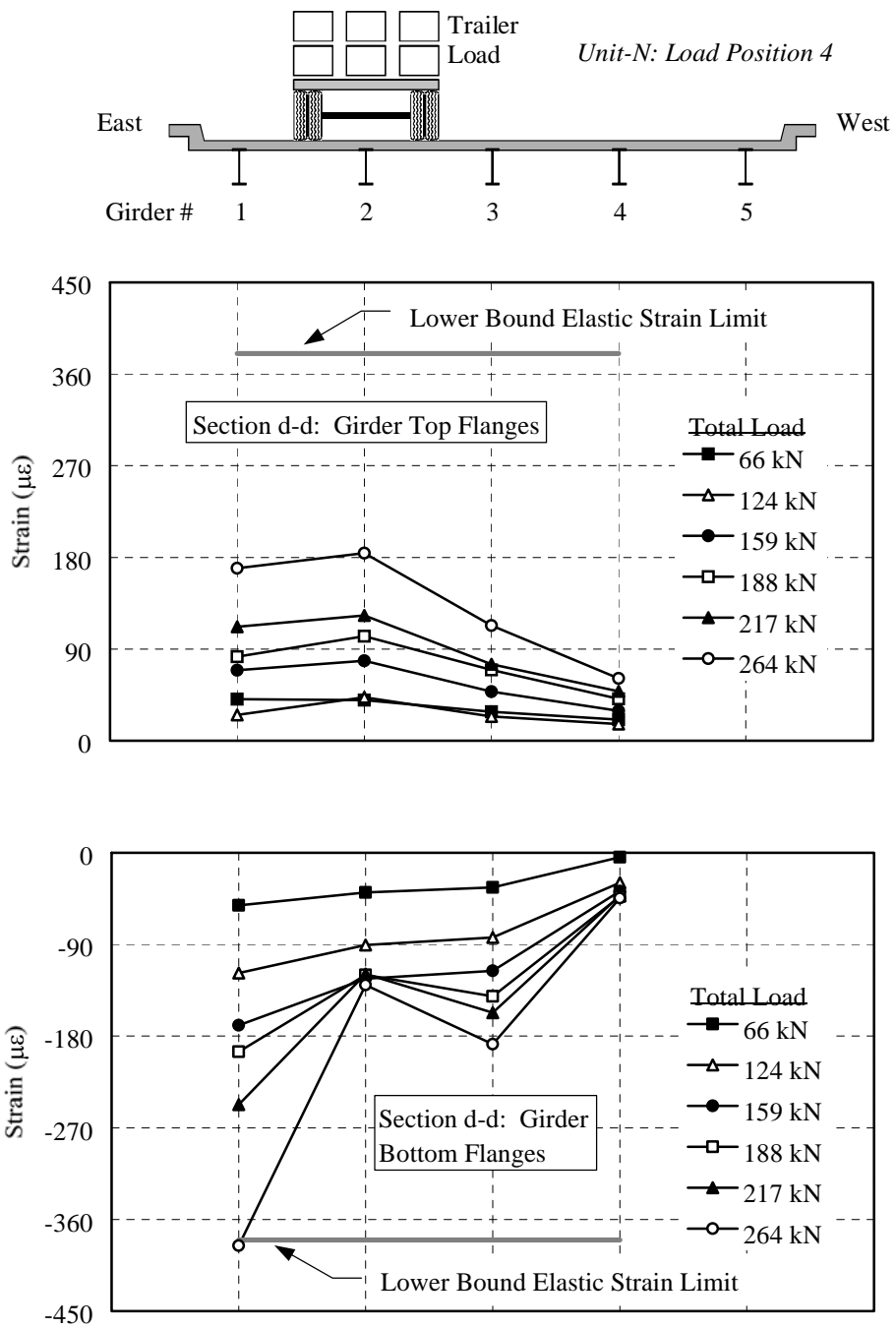
Figure 6.11 Girder Strain Profile at Section d-d of Unit-N during Stage 1 Loading.

143
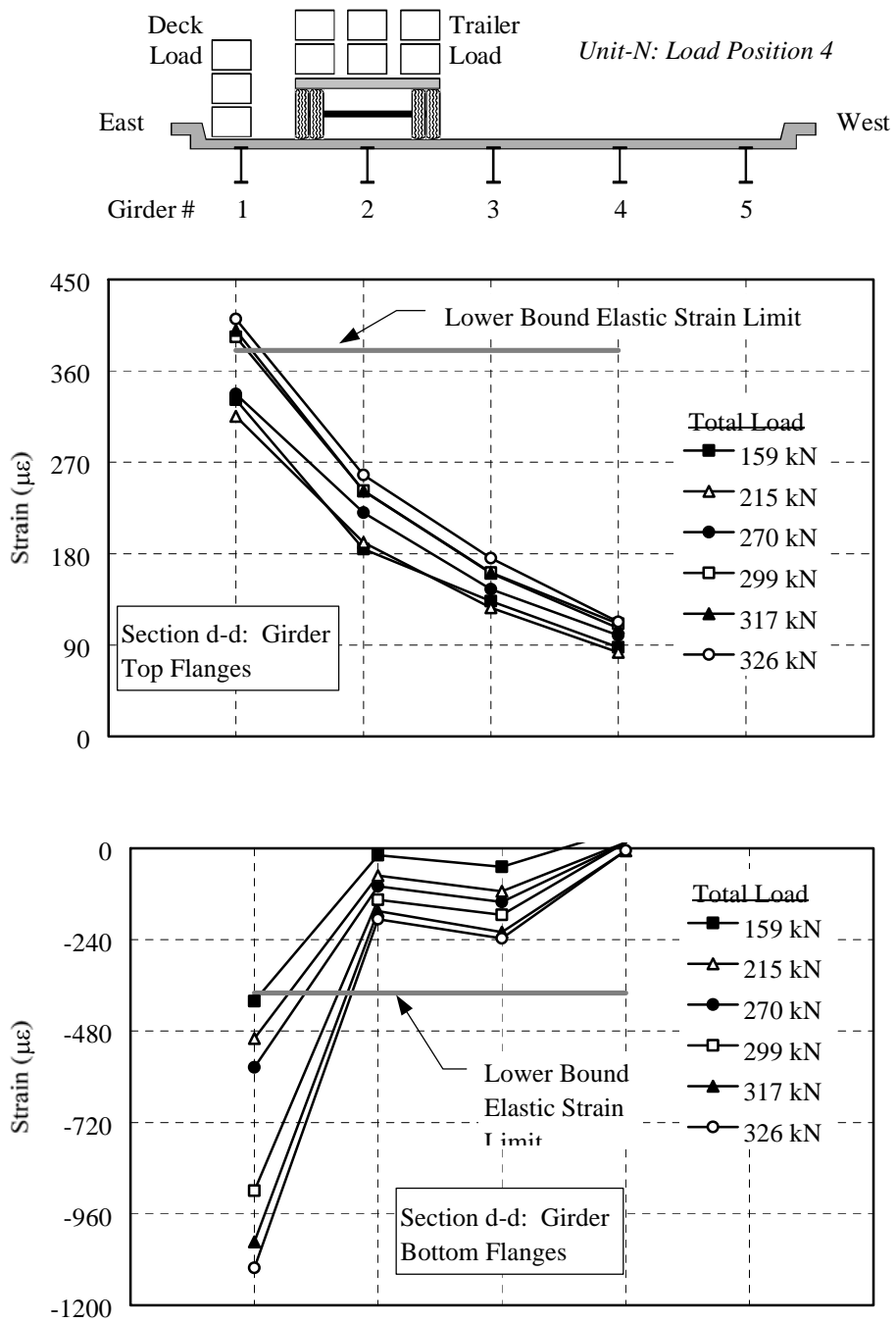
Figure 6.12 Girder Strain Profile at Section d-d of Unit-N during Stage 2 Loading.

144

The yielding of girder 1 at Section d-d appeared to have no measurable effect on the load-strain behavior of the girders at Section c-c based on Figure 6.8. In this figure, the slopes of the strain curves correlated well between the two loading stages. Again, only a gradual non-linear response was observed in the girders during Stage 2. From Figure 6.8, no signs of yielding were obvious although the strains for girders 1 and 2 were close to the upper elastic limit. As described in Chapter 4, however, two strain gages were installed on the bottom flange of girder 2 on opposite sides of the web. Strains plotted in Figure 6.8 correspond to the readings for the strain gage placed on the east side. Figure 6.13 shows a comparison of the strains measured at the gage installed on the east and west sides of the flange.
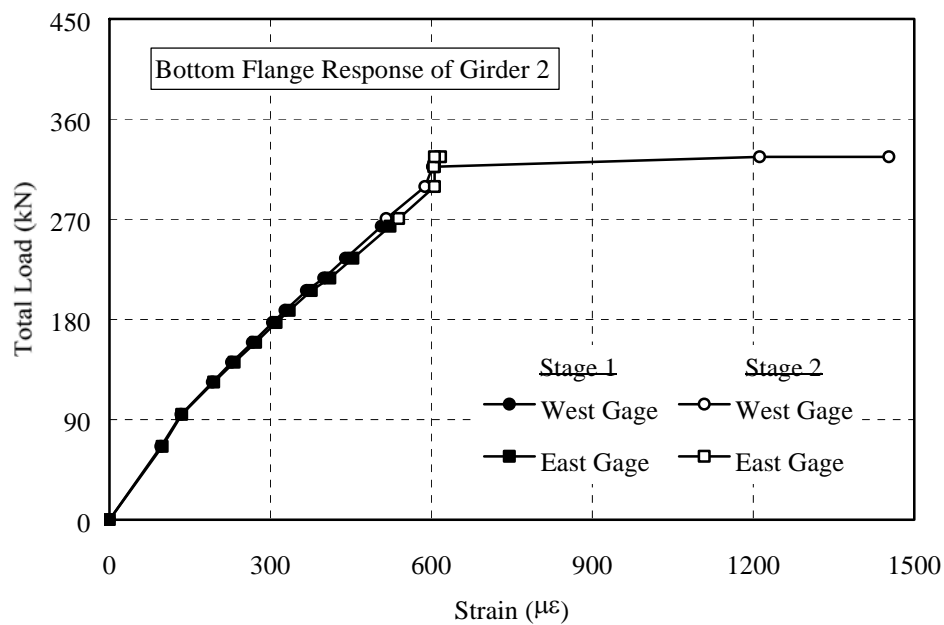
Figure 6.13 Measured Strains on Bottom Flange of Girder 2 at Unit-N.

145

There was essentially no difference between the two gages during Stage 1 loading. During Stage 2, however, a sudden strain increase occurred at only the west-side gage at a load of 317 kN (71.3 kips), a possible indication that the flange had indeed yielded. Furthermore, since the gage was positioned on the top surface of the flange, yielding had to have propagated through the thickness. A possible reason for the strain increase on only one side of the flange is that the yield lines happened to traverse only the west-side gage. However, this behavior could not be verified since the girders were coated with a lead-based paint and thus, whitewash could not be used as a visible aid to detect yielding.

Figure 6.14 shows the strain contours on the girder bottom flanges across Section c-c at various load levels in Stage 1 and Stage 2. In Stage 2, the deck load remained constant at 122 kN (27.5 kips) and as a result, the trailer load ranged from 23 to 63 percent of the total load. As shown, girder 2 experienced the largest strains in Stage 1 followed by girder 3 and then girder 1. It is interesting to note that the interior girder adjacent to girder 2 (i.e., girder 3) showed larger strains than the exterior girder (i.e., girder 1) even though both girders were the same distance from the trailer. The lower strains on the exterior girder occurred because of the flexural participation of the curb. In addition, partial composite action was higher in this girder since it was located away from the centerline of the traffic lane and thus, could not be loaded as heavily as the interior girders.
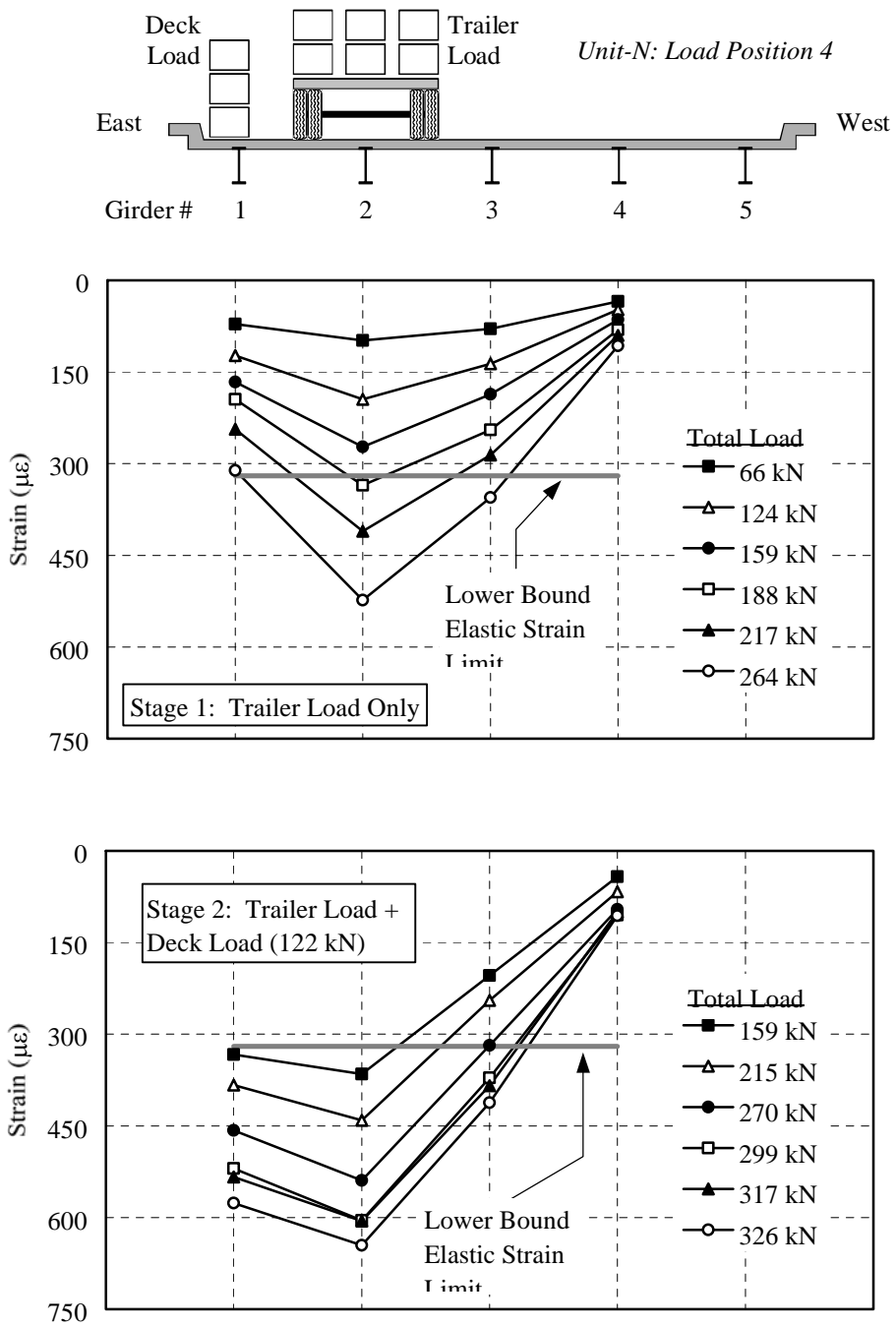
Figure 6.14 Bottom Flange Strains at Section c-c of Unit-N for Load Position 4.

147

Comparison of Figure 6.8 with Figure 6.9 shows that the overall behavior of the girders in the positive moment region was similar for the two tests. As in Unit-N, the girders of Unit-S displayed non-linear behavior as seen in the trends of bottom flange strains given in Figure 6.9. Measured strains exceeded the lower elastic limit at girder 2 only by 20 percent suggesting that the girders were perhaps still elastic at Section c-c as Stage 1 loading was completed.

Figure 6.15 shows the top and bottom flange response for girder 1 in the negative moment region. The figure shows a sudden increase in the top flange strain to 320 $\mu\varepsilon$ (approximately 85% of the lower elastic limit) at the final load applied in Stage 1 of 235 kN (52.8 kips). Measured strains on both the top and bottom flange exceeded the lower elastic limit in Stage 2.
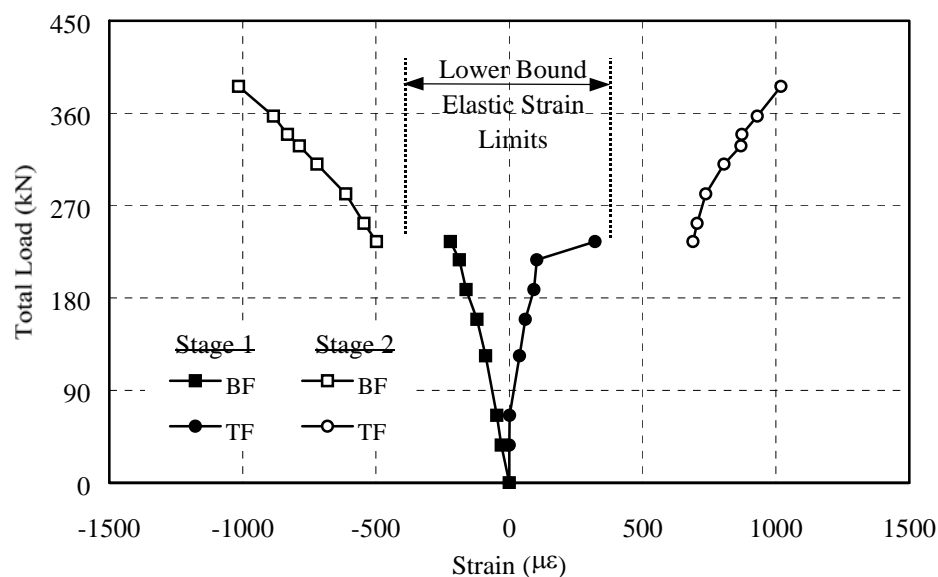
Figure 6.15 Measured Strains on Bottom Flange (BF) and Top Flange (TF) of Girder 1 at Section d-d of Unit-S.

148

Since the measured strains were below the lower elastic limit in Stage 1, the strain increase could not be attributed to yielding as in Unit-N. Another explanation for the abrupt increase in the top flange strain of girder 1 was the loss of partial composite action. As shown in Figure 6.15, the strain measured on the top flange was approximately half of the bottom flange strain before the final load applied in Stage 1. Cracking of the deck slab above girder 1 may have weakened the connection with the top flange thus causing the girder to act non-composite.

Strain contours for girders 1 through 4 at Section d-d are plotted in Figure 6.16 and 6.17 for Stage 1 and Stage 2, respectively. Comparison of Figures 6.11 and 6.16 shows that yielding of girder 1 at Unit-N occurred at about the same load that girder 1 experienced a loss of partial composite action at Unit-S. The loss of partial composite action of girder 1 appeared to have little effect on the response of the remaining girders. For loads below the final load applied in Stage 1, the girders exhibited a rather uniform distribution. Bottom and top flange strains were nearly identical on girders 2 through 4, which indicated that the bending resistance of these three girders resembled a non-composite section. During Stage 2 loading, the loss of partial composite action resulted in top and bottom flange strains in girder 1 well above the lower elastic limit. As shown by the strains plotted in Figure 6.17 for Stage 2, the strain profiles were consistent between load levels although the flange strains for girder 1 were clearly inelastic. The equal strains on the top and bottom flange also show that girder 1 is non-composite.
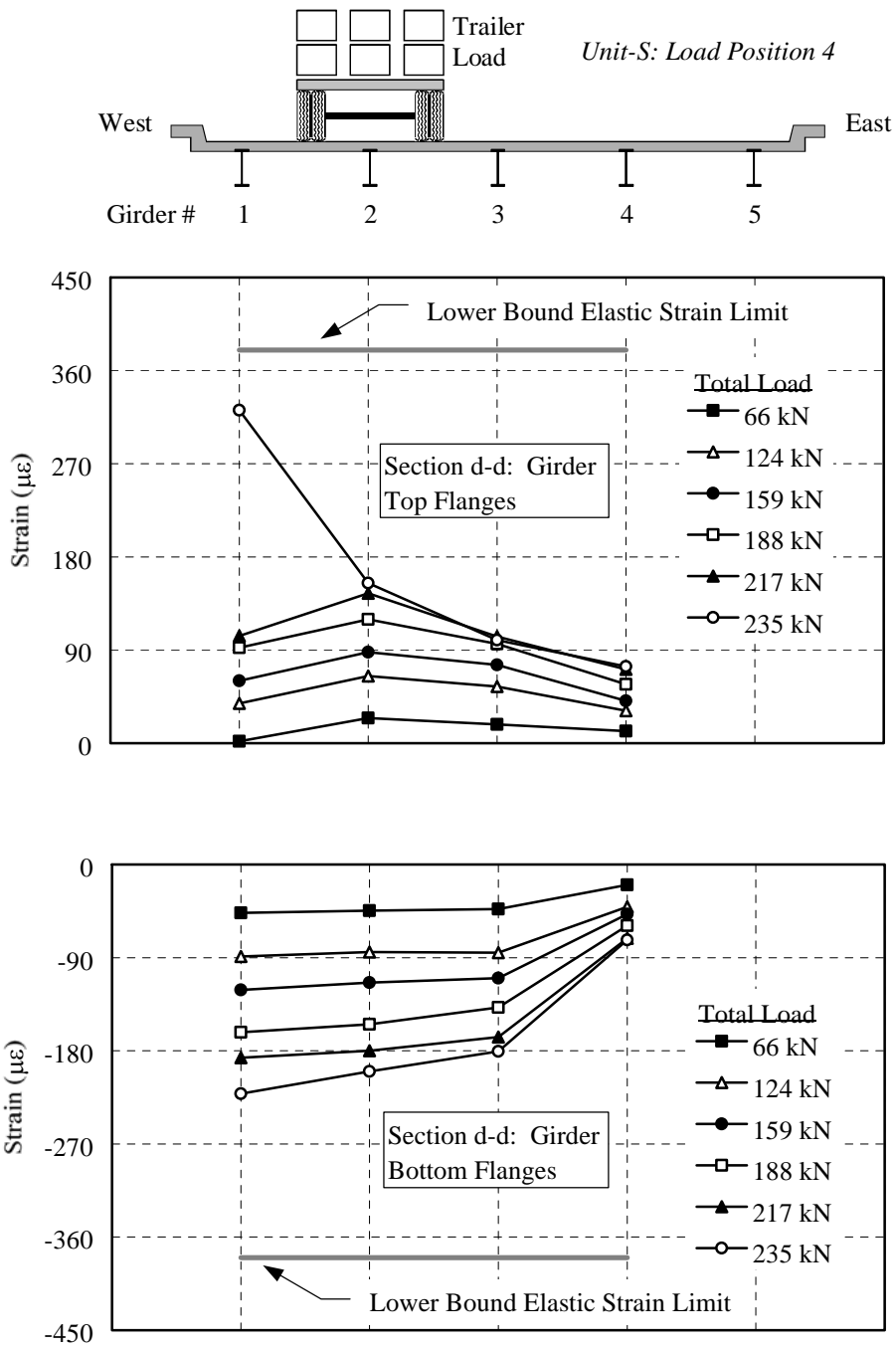
Figure 6.16 Girder Strain Profile at Section d-d of Unit-S during Stage 1 Loading.
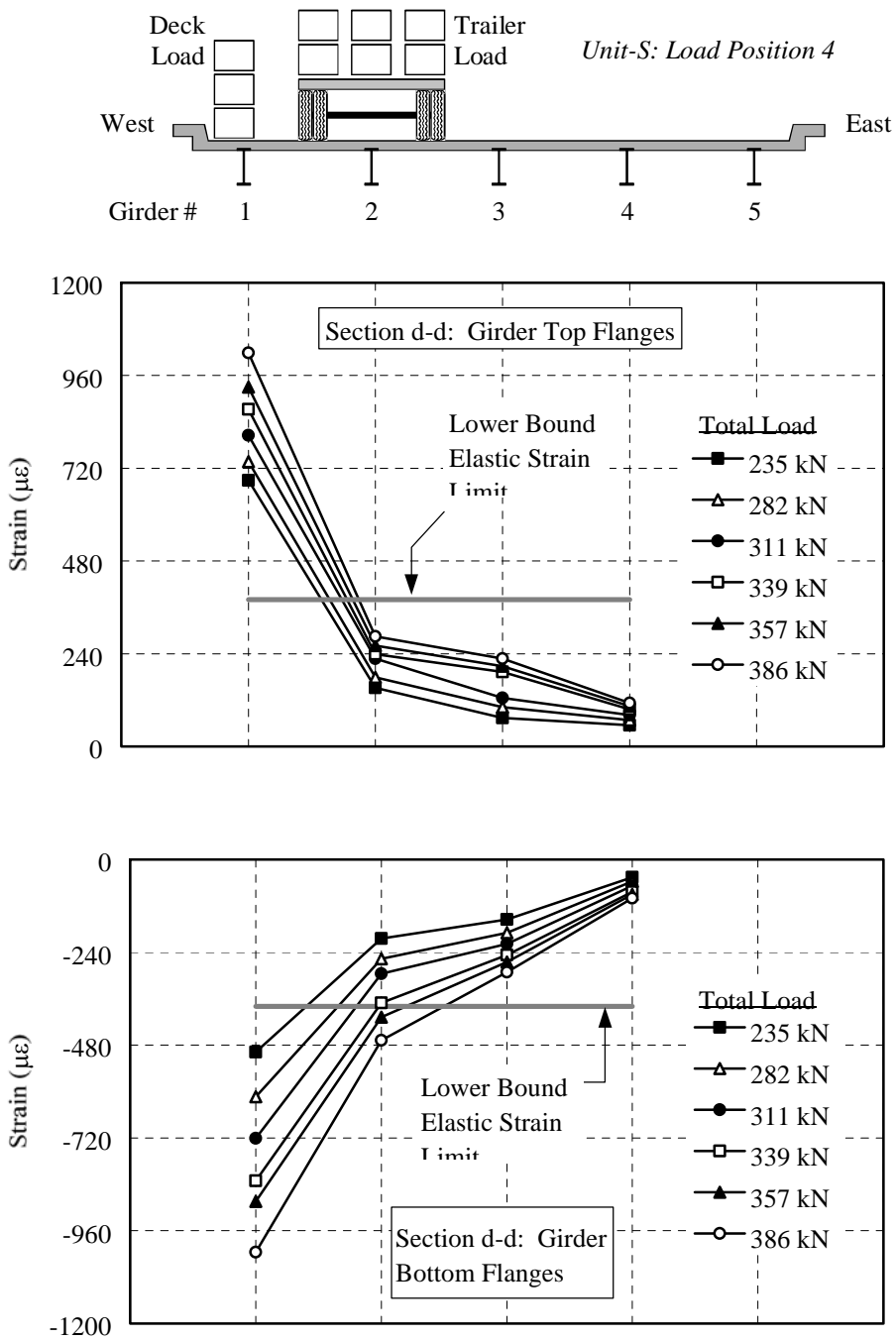
Figure 6.17 Girder Strain Profile at Section d-d of Unit-S during Stage 2 Loading.

151

In the middle of Stage 2, inelastic behavior occurred simultaneously at Section c-c in girders 1 and 2 at a load of about 311 kN (69.8 kips) as shown by the top flange strains plotted in Figure 6.18.
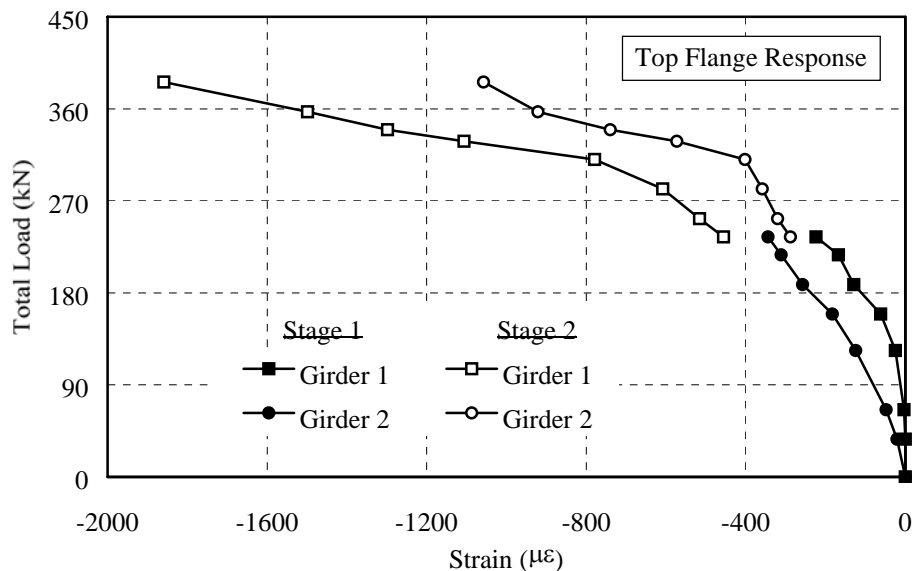
Figure 6.18 Strain Response at Top Flanges of Girders 1 and 2 at Section c-c of Unit-S.

From Figure 6.9, it can also be seen that the strains on the bottom flanges were also approaching the upper elastic limit for the same two girders. With only the web possibly elastic, the bending stiffness of girders 1 and 2 was greatly reduced. Bottom flange strains for the third and fourth girder, however, indicated that these girders were still elastic and therefore, flexurally stiffer than girders 1 and 2. As a result, the increase in strain for girders 3 and 4 that occurred at the yield load suggested that the load was redistributed in the transverse direction as girders 1 and 2 yielded (see Figure 6.9). Strain contours are provided in Figure 6.19.

152
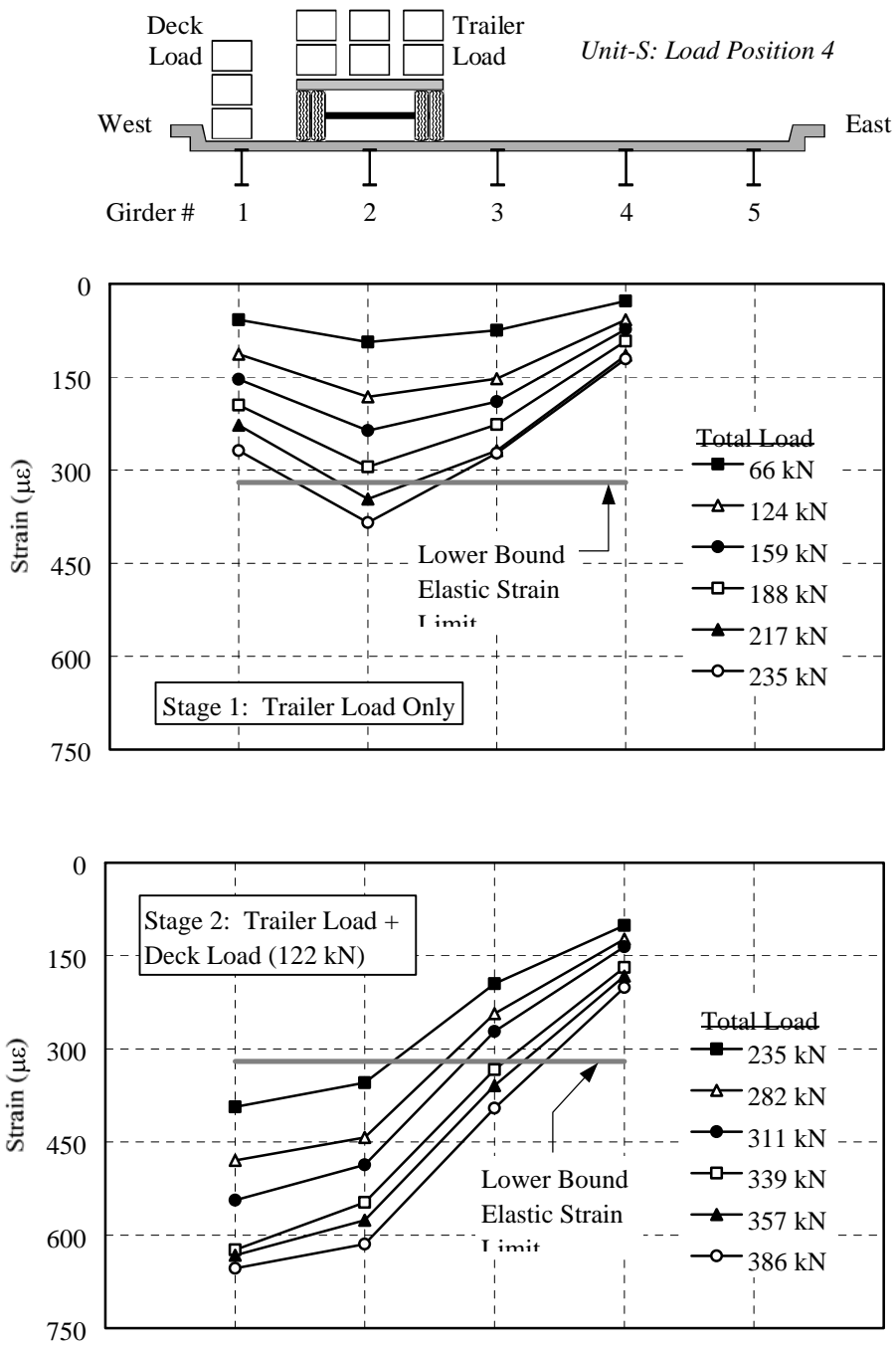
Figure 6.19 Bottom Flange Strains at Section c-c of Unit-S for Load Position 4.

The contours show a similar pattern to that recorded for Unit-N. Within each loading stage, the strains show a consistent increase with load. At the end of Stage 1, however, the bottom flange strains did not change for girders 3 and 4 in accordance with the changes for girders 1 and 2. The yielding of girder 1 at the end of Stage 1 in the negative moment region possibly caused this behavior since girder 1 would have experienced plastic hinge rotations at Section d-d. It appears that the reduced bending stiffness of girder 1 at Section d-d caused a longitudinal redistribution of load towards Section c-c, particularly to girders located on the loaded side of the bridge width (i.e., girders 1 and 2).

6.3.2   Girder Deflections

Figures 6.20 and 6.21 show the deflection response for girders 1 through 4 measured at Section c-c of Unit-N and Unit-S, respectively. On the horizontal axis, positive deflection represents downward movement of the girders. Problems occurred with the deflection transducer under girder 1 of Unit-N, which is why no data are shown for Stage 2. Deflections are also not shown at girder 5 of both units for the same reason. Based on the deflected shape of the cross-section, however, it appears that girder 5 would have had very small deflections, possibly in the upward direction. Therefore, since girders 1 through 4 resisted the majority of the load, the absence of data for girder 5 did not pose any major difficulties in evaluating the deflection response of the units. Contours of the measured vertical deflections of the girders across Section c-c are provided in Figures 6.22 and 6.23. Again, the vertical grid lines of the plots line up with the girder locations.

154
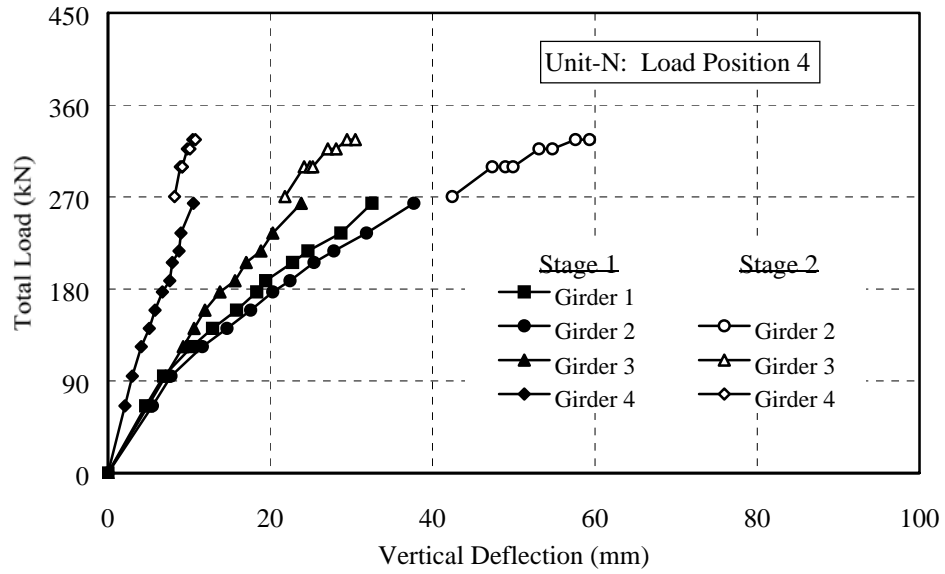
Figure 6.20 Vertical Deflection of Girders 1 through 4 at Section c-c of Unit-N.
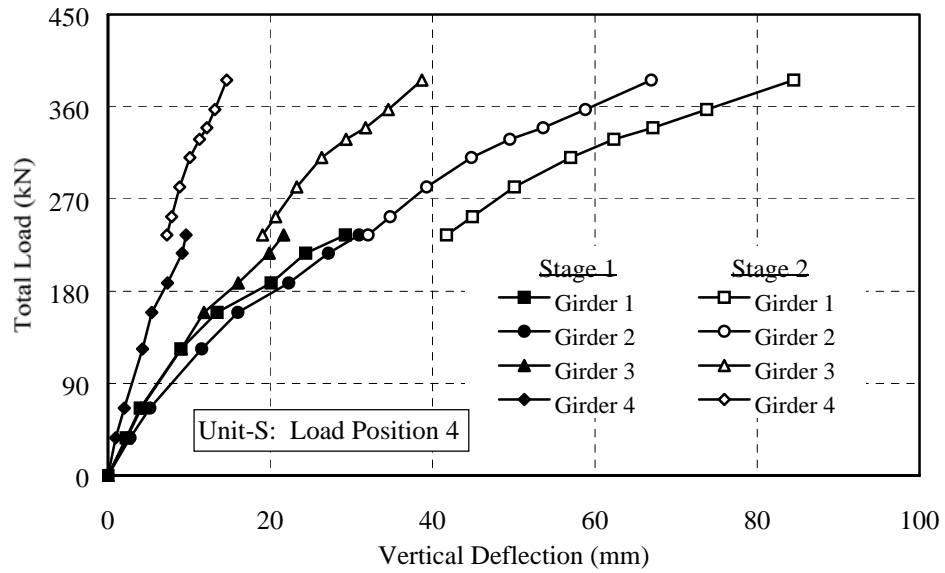
Figure 6.21 Vertical Deflection of Girders 1 through 4 at Section c-c of Unit-S.

155
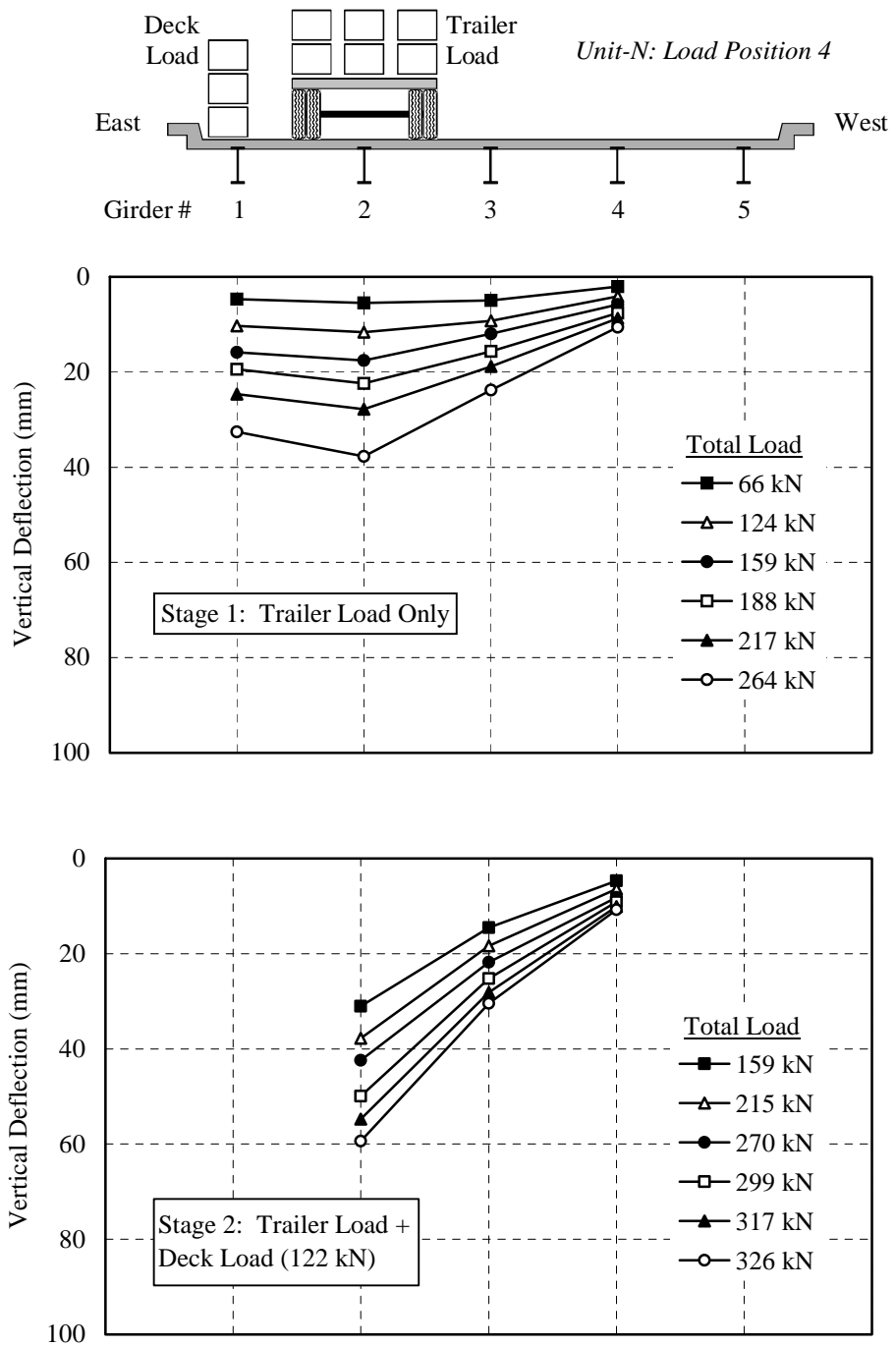
Figure 6.22 Vertical Deflections at Section c-c of Unit-N for Load Position 4.

156
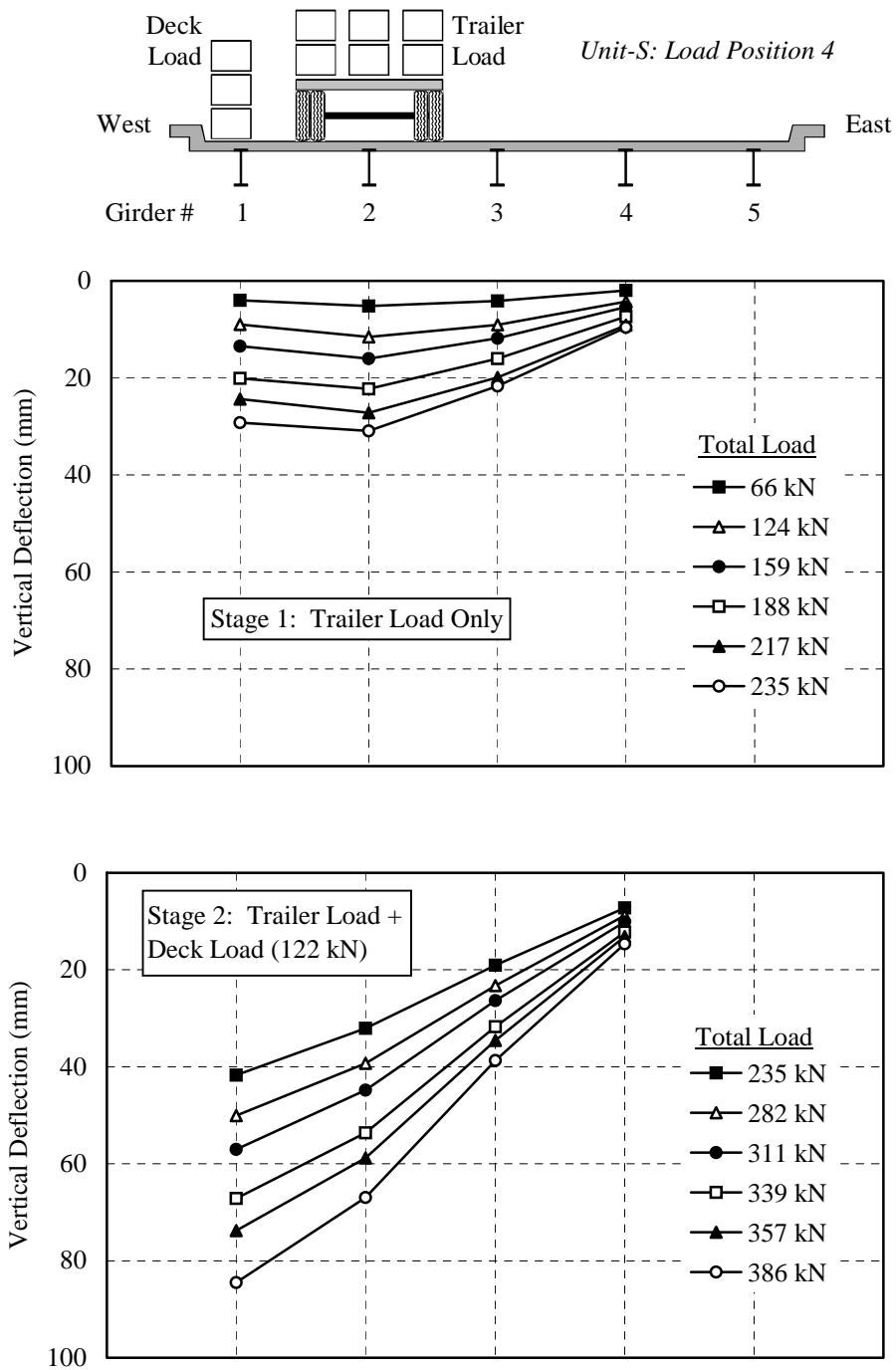
Figure 6.23 Vertical Deflections at Section c-c of Unit-S for Load Position 4.

157

The load-deflection response of the four girders shown in Figures 6.20 and 6.21 correlated well with the measured bottom flange strains presented in Section 6.3.1. Overall, girder 2 (directly below the axles of the trailer) deflected the most in load Stage 1, followed by girder 1 and then girder 3. It is interesting to note that girder 1 deflected more than girder 3 although the latter girder showed higher strains on the bottom flange (see Figures 6.8 and 6.9). The lower deflections and higher strains of girder 3 compared with girder 1 is possibly attributed to the differences in the moment-curvature relationship (i.e., bending stiffness) for each girder. As will be shown in Chapter 7, the bending stiffness varied from girder to girder because there was no definite connection between the girders and the slab.

Table 6.6 lists the measured deflections for the four girders at selected load levels during Stage 1. Beneath the deflection values, the ratios of the girder deflections relative to girder 2 are shown in parentheses, which increased for girder 1 and decreased for girders 3 and 4. These trends show that the deflected shape of the cross section became more distorted towards the loaded side of the deck as the load increased. The vertical deflections of the girders between Unit-N and Unit-S compared well in Stage 1. For the load range between 188 kN (42.3 kips) and 235 kN (52.8 kips), the percent difference in deflection ranged from 1 to 6 percent. For lower loads, the margin broadened from 1 to 20 percent. This increase occurred because there is more chance for error at the start of loading as the instrumentation and data acquisition systems set up and also because smaller deflections are measured. In addition, as load is first applied, initial slip at the girder-slab interface occurs and movement may release the support bearings

158

(previously locked by corrosion), the amount of which is likely different between bridge units.

Table 6.6 Vertical Deflections and Deflection Ratios for Girders 1 through 4 during Stage 1 Loading.

Bridge Unit	Girder #	Vertical Deflection (mm) versus Load (kN)					
		66 kN	124 kN	159 kN	188 kN	217 kN	235 kN
Unit-N	1	4.7 (0.85) *	10.3 (0.89)	15.8 (0.90)	19.5 (0.87)	24.7 (0.89)	28.7 (0.90)
	2	5.5	11.7	17.6	22.4	27.8	31.9
	3	4.9 (0.90)	9.3 (0.80)	12.0 (0.68)	15.6 (0.70)	18.9 (0.68)	20.3 (0.64)
	4	2.1 (0.38)	4.1 (0.35)	5.8 (0.33)	7.6 (0.34)	8.7 (0.31)	9.1 (0.28)
Unit-S	1	4.0 (0.77)	9.0 (0.78)	13.5 (0.84)	20.1 (0.90)	24.4 (0.90)	29.3 (0.94)
	2	5.2	11.5	16.0	22.3	27.2	31.0
	3	4.1 (0.80)	9.0 (0.78)	11.8 (0.74)	16.0 (0.72)	19.9 (0.73)	21.7 (0.70)
	4	2.0 (0.39)	4.3 (0.37)	5.4 (0.34)	7.3 (0.33)	9.1 (0.34)	9.6 (0.31)

* Deflection ratio relative to the deflection of girder 2.

The addition of the 122 kN (27.5 kips) deck load caused the cross-section to distort more towards the "loaded side" of the bridge width. Table 6.7 lists the girder deflections measured at Point B of Stage 1 and at Point E of Stage 2 (see Figure 6.7 and Table 6.2) with the loads about equal between the two stages. The table illustrates the shift in deflections caused by the addition of the deck load. As mentioned earlier, the deflection instrument beneath girder 1 of Unit-N failed during Stage 2. At Unit-S, the average deflection of the four girders was 23 mm (0.90 inches) at Point B and 25 mm (0.99 inches) at Point E, a difference of approximately 9%. A slightly better comparison may have been achieved had the

deflection of girder 5 been measured and included in the average. Nevertheless, the discrepancy of 9 percent showed that in spite of the deflection shifts that occurred in the girders at Stage 2, the average deflection across the cross section was reasonably close for the two loading stages.

Table 6.7 Girder Deflections Between Stage 1 and Stage 2 at Equal Loads.

| Bridge Unit | Girder # | Vertical Deflection (mm) | |
		Point B of Stage 1	Point E of Stage 2
Unit-N	1	33	
	2	38	42
	3	24	22
	4	11	8
Unit-S	1	29	42
	2	31	32
	3	22	19
	4	10	7

Note: At point B, the total loads equaled 264 kN (59.3 kips) for Unit-N and 235 kN (52.8 kips) for Unit-S.

As shown in Figures 6.20 and 6.21, discontinuities occurred in the load-deflection curves as a result of the deck load. Girder 1 showed a positive shift in deflection since the deck load was placed directly over the girder next to the curb. Consequently, the deflection of girder 1 exceeded the deflection of girder 2 in Stage 2 since the former girder carried more of the deck load. Only a slight difference in the measured deflections occurred at girder 2 between load stages. This strong agreement in deflection shows that the transverse load distribution to girder 2 was consistent between Stage 1 and Stage 2. That is, the girder carried about the same portion of the load whether it was placed directly over the girder (i.e., trailer load) or off to the side (i.e., deck load). Girders 3 and 4 both showed a reduction in deflection between loading stages which shows that they resisted a

160

smaller portion of the deck load than the trailer load. However, within each stage the deflected shape of the cross-section was consistent indicating no significant changes in load distribution.

6.3.3 Slip at Girder-Slab Interface

Slip measurements were taken to measure the relative movement between the girder top flanges and the deck. At Unit-N, slip was measured at all five girders at the end of the 18.3 m (60 ft) span supported at bearing 3 (see Figure 5.12). This location was chosen because the shear was highest and thus, it was expected that slip would be largest at this location. Figure 6.24 shows the slip measured at girders 1 through 3 during Stage 1 loading. No readings were taken during Stage 2 due to problems with the deflection transducers.
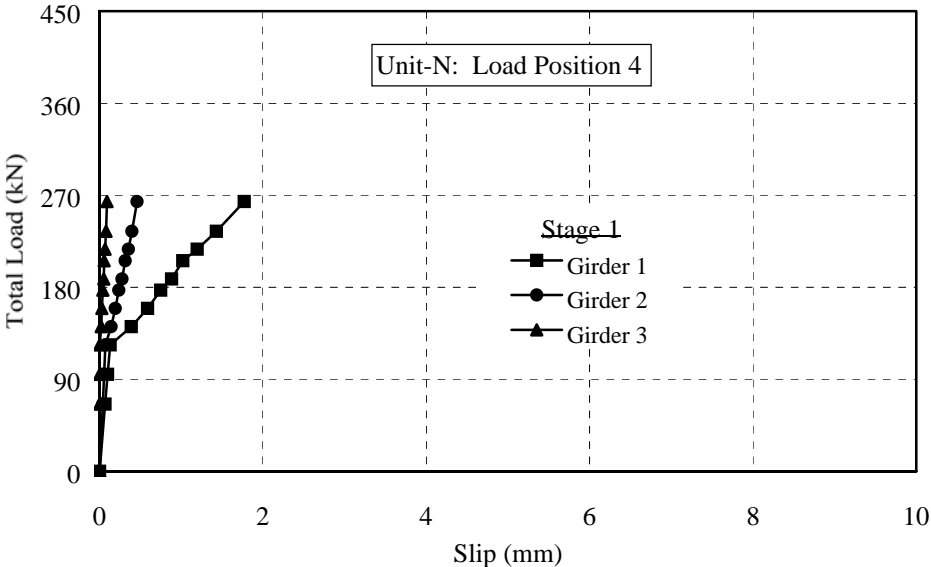
Figure 6.24 Girder-Slab Slip at Bearing 3 of Unit-N during Stage 1 Loading.

161

Positive slip values on the horizontal axis of the figure correspond to a northward movement of the deck slab relative to the girder top flange towards the abutment (see Figure 5.12). Measurements taken for girders 4 and 5 were excluded from the plot since the amount of slip was less than the accuracy of the deflection transducers. Slip measurements for girders 2 and 3 were also very small, not exceeding 0.5 mm (0.02 in). Significant amounts of slip occurred only at girder 1.

The small slip measurements shown in Figure 6.24 indicated that the movement of the slab was being restricted by some means other than just friction. A review of the design plans showed that the expansion bearing detail at bearing 3 consisted of an armored plate placed on the vertical face of the deck slab on either side of the joint. Steel plates were welded onto the armored plate and then bolted to angles welded to the girder top flanges. The armored plate was further anchored to the deck slab by means of hooked reinforcing bars (see Figure 4.9). This detail could have restrained the slab from sliding relative to the girders.

At Unit-S, two additional locations were instrumented along the length of girders 1 through 3. In addition to the location at the end of the span, slip was measured at mid-span and halfway between mid-span and the end. This scheme was chosen to determine the slip distribution over half the span length. It was expected that the slip distribution would provide a more meaningful insight into the girder-slab interaction than a single measurement at the end. Figure 6.25 shows the load-slip curves for the three girders at Section a-a (i.e., end of the span) and Section b-b (i.e., quarter span). Positive slip represents a southward movement of the deck towards the abutment (i.e., bearing 19 of Figure 5.18).

162
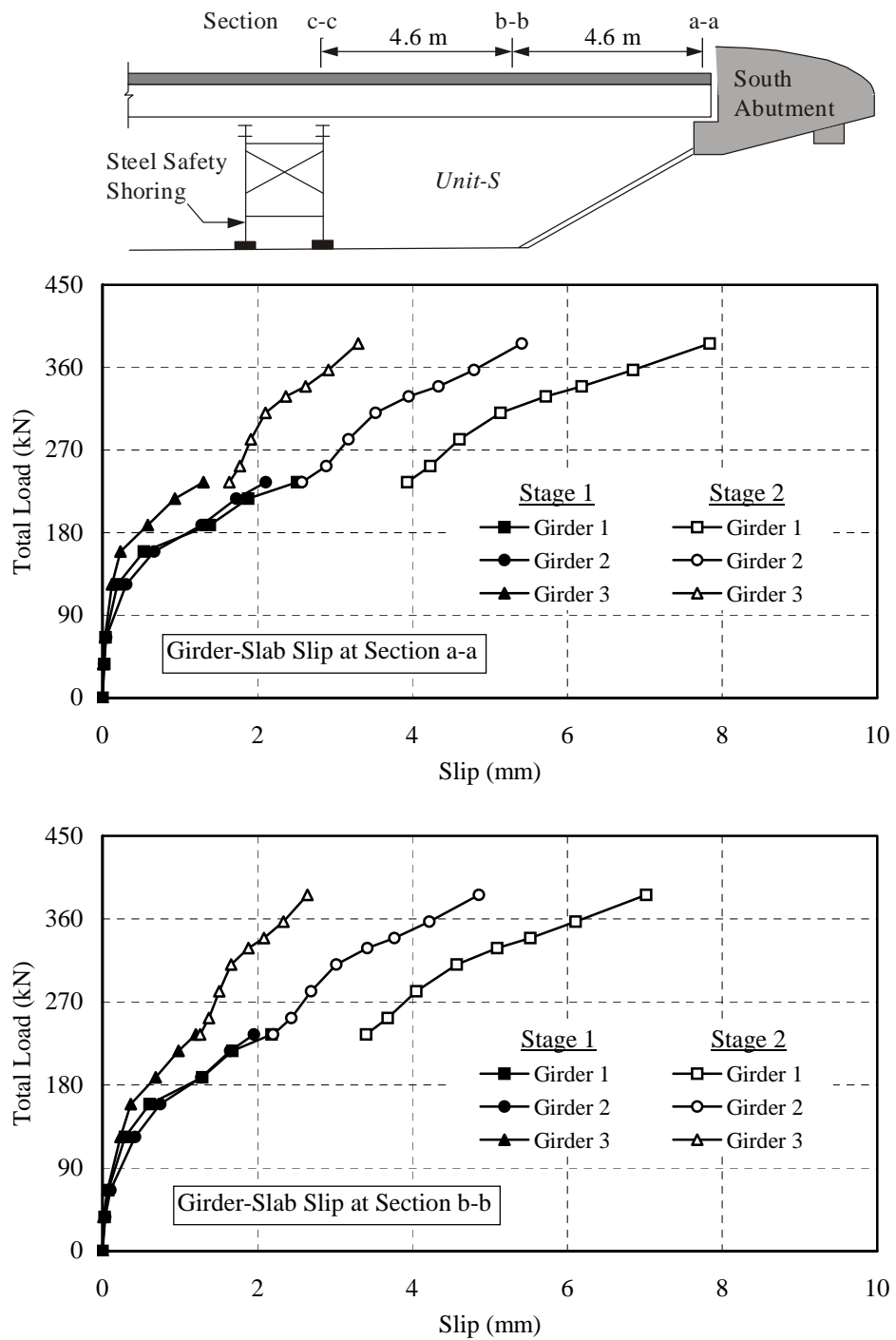
Figure 6.25 Girder-Slab Slip at Section a-a and b-b of Unit-S for Load Position 4.

163

As shown, there was a marked similarity between the girder-slip behavior of girders 1 through 3 at the end and the quarter span of the 18.3 m (60 ft) span of Unit-S. The slip response of girders 1 and 2 were nearly identical in Stage 1 at both Section a-a and Section b-b. In Stage 2, girders 2 and 3 essentially started at the same slip ending Stage 1. Girder 1, on the other hand, experienced a shift in slip of about 1.5 mm (0.06 in) when the deck load was added. This behavior seems appropriate considering that the barriers were placed directly over the girder therefore causing larger shear forces than the trailer load would have caused independently.

Figures 6.26 through 6.28 show the slip distribution along the length of girders 1, 2 and 3, respectfully. The horizontal axis of the figures corresponds to the transverse section at which the slip measurements were taken. A longitudinal view of each girder is provided at the top of each figure to show the three instrumented sections (i.e., Sections a-a, b-b, and c-c). As shown, the distribution of slip was rather uniform within each loading stage. The slip was largest at the end of each girder, however, it was nearly equal to the slip at quarter span. Virtually no slip was recorded at mid-span which was expected since it was the location of maximum deflection and thus, zero slope.

6.4   SUMMARY

The load-deformation behavior of Unit-N and Unit-S has been presented. It was shown that the two tested units exhibited similar behavior. In both tests, first yield of the units occurred at girder 1 in the negative moment region. Before

164

yielding occurred, girder 1 experienced a loss of partial composite action at Unit-S. At Unit-N, girder 1 maintained partial composite action throughout the full range of loading. Interior girders acted as non-composite sections in negative bending. Following first yield, girders 1 and 2 experienced strains in the inelastic range in the positive moment region. However, at this section the strain response of the girders caused difficulty in defining the start of yield although the strains were in the expected range of inelastic behavior. In general, the bottom flange strains and the deflections showed similar profiles across the positive moment region. Yielding was most obvious at Unit-S where higher loads were applied.

There was a significant similarity between the load-slip curves and the load-deflection curves of Unit-S. This similarity suggested that the non-linear girder response was mainly due to the relative movement between the top flanges and the concrete slab. It was also observed that the deformations of the girders did not return to zero after the trailer was removed. The unrecovered slip measurements indicated that the slab did not return to its original position relative to the girders. Shear forces must exist at the interface between the girders and slab which prevent the slab from returning to its original position. Consequently, these shear forces must cause residual strains and deflections in the girders.

Lower strains were measured in the exterior girder compared to the interior girder in the positive moment region due to the stiffening effects of the curb. In addition, partial composite action is likely higher in the exterior girders since they cannot be loaded as heavily as the interior girders. Both these factors are addressed in more detail in Chapter 7.
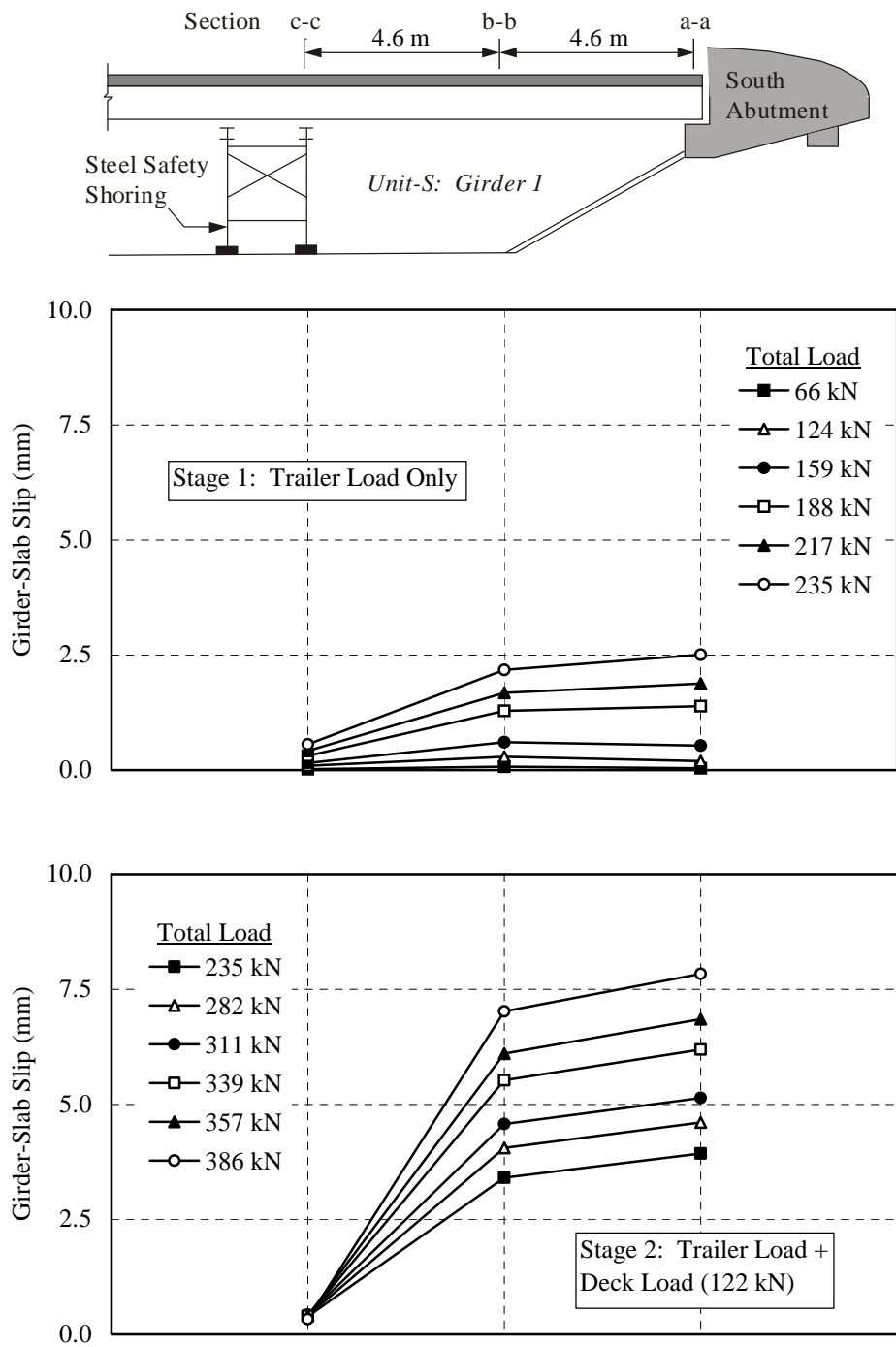
Figure 6.26 Slip Profile Along Length of Girder 1 at Unit-S for Load Position 4.

166
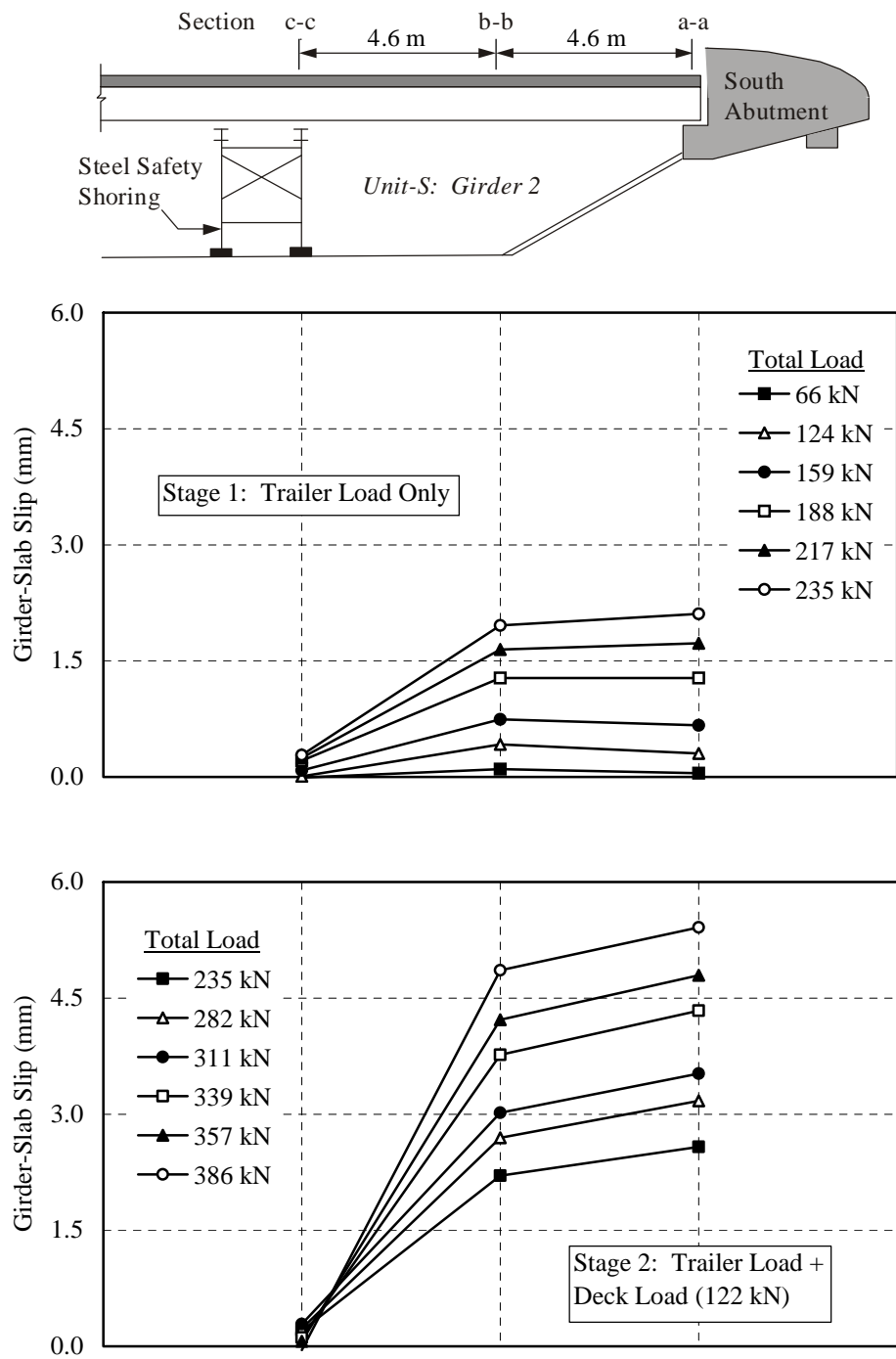
Figure 6.27 Slip Profile Along Length of Girder 2 at Unit-S for Load Position 4.
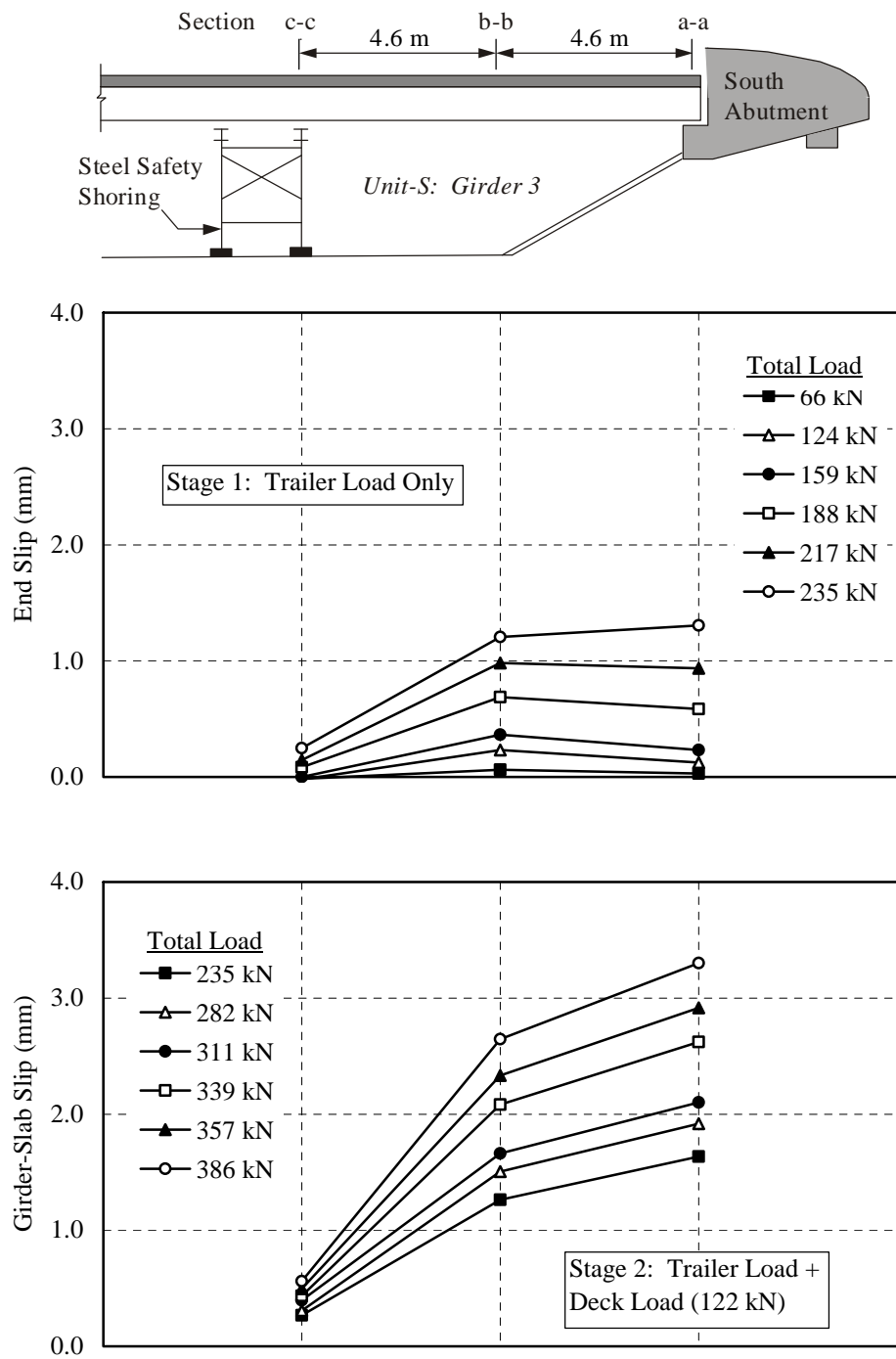
Figure 6.28 Slip Profile Along Length of Girder 3 at Unit-S for Load Position 4.

168

CHAPTER 7

EVALUATION OF BRIDGE RESPONSE

In this chapter, the lateral distribution of load to the girders and the partial composite action between the girders and the deck slab (plus the integral curbs) is investigated. Particular emphasis is given to evaluating the variations in load distribution and girder-slab interaction as the applied trailer loads are taken up to and beyond the initial yielding of the girders.

The analytical procedures for estimating the bending moments carried by the girders from the strains measured over the height of their cross sections are described in Section 7.1. The section also covers the techniques used for deriving experimental girder properties such as the neutral axis position, the moment of inertia, and the section modulus from the measured strains. Lastly, to illustrate the differences in behavior (i.e., section properties, stresses, deflections, etc.) between a non-composite, partial composite, and full composite section, an example analysis of a simply-supported girder is carried out. The example serves as a basic guideline for evaluating the behavior of the Marlin bridge units in subsequent sections of the chapter.

Experimental load distribution factors for the girders are derived from the test measurements in Section 7.2. Factors computed based on moments, strains, and deflections are compared to determine the type of measurement providing the most accurate indication of the girder distribution pattern. The section also covers

169

the relationships given in the AASHTO Standard (1996) and LRFD (1998) Bridge Design Specifications for live load distribution analysis.

In Section 7.3, the load distribution pattern of the bridge units is evaluated experimentally and compared with the empirical results determined in accordance with the AASHTO Specifications. In addition, the degree of partial composite action exhibited by the girders is examined by comparing experimentally derived section properties with those computed assuming full composite and non-composite girder behavior. Qualitative trends in the strain measurements are also used to explain the curb participation and to distinguish partial composite action from other factors of bridge behavior such as bearing restraint. An attempt is made to identify and assess the mechanisms of shear transfer that contribute to unintended partial composite action. Significant findings from the chapter are summarized in Section 7.4.

7.1   GIRDER SECTION ANALYSIS USING MEASURED STRAINS

7.1.1   Computation of Girder Moments

To compute the girder moments, the bridge cross section was divided into five girder sections. Figures 7.1 and 7.2 show the details of a typical interior and exterior girder in the positive moment region (i.e., Section c-c in Figures 5.12 and 5.18). The sections are similar at Section d-d (i.e., the negative moment region) with 8 mm x 127 mm cover plates added on the top and bottom flanges of the girders.
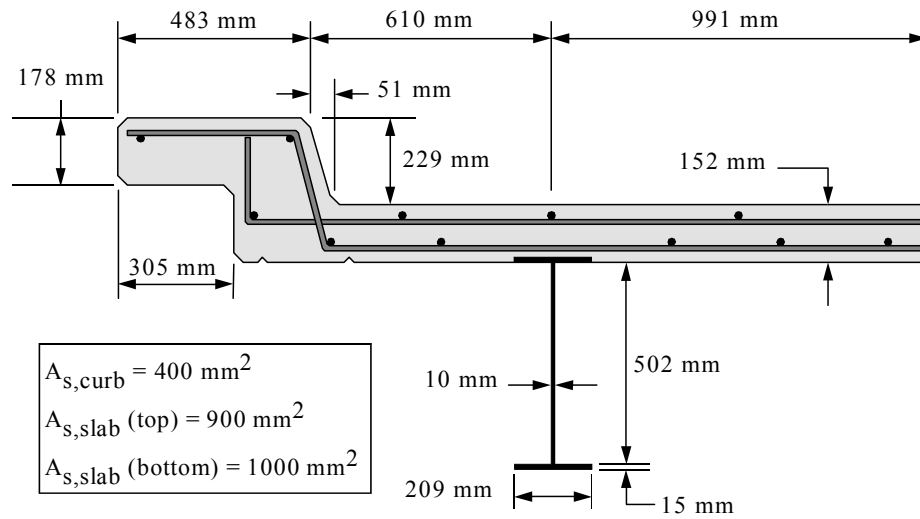
Figure 7.1 Details of a Typical Exterior Girder Section in the Positive Moment
Region of the Bridge Units.
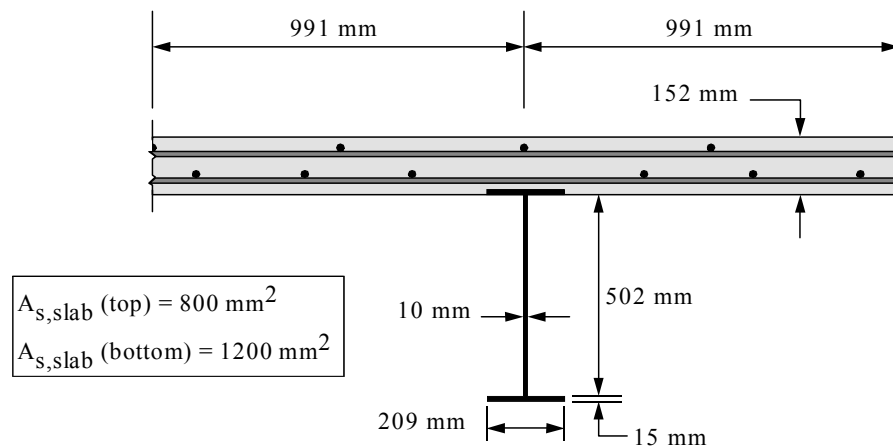
Figure 7.2 Details of a Typical Interior Girder Section in the Positive Moment
Region of the Bridge Units.

171

Interior girders (i.e., girders 2, 3, and 4) were given a tributary slab width equal to the girder spacing while exterior girders (i.e., girders 1 and 5) were assigned a width of half the girder spacing plus the overhanging portion of the slab (counting the curb). The curb was included as part of the tributary slab section for the exterior girder since it was cast monolithic with the deck slab. In addition, the transverse reinforcement in the slab extended into the curb, thus providing full continuity.

The added stiffness provided by the steel railing to the curb was ignored since the connection detail (see Figure 4.5) was not considered adequate to provide complete load transfer between the two elements. Also, the rail was not considered reliable under normal traffic conditions since vehicular impact could eliminate its ability to carry load. Previous research (Burdette and Goodpasture, 1988) also showed that the rail added less than 5 percent additional resistance. Thus, the potential benefits from the rail contribution were greatly outweighed by the difficulty of quantifying the effect of the rail connection detail and its damage by impact.

Table 7.1 lists the properties for the interior and exterior girder sections at Section c-c and Section d-d of the bridge units (see Figures 5.12 and 5.18). Since the bridge was built with no shear studs, the tributary slab section and the girder were treated as two independent beams bending about their respective neutral axes. The moment of inertia of the tributary slab section was computed assuming that the concrete was uncracked (i.e., gross section). There was a slight difference in the slab moment of inertia between Sections c-c and d-d due to the cover plates.

Table 7.1 Properties of Tributary Slab Section and Steel Girder at Section c-c and Section d-d.

Property	Section c-c		Section d-d	
	Interior Girder	Exterior Girder	Interior Girder	Exterior Girder
Girder-Slab Eccentricity, e	328 mm (12.9 in)	384 mm (15.1 in)	328 mm (12.9 in)	384 mm (15.1 in)
Girder Moment of Inertia, I_g	0.519×10^9 mm^4 (1247 in^4)	0.519×10^9 mm^4 (1247 in^4)	0.665×10^9 mm^4 (1599 in^4)	0.665×10^9 mm^4 (1599 in^4)
Girder Area, A_g	11200 mm^2 (17.36 in^2)	11200 mm^2 (17.36 in^2)	13220 mm^2 (20.49 in^2)	13220 mm^2 (20.49 in^2)
Slab Moment of Inertia, I_s	0.567×10^9 mm^4 (1363 in^4)	3.901×10^9 mm^4 (9372 in^4)	0.566×10^9 mm^4 (1359 in^4)	3.897×10^9 mm^4 (9363 in^4)

The cross-sectional area and moment of inertia listed in Table 7.1 for the girder (A_g and I_g) and the gross moment of inertia for the tributary slab section (I_s) were determined separately with respect to the center of gravity of each member. That is, the two bending members were not transformed into one material but rather left as two separate beams of different materials since there was no definite connection between the girders and the slab. For example, the gross moment of inertia for the tributary slab section for the interior girder was approximately equal to one-twelfth the tributary width times the slab thickness cubed. The longitudinal reinforcing steel in the tributary slab sections (see Figures 7.1 and 7.2) was also considered in computing the moment of inertia.

The girder-slab eccentricity, e, listed in Table 7.1 corresponds to the distance between the centroids of the girder and the tributary slab section. For an interior girder, the neutral axis of the slab section lies approximately at mid-depth. Accordingly, the eccentricity equals half the slab thickness plus half the depth of the girder web since the top flange was embedded into the bottom of the slab.

Due to the curb, the center of gravity for the slab section above the exterior girder was closer to the top of the slab. Consequently, there was an increase of 56 mm (2.20 in) in the girder-slab eccentricity compared to the interior girder section. The curb also increased the moment of inertia of the tributary slab section by 28 percent. For the girders, the addition of the cover plates in the negative moment region at Section d-d increased the moment of inertia by 28% and the cross-sectional area by 18%.

Table 7.2 lists the calculated section properties for the five girders without the cover plates. The table includes the bending moment of inertia, the location of the neutral axis, and the section modulus relative to the bottom flange assuming composite and non-composite action of the girders. The properties are based on the gross section for the slab and curbs (i.e., cracking was ignored).

Table 7.2 Theoretical Girder Section Properties.

Girder #	Composite Action		
	Moment of Inertia, I (10^9 mm^4)	Neutral Axis, y (mm)	Section Modulus, S (10^6 mm^3)
1 and 5	2.306	572	4.031
2, 3, and 4	1.505	516	2.917
Girder #	Non-Composite Action (including deck slab and curbs)		
	Moment of Inertia, I (10^9 mm^4)	Neutral Axis, y (mm)	Section Modulus, S (10^6 mm^3)
1 and 5	0.973 (0.42)*	266 (0.47)	3.663 (0.91)
2, 3, and 4	0.585 (0.39)	266 (0.52)	2.202 (0.75)
Girder #	Non-Composite Action (ignoring deck slab and curbs)		
	Moment of Inertia, I (10^9 mm^4)	Neutral Axis, y (mm)	Section Modulus, S (10^6 mm^3)
1 and 5	0.519 (0.23)	266 (0.47)	1.955 (0.48)
2, 3, and 4	0.519 (0.34)	266 (0.52)	1.955 (0.67)

∗   Ratio with respect to theoretical section properties for a composite girder.

174

For the case of non-composite behavior, properties were computed first including the bending stiffness of the deck slab and curbs. Subsequently, the deck slab and curbs were ignored in which case the section properties corresponded to those of the bare girder. A ratio is given in parentheses next to the values for the non-composite properties, which represents the percentage with respect to the properties of a fully composite section. Values reported for girders 1 and 5 (i.e., the exterior girders) include the participation of the curbs. For girders 2 through 4 (i.e., the interior girders), the tributary width includes only the deck slab.

The flexural stiffness of the tributary slab section and the girder was approximated as the product of the moments of inertia listed in Table 7.1 and the modulus of elasticity of each material. Hence, the bending stiffness for the girders was computed as $E_{stl}I_g$ where E_{stl} is the modulus of elasticity for steel, which was assumed to be 200 GPa (29000 ksi). Similarly, the tributary slab sections were given a bending stiffness equal to $(E_{conc}I_s)$ where E_{conc} is the modulus of elasticity for concrete. Section 8.5.1 of the ACI Building Code (1995) provides the following relationship for the elastic modulus of normal weight concrete

$$E_{conc} = 4700\sqrt{f_c'} \ (MPa) \eqno(7.1)$$

where f_c' equals the compressive strength of the deck concrete (in units of MPa). As described in Section 4.3 of Chapter 4, the concrete compressive strength was estimated from core testing to be 24.1 MPa (3500 psi) resulting in a modulus of elasticity of 23.2 GPa (3372 ksi) for the tributary slab sections.

175

In order to estimate the moments in the girders from the measured strains, a few assumptions were necessary since there was no mechanical connection (i.e., shear studs) to prevent the slab from slipping relative to the girder top flanges. The following four assumptions were made in order to analyze the girder sections (adopted from Baldwin, 1965).

1. The distribution of strain is linear over the depth of the girder and the height of the tributary slab section. Plane sections are assumed to remain plane in both the girder and the tributary slab section individually. However, a strain discontinuity is allowed at the girder-slab interface meaning plane sections do not remain plane over the entire depth of the girder section (i.e., from the bottom fiber of the girder to the top fiber of the slab section). This assumption also ignores the effects of torsion and shear deformation.

2. The flexural curvature of the steel girder is equal to the curvature of the slab section. Under this assumption, the strain gradient over the height of the tributary slab section is assumed to be parallel to the profile over the girder depth.

3. The slab section remains in contact with the girder top flange. This statement assumes that the tributary slab section does not separate vertically from the girders. However, the slab may slide longitudinally relative to the girder top flanges.

4. There is no net axial force at the girder cross-section. Hence, any axial force in the slab is assumed to be equal and opposite of the force acting on the girder. In both members, the axial forces are assumed to act at the centroids.

Although there was no definite connection, some degree of partial composite action was expected in the girders of the Marlin bridges due to the friction caused by the weight of the deck slab bearing down on the top flanges of the girders. Mechanical interlock was another possible mode of shear transfer at the girder-slab interface since the top flanges of the girders were embedded into the bottom of the slab.

Based on the four assumptions given above, Figures 7.3 and 7.4 show a visual representation of the strain distribution over the depth of an interior and exterior girder section under positive bending. Partial interaction between the girders and the deck slab was assumed. At the plane of contact between the slab and the girder top flanges, there is a strain discontinuity signifying the relative slip between the two members. The amount of slip and thus, degree of partial composite action depends on the strength of the shear restraint provided by the inadvertent effects of friction and mechanical interlock.

The total flexural moment resisted by a partial composite girder may be divided into three components: the moment in the steel girder (M_g), the moment in the tributary slab section (M_s), and the moment couple due to the equal and opposite axial forces acting on the girder and the slab section (M_c). The latter moment equals the axial force (P) times the distance between the neutral axes of the girder and the slab section, defined as the girder-slab eccentricity (e). Complementary to the axial forces, the moments in the steel girder and the tributary slab section are also assumed to act at the center of gravity of the members.

As shown in Figures 7.3 and 7.4, measured girder strains may be divided into the discrete strain components caused by the combined loading of bending moment and axial force, ε_f and ε_a. Under pure flexure, the strains at the top and bottom flange of the girder are equal with opposite signs. A positive sign indicates tension and a negative sign indicates compression. At the neutral axis, the flexural strain is zero. Hence, strains measured at mid-height of the web are caused solely

by the axial force. This force causes a uniform strain distribution over the depth of the girder and is largest under the condition of full composite action when there is complete transfer of the shear forces at the girder-slab interface and thus, no relative slip between the girder top flange and the slab. If the plane of contact between the girder and the slab is assumed to be frictionless (i.e., non-composite action), then there is no shear transfer at the interface and therefore, no axial force.
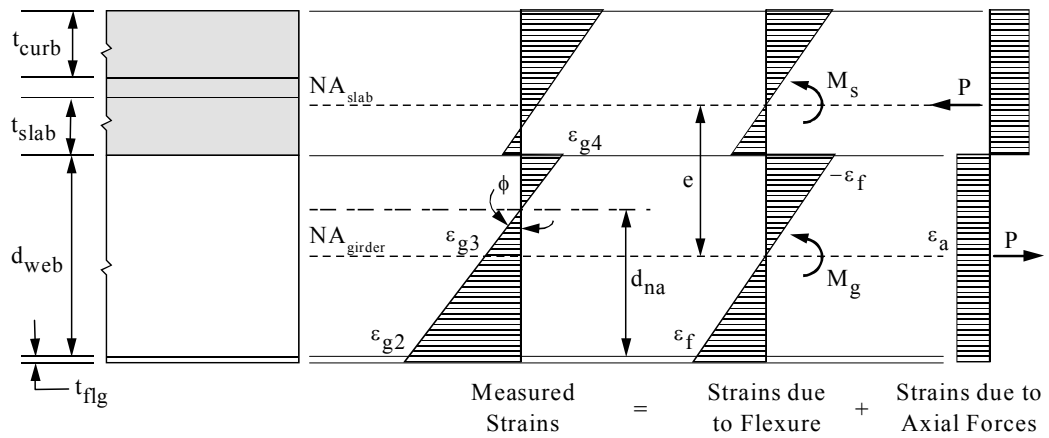
Figure 7.3 Assumed Strain Distribution for a Typical Exterior Girder Section.
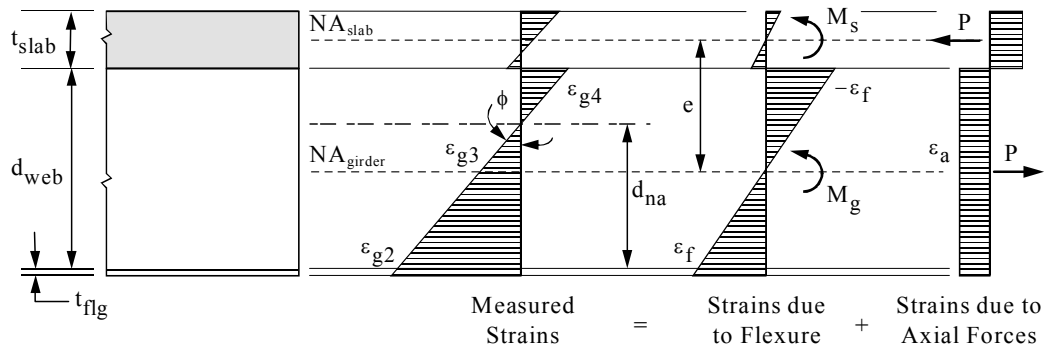
Figure 7.4 Assumed Strain Distribution for a Typical Interior Girder Section.

178

The strain equilibrium relationships at the three gage locations on the girder are written as

$$\varepsilon_{g2} = \varepsilon_f + \varepsilon_a \qquad (7.2)$$

$$\varepsilon_{g3} = \varepsilon_a \qquad (7.3)$$

$$\varepsilon_{g4} = -\varepsilon_f + \varepsilon_a \qquad (7.4)$$

where ε_{g2}, ε_{g3}, and ε_{g4} represent the measured strains on the topside of the bottom flange, at mid-depth of the web, and on the underside of the top flange of the steel girder. The flexural and axial strain components may be determined by solving any pair of the Equations (7.2) through (7.4). That is, two strain readings over the girder depth are needed in order to determine the flexural and axial strain components. The three strain combinations that may be used are the top and bottom flange, the mid-web and bottom flange, and the top flange and mid-web strain readings. Since the maximum strain in the positive moment region occurs on the bottom flange, the two logical combinations were the bottom flange strain reading paired with either the top flange or the mid-web strain reading.

By solving Equations (7.2) and (7.4), the pure bending and axial strains are both functions of the strains on the top and bottom flange, ε_{g2} and ε_{g4}.

$$\varepsilon_f = 0.5(\varepsilon_{g2} - \varepsilon_{g4}) \qquad (7.5)$$

$$\varepsilon_a = 0.5(\varepsilon_{g2} + \varepsilon_{g4}) \qquad (7.6)$$

Similarly, the bending and axial strains may be expressed in terms of the strains measured at the mid-height and bottom flange of the girder, ε_{g2} and ε_{g3}. Solving Equations (7.3) and (7.4) results in the relationships

$$\varepsilon_f = \varepsilon_{g2} - \varepsilon_{g3} \tag{7.7}$$

$$\varepsilon_a = \varepsilon_{g3} \tag{7.8}$$

Now, using the bending and axial strains from either Equations (7.5) and (7.6) or (7.7) and (7.8), the moment in the steel girder, M_g, is computed as

$$M_g = E_{stl}\varepsilon_f S_f \tag{7.9}$$

where S_f equals the section modulus of the steel girder with respect to the top of the bottom flange. Applying the assumption of equal curvatures between the tributary slab section and the girder, the moment taken by the slab section, M_s, may be estimated as

$$M_s = M_g\left(\frac{E_{conc}I_s}{E_{stl}I_g}\right) \tag{7.10}$$

Equation (7.10) assumes that the tributary slab section is uncracked. The final term of the total moment corresponds to the moment couple caused by the equal and opposite axial forces acting on the girder and the slab section. As mentioned earlier, the axial force in the concrete slab section is assumed to be equal to the axial force in the girder. Thus, the moment couple, M_c, is determined as

$$M_c = Pe = \left(E_{stl}\varepsilon_a A_g\right)e \tag{7.11}$$

180

Summation of the three moment terms produces the total moment carried by the girder section

$$M_T = M_g + M_s + M_c \tag{7.12}$$

7.1.2 Computation of Girder Section Properties

Bending strains recorded over the girder height may also be used to estimate girder section properties. For a partial composite section with varying girder-slab interaction, the neutral axis will reside at some location between the neutral axis for a fully composite and non-composite section. Using the measured strains on the top and bottom flanges, the neutral axis location with respect to the top face of the bottom flange, d_{na}, is determined by similar triangles as

$$\frac{\varepsilon_{g2} - \varepsilon_{g4}}{d_{web}} = \frac{\varepsilon_{g2}}{d_{na}} \quad \Rightarrow \quad d_{na} = \frac{\varepsilon_{g2} d_{web}}{\varepsilon_{g2} - \varepsilon_{g4}} \tag{7.13}$$

where d_{web} is the depth of the girder web. Similarly, the neutral axis position can be determined using the bottom flange and mid-web strain readings as follows

$$\frac{\varepsilon_{g2} - \varepsilon_{g3}}{d_{web} / 2} = \frac{\varepsilon_{g2}}{d_{na}} \quad \Rightarrow \quad d_{na} = \frac{\varepsilon_{g2} d_{web}}{2(\varepsilon_{g2} - \varepsilon_{g3})} \tag{7.14}$$

The neutral axis position with respect to the bottom face of the girder is then

$$y_{na} = d_{na} + t_{flg} + t_{cover} \tag{7.15}$$

where t_{flg} and t_{cover} represent the thickness of the girder flange and the cover plate, respectively. The t_{cover} term does not apply in the positive moment region since

181

cover plates were installed on the exterior face of both the top and bottom girder flanges in the negative moment region only.

With the neutral axis located, the bending curvature of the girder may be determined with the following equation assuming small deflections

$$\tan\phi \approx \phi = \frac{\varepsilon_{g2}}{d_{na}} \tag{7.16}$$

The slope of the moment-curvature diagram represents the effective stiffness (i.e., EI) of the girder. Hence, the computed curvature, total moment, and neutral axis position of the girder section may then be used to approximate the moment of inertia, $I_{partial}$, and section modulus, $S_{partial}$, of the partial composite steel girder section using the relationships

$$\phi = \frac{M_T}{E_{stl}I_{partial}} \quad \Rightarrow \quad I_{partial} = \frac{M_T}{\phi E_{stl}} \tag{7.17}$$

and

$$S_{partial} = \frac{I_{partial}}{y_{na}} \tag{7.18}$$

There are a variety of ways to evaluate the degree of partial composite action in the girders of a bridge built with no shear connectors. One approach is to compare the section properties for the partial composite girder that are derived experimentally with the section properties for a composite and non-composite section. The latter properties represent an upper and lower bound to stiffness and can be determined based solely on the geometry of the girder section. For a

182

partial composite girder, the section properties must be determined experimentally since the girder-slab interaction is unknown.

7.1.3 Levels of Girder-Slab Interaction

There are three terms used to refer to the degree of interaction between the deck and girders of a slab-on-girder bridge: non-composite, partial composite, and full composite action. To demonstrate these three cases, consider the simple-supported girder section shown in Figure 7.5 of length L under a concentrated load P at mid-span. A cross section of the girder is given on the right side of the figure with dimensions and properties as defined in Section 7.1.1. The following paragraphs provide a general description of the three levels of interaction. An illustrative example is then conducted to highlight in more detail the major differences in behavior between the three cases.

(a) Non-Composite Action

(b) Partial Composite Action *

(c) Full Composite Action
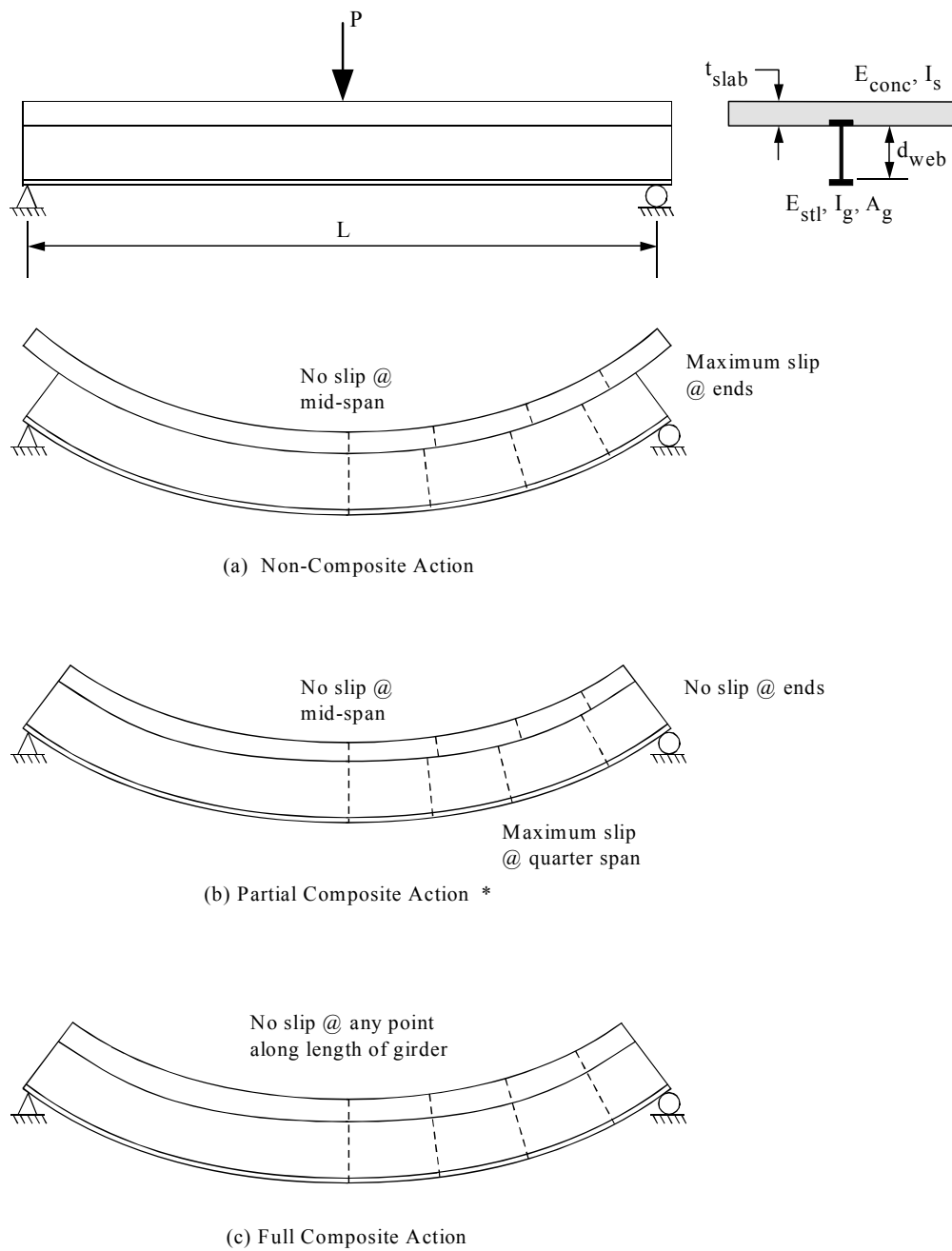
* Assuming only the ends of the girders and the deck slab are connected.

Figure 7.5 Varying Levels of Girder-Slab Interaction for a Simple Beam Subjected to a Concentrated Load at Midspan.

184

<u>Non-Composite Action</u>

Non-composite action refers to the condition where there is no interaction between the girders and the slab. The effective moment of inertia of a non-composite section equals

$$I_{eff} = I_g + \frac{I_s}{n} \tag{7.19}$$

where n is the modular ratio, (E_{stl} / E_{conc}). Shear forces are not transferred between the two members along their contact surface. As a result, the bottom of the slab slides freely with respect to the girder top flange in the longitudinal direction. Applied loads are distributed to the girder and slab in proportion to their individual flexural stiffness (i.e., $E_{stl}I_g$ and $E_{conc}I_s$) according to Equations (7.9) and (7.10).

In Equation (7.12), the moment couple term is zero since there are no axial forces in the girder and the slab. Since the slab and girder act independently, each bending about their respective neutral axes (i.e., mid-height of the member), the stresses on the top and bottom of each member are equal and opposite. Thus, the moment in the slab causes the bottom fiber to elongate while the moment in the bare girder causes the top fiber to shorten. The difference in the deformed chord lengths represents the interface slip, which is largest at the ends of the girder as shown in Figure 7.5(a).

<u>Partial Composite Action</u>

Partial composite action represents the condition when shear resistance does exist at the girder-slab interface, however, the connection does not prevent

slip along the entire length of the girder section. The amount of slip is reduced therefore increasing the effective girder stiffness compared to a non-composite section.

An example of a partial composite section is one where the girder and slab are connected only at their ends as shown in Figure 7.5(b). In this case, the analysis of the girder section requires slip compatibility to be enforced at the ends of the girder. However, slip may occur at intermediate points between mid-span and the end. Later in this section, it is shown that the maximum slip occurs at the quarter points of the span. In addition to modifying the slip distribution over the length of the girder, a moment couple (i.e., the third term in Equation (7.12)) is produced due to the horizontal shear forces that develop to prevent end slip.

Composite Action

In a composite girder section, the girder and the slab are joined along the entire length. As a result, the girder and slab act as a single unit and there is no slip at any point along the girder-slab interface (i.e., plane sections remain plane over the depth of the girder section) as illustrated in Figure 7.5(c). The no slip condition will be appropriate until the shear strength at the interface is reached. The complete transfer of the interface shear forces causes the strain profile to be continuous over the height of the section from the bottom of the girder to the top of slab. In practice, strain compatibility is usually enforced with the use of shear connectors that are welded to the top flange and protrude into the bottom of the deck slab.

To determine the flexural stiffness of a composite girder section, the slab section is transformed into an equivalent section of steel by reducing the width of the slab by the modular ratio. Total moment in a composite girder equals the summation of the girder moment, the slab moment, and the moment couple from the axial force.

Illustrative Example of Girder Section Behavior

Table 7.3 summarizes the results of an analysis conducted for the three levels of interaction just discussed. For purposes of the illustrative example, the magnitude of the concentrated load and the length of the girder of Figure 7.5 were assumed to be 44.5 kN (10 kips) and 15.2 m (50 ft), respectively, producing a mid-span moment of 169 kN-m (125 kip-ft). In addition, the properties listed in Table 7.1 for an interior girder section were used.

Table 7.3 provides a direct comparison of the neutral axis position, bending stress, vertical deflection, and maximum slip as affected by the varying stiffness of the girder sections. The table also shows the magnitude of the normal force, the girder moment, the slab moment, and the moment couple for the three conditions. Based on the table, the following changes were observed as the connection between the girder and the slab was increased. The observations were made with respect to the response of the non-composite girder section.

187

Table 7.3 Maximum Stress, Deflection, and Slip for Varying Levels of Girder-Slab Interaction for an Interior Girder Section.

Variable	Degree of Girder-Slab Interaction		
	Non-Composite Action	Partial Composite Action °	Full Composite Action
Bottom Flange Stress @ Midspan	77.0 MPa (11.2 ksi)	70.1 MPa (10.2 ksi)	58.1 MPa (8.43 ksi)
Top Flange Stress @ Midspan •	-72.7 MPa (-10.5 ksi)	-46.9 MPa (-6.80 ksi)	-0.07 MPa (-0.01 ksi)
Bottom of Slab Stress @ Midspan	2.56 MPa (0.372 ksi)	1.63 MPa (0.237 ksi)	-0.007 MPa (-0.001 ksi)
Top of Slab Stress @ Midspan	-2.56 MPa (-0.372 ksi)	-2.39 MPa (-0.346 ksi)	-2.00 MPa (-0.290 ksi)
Vertical Deflection @ Midspan	28.0 mm (1.10 in)	22.0 mm (0.864 in)	11.7 mm (0.459 in)
Maximum Relative Slip ▪	1.80 mm (0.071 in)	0.46 mm (0.018 in)	0
Bottom Flange Stress @ Ends •	0	-4.41 MPa (-0.640 ksi)	0
Top Flange Stress @ Ends •	0	23.7 MPa (3.44 ksi)	0
Maximum Normal Force in Slab and Girder	0	113 kN (25.3 kips)	303 kN (68.0 kips)
Girder Neutral Axis Position *	266 mm (10.5 in)	310 mm (12.2 in)	516 mm (20.3 in)
Effective Girder Stiffness	0.585×10^9 mm^4 (1405 in^4)	0.747×10^9 mm^4 (1795 in^4)	1.506×10^9 mm^4 (3617 in^4)
Girder Moment	150 kN-m (111 k-ft)	118 kN-m (86.8 k-ft)	62.5 kN-m (46.1 k-ft)
Slab Moment	19.1 kN-m (14.1 k-ft)	14.9 kN-m (11.0 k-ft)	7.9 kN-m (5.83 k-ft)
Moment Couple	0	36.9 kN-m (27.2 k-ft)	99.0 kN-m (73.0 k-ft)

°   Slip restrained only at the ends of the girder.
•   Stresses reported are at the bottom face of the flanges.
▪   Maximum slip occurred at the ends of the girder for non-composite action and at the quarter span for partial composite action (see Figure 7.5).
*   The reported neutral axis position is with respect to the bottom of the girder.

1. The neutral axis shifts to a higher vertical position on the depth of the girder. By preventing slip at the ends of the girder and slab, the neutral axis moved up a distance of 44.3 mm (1.74 in) from the mid-web of the girder, approximately 8.3% of the girder depth. When the section was made completely composite, the neutral axis shifted upward 251 mm (9.86 in) to the top of the girder web. This distance was about 47.2% of the girder height.

2. The shear force at the girder-slab interface (i.e., the normal force in the slab and girder) increases. The force is largest under full composite action and zero when there was no connection (i.e., non-composite action). For a partial composite section connected only at the ends, the axial force is 37.2% of the force that developed under full composite action.

3. Due to the increase in the normal force, the moment couple also increases. Hence, the moment couple represents a more significant portion of the total moment in the girder section as the interaction between the girder and slab improves. Conversely, the individual contributions of moment from the bare girder and the slab section become less significant. A percent breakdown of the total moment in the girder section is provided in Table 7.4.

Table 7.4 Percentage Breakdown of Total Moment.

Moment Component	Percent of Total Moment (%)		
	Non-Composite Action	Partial Composite Action	Full Composite Action
Girder Moment	89	69	37
Slab Moment	11	9	5
Moment Couple	0	22	58

4. The effective bending stiffness (i.e., moment of inertia) increases, which reduces the vertical deflection of the girder section at mid-span. Flexural stresses on the girder flanges and on the top and bottom of the slab at mid-span also decreases. Connecting the girder and slab at the ends increases the effective moment of inertia by 28% which causes a 9% decrease in stress on the girder bottom flange and a 22% decrease in mid-span deflection. When the girder section is considered fully composite, the moment of inertia increases by a factor of 2.6 which reduces the bottom flange stress and deflection at mid-span by 24 and 58 percent, respectively.

5. Bending stresses are produced over the girder height at the ends of a partial composite section. The stresses are caused by the shear force shown in Figure 7.6(a) needed to keep the girder from slipping relative to the slab at the ends. This horizontal force (designated as H) acts as a compressive load on the bottom of the slab and as a tensile load on the top of the girder as shown in Figure 7.6(b). When transferred to the centroid of the girder, the tensile load induces both an axial tension and negative bending moment equal to the axial load times half the depth of the girder web. This combined loading causes a tensile stress on the top flange that exceeds the compressive stress produced on the bottom flange as shown qualitatively in Figure 7.6(c). There are no bending stresses at the ends of the girder for a fully composite or non-composite section.

(a) (b) (c)

H

$Ht_s/2$

H

Slip

H

$Hd_{web}/2$

+

−
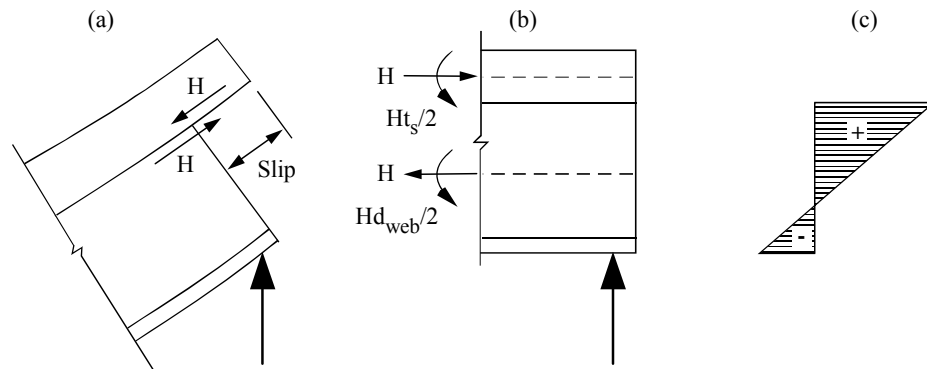
Figure 7.6 Strain Compatibility at the Ends of a Partial Composite Section.

6. The amount of slip between the girder and tributary slab section decreases. There is no slip at any point along the girder span for a fully composite section. For the cases of non-composite and partial composite behavior, the slip distribution starts at zero at mid-span and varies parabolically over half the length of the girder as shown in Figure 7.7. Maximum slip occurs at the ends of the non-composite section and at the quarter points of the span of the partial composite section. In addition, restraining slip at the ends reduces the maximum slip by a factor of 4.

This example illustrated the positive effects that partial composite action can have on the stresses and deflections of a girder section. For a bridge built as non-composite, any partial composite action that develops in the girders will cause measured stresses and deflections to be lower than expected. Thus, because of the potential benefits of partial composite action to the capacity of the bridge, the procedures given in Sections 7.1.1 and 7.1.2 for quantifying this phenomenon are critical.
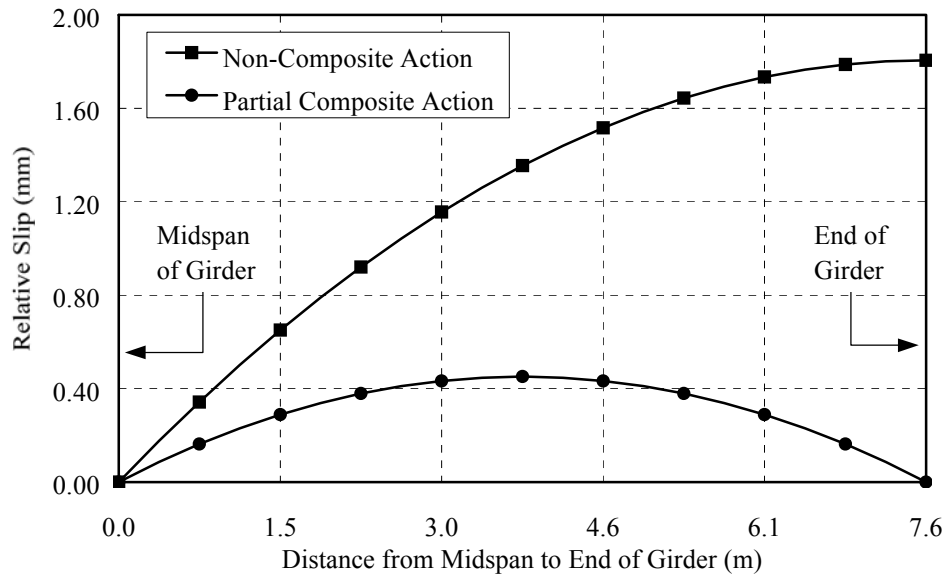
Figure 7.7 Slip Distribution between Girder and Slab for Non-Composite and
Partial Composite Action (Slip Restricted at Ends only).

7.2   EVALUATION OF LATERAL LOAD DISTRIBUTION

A load distribution study was performed using the measurements from both the (a) increasing trailer loads and the (b) constant dump truck loads. The former readings provided the information needed for evaluating shifts in lateral distribution as applied loads were taken up to and beyond initial yielding of the girders. The latter readings, which were taken between trailer load increments, were used in a companion study (presented in Chapter 8) to monitor the behavior of the bridge units under normal traffic loads after each stage of overload.

192

7.2.1   Experimental Girder Distribution

The share of the live load (i.e., trailer load or dump truck load) carried by each of the five girders was estimated experimentally by dividing the moment in each girder by the summation of girder moments across the bridge cross-section. Hence,

$$LDF_{M,i} = \frac{M_{T,i}}{\sum\limits_{i=1}^{5} M_{T,i}} \tag{7.20}$$

where $M_{T,i}$ represents the total bending moment (as computed by the procedure outlined in Section 7.1.1) and $LDF_{M,i}$ is the load distribution factor for the ith girder. As discussed in Chapter 5, strain gages were installed on all the girders in the positive and negative moment region (i.e., Sections c-c and d-d of Figures 5.12 and 5.18) of both test units. Gaging all five girders was necessary in order to determine the total bending moment across the transverse section of the bridge units and thus, the lateral distribution factors.   This instrumentation plan was needed especially during the service load tests when the dump trucks were driven down the middle of the roadway. For this load case, all five girders carried a significant amount of the load. Had strain gages not been installed on each girder, the total bending moment across the bridge cross-section would have been underestimated thus leading to an overestimation of the distribution ratios computed with Equation (7.20). In some load situations, however, the girder located most remote from the applied load does not contribute much (if any) to the total bending moment across the bridge cross section. For example, when the

dump trucks were driven along the first transverse path (i.e., 2 feet from the curb), the exterior girder on the unloaded side of the bridge deck (i.e., girder 5) carried a very small portion of the applied load. Consequently, the sum of the bending moments in girders 1 through 4 amounts to close to 100 percent of the total bridge moment, in which case the distribution factors may be computed accurately without accounting for girder 5.

Experimental distribution factors may also be estimated directly using the measured bottom flange strains, ε_i, of the girders. Stallings and Yoo (1993) proposed one such approach with the equation

$$\text{LDF}_{\varepsilon,i} = \frac{\varepsilon_i w_{S,i}}{\sum\limits_{i=1}^{j} \varepsilon_i w_{S,i}} \qquad (7.21)$$

where $w_{S,i}$ is the ratio of the section modulus between the ith girder and a typical interior girder while j represents the number of girders. The weighting factor for the section moduli is applied as an approximation to the bending moment in the girders. Figure 7.8 shows the load distribution factors computed for Unit-S in the positive moment region based on moments (Eq. 7.20) and strains (Eq. 7.21). The distribution factors were evaluated for a trailer load of 217 kN (48.8 kips) at load position 4 (see Figure 5.21). In the figure, the portion of the trailer load carried by girders 1 through 5 is plotted on the vertical scale versus the girder number on the horizontal scale.

194
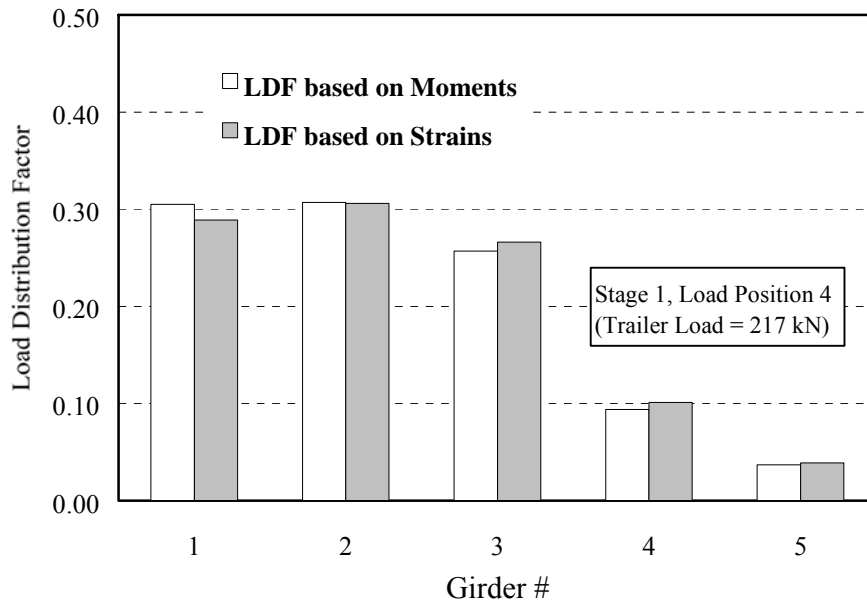
Figure 7.8 Load Distribution at Section c-c for (a) Unit-N and (b) Unit-S based
on Girder Moments, Deflections, and Bottom Flange Strains.

As shown in Figure 7.8, the girder distribution factors that were estimated based on measured strains agreed well with those based on bending moments in the girder sections since the bending resistance was taken into account.   The weighting ratios used to compute load distribution factors based on measured strains using Equation (7.21) are listed in Table 7.5.   The values represent the ratio of the section modulus of the girders to that of girder 2 and were determined based on the experimentally derived section properties that are derived later in Section 7.3.   Ratios greater than one indicate that the girder in question has a section modulus greater than that of girder 2 whereas if less than unity, the girder has a lower bending resistance.   The weighting factor gets larger in proportion to

the magnitude of the relative difference in bending resistance of the girders to girder 2 and results in more load distribution to the stiffer girders.

Table 7.5 Weighting Factors for Section Modulus at Unit-S.

Girder #	Weighting Factor *
1	1.52
2	1.00
3	1.12
4	1.21
5	1.70

* Note: Relative to girder 2.

Assigning a weighting ratio of one to the five girders would signify that the girders have the same flexural resistance, which is not true. In Section 7.3, the stiffness properties (e.g., moment of inertia, section modulus) are shown to vary from girder to girder across the bridge cross-section. Due in part to the flexural participation of the curb, the exterior girders have the largest bending resistance, which explains the larger weighting factors given in Table 7.5. In addition, the exterior girders cannot be loaded as heavily as the interior girders, which results in smaller shear stresses between the slab and the top flange of the exterior girders and thus, a higher level of partial composite action.

To demonstrate the errors induced by ignoring the bending stiffness of the girders when computing distribution factors, consider a 14.2 m (46.5 ft) simply supported bridge with five girders subjected to a load of 89.0 kN (20.0 kips) at mid-span. By idealizing each of the girders as an elastic spring, the bridge may be reduced to a beam supported on an elastic foundation as shown in Figure 7.9.

196
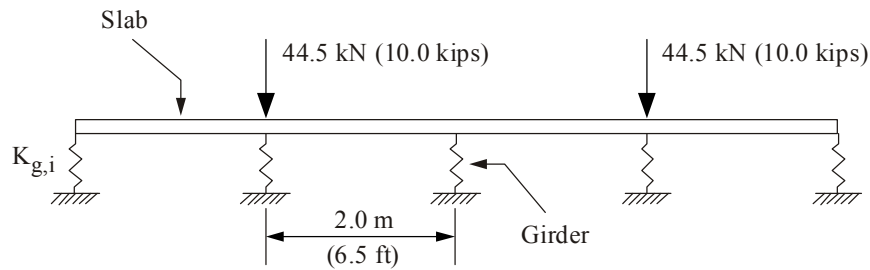
Figure 7.9 Elastic Spring Representation of a Transverse Bridge Section.

The transverse beam represents the deck slab spanning across the girders (i.e., the elastic springs). The 44.5 kN (10.0 kip) loads are positioned directly over the second and fourth girders. For a simply-supported bridge, the spring constants representing the stiffness of the girders at mid-span are computed as

$$K_{g,i} = \frac{48E_{stl}I_{g,i}}{L^3} \tag{7.22}$$

where L is the span length of the bridge. The force in each spring, $F_{g,i}$, is the product of the spring deformation (i.e., vertical deflection of the girder), $\Delta_{g,i}$, and the spring constant, $K_{g,i}$. Thus, the force in each ith spring (or the load distributed to the ith girder) is

$$F_{g,i} = \Delta_{g,i}K_{g,i} \tag{7.23}$$

The amount of load distributed to the girders is a function of the stiffness of the transverse beam representing the slab. For this analysis, the slab stiffness was arbitrarily modeled with a 1400 mm x 150 mm (55 in x 6 in) strip of the deck. Incidentally, the AASHTO LRFD (1998) Bridge Design Specifications

197

require an analysis in which the deck is assumed rigid for investigating the load distribution factor for exterior girders. Table 7.6 contains the results from a structural analysis performed on the elastic spring model given in Figure 7.9 for two separate cases. In Case I, the spring constants for all the girders were assumed equal to 1.75 kN/mm (10.0 kips/in) while in Case II, the two exterior springs had twice the stiffness of the interior springs. The second case is analogous to a structure with stiffer outer girders such as the Marlin units.

Table 7.6 Load Distribution Results of Beam Supported by Elastic Springs.

Girder #	Case I		Case II	
	(a) Force (kN)	(b) Deflection (mm)	(c) Force (kN)	(d) Deflection (mm)
1	10.5	6.0	12.1	3.5
2	22.0	12.6	20.6	11.8
3	23.8	13.6	23.6	13.5
4	22.0	12.6	20.6	11.8
5	10.5	6.0	12.1	3.5
Σ	89.0	50.8	89.0	43.9
Girder #	Case I		Case II	
	(e) Percent Force	(f) Percent Deflection	(g) Percent Force	(h) Percent Deflection
1	0.119	0.119	0.136	0.079
2	0.248	0.248	0.232	0.268
3	0.268	0.268	0.265	0.307
4	0.248	0.248	0.232	0.268
5	0.119	0.119	0.136	0.079

The top half of the table (i.e., columns a through d) contains the spring forces and deflections from the analyses. In the bottom half of the table, the distribution of load to the springs was investigated by expressing the force in each spring as a percentage of the total load of 89.0 kN (20.0 kips) applied to the beam. These

results are given in columns (e) and (g). Similarly, the load distribution was also estimated by dividing the deflection of each spring by the sum of the spring deflections. Columns (f) and (h) of the table contain these ratios.

When the girders are all assumed to have the same stiffness (i.e., Case I), a comparison of columns (e) and (f) of the table show that the distribution factors based on either load or deflection are identical. However, when the exterior springs are given a larger stiffness than the interior springs (i.e., Case II), the load distribution factors computed from the deflections underestimates the load to the exterior springs and overestimates the load to the interior springs. This observation was made by comparing columns (g) and (h) of Table 7.5. Another important observation made from the table is that the exterior springs carry a larger amount of the load when the larger stiffness constant was assigned to these springs. Consequently, the interior springs showed a decrease in the percentage of load as shown by comparing columns (e) and (g). The middle spring showed virtually no change in the percentage of load taken.

7.2.2   AASHTO Girder Distribution

Distribution factors determined from the bridge tests using Equation (7.20) were compared with the values computed based on the AASHTO Standard (1996) and LRFD (1998) Specifications. Table 7.7 lists the formulas contained in these two standards for the distribution of live load (per lane) to interior and exterior girders for single and multiple-lane loading. A legend is provided at the bottom of the table defining the variables that are used in the equations.

199

Table 7.7 Distribution of Live Load (per lane) according to the AASHTO Standard (1996) and LRFD (1998) Specifications.

Girder	AASHTO Standard Specifications (1996): Article 3.23.2	
	Distribution Factor (One Design Lane Loaded)	Distribution Factor (Multiple Lane Loading)
Interior	$\dfrac{S}{4300}$	$\dfrac{S}{3400}$
Exterior	* Lever Rule $\geq \dfrac{S}{4300 + 0.5S}$	* Lever Rule $\geq \dfrac{S}{4300 + 0.5S}$
Girder	**AASHTO LRFD Specifications (1998): Article 4.6.2.2**	
	Distribution Factor (One Design Lane Loaded)	Distribution Factor (Multiple Lane Loading)
Interior	$0.06 + \left(\dfrac{S}{4300}\right)^{0.4}\left(\dfrac{S}{L}\right)^{0.3}\left(\dfrac{K_g}{Lt_s^3}\right)^{0.1}$	$0.075 + \left(\dfrac{S}{2900}\right)^{0.6}\left(\dfrac{S}{L}\right)^{0.2}\left(\dfrac{K_g}{Lt_s^3}\right)^{0.1}$
Exterior	* Lever Rule	e x (distribution factor for interior girder)

* Method of analysis in which the concrete deck slab is assumed to act as a simple supported beam between girders.

Legend

S, L = girder spacing (mm) and length of span (mm)
t_s = thickness of concrete deck slab (mm)
K_g = longitudinal stiffness parameter (mm^4) = $n(I_g + A_g e_g^2)$
n = modular ratio between steel girder and concrete deck slab = E_{stl} / E_{conc}
E_{stl}, E_{conc} = modulus of elasticity for steel (MPa) and concrete (MPa)
I_g, A_g = moment of inertia (mm^4) and cross-sectional area (mm^2) of steel girder
e_g = distance between the center of gravity of the steel girder and the concrete deck slab (mm)
e = load distribution correction factor for exterior girder = $0.77 + 0.00328d_e / 9.1 \geq 1.0$
d_e = distance between the center of the exterior girder and the interior edge of the curb (mm)

As shown in Table 7.7, the formulas in the AASHTO Standard (1996) Specifications solely consider the spacing of the girders to compute the fraction of the load distributed to the interior girders. Because of this simplicity, a load distribution study was carried out under National Cooperative Highway Research Program (NCHRP) Project 12-26 (Zokaie, et al., 1991) to improve the accuracy of the load distribution formulas. The formulas developed as part of this NCHRP project subsequently made their way into the more recent AASHTO LRFD (1998) Specifications and are listed in the bottom half of Table 7.7. In addition to the spacing of the girders, the new LRFD relationships account for the span length, the slab thickness, and other stiffness parameters related to the girders and the deck slab in distributing live load to the interior girders. Moment distribution factors were computed by LRFD for the case of non-composite and composite behavior of the girders. Non-composite action was considered by ignoring the eccentricity term, e_g, when computing the longitudinal stiffness parameter, K_g.

In both standards, with the exception of multiple-lane loading in the AASHTO LRFD (1998) Standard, which applies a correction factor to the interior girder distribution, load distribution to the exterior girders is determined by the "lever rule". This analysis method assumes the deck slab to be simply-supported between the exterior and adjacent interior girder. That is, the girder distribution to the exterior girder is simply the reaction resulting from the summation of moments caused by the wheel loads placed between the adjacent interior girder and the exterior girder. In this approach, wheel loads positioned between interior girders are not carried over to the exterior girder. A lower bound is enforced on

this calculation to prevent the exterior girder from being designed for a load less than the design load for the interior girder. To determine the load distribution with respect to wheel loads, the equations given in Table 7.7 are multiplied by 2.

7.3   BRIDGE RESPONSE UNDER TRAILER LOADING

In this section, the lateral distribution of load to the girders and the partial interaction between the girders and the deck slab is evaluated as the trailer load was increased up to and beyond first yield of the girders. The effects of bearing restrain are also studied. In spite of the good comparison in load distribution factors computed based on strains and moments presented in Section 7.2.1, lateral distribution was evaluated by expressing the moment in each girder as a percentage of the total bending moment at the bridge section using Equation (7.20). This decision was made since the use of bending moments provided better indication of the distribution of forces within each girder section. The procedures outlined in Sections 7.1.1 and 7.1.2 were followed to compute the girder moments and section properties from the measured strains. This same approach is used in Chapter 8 to evaluate the bridge response under the service load runs.

Permanent strains remaining from previous load cycles were deducted so that the strain values would represent strictly the change in strain experienced by the girders for the particular trailer load under investigation. Adjusting the strain readings in this way made it possible to isolate the bridge response for each trailer load increment and thus, evaluate changes in distribution between load levels.

As discussed in Sections 7.1.1 and 7.1.2, the girder moments and section properties may be computed using the following three pairs of strain gage readings: (a) top flange-bottom flange, (b) top flange-web, and (c) web-bottom flange. Since no significant differences were noted in the computed moments and properties regardless of which one of these pairs was used, the evaluation of the bridge response presented herein is based on strain combination (a). This decision was also made because the bottom flange strain always represents a maximum strain on the girder cross-section whether at a positive or negative moment region. Furthermore, the gage positions on the girder flanges are defined by a horizontal surface whereas the location of the web gage can only be approximated at mid-depth of the girder through measurement, which introduces an error associated with the gage position. Out-of-plane bending of the web may also lead to the misinterpretation of the web strains.

Cracking of the concrete slab and curbs was ignored in order to simplify the calculation of the girder moments and section properties. This assumption was made because of the difficulty in quantifying the cracked condition of the deck slab and curbs caused by the previous loading history of the bridge units. Although this assumption may lead to errors in absolute girder moments, it was considered appropriate for evaluating changes in moment distribution between trailer load levels and also for deriving approximate experimental quantities for the girder section properties.

203

7.3.1   Lateral Load Distribution

Figures 7.10 and 7.11 display the experimental girder distribution factors for Unit-N and Unit-S, respectively, in the positive moment region (Section c-c in Figures 5.12 and 5.18).   Distribution factors are plotted on the vertical scale versus the girder number on the horizontal scale.   The top plot of each figure (labeled "a") represents the moment distribution during Stage 1 loading and the bottom plot (labeled "b") corresponds to Stage 2.   In each stage, the factors were computed for three levels of load with the trailer at its fourth position on the deck (see Figures 5.17 and 5.21).

At position 4, the trailer load was at the critical longitudinal location to maximize the positive moment at Section c-c.   Also, in Stage 2, a concrete barrier load of 122 kN (27.5 kips) rested on the loaded side of the bridge deck next to the curb as the trailer loads were applied.   The AASHTO Standard and LRFD distribution factors for an interior girder are also plotted on Figures 7.10 and 7.11 for comparison with the experimental values for girder 2 (i.e., the heaviest loaded girder).   The two LRFD quantities represent the cases of composite (C) and non-composite (N-C) girder behavior.

204
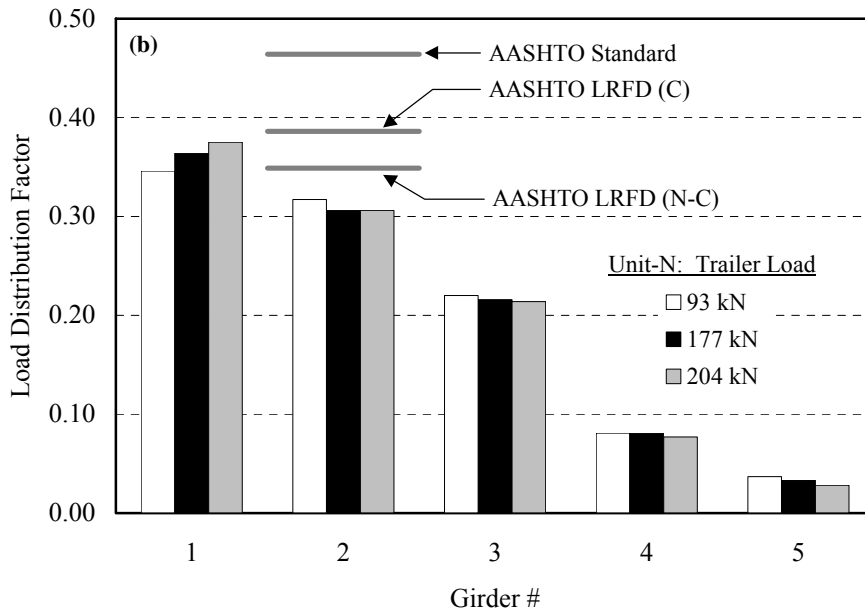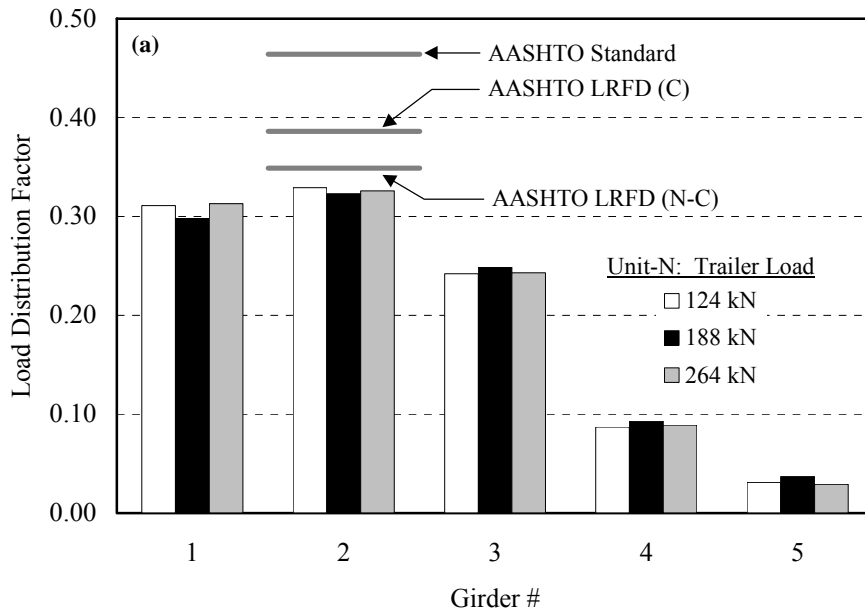
Figure 7.10 Lateral Distribution of Positive Moment at Section c-c of Unit-N for Different Trailer Loads during (a) Stage 1 and (b) Stage 2 Loading.
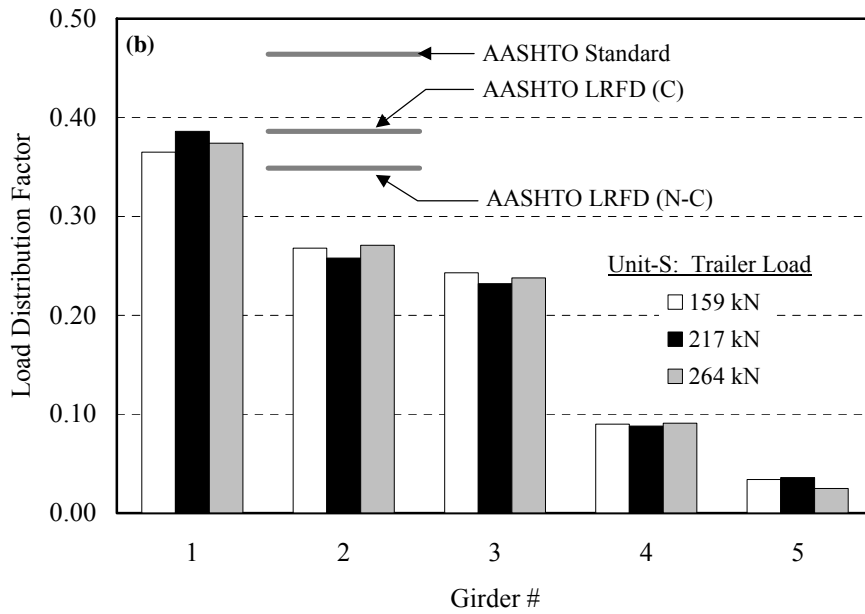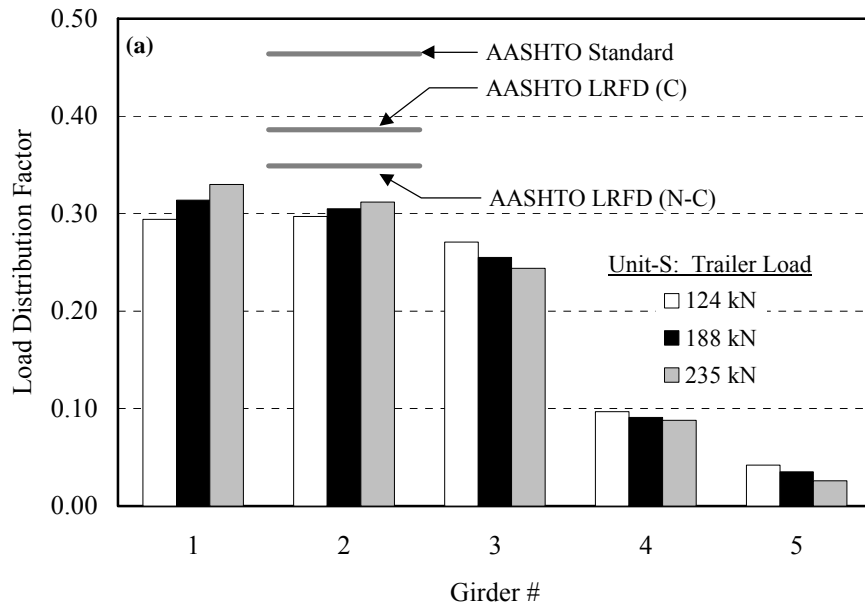
Figure 7.11 Lateral Distribution of Positive Moment at Section c-c of Unit-S for
Different Trailer Loads during (a) Stage 1 and (b) Stage 2 Loading.

206

<u>Response of Unit-N</u>

In Stage 1, no significant or uniform changes were observed in the lateral distribution of positive moment to the girders as the trailer load increased, as shown in Figure 7.10(a). The most notable difference in the load distribution factors occurred at a trailer load of 188 kN (42.3 kips) for girder 1. At this girder, the distribution ratio at a load of 188 kN (42.3 kips) differed by only 4% from the factors computed for 124 kN (27.9 kips) and 264 kN (59.4 kips). Similar comparisons at girders 2 and 3 showed variations of 2 and 3 percent, respectively. These minute changes suggest that the girders maintained relatively the same bending stiffness throughout the first stage of loading.

The AASHTO LRFD (1998) Specifications provided a significantly better estimate of the distribution factor for girder 2 than the Standard (1996) provisions. The experimental distribution factor for girder 2 was 7 percent lower than the LRFD value based on assumed non-composite action and 18 percent lower for composite action. Assuming composite action in the LRFD approach results in a larger distribution factor because the equations relate directly to the bending stiffness through the $(K_g / Lt_s)^{0.1}$ term as shown in the bottom half of Table 7.7. The AASHTO Standard (1996) factor exceeded the experimental value for girder 2 by about 40 percent. A larger deviation was expected using the AASHTO Standard (1996) provisions since only the girder spacing is considered in the load distribution relationships as shown in the top half of Table 7.7.

Figure 7.10(b) shows a continual increase in the distribution factor for girder 1 during Stage 2. Between the trailer loads of 93 kN (20.9 kips) and 204

kN (45.9 kips), the distribution factor for this girder increased by 8%. As discussed in Chapter 6, girder 1 showed signs of yielding in the flanges at the negative moment region (Section d-d in Figure 5.12) towards the end of Stage 1. Thus, it appears that girder 1 continued to undergo plastic rotations at Section d-d as the trailer loads were applied during Stage 2, reducing the continuity with the adjacent span. Also, the extra dead weight of the concrete barriers resting on the deck throughout Stage 2 may lead to continual creep of plastic deformations at Section d-d. As a result, girder 1 acts more as a simply-supported beam between Section d-d and the end of the girder (bearing 3 in Figure 5.12) causing larger positive moments at Section c-c. Consequently, girders 2 and 3 both showed a 3% decrease in the distribution factor of positive moment as the trailer load increased in Stage 2. A comparison of the distribution factors between Stage 1 and Stage 2 showed an 18% increase for girder 1, a 5% decrease for girder 2, and an 11% decrease for girder 3. These changes further show that yielding (i.e., loss of continuity) of girder 1 at Section d-d at the end of Stage 1 altered the load distribution pattern of positive moment at Section c-c during Stage 2.

Response of Unit-S

As shown in plot (a) of Figure 7.11, there was a regular trend in the load distribution factors for all five girders as the trailer load increased in Stage 1. Increases on the order of 12% and 5%, respectively, occurred at girders 1 and 2 as the load progressed from 124 kN (27.9 kips) to 235 kN (52.8 kips). The three remaining girders each showed a decrease in the percentage of load carried. At girder 3, the distribution factor at 124 kN (27.9 kips) was 10% lower than at the

load of 235 kN (52.8 kips). Compared with Unit-N, the variation of distribution factors was larger and more uniform at Unit-S between the three loads applied during Stage 1. The larger variation and the regular shift in load distribution of the girders suggested that girder 2 (directly beneath the trailer load) was losing stiffness with increasing trailer load due to a continual loss of interaction with the slab. This loss of stiffness of girder 2 resulted in a westward redistribution of load to girder 1, which subsequently reduced the load to girders 3, 4, and 5.

As with Unit-N, the AASHTO based distribution factors for Unit-S all exceeded the load test results for girder 2. The differences between experimental distribution factors and the AASHTO LRFD (non-composite), AASHTO LRFD (composite), and AASHTO Standard were 14%, 27%, and 52%, respectively. Again, the AASHTO LRFD equation assuming non-composite action provided the best approximation to the test results. In Stage 2, the distribution factors for girder 1 at Section c-c were about 20% higher than the values for Stage 1 due to the location of the deck load and to yielding in the negative moment region at the end of Stage 1. Girders 2 and 3 both showed decreases of 13% and 7%, respectively, between Stage 1 and Stage 2 loading. Similar behavior was also observed at Unit-N.

7.3.2   Curb Participation

One of the assumptions made to simplify the computation of the girder moments was that the curvatures of the girder and the tributary slab section were equal. In other words, the strain profile over the depth of the slab section was assumed to be parallel to the distribution over the girder depth.   Another assumption was that the strain profiles were linear over the depths of both the slab section and the girder.

The validity of the aforementioned assumptions was evaluated based on Figure 7.12, which shows the strain profiles measured over the depths of girder 1 and the curb for trailer loads applied during Stage 1 loading at Unit-S. At the top of the figure, a sketch of girder 1 and the slab section is provided showing the layout of strain gages where measurements were made. Four strain measurements were made over the depth of the west curb (labeled C1 through C4) and three over the girder depth (labeled GB20, GM20, and GT20). The vertical distances from the bottom surface of the girder to the gage locations are noted in parentheses. In each of the strain gradient plots, the measured bending strains at the seven gage locations are plotted on the horizontal axis versus the vertical distance to the gage on the vertical axis. The solid line represents the best-fit line based on a linear regression analysis of the measured curb and girder strains. A comparison of the slope of the line (i.e., curvature) between the curb and girder gave an average percent difference of 10 percent indicating the curvatures were about equal.
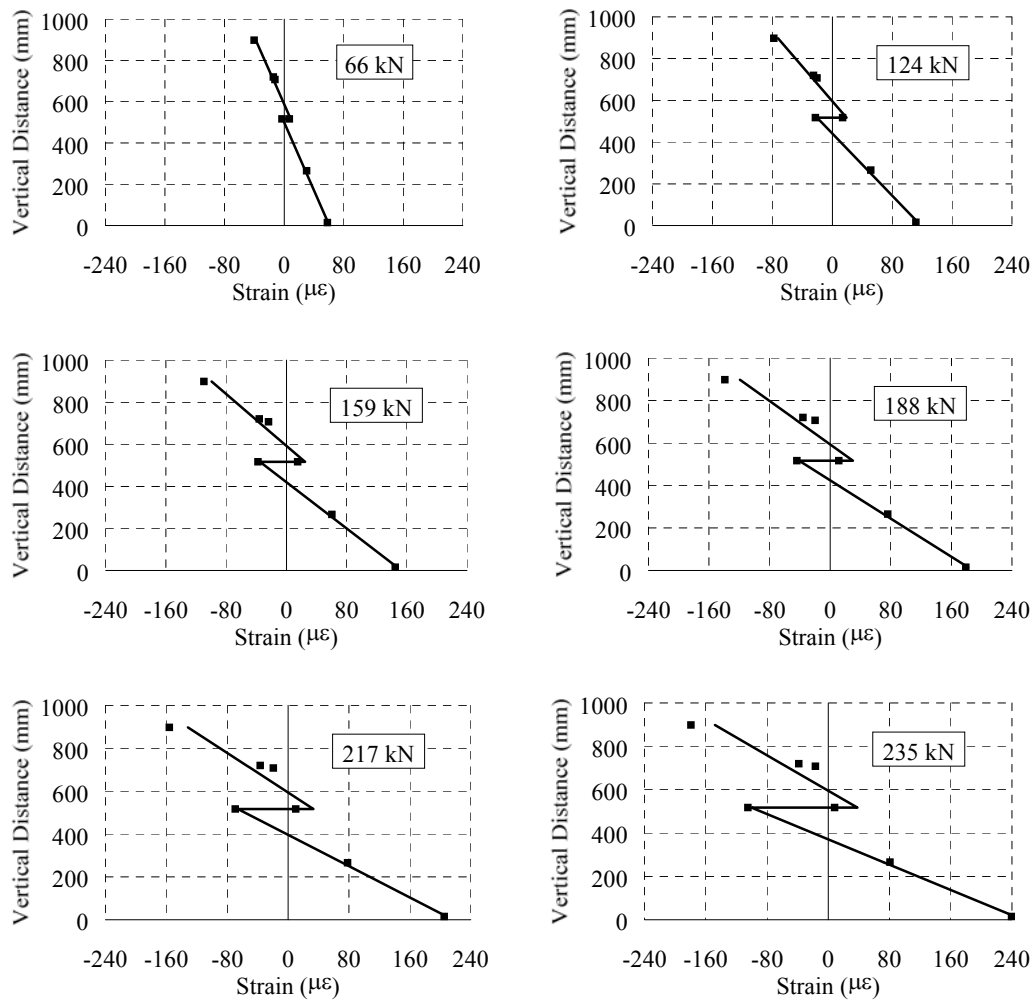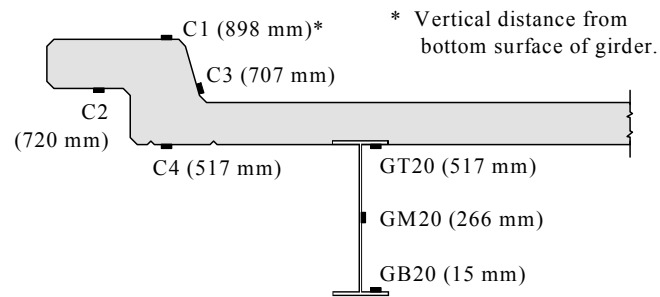
Figure 7.12 Bending Strain Profile over Depths of Girder 1 (and Curb) of Unit-S during Stage 1 Loading at Load Position 4.

211

Over the curb depth, the bending strain measured at one gage (C4) did not line up with the strain readings for the other three gages (C1 through C3). From this observation, it appears that gage C4 may have given inaccurate strain readings causing errors in the calculated curvature of the curb. However, as stated earlier, the slope of the best-fit line through the curb readings was relatively parallel to the strain gradient measured over the girder depth. This observation confirms the assumptions made for calculating girder moments and also proves that the curb contributes to the bending stiffness of the exterior girder, which will effect the distribution of live load to the girders.

7.3.3 Partial Composite Action and Bearing Restraint

Strain readings taken at the abutment bearing 19 of Unit-S (Section a-a in Figure 5.18) showed evidence that the girders were acting partially composite with the deck slab. Table 7.8 lists the strain readings on the top flange and bottom flange of the girders at Section a-a measured during Stage 1 and Stage 2 loading. Strain measurements are listed below the load applied by the trailer axles at load position 4. The gage labels are defined in Figure 5.20.

With the exception of girder 5, the most remote girder from the trailer load, the remaining girders all showed a strain distribution with tensile strains on the girder top flange exceeding the compressive strains measured on the bottom flange. As illustrated in the sample analysis in Section 7.1.3, this type of behavior occurs when the girder top flange is partially restrained from sliding relative to the bottom of the deck slab. At the ends of the girders (i.e., bearing 19 or Section

a-a of Figure 5.18), the slab attempts to slide southward relative to the girder top

flange towards the abutment under loading.

Table 7.8 Measured Girder Strains at Section a-a of Unit-S for Trailer Loads
applied during Stage 1 and Stage 2 at Load Position 4.

Girder No.	Gage Label	Girder Strains (µε) for Stage 1 Loading					
		66 kN	124 kN	159 kN	188 kN	217 kN	235 kN
1	GT26	30	57	79	122	124	127
	GB26	-7	-5	-18	-27	-27	-30
2	GT27	34	55	99	109	127	129
	GB27	-16	-21	-45	-66	-74	-69
3	GT28	27	51	69	86	102	113
	GB28	-21	-37	-53	-75	-87	-98
4	GT29	10	23	26	33	41	41
	GB29	2	0	1	-6	-12	-15
5	GT30	1	0	0	-3	-4	-9
	GB30	14	26	33	35	40	44

Girder No.	Gage Label	Girder Strains (µε) for Stage 2 Loading					
		113 kN	159 kN	188 kN	217 kN	235 kN	264 kN
1	GT26	54	83	104	145	157	178
	GB26	-17	-34	-45	-61	-70	-90
2	GT27	67	90	101	109	113	129
	GB27	-48	-62	-63	-60	-59	-62
3	GT28	50	71	82	96	101	103
	GB28	-46	-63	-70	-79	-77	-72
4	GT29	21	28	32	42	46	49
	GB29	0	-6	-4	-15	-18	-17
5	GT30	3	-1	-4	-2	-2	-4
	GB30	16	32	40	41	48	50

Since relative slip is restricted by friction caused by the deck weight and by

mechanical interlock, an equal and opposite shear force develops at the contact

surface between the girder top flange and the deck slab. These forces have the

effect of pulling on the top flange of the girder and compressing the bottom

surface of the deck slab. Transferring the shear force from the top flange down to

the centroid of the bare girder results in a combined loading condition of axial

tension and negative bending moment as shown previously in Figure 7.6(b). Consequently, a strain profile resembling plot (c) of Figure 7.6 develops over the girder height marked by tensile strains on the top of the girder that exceed the compressive strains measured on the bottom of the girder.

There are factors other than partial composite action that may contribute to the girder strain field at the supports of a bridge such as bearing restraint and unintended continuity (Burdette and Goodpasture, 1988; Pinjarkar et al. 1990; Lichtenstein, 1993). As a result, the force distribution may become quite complex at the supports making it difficult to separate the effects caused independently by the different inadvertent factors. Nevertheless, the general trend of the strain distribution for the girders at the expansion bearing locations can provide useful information for recognizing the particular aspect of unintended behavior that may be acting. For example, the phenomenon of bearing restraint represents the condition where the expansion bearings do not perform their intended function of allowing the bridge girders to move longitudinally outward under the actions of live load or temperature fluctuations (Bakht and Jaeger, 1988). Relative movement between the bottoms of the girders and the bearings may be prevented by friction at the contact surface between the girder and the bearings as shown in Figure 7.13(a). In the figure, N represents the normal vertical force (i.e., reaction) at the support and F is the friction force which equals the normal force times a coefficient of friction, μ, between the underside of the bottom flange and the bearing support. The bearings may also "lock" due to the accumulation of debris or corrosion. In either case, equal and opposite forces develop between the

214

bearing and the girder bottom flange. The force acting on the bearing is ultimately transferred into the abutment or pile cap supporting the bearing. At the centroid of the girder, the friction force applies a combined loading of axial compression and negative moment equal to the friction force times half the depth of the girder, d, as shown in Figure 7.13(b). This load combination results in a strain distribution where compression strains on the bottom flange exceed the tensile strains on the top flange as shown in Figure 7.13(c). This profile is opposite to that which occurs under the forces associated with partial composite action where the magnitude of the top flange tensile strain exceeds the magnitude of the compressive strain on the bottom flange (see Figure 7.6(c)).
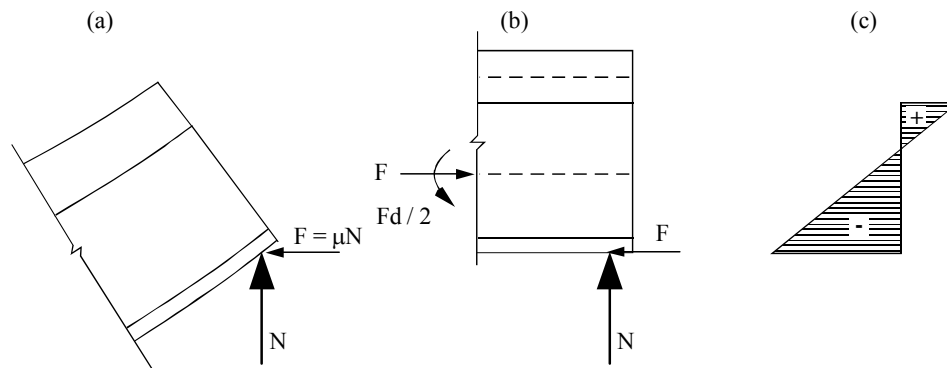
Figure 7.13 Strain Distribution at End of Girder Caused by Bearing Restraint Forces.

To illustrate the strain distribution caused at the girder ends by bearing restraint forces, Table 7.9 contains the results from a three-dimensional analysis performed on Unit-S under the final trailer load of 235 kN (52.8 kips) applied during Stage 2. The BRUFEM (Bridge Rating using the Finite Element Method) program was

215

used for the analysis (Hays et al., 1994). Further details regarding this program are provided in Chapter 8.

Table 7.9 Forces and Strains at Girder Ends Caused by Bearing Restraint under a Total Load of 235 kN (52.8 kips).

	Girder				
	1	2	3	4	5
Support Reaction (kN)	33.7	19.4	19.3	16.6	
Friction Force (kN) *	16.9	9.70	9.63	8.32	
Bending Moment (kN-m)	4.48	2.58	2.56	2.21	
Top Flange Strain ($\mu\varepsilon$)	4	2	2	2	
Bottom Flange Strain ($\mu\varepsilon$)	-19	-10	-10	-8	

The first row of the table shows the support reactions at girders 1 through 4. No value is shown for girder 5 since the analysis indicated that the girder was lifting off of the support and thus, there was no friction force. The second and third rows of the table show the friction force (computed assuming a coefficient of friction of 0.5 between the bottom of the girder and the support) and the bending moment caused by the friction force. In the final two rows, the tensile top flange strains are shown to exceed the compressive bottom flange strains as expected due to the combined axial and moment forces.

Examination of the strains given in Table 7.8 at the abutment end of the girders of Unit-S suggests that the effects of partial composite action dominate over those associated with bearing restraint. However, it is difficult to determine the amount of strain that is caused individually by the two different factors. In addition to contributing to the strain field at the ends of the girders, the negative bending moments caused by the bearing restraint forces can reduce the positive bending moments towards the center of the 18.3 m (60 ft) span.

216

Table 7.10 lists the bending moments and axial forces for the five girder sections at Section c-c that were computed for the different trailer loads (at load position 4) of Stage 1. Results listed for 66 kN (14.8 kips) are inaccurate due to problems with the test data for this load but are shown for completeness. Girder section moments were evaluated using Eq. (7.12), which includes the moment in the tributary slab section, the moment in the bare girder, and the moment couple caused by the axial forces acting at the centroids of the tributary slab section and the bare girder. The moment couple is the product between the axial forces and the vertical offset between the centroids of the bare girder and the slab section as given by Equation (7.11). Axial forces signify the amount of longitudinal force that was transferred between the girders and their respective slab sections along their plane of contact by friction and mechanical interlock.

For each trailer load, the moments and axial forces derived from the measured strains in each of the five girder sections are summed and shown in the rightmost column of Table 7.10. These total amounts represent the total measured bending moments (designated as "Bridge Moment") and axial forces in the deck slab (specified as "Deck Force") over the bridge cross section at Section c-c. The ratio of the experimental bridge moment to the statical bridge moment computed by treating the bridge unit as a one-dimensional beam is noted in parentheses next to the total measured moments. The magnitude of the statical bridge moments for the different trailer loads may be "back-calculated" by simply dividing the experimental moments by these moment ratios.

217

Table 7.10 Experimental Girder Section Moments and Axial Forces at Section c-c for Trailer Loads (Position 4) applied during Stage 1.

(a) Unit-N

Load (kN)	Section Moments, M_T (kN-m)					Bridge Moment Σ, (kN-m)
	Girder 1	Girder 2	Girder 3	Girder 4	Girder 5	
66	58	54	46	22	12	192 (0.97)∗
124	100	106	78	28	10	322 (0.87)
159	130	134	97	36	11	408 (0.86)
188	147	159	123	46	18	493 (0.88)
217	175	186	139	52	18	570 (0.88)
264	218	227	169	62	20	696 (0.88)

Load (kN)	Axial Forces, P (kN)					Deck Force Σ, (kN)
	Girder 1	Girder 2	Girder 3	Girder 4	Girder 5	
66	72	69	76	45	24	286 [0.95]●
124	111	126	118	47	12	414 [0.66]
159	148	154	148	64	13	527 [0.52]
188	165	181	191	86	22	645 [0.42]
217	194	203	212	95	22	726 [0.38]
264	234	237	250	112	23	856 [0.32]

(b) Unit-S

Load (kN)	Section Moments, M_T (kN-m)					Bridge Moment Σ, (kN-m)
	Girder 1	Girder 2	Girder 3	Girder 4	Girder 5	
66	47	49	42	15	7	160 (0.81)∗
124	91	92	84	30	13	310 (0.84)
159	117	119	103	37	15	391 (0.82)
188	145	141	118	42	16	462 (0.82)
217	165	166	139	51	20	541 (0.83)
235	192	181	142	51	15	581 (0.83)

Load (kN)	Axial Forces, P (kN)					Deck Force Σ, (kN)
	Girder 1	Girder 2	Girder 3	Girder 4	Girder 5	
66	62	45	61	26	8	202 [1.35]●
124	100	66	113	49	16	344 [0.79]
159	120	84	136	62	18	420 [0.65]
188	152	94	153	69	18	486 [0.56]
217	152	108	166	82	24	532 [0.51]
235	152	117	172	84	16	541 [0.50]

∗   ( ) Ratio of strain developed bridge moment to statical bridge moment.
●   [ ] Ratio of friction resistance to deck force.

218

The beam analysis was performed assuming point supports with no rotational stiffness and using the centerline dimensions between supports for the span lengths.

As shown in Table 7.10, the moment ratios averaged approximately 88% for Unit-N and 83% for Unit-S. In other words, the longitudinal moments derived experimentally from the measured strains at the positive moment region were 12% and 17% lower than the expected values for the bridge units. In the negative moment region, the experimental bridge moments underestimated the statical bridge moments by about the same amounts as shown in Table 7.11. Hence, the level of accuracy of the derived experimental bridge moments was relatively the same in both the positive and negative moment regions.

Table 7.11   Experimental Girder Section Moments at Section d-d for Trailer Loads (Position 4) applied during Stage 1.

Unit-N		Unit-S	
Load (kN)	Bridge Moment Σ, (kN-m)	Load (kN)	Bridge Moment Σ, (kN-m)
66	-130 (0.90) *	66	-113 (0.79)
124	-247 (0.92)	124	-211 (0.78)
159	-320 (0.93)	159	-268 (0.78)
188	-369 (0.90)	188	-312 (0.76)
217	-427 (0.91)	217	-365 (0.78)
264	-528 (0.92)	235	-388 (0.76)

∗   ( ) Ratio of strain developed bridge moment to statical bridge moment.

One factor that has been shown to reduce the positive bending moment at a given section of a bridge is the counteracting moment caused by bearing restraint forces at the supports (Bakht and Jaeger, 1988). Compressive forces may

develop at the underside of the girder bottom flanges due to friction, corrosion, and/or deposited debris. Consequently, these forces will induce a bending moment to the bridge girders that opposes the moment caused by the live load. For example, if longitudinal translation was completely restrained at the roller support of the girder shown in Figure 7.5, the positive moment at mid-span would have reduced from PL/4 to PL/8 by the negative moment at the ends of the girder caused by the compressive bearing forces. That is, the restraint forces would have altered the girder behavior from a simple supported beam to that resembling one with fixed ends. The amount of moment reduction depends on how much longitudinal movement of the girder is prevented at the bearing.

To examine the effect of bearing restraint on the Marlin bridge, consider the final trailer load of 235 kN (52.8 kips) applied to Unit-S during Stage 1. At this load, the total statical bridge moment across Section c-c is 700 kN-m (518 kip-ft) which was computed from a one-dimensional analysis of the bridge unit with the trailer at load position 4. Summation of the bending moments listed in Table 7.9 equals 11.8 kN-m (8.73 kip-ft) which represents the negative moment caused by the bearing restraint forces over the length of the 18.3 m (60 ft) span. It is assumed that the bearings on either side of the span develop equal and opposite friction forces thus, producing a constant moment equal to the force times half the girder depth as shown in Figure 7.14. As mentioned in an earlier discussion, the restraint forces were computed assuming a coefficient of friction equal to 0.5 at the interface between the topside of the bearings and the bottom of the girders.
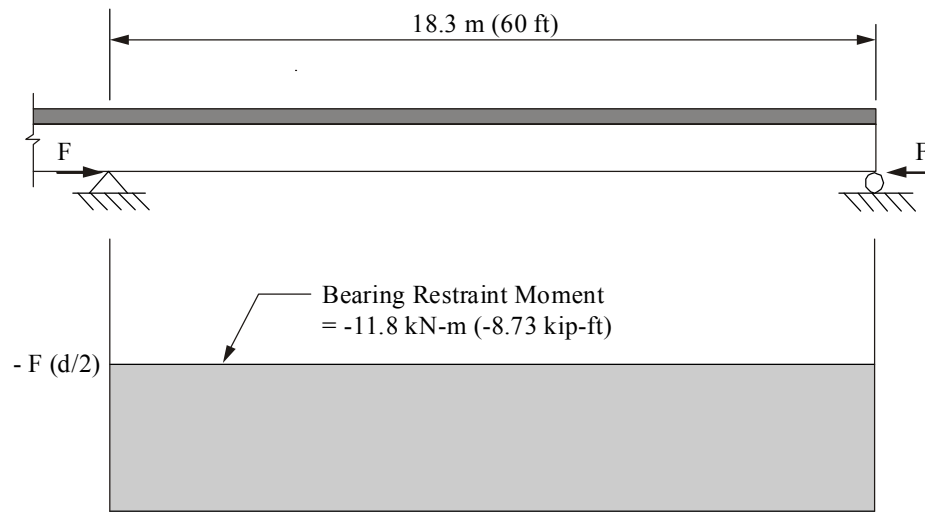
Figure 7.14 Bending Moment Caused by Bearing Restraint Forces over Length of 18.3 m (60 ft) Span.

The bearing restraint moment represents less than 2% of the total statical moment at Section c-c. Thus, it appears that the difference between the measured and statical moments given in Table 7.10 is not attributed to bearing restraint but rather to some other factor. One possible explanation is that the procedures given in Section 7.1.1 to compute the girder moments experimentally become unreliable with decreased interaction between the girder and the slab. For instance, there is more possibility for the girder to separate from the deck slab thus violating one of the assumptions made in Section 7.1.1. Torsional effects were also ignored in the equations, which may lead to errors in the computed moments particularly under conditions when the live load is applied at a transverse position eccentric to the bridge centerline. In Chapter 8, the experimental response under the dump truck loading is shown to approximate the theoretical response more accurately as the

221

transverse position of the dump truck approaches the third path (i.e., the dump truck axles straddle the bridge centerline), where the torsional effects are minimal.

Another possibility for the discrepancy between the experimental and theoretical moments is that the bending moment carried by the deck slab was underestimated. In Table 7.12, the total measured moments are separated into the individual bending moments in the girder and deck slab plus the moment couple caused by partial composite action.

Table 7.12   Breakdown of Total Bridge Moment at Section c-c for Trailer Loads (Position 4) applied during Stage 1.

(a) Unit-N

Load (kN)	Moment Components, (kN-m)			Bridge Moment Σ, (kN-m)
	M_g	M_s	M_c	
66	71 (0.37)*	22 (0.12)	99 (0.52)	192
124	136 (0.42)	42 (0.13)	143 (0.44)	322
159	173 (0.42)	54 (0.13)	182 (0.45)	408
188	207 (0.42)	63 (0.13)	222 (0.45)	493
217	244 (0.43)	75 (0.13)	250 (0.44)	570
264	307 (0.44)	95 (0.14)	295 (0.42)	696

(b) Unit-S

Load (kN)	Moment Components, (kN-m)			Bridge Moment Σ, (kN-m)
	M_g	M_s	M_c	
66	71 (0.44)*	20 (0.12)	70 (0.44)	160
124	148 (0.48)	42 (0.14)	119 (0.38)	310
159	189 (0.49)	55 (0.14)	145 (0.37)	391
188	226 (0.49)	67 (0.14)	169 (0.37)	462
217	275 (0.51)	82 (0.15)	185 (0.34)	541
235	300 (0.52)	95 (0.16)	187 (0.32)	581

* Ratio between individual moment component and total bridge moment.

As shown in the table, the moment in the deck slab ranged from 12 to 16 percent of the total measured moment. Recall that the deck moment was computed by multiplying the girder moment by the stiffness ratio between the tributary slab section and the girder. To determine the slab stiffness, the empirical formula given in ACI (1995) was used to approximate the modulus of elasticity for the concrete. This formula was developed based on a least squares fit of measured static moduli for a variety of concrete mixes (Pauw, 1960). That is, the measured static modulus may fall either above or below the ACI formula. In a study by Parsley (1998), the ACI formula underestimated the elastic modulus by about 20% compared to the results from short column and unconfined cylinder tests (i.e., methods for measuring the elastic modulus for concrete). Thus, increasing the concrete elastic modulus by 20% causes the deck moments in Table 7.12 to increase by about 20%. Consequently, the larger deck moments results in an increase of about 3 percent in the total measured bridge moment. In summary, the moment due to bearing restraint together with the possibility of larger moment in the bridge deck may account for as much as 5 percent of the difference between the measured and calculated moments.

Figure 7.15 shows the internal forces at Section c-c for Unit-S with the trailer at load position 4. In the figure, the variables M_{bridge} and P_{deck} represent the bridge moment and deck force listed in Table 7.10. The shear resistance at the girder-slab interface was taken as the frictional restraint provided by the weight of the deck slab bearing down on the top flanges of the girders ($v_{friction}$) and the restraint due to the mechanical interlock at the girder-slab interface ($v_{interlock}$).
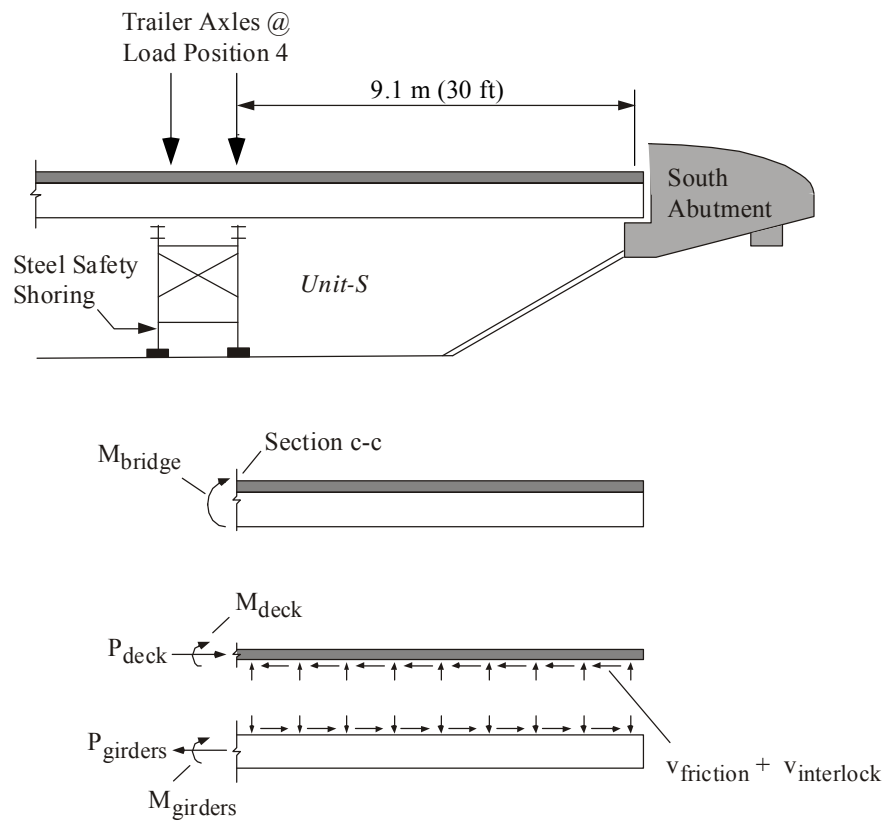
Figure 7.15 Free Body Representation of Unit-S at Section c-c with Trailer Axles at Load Position 4.

The length of the slab providing shear resistance was taken from Section c-c to the end of the bridge units, which amounted to 9.1 m (30 ft). Shear restraint due to friction was computed as the product of the weight of the deck slab and the coefficient of static friction between steel and concrete. A friction coefficient of 0.57 was assumed in the computations as recommended by Rabbat and Russell (1985). The extra shear resistance provided by the natural bond between the steel and the concrete at the girder-slab interface was ignored due to the complexities in quantifying the amount of shear restraint it would provide. In addition, this

shear component was most likely broken from the previous traffic loading on the bridge and was unrecoverable. On the other hand, the friction component was considered a recoverable force.

For a length of 9.1 m (30 ft), the weight of the tributary slab section was 101 kN (22.6 kips) for the exterior girders and 92.1 kN (20.7 kips) for the interior girders. The slab weight was slightly higher for the exterior girders since the curbs were included as part of the tributary slab section. The average bearing pressure exerted by the deck slab on the top flanges was only about 0.05 N/mm^2 (7.3 psi). Based on the friction coefficient of 0.57, the shear-friction came out to 57.4 kN (12.9 kips) for the exterior girders and 52.5 kN (11.8 kips) for the interior girders. Summation of these forces for the five girders resulted in a total shear-friction resistance at the girder-slab interface of 272 kN (61.2 kips). The extra friction caused by the weight of the trailer was ignored since the axles were at Section c-c where there was minimal slip between the girders and the slab (see Figures 6.24 through 6.26). Hence, the position of the trailer causing maximum moment in the girders (and maximum girder-slab slip at the ends) coincides with the position where the trailer weight offers little contribution to partial composite action since there is minimal relative slip between the girders and the slab. This loading position is as ineffective as placing shear studs only at mid-span of a simple supported beam (i.e., areas of zero shear or shear reversal).

As shown in Table 7.10, the experimental bridge moment was closer to the calculated value at Section c-c for Unit-N. Incidentally, the bending stiffness derived experimentally for girders 1 through 4 of this unit exceeded those for

Unit-S as shown in Table 7.13. The table lists the experimental section properties at Section c-c derived using the procedures given in Section 7.1.2 including the moment of inertia, the neutral axis location, and the section modulus with respect to the bottom flange of the girders.

Table 7.13 Experimental Girder Section Properties at Section c-c derived from Measured Strains (Trailer at Load Position 4) before First Yield.

Girder #	Experimental Girder Section Properties for Unit-N		
	Moment of Inertia, I (10^9 mm^4)	Neutral Axis, y (mm)	Section Modulus, S (10^6 mm^3)
1	1.752 (0.76)*	437 (0.76)	4.009 (0.99)
2	0.944 (0.63)	365 (0.71)	2.590 (0.89)
3	1.205 (0.80)	426 (0.83)	2.829 (0.97)
4	1.489 (0.99)	504 (0.98)	2.954 (1.00)
5	1.838 (0.77)	461 (0.81)	3.987 (1.00)
Girder #	Experimental Girder Section Properties for Unit-S		
	Moment of Inertia, I (10^9 mm^4)	Neutral Axis, y (mm)	Section Modulus, S (10^6 mm^3)
1	1.690 (0.73)	466 (0.81)	3.627 (0.90)
2	0.747 (0.50)	312 (0.60)	2.394 (0.82)
3	1.035 (0.69)	387 (0.75)	2.678 (0.92)
4	1.300 (0.86)	449 (0.87)	2.895 (0.99)
5	1.877 (0.81)	463 (0.81)	4.058 (1.00)

- Ratio with respect to calculated section properties for a composite girder.

The ratios of the experimental properties to the calculated properties given in Table 7.2 for a full composite section are noted in parentheses. As shown, girders 1 through 4 of Unit-N had a larger moment of inertia and section modulus than the same four girders at Unit-S. Girder 5 had larger values for Unit-S, however, there were more possibilities of error in the strain data for this girder since it was located most remote from the trailer load. The moment of inertia of the girders varied from 63% to 99% of the stiffness of a full composite section for Unit-N

and from 50% to 86% for Unit-S. The percentage was lowest for girder 2, which was located directly beneath the trailer load, and highest for girder 4. Girders 1 and 3, which were located on either side of girder 2, showed about the same relative stiffness percentage with respect to a theoretical composite section (approximately 78% at Unit-N and 71% at Unit-S).

The observations noted above show that the stiffness of the girders with respect to a full composite section was lowest at girder 2 (i.e., the most heavily loaded girder) and increased for the other girders in relation to the distance of the girder from girder 2. The same observation was made for the section modulus, however, the values were closer to the fully composite section. With the exception of girder 2 which had a section modulus equal to 90% of that for a fully composite section, the remaining girders of Unit-N all had a section modulus equal to a composite girder section. At Unit-S, the experimental section modulus of girders 1 and 3 was about 91% of the composite section and 100% for girders 4 and 5. Girder 2 was the lowest at 82%. These percentages show that the section modulus is less sensitive to the degree of partial composite action as the moment of inertia.

In Table 7.10, the values in brackets next to the deck forces represent the ratio between the shear friction resistance of 272 kN (61.2 kips) at the girder-slab interface and the deck forces. As shown in the table, the ratios were smaller at Unit-N, which once again shows that the girders of this unit had a higher degree of partial composite action compared to Unit-S since larger forces developed in the deck. A possible explanation for the increased partial interaction at Unit-N is

227

the expansion joint detail at bearing 3 (see Figure 5.12). This detail consisted of an armored plate connected to clip angles welded to the girder top flanges (see Figure 4.9(b)). Since the plate was oriented vertically on the outside face of the slab and was definitely connected to the girder top flanges, the connection may have prevented relative slip between the girders and the slab thus improving the girder-slab interaction. On the other hand, a filler material separated the slab from the abutment (see Figure 4.9(a)) at Unit-S which offered virtually no means of shear transfer.

Starting at a load of 124 kN (27.9 kips), the deck forces exceeded the frictional resistance by more than 34% at Unit-N and 20% at Unit-S. As the loads increased, the deck forces also continued to increase up until the final load applied in Stage 1. At the final loads, the deck force was about 70% larger than the friction restraint at Unit-N and 50% for Unit-S. These percentages represent the shear transfer attributed to mechanical interlock. In addition, extra shear transfer is provided by the expansion joint connection for Unit-N which accounts for the higher percentage compared to Unit-S. If only girders 1 through 3 are considered, however, the ratio of the friction resistance to the deck force for just these three girders decreases substantially as shown in Table 7.14. For the ratios given in the table, the friction was taken as 162 kN (36.5 kips) to account for the friction resistance for girders 1 through 3 only.

Table 7.14 Deck Force to Friction Resistance Ratios considering Girders 1 through 3.

Load (kN)	Axial Forces for Unit-N, P (kN)			Σ, (kN)
	Girder 1	Girder 2	Girder 3	
66	72	69	76	217 [0.75]•
124	111	126	118	355 [0.46]
159	148	154	148	450 [0.36]
188	165	181	191	537 [0.30]
217	194	203	212	609 [0.27]
264	234	237	250	721 [0.23]
Load (kN)	Axial Forces for Unit-S, P (kN)			Σ, (kN)
	Girder 1	Girder 2	Girder 3	
66	62	45	61	168 [0.97]•
124	100	66	113	279 [0.58]
159	120	84	136	340 [0.48]
188	152	94	153	399 [0.41]
217	152	108	166	426 [0.38]
235	152	117	172	441 [0.37]

- [ ] Ratio of friction resistance to deck force for girders 1 through 3 only.

The deck force to friction resistance ratios were larger when the total bridge cross section was considered since the individual forces in the tributary slab section of girders 4 and 5 were small. Hence, the small values for girders 4 and 5 do not reflect a lower degree of partial composite action for these girders but are rather due to the transverse position of the trailer load. When these forces are considered the ratios give misleading indications that the friction resistance is a higher percentage of the deck force.

Based on the ratios given in Table 7.14, it appears that the mechanical interlock provides the most substantial amount of shear transfer exceeding that provided by friction. Past research has also justified this to be true as discussed by Suetoh et al. (1988). In that investigation, various case studies of non-

composite bridges were presented. An observation made from the case studies was that when the deck slab simply rested on the top flange of the girders, virtually no partial composite action occurred in the girders. Evidence of partial composite action was shown mainly when the top flange was embedded into the bottom of the deck slab as with the Marlin bridges. Embedment of the top flange maximizes the shear restraint provided by mechanical interlock since the topside and the sides of the flange interact with the slab.

7.4   SUMMARY

The load distribution response and girder-slab interaction of the tested Marlin bridge units under the load of the trailer has been presented. To evaluate the behavior, relationships were developed for approximating the moments in the girder sections as well as the stiffness properties such as moment of inertia and section modulus. Girder distribution was evaluated experimentally by expressing the moment in each of the girders as a percentage of the total bridge moment at the instrumented sections. Distribution factors based on measured strains were shown to provide accurate results when the effective bending resistance (i.e., section modulus) of the girders was considered.

Strain measurements taken over the depth of the curb (during the test of Unit-S) proved that it contributed to the stiffness of the exterior girder. These measurements also justified the assumptions made to compute the girder moments and section properties from the measured girder strains. A qualitative evaluation of the strains measured at the expansion bearings showed evidence of partial

230

composite action. In addition, the strain field at the bearings provided stronger evidence of the partial composite action than other inadvertent types of behavior such as bearing restraint. The moments caused by bearing restraint along with the possibility for the deck stiffness to be larger than predicted are two potential factors that may improve the comparison between the measured bridge moment and the calculated moment and thus, must be accounted for.

A change in load distribution occurred in the positive moment region from Stage 1 to Stage 2 due to the yielding of girder 1 in the negative moment region. Yielding of this girder in negative moment resulted in a reduction of continuity at the interior support thus causing girder 1 to experience larger positive moments during Stage 2 compared to Stage 1. Consequently, the load distribution factors for girder 1 in positive bending increased in Stage 2 and decreased for the remaining girders.

The girders showed a larger degree of partial composite action at Unit-N than at Unit-S. The increase in girder-slab interaction was believed to be due to the expansion joint detail used at Unit-N in which the armored plate restricted relative slip between the girders and the slab at the expansion ends of the girders. At Unit-S, no means of shear transfer other than friction and mechanical interlock existed since the joint separating the slab from the abutment end of the girders was filled with a bituminous material only. Mechanical interlock provided the larger amount of shear transfer compared with friction.

CHAPTER 8

BRIDGE RATING BASED ON MEASURED RESPONSE

This chapter covers the application of the measured bridge response to the load rating process. The response of the bridge units subjected to partially loaded dump trucks (hereafter referred to as the service load runs) is presented in Section 8.1. As described in Chapter 5, the bridge units were loaded with the dump trucks along three transverse paths between trailer load cycles. The service load runs started when the gross weight of the dump trucks was just less than the last trailer load applied. Measurements taken during the service load runs served as a continuous monitor of the lateral load distribution and girder-slab interaction exhibited by the bridge units as affected by the heavy loads applied with the trailer-concrete barrier system.

Based on the service load response and on the findings of Chapter 7, suggestions are made in Section 8.2 for implementing the measured behavior of the bridge units (e.g., distribution factors and section properties) in the AASHTO rating process. Attention is given only to the Allowable Stress (AS) and Load Factor (LF) methods, which are the two primary methods used to rate bridges in the state of Texas. Limitations associated with these two AASHTO techniques for using load test results to possibly improve the bridge rating are particularly addressed. The more recent Load and Resistance Factor (LRF) method is yet to be adopted in Texas and thus no experimental rating suggestions are made for this approach. Important findings in the chapter are summarized in Section 8.3.

8.1 BRIDGE RESPONSE UNDER SERVICE LOADS

As part of the evaluation of the service load response, a load distribution study was conducted using the bending moments in the girder sections estimated from the strains measured under the dump truck loading. This investigation was performed to check if changes in the structural condition of the bridge units observed under the increasing trailer loads were also evident in the behavior under normal traffic loads. In addition, since the dump trucks were driven across the bridge deck along various transverse positions, the effects of lateral load position on the girder distribution was evaluated. The investigation was carried out at both the positive and negative moment regions of the bridge units (i.e., Sections c-c and d-d of Figures 5.12 and 5.18).

Separate distribution analyses were done for the three transverse load paths of the dump trucks (described in Figures 5.17 and 5.21). For each path, the measured distribution factors were subsequently judged against the AASHTO values based on a single loaded traffic lane. Further comparisons were made with the calculated distribution factors from a linear elastic finite element analysis of the bridge units. Specific details regarding the modeling and analysis of the Marlin bridge units are given in Section 8.1.1. Statistical analysis of the experimental distribution factors was also performed to assess the variance in lateral distribution as influenced by the heavy loads applied during the trailer load cycles.

In both the positive and negative moment regions, the girder neutral axes (measured under the constant weight of the dump trucks) are used to investigate girder-slab interaction following the various load increments applied during the trailer load cycles. In addition, the influence of the transverse position of the service load vehicle on the interaction between the girders and the deck slab is examined. Experimental section properties are also used to further evaluate partial composite action of the girders in the positive moment region at the service load level following the passing of heavy loads.

8.1.1 Finite Element Modeling/Analysis of Bridge Units

Finite element analyses of the bridge units were carried out with the BRUFEM (Bridge Rating using the Finite Element Method) program to compute lateral load distribution factors for the girders. This program performs linear elastic analysis and was developed specifically for modeling, analyzing, and rating slab-on-girder bridge types (Hays, et al., 1994). Two of the main pre-processing features of the program include an automated mesh generator and a moving live load utility. Girders may be modeled as either non-composite or composite with the deck slab. The post-processor provides the ability to compute bending moments in the girder sections based on an assumed tributary slab width.

Figure 8.1 shows a plan view of a representative section of the finite element model created to evaluate the elastic behavior of the Marlin bridge units under the service load vehicles. A sketch of the bridge cross section is provided at the top of the figure as an aid for interpreting the model.

234
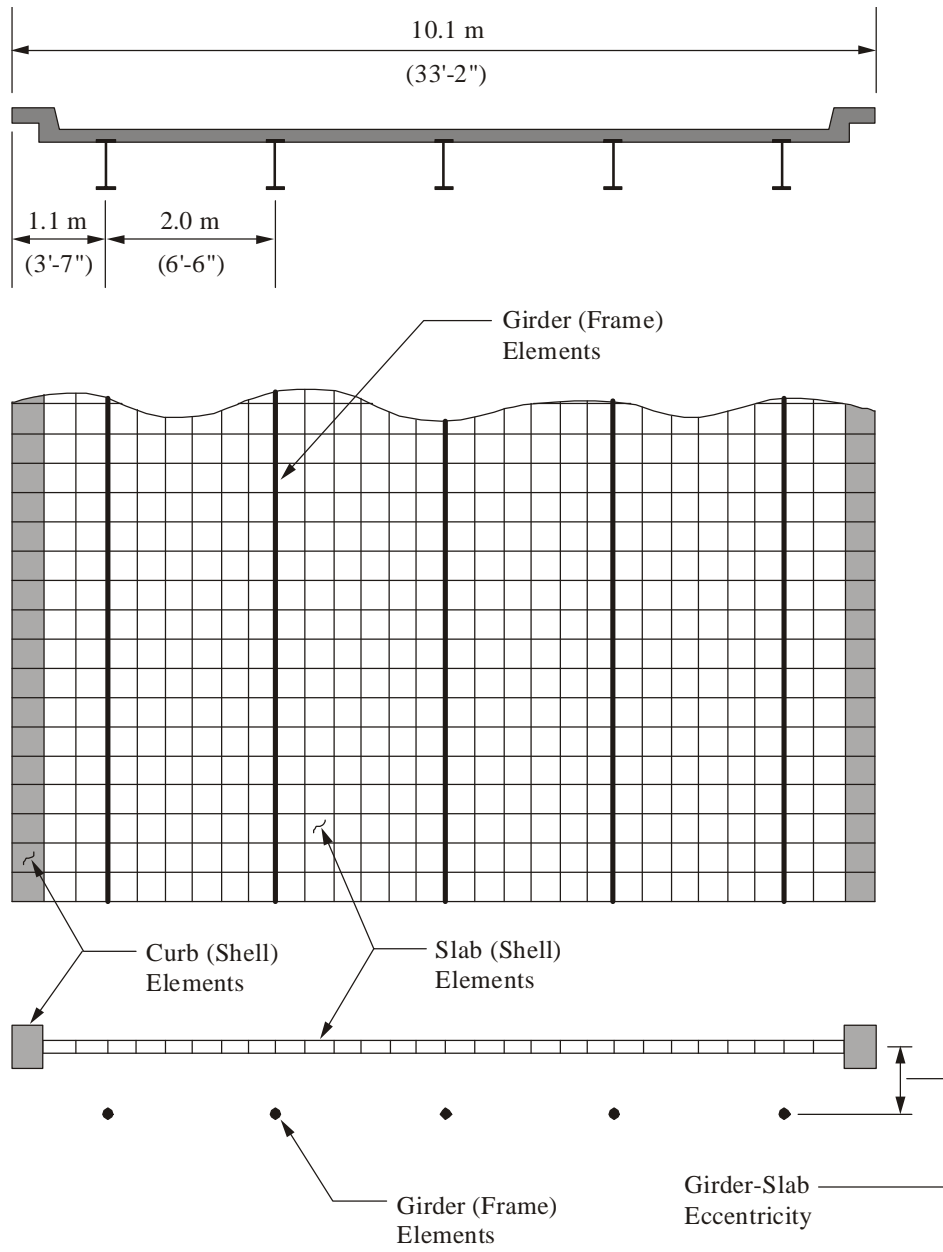
Figure 8.1 Finite Element Modeling of Marlin Bridge Units.

235

The steel girders were modeled using 2-node beam elements with six degrees of freedom (three rotation and three translation) per node. Each girder was divided into a total of 120 frame elements along its length resulting in an average element size of 305 mm (1 ft). Beam elements were given section properties representing the bare girders, which included a moment of inertia equal to 0.519 x 10^9 mm^4 (1247 in^4) and a cross-sectional area of 11200 mm^2 (17.36 in^4). Over a 2.0 m (6.5 ft) section about the center support of each girder, the moment of inertia and cross-section area were increased to 0.665 x 10^9 mm^4 (1599 in^4) and 13220 mm^2 (20.49 in^2) to account for the cover plates attached to the top and bottom flanges.

Four-node shell elements were used to model the deck slab and the monolithic curbs. As with the beam element, there are three translation and three rotation degrees of freedom per node of a shell element. Between girders, the deck slab was divided into six rows of shell elements over the 2.0 m (6.5 ft) spacing. Three rows of shell elements were used to model the 1.1 m (3.58 ft) deck overhang on either side of the exterior girders, one of which corresponded to the curb. With this mesh, the size of each shell element came out to roughly 305 mm (1 ft) by 305 mm (1 ft), which provided an ideal aspect ratio of one.

Slab elements were assumed to have a constant thickness of 152 mm (6 in) over the entire span length of the bridge units. The two outer rows of shell elements representing the curbs were assigned an effective thickness of 508 mm (20 in). The BRUFEM pre-processor has an option to reduce the thickness of the shell elements in the negative moment region to account for cracking in the deck.

Although reducing the girder stiffness in negative moment regions will certainly alter the distribution of load in the longitudinal direction, a study done by Tarhini et al. (1998) showed virtually no change in the transverse distribution pattern. Since the lateral girder distribution was of primary interest, no reductions were made to the thickness of the shell elements (both deck and curb elements) in the negative moment region.

Separate analyses were done for the three transverse paths of the dump truck vehicles. For each path, an analysis was performed with the dump truck in the critical longitudinal position causing maximum positive and negative bending moments. Thus, a total of six load cases were considered (two per load path). Positive moment at Section c-c and negative moment at Section d-d were largest when the front axle of the dump truck was about 12.2 m (40 ft) and 10.7 m (35 ft), respectively, from the center support as shown in Figure 8.2. The center support corresponds to bearing 5 of Unit-N and bearing 17 of Unit-S. Nodal loads representing the wheels of the service load vehicles were computed automatically by the BRUFEM pre-processor and applied to the finite element bridge model.

The bottom sketch of Figure 8.1 shows a cross sectional view of the finite element bridge models. In BRUFEM, composite action is modeled by offsetting the centroids of the girder elements and the deck elements in the vertical direction with a rigid link. Similarly to the procedure described in Chapter 7, the theoretical bending moment in each girder section equals the sum of the girder moment, the moment in the tributary slab segment, and the moment couple caused by the axial forces acting at the centroids of the girders and the slab elements.
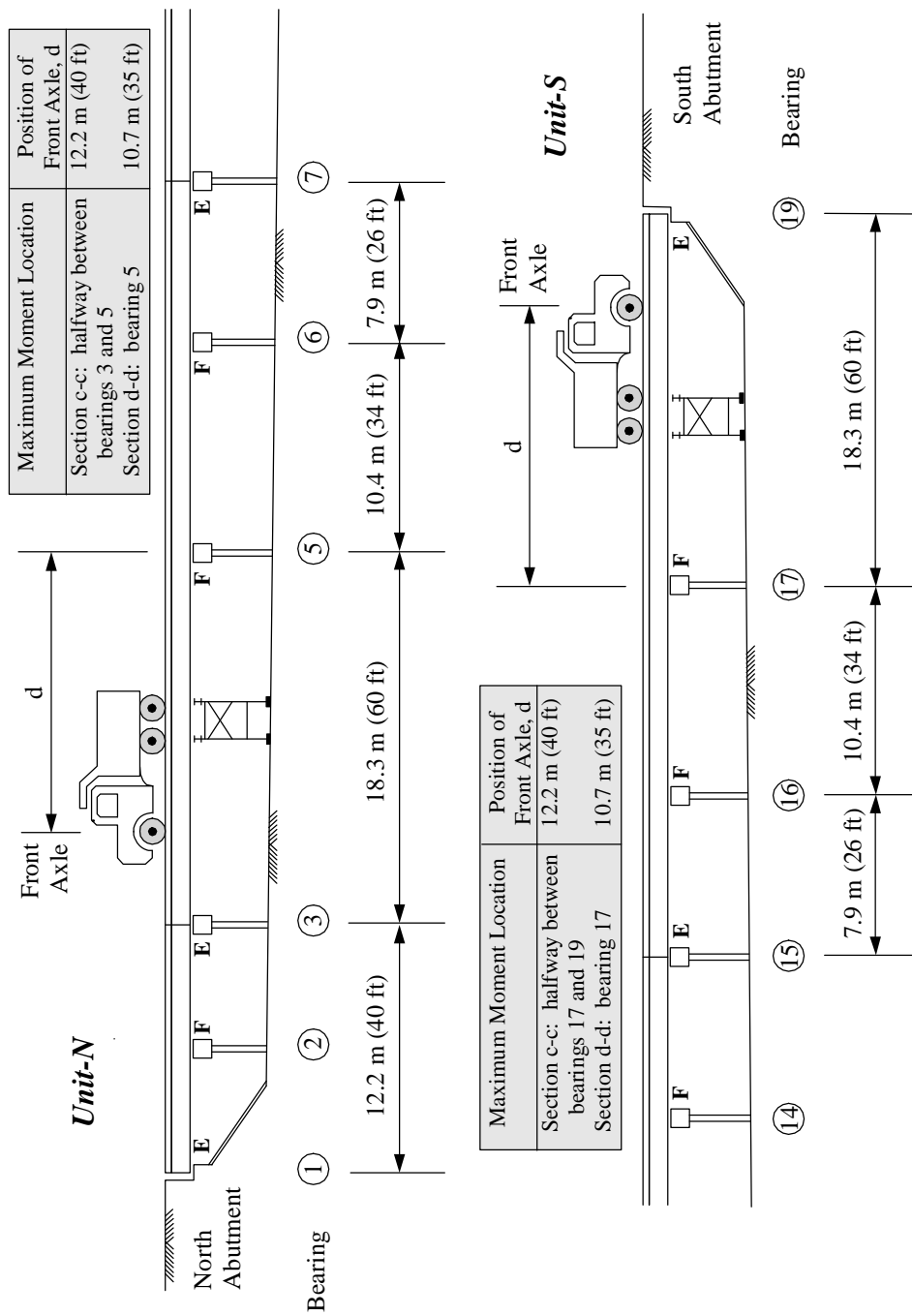
Figure 8.2 Critical Dump Truck Positions for Maximum Positive Moment at Section c-c and Maximum Negative Moment at Section d-d.

238

This calculation is performed routinely by the BRUFEM post-processor assuming a tributary slab section for the girders. For interior girders, the tributary slab width is taken as the girder spacing while for the exterior girders, the width is equal to half the girder spacing plus the overhang (including the curbs). To model non-composite action, the rigid link is removed which eliminates the moment couple term since there are no axial forces in the girder and deck elements for this case. For both the composite and non-composite models, the total bridge moments at Sections c-c and d-d (determined by summing the individual moments of the girder sections) converged to the exact solution for the six load cases, which validated the accuracy of the models.

8.1.2   Lateral Load Distribution

Experimental distribution factors for positive moment at Section c-c and negative moment at Section d-d were determined for the girder sections during the service load runs using Equation (7.20). For both moment regions, the bending moments in the girder sections applied in Equation (7.20) were derived from the measured strains according to the procedures given in Section 7.1.1. Girder strains used for the service load distribution analysis were extracted for the three transverse paths when the dump truck was at the critical longitudinal positions causing the maximum moments (see Figure 8.2). The total weight of the service load vehicle was 160 kN (36.0 Kips) for Unit-N and 153 kN (34.4 Kips) for Unit-S. Axle spacing and axle weights for these vehicles can be found in Figure 5.11.

Figure 8.3(a) shows the measured strain on the bottom flange of girder 3 of Unit-S with the dump truck at the critical position along path 3. The total load (trailer load plus deck load) applied previously to the bridge before the service load runs is plotted on the horizontal scale. A load of 253 kN (56.8 kips) marks the end of Stage 1 and the beginning of Stage 2. There was not much variation in the measured strain as the bridge unit was subjected to increasing load. A similar trend was observed in the distribution factor as shown in Figure 8.3(b). In fact, none of the girders experienced any major changes in load distribution during the service load runs. The small variation in distribution indicates that the girders maintained the same stiffness as the bridge was loaded incrementally to yield. Hence, no sudden loss of partial composite action occurred to significantly reduce the stiffness of the girders and thus, alter the load distribution pattern.

Table 8.1 lists the results from a statistical analysis of the experimental distribution factors for positive and negative bending moment during the service load runs. In the negative moment region, cracking of the deck slab was ignored. Although this assumption is untrue since the deck concrete is in tension, the procedures given in Chapter 7 for computing experimental distribution factors were considered adequate to make a rational judgment of the negative moment distribution and for comparison with the BRUFEM and AASHTO based values. Statistical quantities listed in Table 8.1 include the mean and the coefficient of variation (i.e., standard deviation divided by the mean) of the experimental load distribution factors for the various service runs made along each of the transverse paths between trailer load cycles.
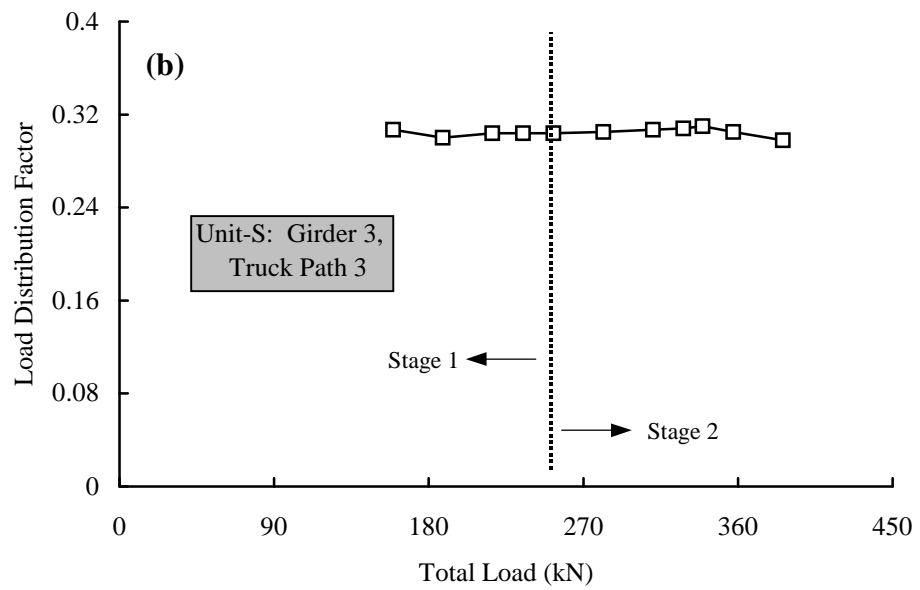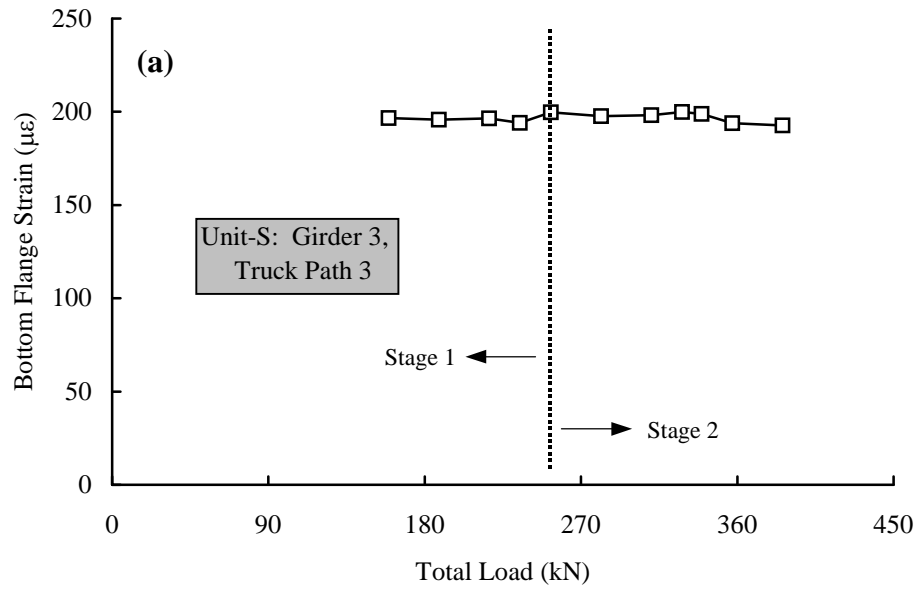
Figure 8.3 (a) Measured Strain on Bottom Flange and (b) Load Distribution
Factor for Girder 3 of Unit-S with Dump Truck at Transverse Path 3.

241

Table 8.1 Experimental Distribution Factors (Mean and Coefficient of Variation)
at Positive and Negative Moment Regions for Service Load Runs.

(a) Unit-N

Truck Path	Girder #	Positive Moment Distribution (@ Section c-c)		Negative Moment Distribution (@ Section d-d)	
		Mean	Coefficient of Variation	Mean	Coefficient of Variation
1	1	0.446	0.007	0.590	0.012
	2	0.310	0.003	0.230	0.013
	3	0.177	0.011	0.173	0.012
	4	0.062	0.016	0.032	0.031
	5	0.005	0.400	-0.024	0.125
2	1	0.329	0.049	0.450	0.029
	2	0.302	0.036	0.230	0.009
	3	0.228	0.031	0.236	0.025
	4	0.095	0.021	0.074	0.095
	5	0.046	0.109	0.010	1.000
3	1	0.160	0.056	0.215	0.093
	2	0.224	0.022	0.184	0.038
	3	0.290	0.017	0.300	0.070
	4	0.184	0.033	0.166	0.036
	5	0.142	0.049	0.136	0.110

(b) Unit-S

Truck Path	Girder #	Positive Moment Distribution (@ Section c-c)		Negative Moment Distribution (@ Section d-d)	
		Mean	Coefficient of Variation	Mean	Coefficient of Variation
1	1	0.428	0.023	0.550	0.025
	2	0.316	0.006	0.259	0.039
	3	0.185	0.016	0.199	0.010
	4	0.063	0.048	0.038	0.158
	5	0.009	0.778	-0.046	0.152
2	1	0.348	0.126	0.398	0.043
	2	0.296	0.051	0.263	0.015
	3	0.226	0.071	0.269	0.030
	4	0.093	0.097	0.093	0.086
	5	0.038	0.211	-0.024	0.250
3	1	0.137	0.051	0.132	0.091
	2	0.223	0.022	0.184	0.043
	3	0.305	0.010	0.319	0.034
	4	0.203	0.020	0.245	0.020
	5	0.132	0.068	0.120	0.108

Along transverse path 1 (i.e., closest to the curb on the loaded side of the bridge deck), service load runs were performed only during the first stage of trailer load cycles since concrete barriers were stacked next to the curb (to simulate additional dead load) during the second stage. With the barriers on the bridge deck during Stage 2, the dump truck could not be driven along path 1. Thus, the statistical analysis of the distribution factors for truck path 1 included values obtained only during Stage 1. For transverse paths 2 and 3, the evaluation was performed using service load data collected during the two stages of trailer load cycles since the barriers on the deck did not block these load paths.

At Unit-N, the average coefficient of variation for the distribution factors was 5% in the positive and negative moment regions for the three girders closest to the load (i.e., girders 1 through 3 for the first two truck paths and girders 2 through 4 for the third path). Deviations of such small magnitude were most likely due to minor differences in the transverse position of the dump trucks between the various runs made along each load path. Distribution factors for the girders of Unit-S also showed variations averaging about 5% with one exception. During truck path 2, the distribution factor for girder 1 varied by about 10%. A possible cause of this larger discrepancy is the yielding of girder 1 in the negative moment region. As discussed in Chapter 7, inelastic action at Section d-d (bearing 17 of Figure 8.2) resulted in a redistribution of load in the longitudinal direction to Section c-c (halfway between bearings 17 and 19 of Figure 8.2). This load transfer was obvious mainly in the response of Unit-S since this unit was loaded to a higher level during the trailer load cycles than Unit-N.

Table 8.2 shows the difference in girder distribution between Unit-N and Unit-S. The differences are taken with respect to the distribution factors for Unit-N. Hence, a positive value means that the girder distribution was larger at Unit-N while a negative value signifies a smaller distribution. As shown in the table, the girder distribution varied by as much as 2.5% for positive moment and 8.3% for negative moment. The first percentage suggests a rather consistent distribution of positive moment between the two units. However, the agreement was not as good in the negative moment region possibly because of the more irregular girder stiffness in this area due to the cracking of the deck slab.

Table 8.2 Comparison of Experimental Distribution Factors between Unit-N and Unit-S for Service Load Runs.

Truck Path	Girder #	Difference in Distribution	
		Positive Moment	Negative Moment
1	1	+0.018	+0.040
	2	-0.006	-0.029
	3	-0.008	-0.026
	4	-0.001	-0.006
	5	-0.004	+0.022
2	1	-0.019	+0.052
	2	+0.006	-0.033
	3	+0.002	-0.033
	4	+0.002	-0.019
	5	+0.008	+0.034
3	1	+0.023	+0.083
	2	+0.001	+0.000
	3	-0.015	-0.019
	4	-0.019	-0.079
	5	+0.010	+0.016

Table 8.3 lists the experimental bridge moments at Section c-c determined for the set of service load runs. Also given in the table is the bridge moment calculated by BRUFEM. There was a slight difference in the BRUFEM bridge

244

moments between the two bridge units since the axle weights of the service load vehicles were not the same. Ratios of the experimental to BRUFEM moments are also listed in the table.

Table 8.3 Comparison of Experimental (EXP) and Calculated (CALC) Bridge Moments during Service Load Runs.

| | Truck Path | Positive Bridge Moment (kN-m) | | |
		EXP	CALC	EXP / CALC (%)
Unit-N	1	331	393	84.1
	2	349	393	88.8
	3	357	393	90.7
Unit-S	1	306	380	80.5
	2	342	380	90.1
	3	344	380	90.6

As shown, the experimental bridge moment was closer to the calculated bridge moment as the load approached the third transverse path. Along this path, the participation of the curb is minimal as well as the torsional response of the bridge since the truckload is centered about the roadway. It appears that the procedures given in Section 7.1.1 to compute the girder moments improve as the girders experienced mainly the effects of bending while torsional effects were minimized. Chapter 7 also showed that the experimental moment may increase by as much as 5% by accounting for the counteracting moments caused by bearing restraint forces and by using an experimentally derived stiffness (i.e., concrete modulus of elasticity) to determine the bending moment carried by the deck slab. With these changes, the experimental to calculated moment ratio would improve to 95%.

In spite of the differences between the experimental and calculated bridge moments in the positive moment region, there was a relatively good agreement between the measured distribution factors and the BRUFEM based values. In Figures 8.4 through 8.9, the mean experimental distribution factors given in Table 8.1 are plotted along with the load percentages determined with the BRUFEM bridge models assuming composite (C) and non-composite action (N-C) of the girders. The first set of three figures provides the service load girder distribution at Unit-N (in order of transverse path 1 to 3) while the second set corresponds to Unit-S. A drawing of the bridge cross section is provided on the top of each figure to show the transverse position of the dump truck on the bridge deck.

Distribution factors are displayed on the vertical axis in the top graph of each figure for positive moment and in the bottom graph for negative moment. The horizontal axis of each graph represents the girder number, which are labeled on the top sketch of each figure along with the east-west orientation of the bridge cross section. Also shown on the graphs are the moment distribution factors that were computed according to the AASHTO Standard (1996) and LRFD (1998) Bridge Design Specifications. The AASHTO factors for truck path 1 were determined with the relationships specified for an exterior girder while for truck paths 2 and 3, the factors were determined based on the equations given for an interior girder. Only in the LRFD (1998) moment distribution formulas for an interior girder is the stiffness of the girders taken into account. Accordingly, two LRFD values are shown in the figures for truck paths 2 and 3; one based on composite (C) girder behavior and the other assuming non-composite (N-C).
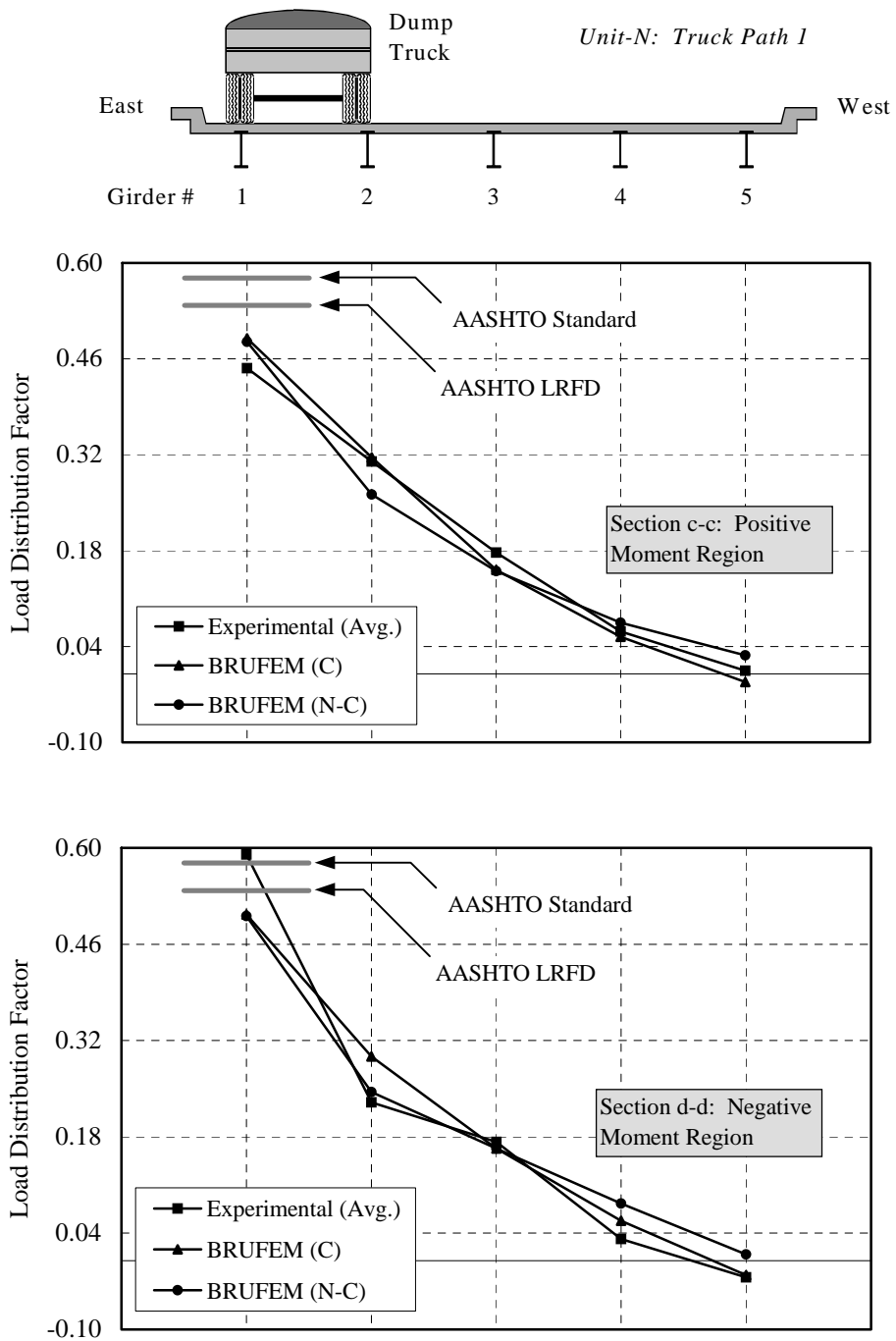
Figure 8.4 Load Distribution at Section c-c and d-d of Unit-N for Truck Path 1.
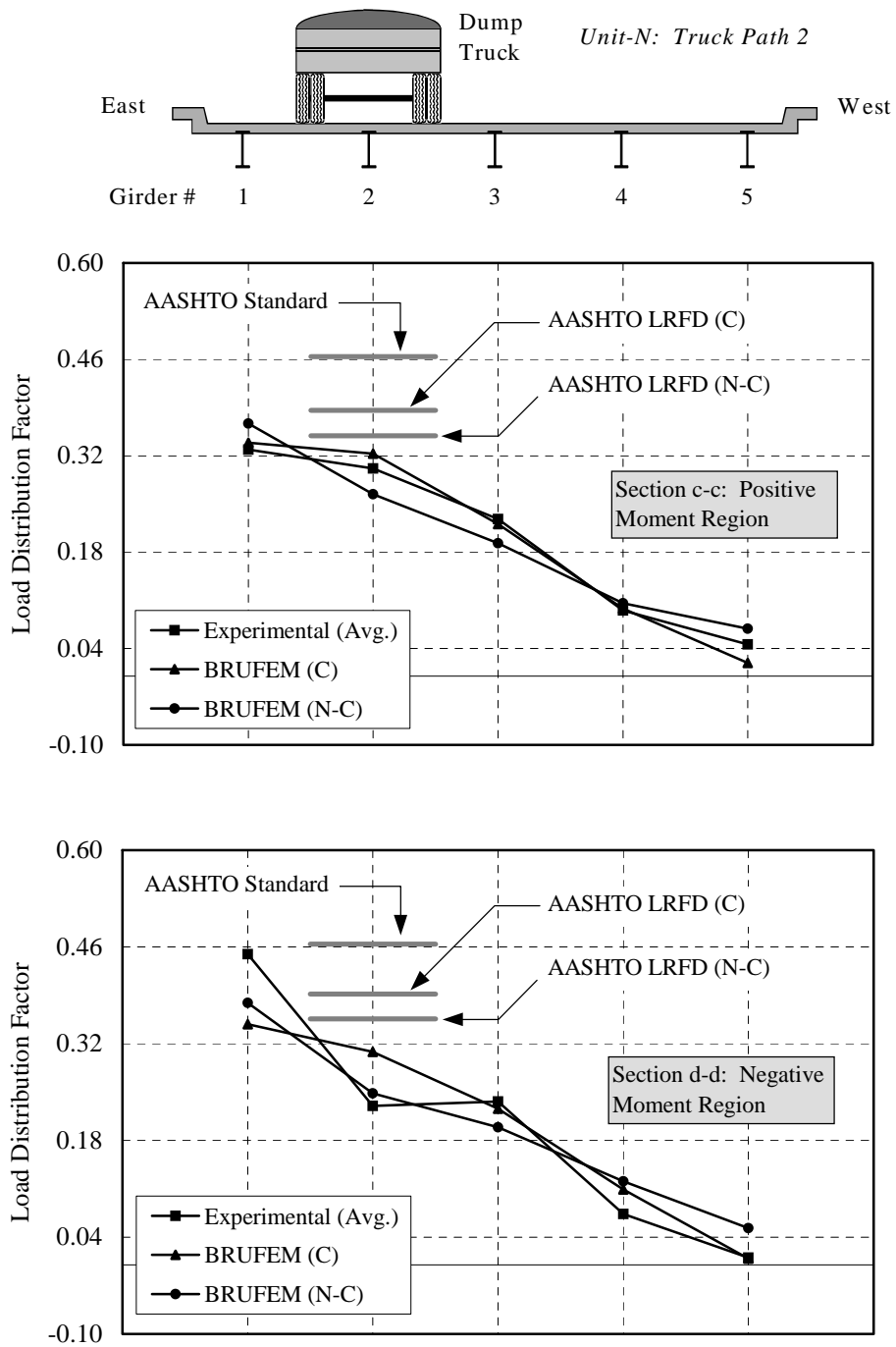
Figure 8.5 Load Distribution at Section c-c and d-d of Unit-N for Truck Path 2.
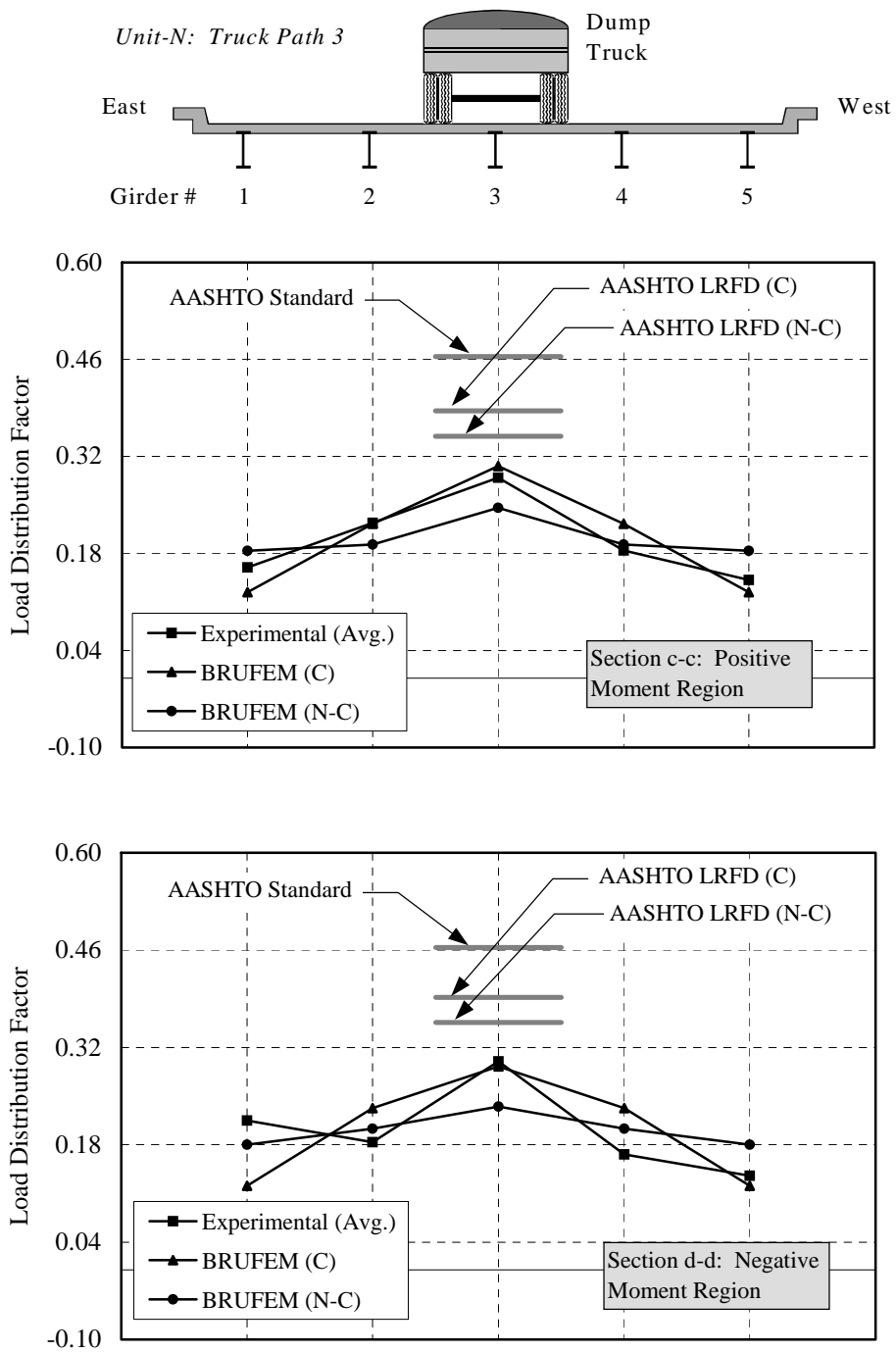
Figure 8.6 Load Distribution at Section c-c and d-d of Unit-N for Truck Path 3.

249
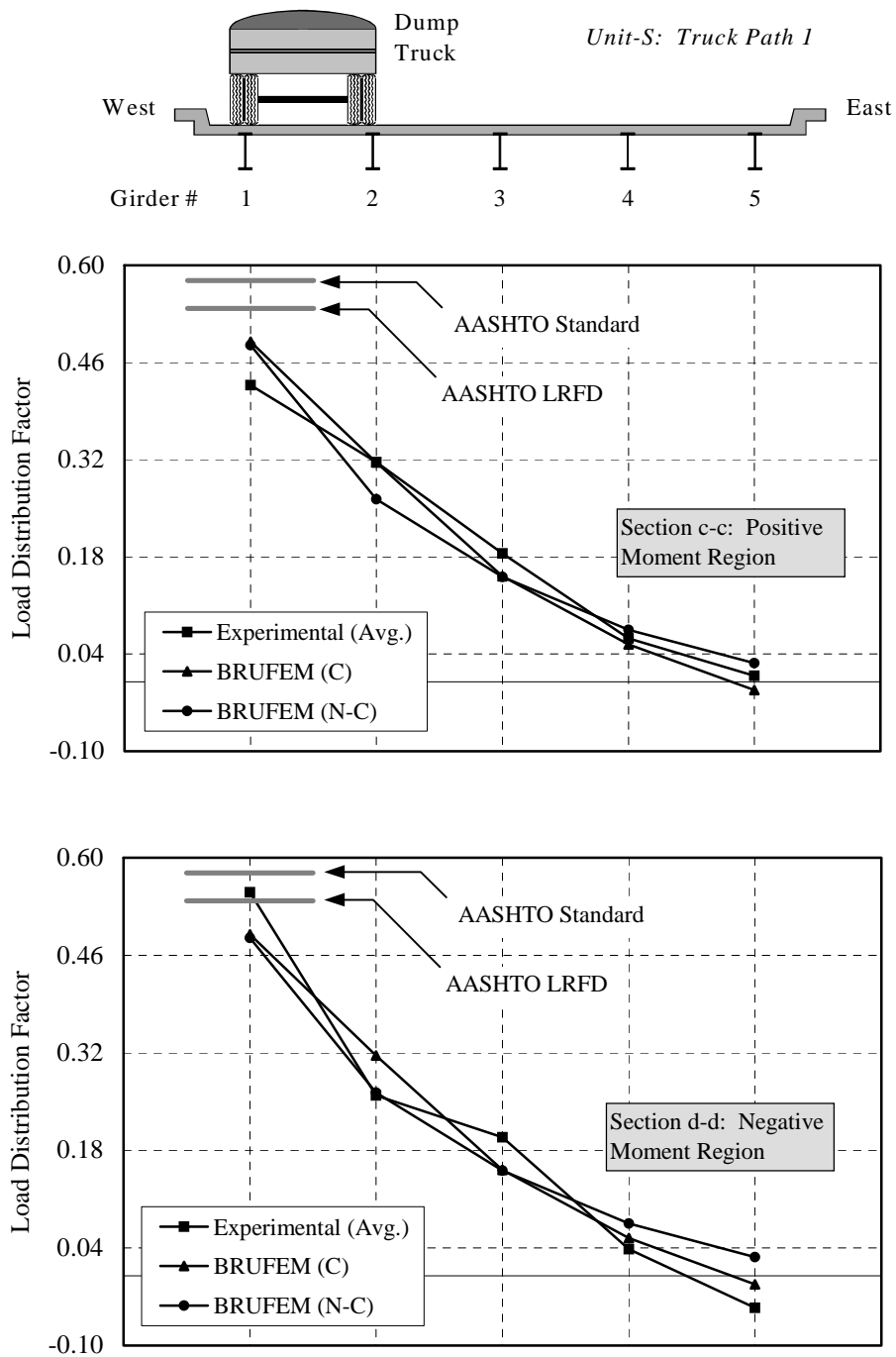
Figure 8.7 Load Distribution at Section c-c and d-d of Unit-S for Truck Path 1.
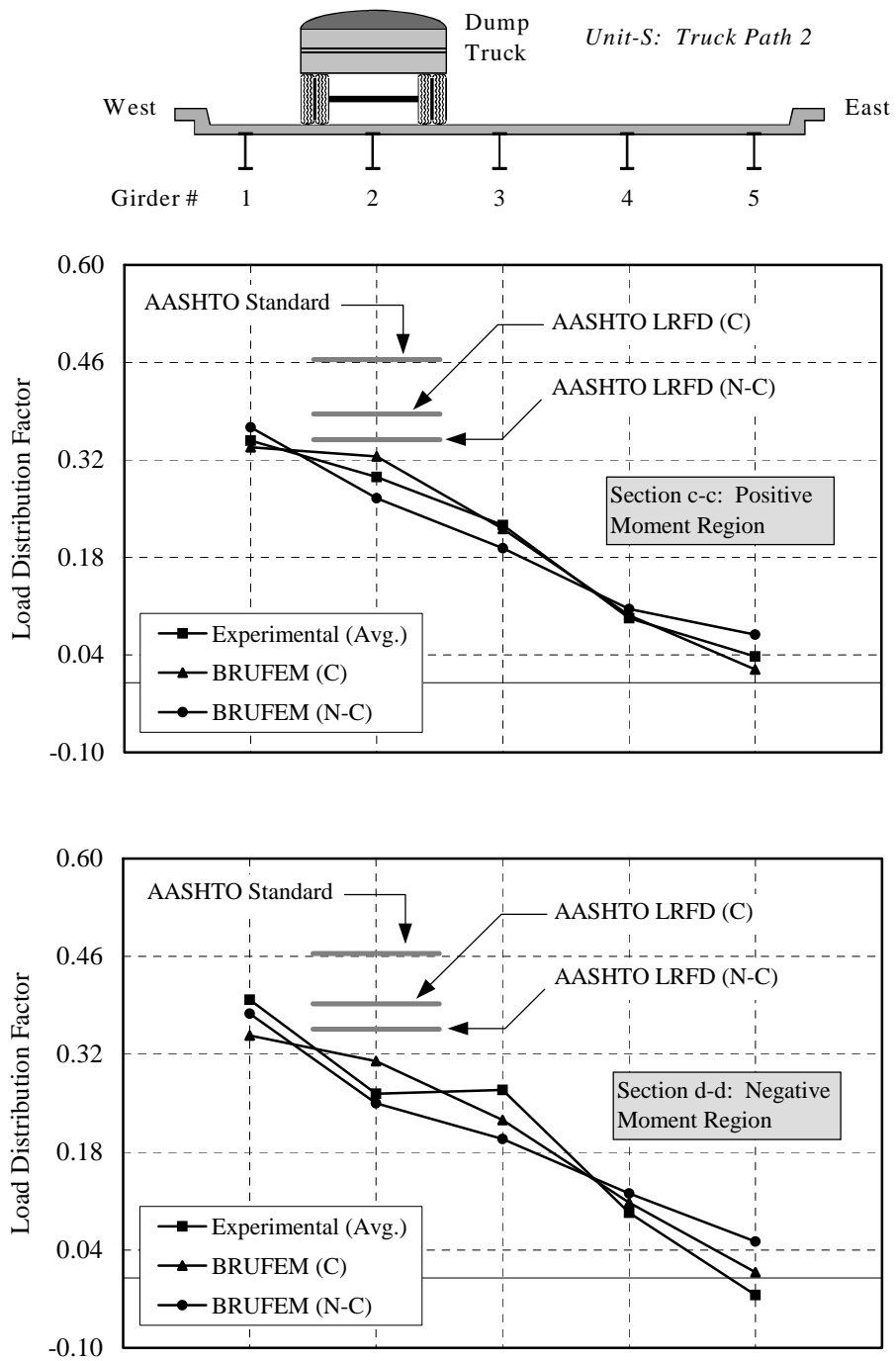
Figure 8.8 Load Distribution at Section c-c and d-d of Unit-S for Truck Path 2.

251
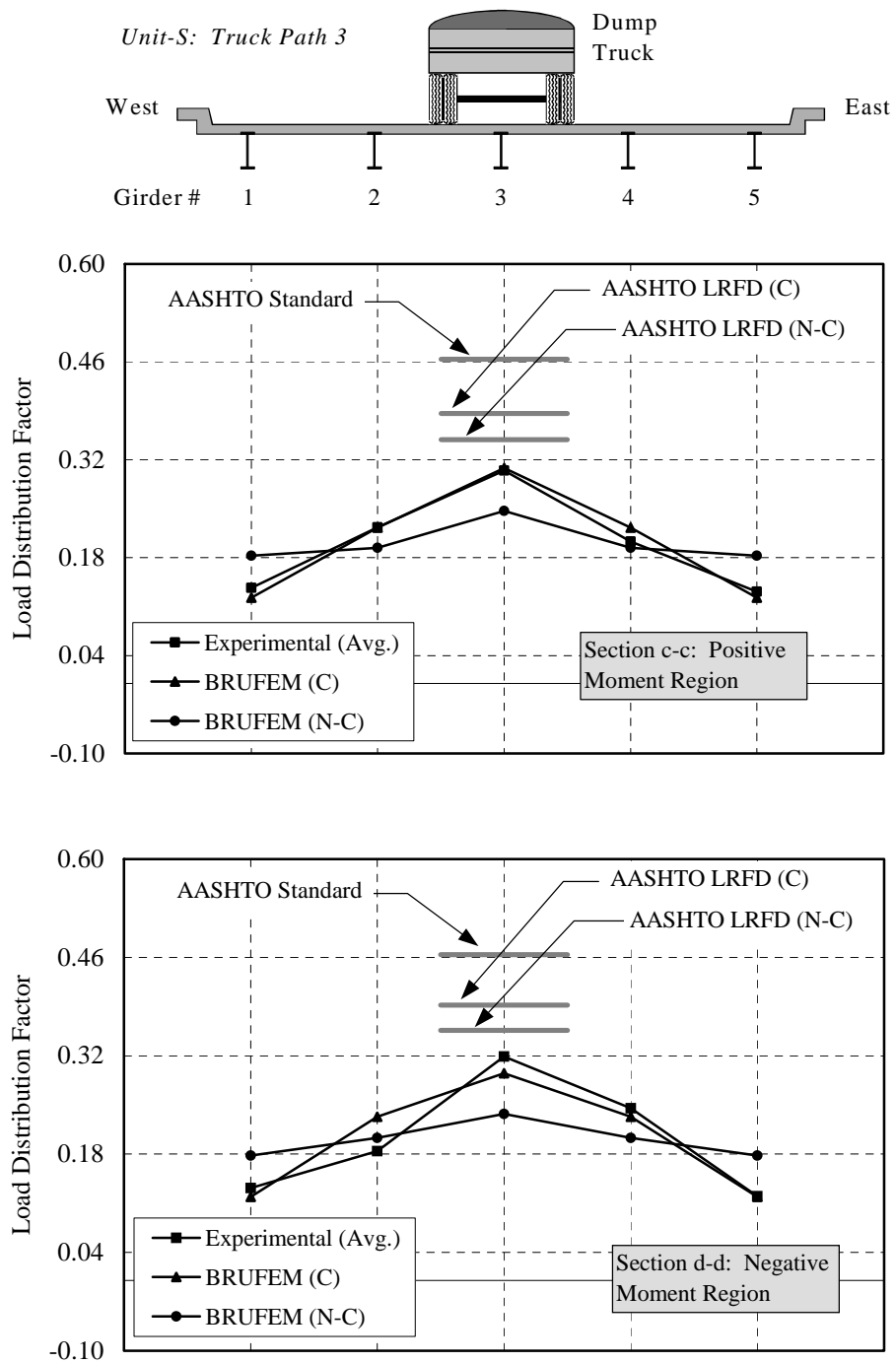
Figure 8.9 Load Distribution at Section c-c and d-d of Unit-S for Truck Path 3.

252

There were slight differences in the distribution factors computed with the two BRUFEM models (composite and non-composite) since the relative stiffness between the exterior and interior girder sections were not the same between the two models. Load is distributed in proportion to the relative stiffness between the girders. Using the values listed in Table 7.2, the ratio of the exterior to interior girder stiffness was about 1.53 for composite action and 1.66 for non-composite action (including the deck slab and curbs). As a result, the distribution factor for girder 2 based on composite action constantly exceeded the factor based on non-composite action. Hence, less load was distributed to girder 1 (i.e., the exterior girder) and more to girder 2 (i.e., the interior girder) in the bridge model with the lower relative stiffness between the exterior and interior girder.

The distribution factors from each of the BRUFEM models were nearly identical in the positive and negative moment regions since the girder stiffness is based on gross section properties in both areas. In general, the BRUFEM results based on composite action compared the best to the service load test results. In addition, the better agreement between the finite element and experimental results was observed in the positive moment region, most likely because the effects of cracking of the concrete deck in the negative moment region was ignored. Table 8.4 compares the experimental (mean values from Table 8.1) with the BRUFEM distribution factors for the service load runs. Values listed in the table represent the difference between the experimental and BRUFEM distribution factors. Negative differences imply that the BRUFEM results overestimated the measured distribution ratios while a positive difference signifies an underestimate.

Table 8.4 Comparison between Experimental (Mean) and BRUFEM Distribution
Factors for Service Load Runs.

(a) Unit-N

Truck Path	Girder #	Percent Difference in Distribution Factors for Positive Moment		Percent Difference in Distribution Factors for Negative Moment	
		Composite Action	Non-Composite Action	Composite Action	Non-Composite Action
1	1	-10	-9	15	15
	2	-2	15	-29	-7
	3	14	15	6	6
	4	13	-21	-81	-159
	5	340	-440	13	138
2	1	-3	-12	23	16
	2	-7	13	-34	-8
	3	3	15	4	17
	4	-3	-12	-47	-64
	5	59	-50	10	-430
3	1	23	-15	44	16
	2	0	14	-27	-10
	3	-6	15	2	22
	4	-21	-5	-40	-22
	5	13	-30	11	-32

(b) Unit-S

Truck Path	Girder #	Percent Difference in Distribution Factors for Positive Moment		Percent Difference in Distribution Factors for Negative Moment	
		Composite Action	Non-Composite Action	Composite Action	Non-Composite Action
1	1	-14	-13	11	12
	2	0	17	-22	-2
	3	18	18	24	24
	4	14	-19	-42	-97
	5	233	-200	74	159
2	1	3	-5	13	5
	2	-10	10	-18	5
	3	2	15	16	26
	4	-4	-14	-16	-30
	5	50	-82	133	317
3	1	10	-34	10	-35
	2	0	13	-27	-10
	3	-1	19	8	26
	4	-10	4	5	17
	5	7	-39	1	-48

Differences for the heaviest loaded girder for each truck path are highlighted in gray in the table.

As shown in Figures 8.4 through 8.9, the BRUFEM models (composite and non-composite action) were able to follow the basic trend of the measured distribution. The difference between the measured and BRUFEM distribution factors for the heaviest loaded girder averaged 10% for positive bending and 15% for negative bending. Results from the composite BRUFEM model overestimated the measured distribution factors for the heaviest loaded girder in the positive moment region. The non-composite BRUFEM model, however, underestimated the measured distribution factors for the interior girders for truck paths 2 and 3. From these observations, the finite element analysis based on composite action appears to provide conservative distribution factors while the non-composite model may be unconservative in the positive moment region.

In the negative moment region for truck path 1, both of the BRUFEM models underestimated the measured distribution factor for the exterior girder. A possible explanation for this difference is that the relative stiffness between the exterior and interior girders may be larger than that modeled by BRUFEM. As a result, more of the load is distributed to the interior girders and less to the exterior girder in the finite element analysis. The BRUFEM models also underestimated the measured distribution to the interior girder for truck path 3. Thus, for negative moment, the finite element models provided unconservative distribution factors for both the interior and exterior girders.

Based on the comparison between the experimental and BRUFEM load distribution factors, it was shown that the finite element results from a non-composite and composite bridge model do not necessarily provide an upper and lower bound to the distribution factor. In Section 8.1.3, the stiffness of the girders (i.e., moments of inertia) is shown to vary between truck paths and also from girder to girder. Interior and exterior girders are shown not to have the same stiffness as assumed in the BRUFEM bridge models. It is these differences in girder stiffness that lead to disparities between the experimental and BRUFEM distribution factors.

As shown in Figures 8.4 through 8.9, the empirical equations provided in the AASHTO Specifications provided upper limits to the measured distribution factors. Experimental distribution factors for the most heavily loaded girder (i.e., girder 1 for path 1, girder 2 for path 2, and girder 3 for path 3) were judged against AASHTO. For positive moment in girders 1 through 3, the AASHTO LRFD (1998) factors based on non-composite action provided the closest estimate of the experimental results. For negative moment, the measured distribution factor for girder 1 was closer to the AASHTO Standard (1996) provisions while girders 2 and 3 had measured distribution factors closer to the non-composite LRFD (1998) based factors. The exact amounts by which the AASHTO results exceeded the measured distribution factors for the most heavily loaded girder are given in Table 8.5. The differences in distribution, expressed as a percentage of the measured distribution factors, are given in parentheses.

Table 8.5 Difference between AASHTO and Measured Distribution Factors for
Most Heavily Loaded Girder during Service Load Runs.

Bridge Unit	Section	Girder	Maximum Measured DF	Difference in Distribution		
				Standard	LRFD (C)	LRFD (N-C)
Unit-N	+Moment	1	0.446	+0.132 (+29.6) *	+0.092 (+20.6)	+0.092 (+20.6)
		2	0.302	+0.162 (+53.6)	+0.084 (+27.8)	+0.047 (+15.6)
		3	0.290	+0.174 (+60.0)	+0.096 (+33.1)	+0.059 (+20.3)
	-Moment	1	0.590	-0.012 (-2.0)	-0.052 (-8.8)	-0.052 (-8.8)
		2	0.230	+0.234 (+100)	+0.162 (+70.4)	+0.126 (+54.8)
		3	0.300	+0.164 (+54.7)	+0.092 (+30.7)	+0.056 (+18.7)
Unit-S	+Moment	1	0.428	+0.150 (+35.0)	+0.110 (+25.7)	+0.110 (+25.7)
		2	0.296	+0.168 (+56.8)	+0.090 (+30.4)	+0.053 (+17.9)
		3	0.305	+0.159 (+52.1)	+0.081 (+26.6)	+0.044 (+14.4)
	-Moment	1	0.550	+0.028 (+5.1)	-0.012 (-2.2)	-0.012 (-2.2)
		2	0.263	+0.201 (+76.4)	+0.129 (+49.0)	+0.093 (+35.4)
		3	0.319	+0.145 (+45.5)	+0.073 (+22.9)	+0.037 (+11.6)

∗   ( ) Percent of Measured Distribution Factor

8.1.3   Neutral Axis Position

Figures 8.10 through 8.13 show the position of the neutral axes for girders 1 through 4 in the positive moment region, respectively, determined from the girder strains measured during field testing of Unit-N (plot "a") and Unit-S (plot "b"). Similar plots of the neutral axis location of the girders in the negative moment region are given in Figures 8.14 through 8.17.

257
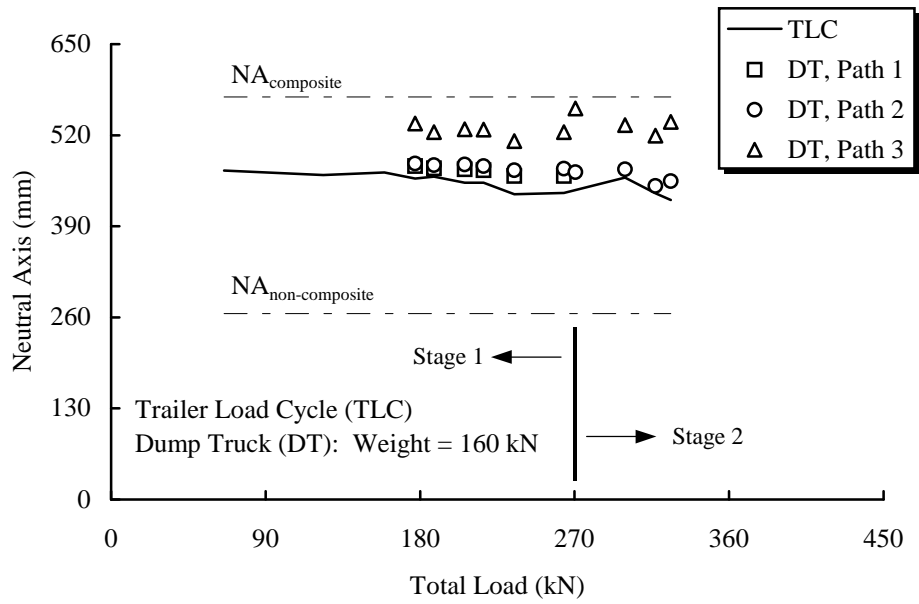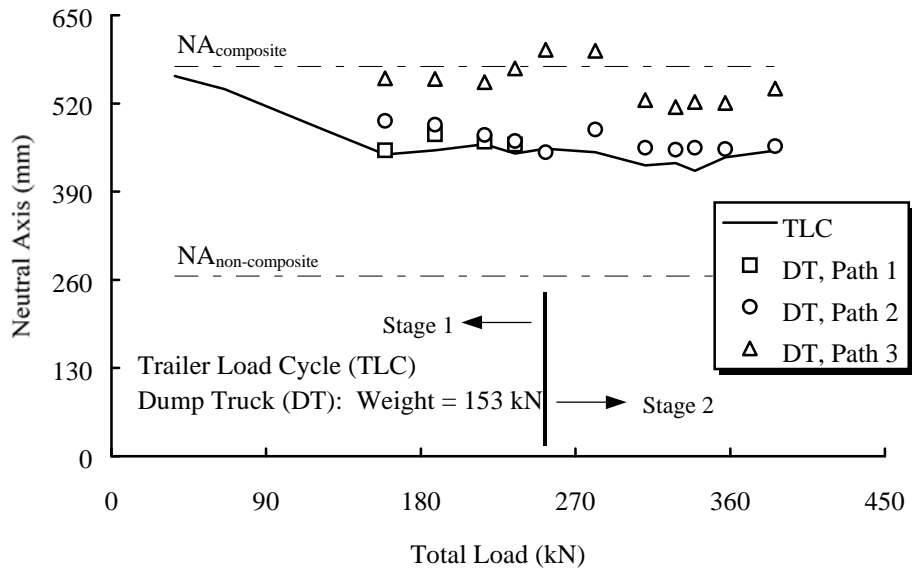
(a) Unit-N

(b) Unit-S

Figure 8.10 Neutral Axis Position for Girder 1 at Section c-c during Trailer Load
Cycles and Dump Truck Load.

258
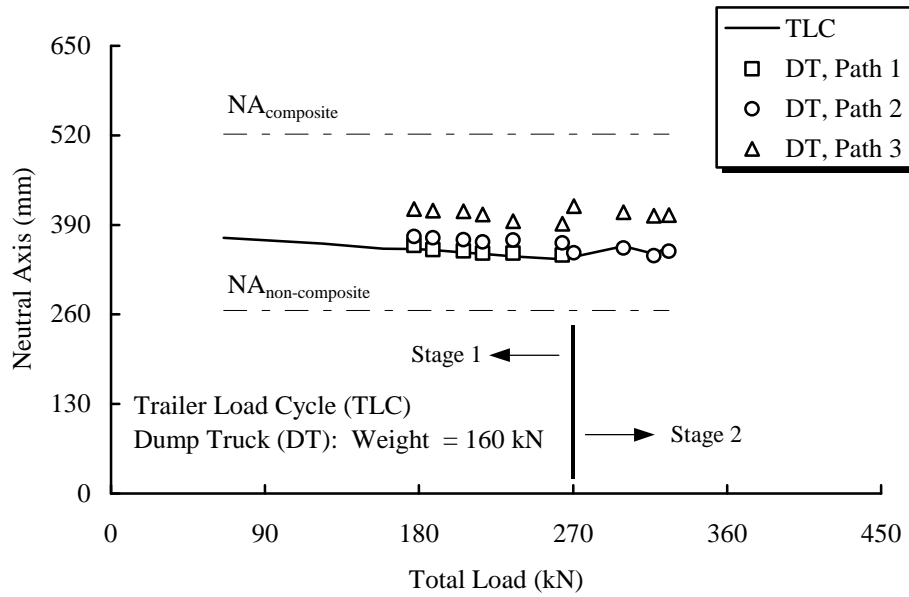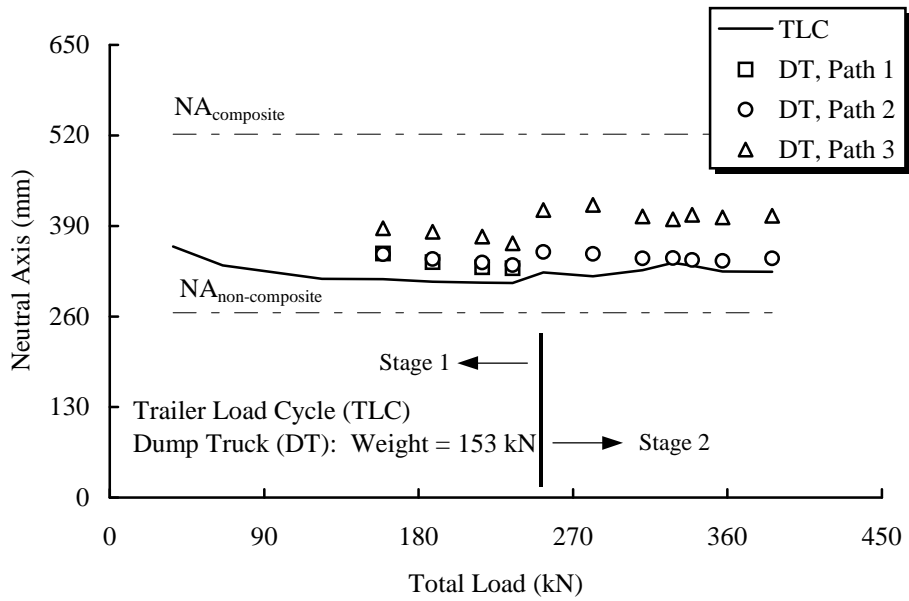
(a) Unit-N

(b) Unit-S

Figure 8.11 Neutral Axis Position for Girder 2 at Section c-c during Trailer Load
Cycles and Dump Truck Load.

259
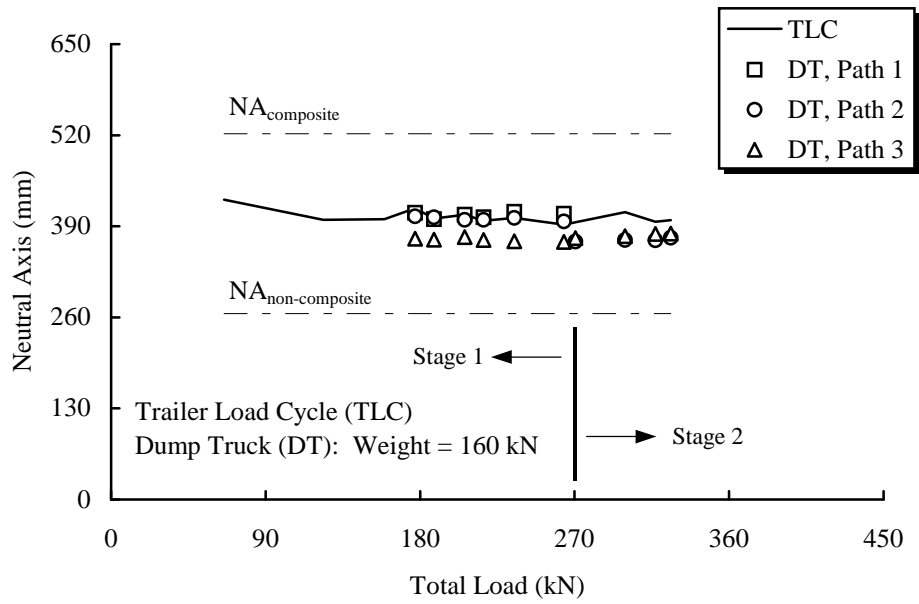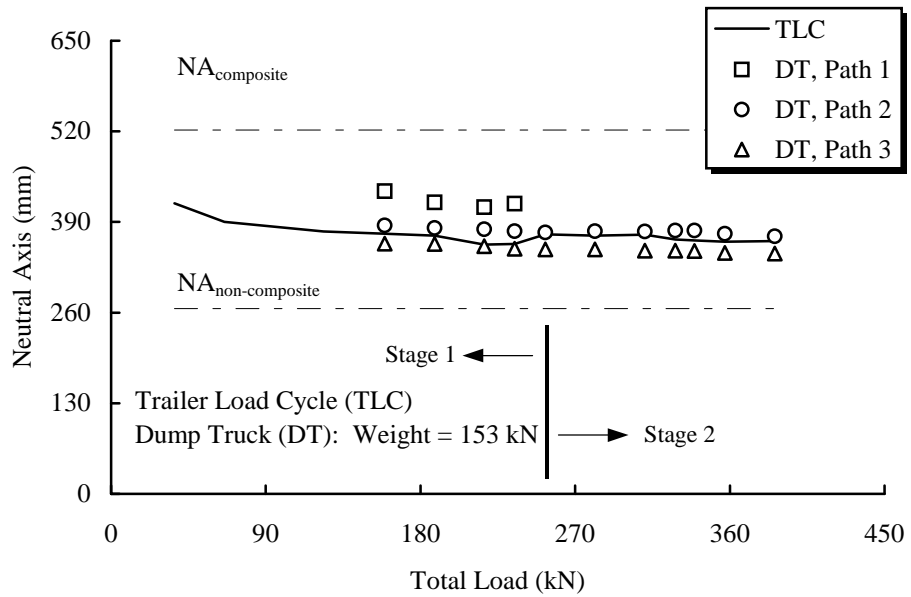
(a) Unit-N

(b) Unit-S

Figure 8.12 Neutral Axis Position for Girder 3 at Section c-c during Trailer Load
Cycles and Dump Truck Load.

260
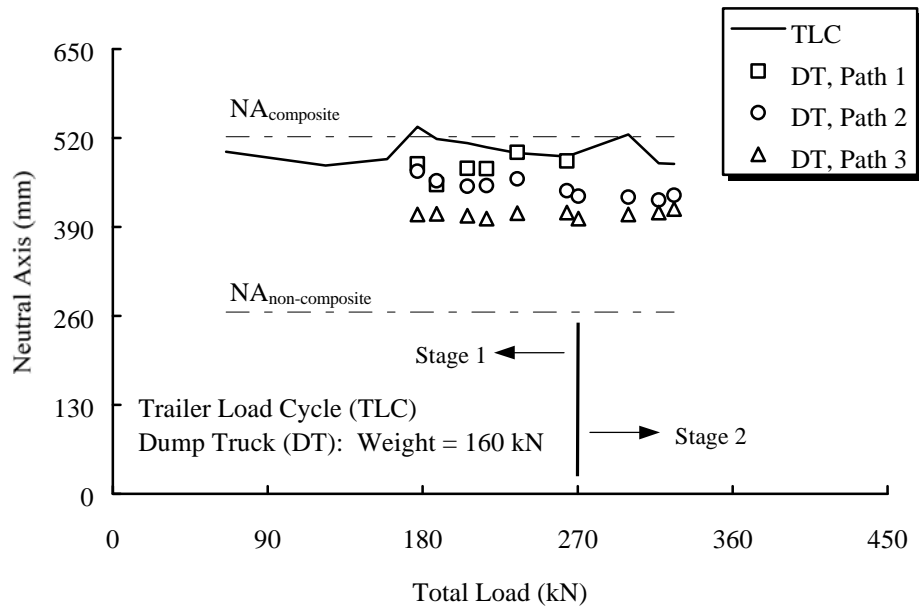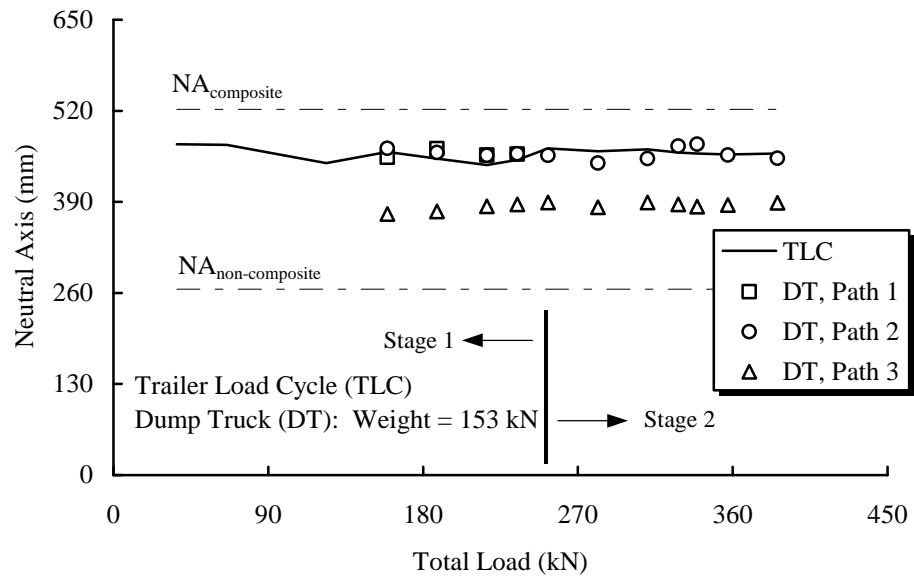
(a) Unit-N

(b) Unit-S

Figure 8.13 Neutral Axis Position for Girder 4 at Section c-c during Trailer Load
Cycles and Dump Truck Load.

261
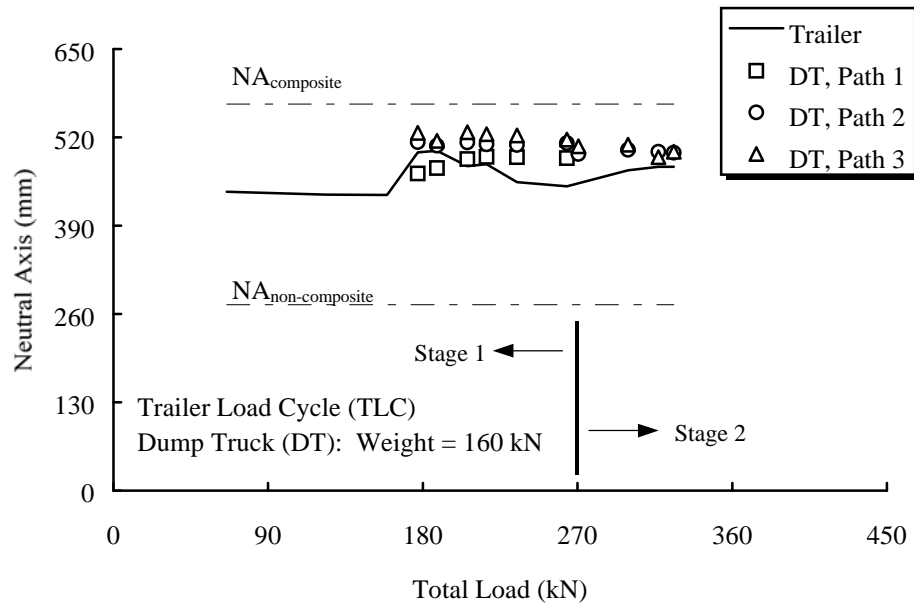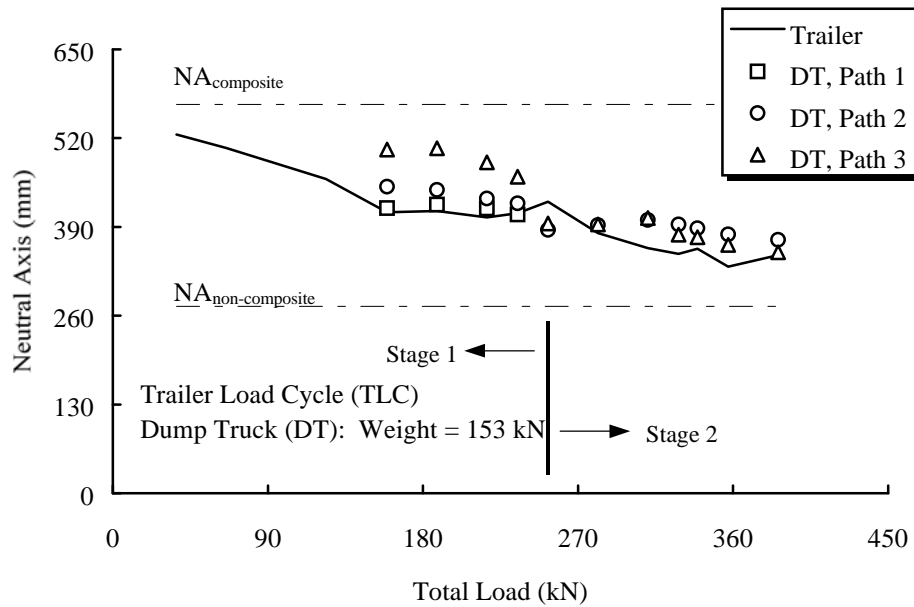
(a) Unit-N

(b) Unit-S

Figure 8.14 Neutral Axis Position for Girder 1 at Section d-d during Trailer Load
Cycles and Dump Truck Load.
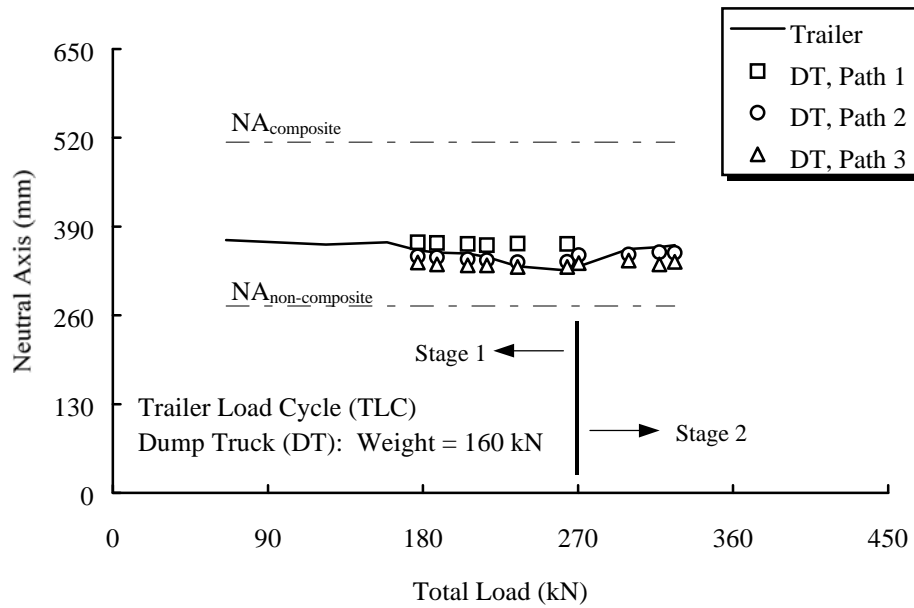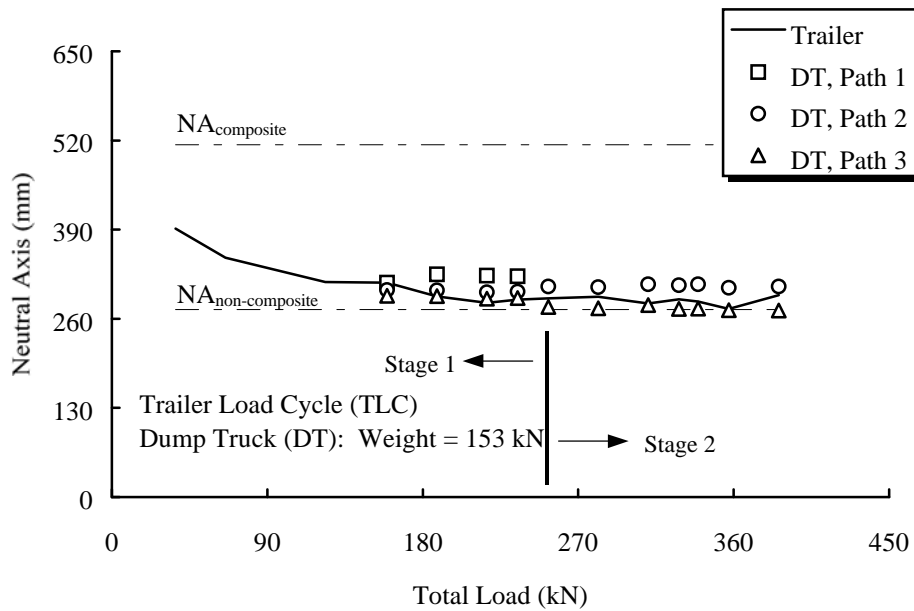
(a) Unit-N

(b) Unit-S

Figure 8.15 Neutral Axis Position for Girder 2 at Section d-d during Trailer Load
Cycles and Dump Truck Load.
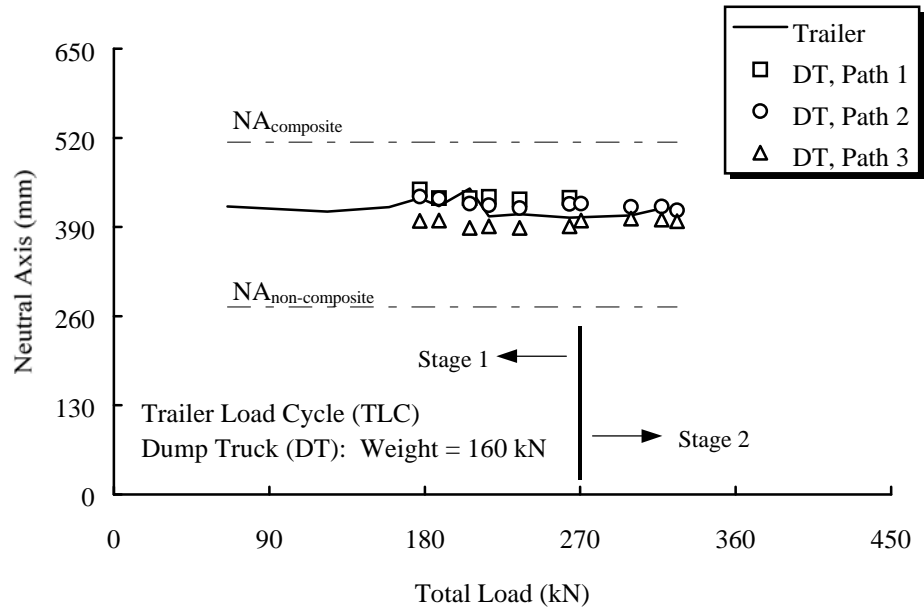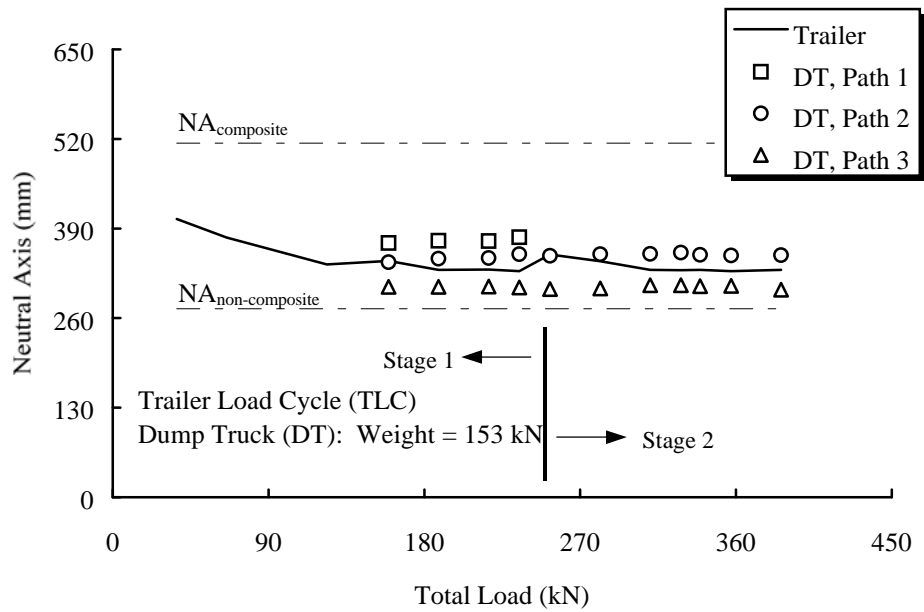
(a) Unit-N

(b) Unit-S

Figure 8.16 Neutral Axis Position for Girder 3 at Section d-d during Trailer Load
Cycles and Dump Truck Load.

264
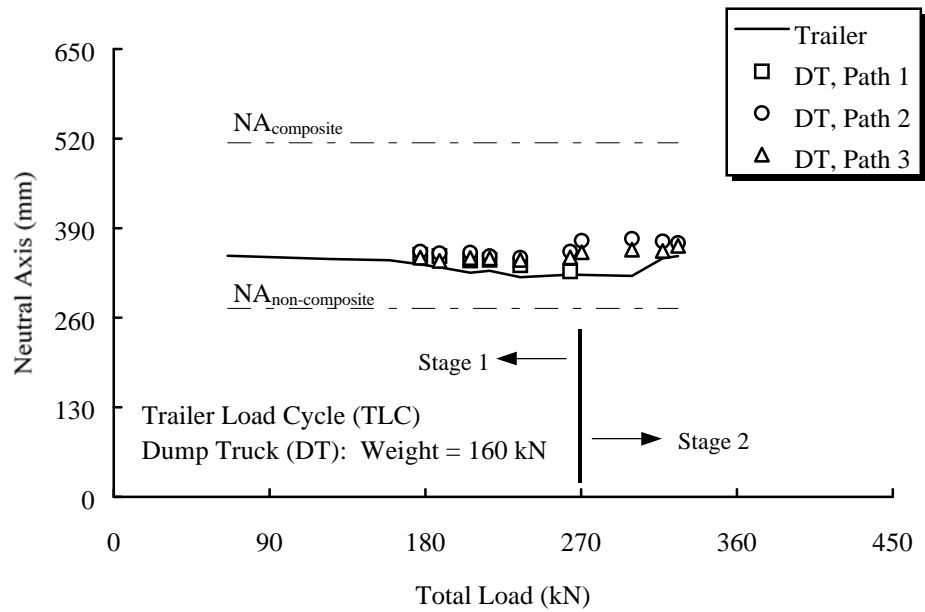
(a) Unit-N
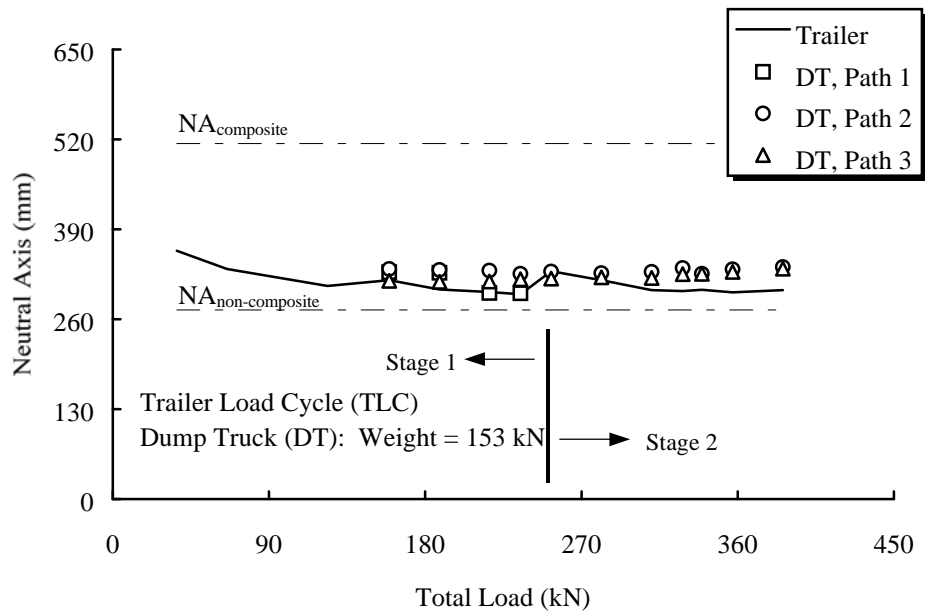
(b) Unit-S

Figure 8.17 Neutral Axis Position for Girder 4 at Section d-d during Trailer Load
Cycles and Dump Truck Load.

265

In Figures 8.10 through 8.17, the neutral axis positions (taken with respect to the underside of the girder bottom flange) are plotted as a solid line on the vertical axis versus the total load applied incrementally during the trailer load cycles (labeled as TLC). On the horizontal scale, the total load equals the trailer load plus the deck load as discussed in Chapter 5, which reached magnitudes of 326 kN (73.3 kips) for Unit-N and 386 kN (86.8 kips) for Unit-S. Stage 2 began at a total load of 270 kN (60.8 kips) on Unit-N and 253 kN (56.8 kips) on Unit-S. For the trailer load sequence, the neutral axis position was determined with the trailer at position 4.

Starting at a total load of 177 kN (39.8 kips) at Unit-N and 159 kN (35.8 kips) at Unit-S, the neutral axis positions measured during the dump truck runs (labeled as DT) immediately following the respective trailer load cycle are superimposed on the plots in Figures 8.10 through 8.17. For these service load runs, the girder neutral axes were estimated using the strains recorded when the truck was at the critical longitudinal location for maximum positive moment at Section c-c and maximum negative moment at Section d-d as described in Figure 8.2. Open square symbols designate the neutral axis positions for path 1 (determined for Stage 1 loading only), circular symbols represent path 2, and triangular symbols denote path 3. The transverse load positions of the service load vehicles are shown on the top sketch of Figures 8.4 through 8.9. The total weights of the service load vehicles used to test Unit-N and Unit-S were 160 kN (36.0 Kips) and 153 kN (34.4 Kips), respectively. Also shown on the plots are the theoretical limits of the neutral axis location based on composite and non-

composite action. Note that the theoretical neutral axis position for girder 1 (i.e., the exterior girder) based on composite action was higher up than girders 2 through 4 (i.e., the interior girders) since the curbs were included as part of the tributary slab section.

Positive Moment Region

Over the course of the trailer load cycles, the neutral axis locations for the four girders in the positive moment region remained rather steady. There was a good agreement in the measured neutral axis positions for girder 1 between the trailer load cycles and the service load runs along paths 1 and 2 as shown in Figure 8.10. The most notable difference was that the neutral axis positions for the trailer load cycles fell just below those measured under the dump trucks along the first two paths. For these load situations, the neutral axis resided about halfway between the theoretical limits for a non-composite and composite section. Along truck path 3, the neutral axis for girder 1 approached that for a fully composite section. Figure 8.11 shows that the same type of behavior was observed at girder 2, however, the neutral axis was closer to that for a non-composite section along the first two paths of the dump truck and about halfway between a non-composite and composite section for the third path. In addition, there was a greater difference between the neutral axis locations for the trailer load cycles and the service load runs along paths 1 and 2 at Unit-S than at Unit-N.

The neutral axis for girder 3 plotted in Figure 8.12 was at its lowest position under the loading of the dump truck along path 3. It is interesting to note

that the neutral axis was closer to that of a non-composite section for the third path of the dump truck than the trailer load cycles in spite of the larger magnitude of load applied with the latter loading system. The reason for this behavior is that the shear stresses at the interface between the slab and girder 3 caused by the dump truck load along path 3 were larger than those caused by the trailer load. As a result, the friction and mechanical interlock restraint at the interface was overcome under the dump truck load resulting in less partial composite action.

Notable shifts in the neutral axis position were observed for girder 3 as the dump truck moved from path 1 to 2 and from path 2 to 3 at Unit-S and Unit-N. Similar behavior was observed at girder 4 as shown in Figure 8.14, however, there was more of a difference between the neutral axis locations for truck path 3 compared to paths 1 and 2. For paths 1 and 2, the neutral axis for girder 4 was about 75% of the difference between the composite and non-composite neutral axis positions. The percentage dropped to 50% for path 3.

Negative Moment Region

In the negative moment region, girder 1 maintained a certain level of partial composite action through the full range of trailer loading for Unit-N as shown in Figure 8.14. The figure shows that the neutral axis remained steady and near to that of a full composite section. At Unit-S, however, there was a gradual decrease in the position of the neutral axis of girder 1 signifying loss of partial composite action. This behavior is consistent with the strain response observed on the top and bottom flanges of girder 1 presented in Chapter 6.

268

At both bridge units, the measured neutral axis positions of girders 2 and 4 indicated that these girders were acting non-composite as shown in Figures 8.15 and 8.17. On the other hand, girder 3 exhibited partial composite action to a level about halfway between a non-composite and full composite section at Unit-N only as shown in Figure 8.16. The behavior of girder 3 was non-composite at Unit-S. As observed in the positive moment region, the neutral axis positions decreased as the dump truck got closer to the girders in the transverse direction.

8.1.4   Moment of Inertia and Section Modulus

To further evaluate the bending stiffness and resistance of the girders in the positive moment region under the dump truck loading, section properties were derived from the measured strains using the relationships given in Section 7.1.2. Experimental properties included the moment of inertia and the section modulus (with respect to the underside of the bottom flange) for both bridge units as shown in Table 8.6. Again these section properties were determined using the girder strains with the service load vehicle at its critical longitudinal position (see Figure 8.2). Values listed in the table represent the mean and coefficient of variation of both the moment of inertia and section modulus for the various service load cycles along each of the truck paths. The coefficient of variation, in percent, is given in parentheses. In the columns next to the mean value for the measured moment of inertia and section modulus, the ratios of the experimental properties to those corresponding to a theoretical composite section (labeled as composite ratio) are listed.

269

Table 8.6 Experimental Girder Section Properties for Positive Moment Region
derived from Service Load Strains.

(a) Unit-N

Truck Path	Girder #	Moment of Inertia, I		Section Modulus, S	
		Mean (10^9 mm^4)	Composite Ratio	Mean (10^6 mm^3)	Composite Ratio
1	1	1.780 (2.6)*	0.77	3.924 (0.2)	0.97
	2	0.901 (2.0)	0.60	2.562 (0.6)	0.88
	3	1.159 (1.0)	0.77	2.747 (0.3)	0.94
	4	1.366 (4.1)	0.91	2.856 (0.8)	0.98
	5				
2	1	1.796 (1.7)	0.78	3.928 (0.2)	0.97
	2	0.937 (3.8)	0.62	2.592 (1.2)	0.89
	3	1.087 (6.3)	0.72	2.701 (1.7)	0.93
	4	1.250 (4.1)	0.83	2.799 (1.0)	0.96
	5	1.952 (2.0)	0.85	3.956 (0.3)	0.98
3	1	2.056 (2.6)	0.89	3.971 (0.2)	0.99
	2	1.100 (2.6)	0.73	2.711 (0.7)	0.93
	3	0.988 (1.6)	0.66	2.633 (0.5)	0.90
	4	1.110 (1.4)	0.74	2.717 (0.4)	0.93
	5	2.153 (0.8)	0.93	3.984 (0.1)	0.99

(b) Unit-S

Truck Path	Girder #	Moment of Inertia, I		Section Modulus, S	
		Mean (10^9 mm^4)	Composite Ratio	Mean (10^6 mm^3)	Composite Ratio
1	1	1.675 (3.6)*	0.72	3.904 (0.3)	0.97
	2	0.848 (4.1)	0.56	2.514 (1.3)	0.86
	3	1.211 (2.3)	0.80	2.778 (0.6)	0.95
	4	1.305 (2.0)	0.87	2.846 (1.6)	0.98
	5				
2	1	1.574 (8.3)	0.68	3.879 (0.8)	0.96
	2	0.871 (2.4)	0.58	2.536 (0.7)	0.87
	3	1.036 (1.8)	0.69	2.668 (0.5)	0.91
	4	1.294 (2.3)	0.86	2.820 (0.5)	0.97
	5	1.809 (5.0)	0.78	3.932 (0.4)	0.98
3	1	1.958 (2.5)	0.85	3.956 (0.2)	0.98
	2	1.065 (5.8)	0.71	2.686 (1.6)	0.92
	3	0.890 (2.6)	0.59	2.553 (0.8)	0.88
	4	1.020 (1.9)	0.68	2.656 (0.5)	0.91
	5	2.005 (2.6)	0.87	3.962 (0.2)	0.98

∗   Coefficient of Variation (%)

As shown in the table, the measured moment of inertia had a coefficient of variation less than 10% while the section modulus varied by less than 2%. For the three truck paths, the measured moment of inertia for girder 1 was over 77% of the stiffness for a full composite section at Unit-N and 68% at Unit-S. Again, the lower percentage at Unit-S was most likely due to load redistribution following yielding in the negative moment region of the girder. Girder 2 had a measured moment of inertia that was 60% of a full composite section at Unit-N and 56% at Unit-S. The level of composite action for girders 1 and 2 was least for truck paths 1 and 2.

The minimum composite ratios for girder 3 were 66% and 59% at Unit-N and Unit-S, respectively, which occurred under truck path 3. These percentages show that the degree of partial composite action exhibited by the girders was least when the dump truck was placed transversely in the vicinity of the girder. The composite ratio was largest for girders 1 and 2 for truck path 3, where it was smallest for girder 3. Conversely, the composite ratio was largest for girder 3 for truck path 1. Placing the truck closer to a particular girder increases the portion of load carried by the girder. As a result, there are larger shear forces at the girder-slab interface, which increases the relative longitudinal slip between the girder and deck slab, thus reducing the level of partial composite action as discussed earlier.

As shown in Table 7.2, the ratio between the moments of inertia of a non-composite section (including the deck slab and curbs) and a full composite section are 42% and 39% for an exterior and interior girder, respectively. For both bridge

271

units, the composite ratios for the measured moments of inertia for girders 1 through 3 exceeded these theoretical ratios. This observation was further proof that the girders acted partially composite with the deck slab at both bridge units. However, a comparison of the measured composite ratios between the two units showed a higher level of partial composite action at Unit-N.

The measured section modulus did not vary as much between the various service runs along each path (as shown by the smaller coefficient of variation) and between truck paths as the moment of inertia. In addition, the experimental section modulus was a larger percentage of the theoretical section modulus for a full composite section. At Unit-N, the composite ratio for the measured section modulus was 97%, 88%, and 90% for girders 1 through 3, respectively. As shown in Table 7.2, the composite ratio for the section modulus of a theoretical non-composite section was computed to be 91% for an exterior girder and 75% for an interior girder. Again, the measured composite ratios exceeded those for a non-composite girder section (with the deck slab and curbs). In order of girder 1 to 3, the composite ratios for the section moduli at Unit-S were 96%, 86%, and 88%, which depicted only a small drop compared to Unit-N.

Between the two bridge units, much larger differences were observed in the measured moments of inertia than in the section moduli of the girders. The discrepancy in the measured stiffness (i.e., moment of inertia) between the girders of the bridge units explains the different distribution factors given in Table 8.2. In spite of the difference in stiffness, the measured resistance (i.e., section modulus) of the girders did not vary as much between the bridge units.

272

8.2   EXPERIMENTAL BRIDGE RATING CONSIDERATIONS

There are a variety of ways in which the measurements from a diagnostic load test may be incorporated into the load rating process. One possible approach is to adjust the live load expression in the AASHTO rating equation by replacing the AASHTO live load distribution and impact factors with those derived from test measurements. Another way is to modify the resistance expression in the AASHTO rating formula using the measured section modulus for the girders. In many cases, these modifications to the AASHTO rating formula will result in a better load rating. Chapter 2 gives a detailed review of the procedures followed by many agencies to integrate the measured bridge response into the load rating. Of particular importance are the studies done by Lichtenstein (1993), Pinjarkar et al. (1990), Shahawy (1996), Schulz et al. (1991, 1995), and Stallings and Yoo (1993). There are special cases when a load test may show just cause for reducing the original rating for the bridge structure. An example of such a bridge is one where the girders have experienced loss of section due to severe corrosion and deterioration. In this case, measured strains and deflections may be larger than those predicted by an AASHTO or finite element live load analysis, thus indicating that the bridge capacity is lower than estimated.

In the experimental rating approach presented in this section, particular attention is given to the nature of the girder-slab interaction that was observed in the positive moment region during the trailer load cycles presented in Chapter 7. That is, the proposed rating technique applies to areas where the deck is primarily in compression since the procedures given in Chapter 7 to compute the girder

273

moments and section properties are less influenced by the assumption to ignore cracking of the deck slab. In the negative moment region, the bending resistance of the girders should be based on the non-composite section modulus of the bare girder as required by the AASHTO provisions since the deck is primarily in tension and thus, in a cracked condition. In addition, the AASHTO distribution factors should be used in negative moment regions to determine the live load effects since the measured factors are based on girder moments derived assuming the deck is not cracked, which is not true. Adjustments to the live load effects and girder resistance in the AASHTO rating formula based on test measurements are not considered warranted in negative moment regions until further research quantifies the negative bending resistance contributed by the deck slab, curbs, and reinforcing steel to the girders.

In the following paragraphs, recommendations are made to incorporate the live load distribution and bending resistance of the girders (measured during the service load runs) in the AASHTO rating process. These experimental properties account for the partial composite action between the girders and the deck slab, the bending resistance of the slab, and the bending resistance of the curbs; aspects of behavior which are typically ignored in conventional rating analysis. Limitations for using the measured response to improve the bridge rating are discussed. Attention is given to the Allowable Stress (AS) and Load Factor (LF) methods, which are the two primary methods used in the state of Texas to rate bridges. Also, these two methods are more consistent with the procedures used in the 1950's to design the Marlin bridges. The more recent Load and Resistance Factor

274

(LRF) method is a completely different philosophy for rating bridges which has not been adopted in Texas and thus, only a general discussion is made for this method.

8.2.1 The Allowable Stress (AS) Method

As outlined in Chapter 1, the resistance factor (ϕ), the dead load factor (γ_D), and the live load factor (γ_L) all equal one in Equation (1.2) for the AASHTO Allowable Stress (AS) method which reduces the rating factor to the expression

$$RF = \frac{R_n - D}{L\,(1 + I)} \qquad (8.1)$$

where R_n is the nominal resistance, D is the nominal dead load effect, L is the nominal live load effect caused by the rating vehicle, and I is the live load impact factor. The nominal moment resistance (M_n) is determined based on an allowable stress (σ_{all}) and the elastic section modulus of the girder (S_g) with the equation

$$R_n = M_n = S_g\,\sigma_{all} \qquad (8.2)$$

For an inventory rating, the allowable stress is taken as 55% of the yield stress, F_y, and $0.75F_y$ for an operating rating. The nominal dead load moment (M_D) equals the bending moment caused by the weight of the girders, the deck slab (including the curbs), the traffic railing, and the roadway wearing surface. The nominal live load moment (M_L) is the product of the moment caused by the rating vehicle (M_{LL}) and the moment distribution factor (DF)

275

$$L = M_L = M_{LL}DF \qquad (8.3)$$

The vehicles considered in Texas to rate bridges include the AASHTO design vehicles, the AASHTO legal loads, and the Texas legal loads shown in Figures 1.1 through 1.3. Using the nominal moment resistance, dead load moment, and live load moment terms just described, the general expression for the load rating factor given by Equation (8.1) may be rewritten as

$$RF = \frac{M_n - M_D}{M_L\,(1+I)} = \frac{S_g\,\sigma_{all} - M_D}{M_{LL}DF\,(1+I)} \qquad (8.4)$$

The two variables of Equation (8.4) that may be modified based on the test results presented in Section 8.1 are S_g and DF. No adjustments may be made to the live load impact factor since dynamic runs (i.e., truck traveling at normal traffic speed) were not conducted during the Marlin bridge tests. A study by Kim and Nowak (1997) contains procedures for assessing impact factors from field tests.

For steel bridges with non-composite girders, AASHTO provisions require that S_g be taken as the section modulus for the bare girder ($S_{g,n\text{-}c}$) ignoring any contribution from the deck slab and curbs. Thus, using the empirical distribution factor from the AASHTO Standard Specifications (DF_{STD}) for bending moment and the non-composite section modulus for the girder, the initial rating factor based on a conventional Allowable Stress ($RF_{AS,i}$) analysis is

$$RF_{AS,\,i} = \frac{S_{g,\,n\text{-}c}\,\sigma_{all} - M_D}{M_{LL}\,DF_{STD}\,(1+I)} \qquad (8.5)$$

276

A similar expression may be written using the section modulus and distribution factor measured from a diagnostic load test ($S_{g,EXP}$, DF_{EXP}) as shown in Equation (8.6).

$$RF_{AS,EXP} = \frac{S_{g,EXP}\sigma_{all} - M_D}{M_{LL}DF_{EXP}(1+I)} \tag{8.6}$$

Dividing Equation (8.6) by Equation (8.5) and rearranging the terms, a benefit factor is derived that represents the potential increase in the original load rating based on the measured behavior of the bridge. The benefit factor, K_{AS}, equals the product between two separate ratios, $K_{AS,RC}$ and $K_{AS,DF}$, both of which are greater than or equal to one as follows:

$$K_{AS} = \frac{RF_{AS,EXP}}{RF_{AS,i}} = K_{AS,RC}K_{AS,DF} \tag{8.7}$$

The first ratio, $K_{AS,RC}$, accounts for the increase in the reserve capacity available to resist live load. The increase comes from the larger section modulus for the girder that is determined experimentally, which takes into account the partial composite action of the girder and the bending resistance of the deck slab, compared with the modulus for the bare girder that is assumed by AASHTO. The formula for computing this ratio is given as

$$K_{AS,RC} = \frac{S_{g,EXP}\sigma_{all} - M_D}{S_{g,n-c}\sigma_{all} - M_D} \tag{8.8}$$

277

The ratio is different for the inventory and operating rating since the allowable stress limits are not the same.

The second ratio, $K_{AS,DF}$, is the same for both the inventory and operating ratings and accounts for the difference between the experimental and AASHTO Standard (1996) moment distribution factors. This factor is given as

$$K_{AS,DF} = \frac{DF_{STD}}{DF_{EXP}}$$ (8.9)

As shown in Section 8.1.2, the AASHTO Standard (1996) exceeded the measured distribution factors. The final bridge rating, $RF_{AS,f}$, is determined as the product of the original AASHTO rating and the benefit ratio.

$$RF_{AS,f} = RF_{AS,i} \times K_{AS}$$ (8.10)

8.2.2 The Load Factor (LF) Method

A similar rating analysis to that given in Section 8.2.1 for the Allowable Stress (AS) method can be performed for the Load Factor (LF) method. In this method, the general rating equation is given as

$$RF = \frac{R_n - \lambda_D D}{\lambda_L L (1 + I)}$$ (8.11)

where D, L, and I are as defined earlier in Section 8.2.1 for the AS method. The dead load factor, λ_D, is 1.3 and the live load factor, λ_L, is 2.17 for an inventory rating and 1.3 for an operating rating. In addition to the dead load and live load

factors, another difference in the LF method compared with the AS method is that the moment resistance is taken as the plastic capacity of the girder. In AASHTO, the plastic capacity must be determined considering only the bare girder, which gives a rating factor equal to

$$RF_{LF,i} = \frac{M_n - \lambda_D M_D}{\lambda_L M_L (1+I)} = \frac{Z_{g,n-c} F_y - \lambda_D M_D}{\lambda_L M_{LL} DF_{STD} (1+I)} \tag{8.12}$$

where $Z_{g,n-c}$ is the plastic section modulus of the non-composite girder ignoring the slab and curbs. The service load test results confirmed that the deck slab was contributing to the stiffness of the interior girder. However, since the bridge units were loaded just past first yield by the trailer load cycles described in Chapter 7, there was no verification that partial composite action of the girders would continue until ultimate. The conservative approach is taken, which is to ignore partial composite action of the girders at the ultimate moment condition and rely on only the bending resistance of the cracked tributary slab section. Thus, to determine an experimental LF rating factor, the ultimate moment resistance of the non-composite girder is increased by an amount equal to the flexural capacity of the tributary slab section ($M_{u,slab}$). Implementing this change and substituting the experimental distribution factor into Equation (8.11), the LF rating factor based on the service load test is

$$RF_{LF,EXP} = \frac{(Z_{g,n-c} F_y + M_{u,slab}) - \lambda_D M_D}{\lambda_L M_{LL} DF_{EXP} (1+I)} \tag{8.13}$$

279

A benefit ratio for the LF method is determined by dividing Equation (8.13) by Equation (8.12), which eliminates λ_L, M_{LL}, and the (1+I) terms leaving

$$K_{LF} = \frac{RF_{LF,EXP}}{RF_{LF,i}} = K_{LF,RC} K_{LF,DF} \tag{8.14}$$

where

$$K_{LF,RC} = \frac{(Z_{g,n-c} F_y + M_{u,slab}) - \lambda_D M_D}{Z_{g,n-c} F_y - \lambda_D M_D} \tag{8.15}$$

and

$$K_{LF,DF} = \frac{DF_{STD}}{DF_{EXP}} \tag{8.16}$$

The LF benefit ratio related to the reserve capacity, $K_{LF,RC}$, does not contain any measured property for the girders. However, the ratio accounting for the measured distribution factor, $K_{LF,DF}$, is the same as the AS method. Again, to obtain the final LF load rating, $RF_{LF,f}$, the original LF rating is multiplied by the LF benefit factor as shown in Equation (8.17).

$$RF_{LF,f} = RF_{LF,i} \times K_{LF} \tag{8.17}$$

NOTE: Although only the AS and LF methods were treated in detail, a few comments are made regarding the LRF method. Unlike the AS and LF methods, the LRF method allows the impact and live load factors to be set based on the condition of the wearing surface and the average daily truck traffic (ADTT),

respectively. The live load factor ranges from 1.30 for low volume roadways to 1.80 for heavy volume roadways. As shown earlier, the impact factor for the AS and LF methods is based on the span length of the bridge. In the LRF method, the dynamic allowance (i.e., impact factor) ranges from 0.1 for a wearing surface in good condition to 0.3 when the overlay is no longer functioning as designed. In addition, the LRF method uses distribution factors from the AASHTO LRFD (1998) Bridge Specifications which were shown in Section 8.1.2 to be smaller than those specified in the AASHTO Standard (1996) provisions.

The lower impact and distribution factors associated with the LRF method will reduce the live load effects and increase the initial rating factor. Hence, it appears that the LRF method serves to maximize the original rating and thus, avoid the need for load testing. Should testing be required, however, the potential benefits of this method resemble those of the LF method. One difference is that a resistance factor is applied to the moment capacity term in the benefit ratio equation related to reserve capacity. This factor is less than one and is determined based on an examination of structural redundancy, deterioration, inspection, and maintenance. Applying this fraction, will increase the reserve capacity benefit ratio compared to the LF method. The benefit ratio for the distribution factor is the same as the AS and LF methods and is simply the ratio between the empirical and measured distribution factors. As shown in Section 8.1.2, however, there was closer agreement between the AASHTO LRFD (1998) and measured distribution factors. As a result, the increase to the rating factor based on the distribution factor benefit ratio would be smaller compared to the AS and LF methods which

281

use the AASHTO Standard (1996) distribution factors having a larger deviation from the measured factors.

8.2.3 Illustrative Rating Example

The bridge units, as tested, were not rated since the large dead load moments caused by the removal of the piers left only a marginal amount of bending resistance for live load, resulting in small rating factors uncharacteristic of a typical bridge. Instead, an example rating analysis is performed on the Marlin bridge units in their original condition (see Figures 4.1 and 4.2) to illustrate the improvements associated with using the experimental findings from the service load tests. Distribution factors and section properties that were determined from the load testing of the bridge units with the piers removed are assumed to apply to the original structure. It is also assumed that the axle configuration (i.e., weights and spacings) of the loading vehicle do not affect the measured properties of the tested bridge units. This assumption is necessary in to order to use the same distribution factors and section moduli measured under the dump trucks for the AASHTO design vehicles, the AASHTO legal loads, and the Texas legal loads. The axle configurations for these vehicles are provided in Figures 1.1 through 1.3.

The rating analysis was performed based on the bending moment at mid-span of the 10.4 m (34 ft) span of the as-built bridge units. Dead load moments at this location were 47.6 kN-m (35.1 kip-ft) for an interior girder and 51.9 kN-m (38.3 kip-ft) for an exterior girder. The dead load moment for the exterior girder was slightly larger than that of the interior girder since the weight of the curbs and

steel railing were distributed entirely to the exterior girder. That is, more weight from the bridge deck bears down on the exterior girder. In addition to their self-weight, other dead load carried by the girders included the weight of the slab and asphalt-wearing surface, the amount of which depended on the tributary width. Table 8.7 lists the maximum mid-span moments caused by the design vehicles and legal loads.

Table 8.7 Maximum Bending Moments at Mid-span of 10.4 m (34 ft) Span under Design and Legal Vehicles.

Vehicle	Maximum Bending Moments
AASHTO H-20	245 kN-m (181 kip-ft)
AASHTO HS-20	275 kN-m (203 kip-ft)
Texas Concrete Truck	312 kN-m (230 kip-ft)
Texas 18-Wheeler	193 kN-m (142 kip-ft)
AASHTO TYPE 3	225 kN-m (166 kip-ft)
AASHTO TYPE 3S2	183 kN-m (135 kip-ft)
AASHTO TYPE 3-3	163 kN-m (120 kip-ft)

As shown in the table, the Texas concrete truck caused the largest moments followed by the AASHTO HS-20 vehicle. These lower weight vehicles caused higher moments since the load was distributed only to three axles whereas for the heavier vehicles the total load is spread out over more axles. Incidentally, the dump trucks used during the service load runs caused a bending moment equal to 168 kN-m (124 kip-ft), which is 61% and 54% of the moments caused by the HS-20 and TCT, respectively.

Table 8.8 lists the inventory and operating rating factors determined based on the AASHTO AS method using Equation (8.5) and LF method using Equation (8.12) for an HS-20 vehicle and Texas concrete truck (TCT). Only these two loading vehicles are considered since they caused the larger bending moments and thus, will control the load rating. For both vehicles, separate factors were determined for an interior girder (i.e., girders 2 through 4) and an exterior girder (i.e., girders 1 and 5) as shown in the table.

Table 8.8 AS and LF Moment Rating Factors based on HS-20 and Texas
Concrete Truck (TCT) Loading.

	Allowable Stress ($RF_{AS,i}$)		Load Factor ($RF_{LF,i}$)	
	Inventory	Operating	Inventory	Operating
Exterior Girder (TCT)	0.73	1.07	0.76	1.27
Interior Girder (TCT)	0.93	1.36	0.96	1.61
Exterior Girder (HS-20)	0.82	1.22	0.86	1.44
Interior Girder (HS-20)	1.05	1.54	1.09	1.82

In Equations (8.5) and (8.12), the AASHTO Standard (1996) distribution factor (DF_{STD}) for a single loaded traffic lane are used in the analysis. The DF_{STD} equals 0.578 for an exterior girder and 0.464 for an interior girder. These values were used instead of those for multiple-lane loading since the section properties and distribution factors from the service load runs were measured with the dump trucks traveling in only one lane at a time. Experimental distribution factors could be estimated for two loaded lanes by superimposing the results for the individual truck paths, however, it was not considered a proper approach since the girders had different section properties for each path. Had the girders had the

284

same stiffness for the different transverse paths of the truck, the approach would have been valid. The correct way to obtain an experimental distribution factor for multiple lane loading is to load the bridge with two dump trucks side-by-side.

The impact factor, I, used in Equations (8.5) and (8.12) is given in the AASHTO Standard (1996) provisions as

$$I = \frac{50}{3.28L + 125} \left(\text{maximum } 30\%\right) \tag{8.18}$$

which for a span length, L, of 10.4 m (34 ft) comes out to 30 percent. The elastic and plastic section modulus ($S_{g,n-c}$ and $Z_{g,n-c}$) of the bare girder used in the AS and LF rating equations, respectively, are 1.955×10^6 mm^3 (119.3 in^3) and 2.201×10^6 mm^3 (134.3 in^3).

As shown in Table 8.8, the rating factors were lower for the exterior girder since the distribution factor and thus, live load moment was larger that that for the interior girder. Operating factors from the LF method are about 20% higher than the AS method and in both cases exceeded unity meaning that the bridge was safe to carry the TCT and HS-20 on a limited basis. Inventory factors were about the same between the AS and LF methods but were less than one for both girders under the TCT and for the exterior girder subjected to an HS-20 which indicate that load restrictions should be imposed on the bridge for normal traffic loading.

Benefit ratios for the AS and LF inventory ratings were computed using the measured load distribution factors (see Table 8.1) and section moduli (see Table 8.6) for girders 1 through 3 of Unit-S and are given in Table 8.9. There was

no need to improve the operating rating factors since they were all above unity. The equations used to calculate the benefit ratios are noted in the table.

Table 8.9 AS and LF Benefit Ratios (for Inventory Rating) for Girders 1 through 3 of Unit-S.

	Allowable Stress			Load Factor		
	$K_{AS,RC}$ (Eq. 8.8)	$K_{AS,DF}$ (Eq. 8.9)	K_{AS} (Eq. 8.7)	$K_{LF,RC}$ (Eq. 8.15)	$K_{LF,DF}$ (Eq. 8.16)	K_{LF} (Eq. 8.14)
Girder 1	2.30	1.35	3.11	1.38	1.35	1.86
Girder 2	1.38	1.57	2.16	1.08	1.57	1.69
Girder 3	1.39	1.52	2.11	1.08	1.52	1.64

The load distribution factor and section modulus measured with the dump truck traveling along transverse path 1 were used to represent the response of girder 1. Similarly, the distribution factor and modulus of girder 2 was based on the measured behavior for truck path 2 whereas girder 3 was based on path 3.

The benefit ratios related to the distribution factor are the same in both the LF and AS method. For the reserve capacity, the ratios for the AS method were higher since the measured elastic section modulus is considered which takes into account partial composite action of the girders. At the strength limit state, it was believed that any partial composite action between the deck and the girders would disappear. Thus, in the LF method, the reserve capacity is based on the plastic moment of the bare girder plus the ultimate moment of the tributary slab section. Figures 7.1 and 7.2 show the tributary slab sections for an interior and exterior girder for which the flexural capacities were computed with the basic formula

$$M_n = M_{u,slab} = A_s f_y \left(d - \frac{a}{2} \right) \qquad (8.19)$$

286

where A_s is the area of the tensile reinforcement steel, f_y is the yield stress of the reinforcement equal to 276 MPa (40 ksi), d is the vertical distance from the extreme compression fiber to the centroid of the reinforcement, and a is the depth of the Whitney stress block. To determine a, the compressive force in the concrete, C, is equated with the tensile force in the steel, T, as follows

$$C = T \tag{8.20}$$

$$0.85 f_c' ba = A_s f_y \tag{8.21}$$

$$a = \frac{A_s f_y}{0.85 f_c' b} \tag{8.22}$$

where b is the width of the compression zone and f_c' is the compressive strength of the concrete equal to 24.1 MPa (3.5 ksi). The width of the compression zone equals the curb width for the exterior girder and the tributary slab width for the interior girder. Based on these values, the flexural capacities of the tributary slab sections were 147 kN-m (108 kip-ft) and 29.7 kN-m (21.9 kip-ft) for the exterior and interior girders, respectively.

Table 8.10 shows the inventory rating factors for the Texas concrete truck adjusted with the benefit ratios from Table 8.9. The initial load ratings are first modified separately by each benefit ratio, to illustrate the improvements attributed solely to the increase in reserve capacity and to the field-measured distribution factors, and then with the benefit ratios combined.

Table 8.10 Adjusted AS and LF Inventory Ratings for Girders 1 through 3 of Unit-S for Texas Concrete Truck.

	Allowable Stress ($RF_{AS,f}$)		
	$RF_{AS,i}* \times K_{AS,RC}$	$RF_{AS,i} \times K_{AS,DF}$	$RF_{AS,i} \times K_{AS}$
Girder 1	1.68	0.99	2.27
Girder 2	1.28	1.46	2.01
Girder 3	1.29	1.41	1.96
	Load Factor ($RF_{LF,f}$)		
	$RF_{LF,I}\bullet \times K_{LF,RC}$	$RF_{LF,i} \times K_{LF,DF}$	$RF_{LF,i} \times K_{LF}$
Girder 1	1.05	1.03	1.41
Girder 2	1.04	1.51	1.62
Girder 3	1.04	1.46	1.57

* $RF_{AS,i}$ equals 0.73 (exterior girder) and 0.93 (interior girder)

• $RF_{LF,i}$ equals 0.76 (exterior girder) and 0.96 (interior girder)

For both methods, the experimental ratings exceeded unity indicating that weight restrictions may not be necessary on the bridge. Based on the field-measured distribution factors only, the interior girders experienced a larger increase in the original rating since there was a larger margin between the measured and AASHTO Standard (1996) distribution factors compared to the exterior girders. There was more of an increase in the AS load rating based on the reserve capacity since the measured section modulus resulted in a larger benefit than the flexural capacity of the slab in the LF method.

Table 8.10 shows that it may only be necessary to use one of the benefit factors to increase the rating factor to an acceptable level. It is also interesting to note that the exterior girder had the smaller original inventory rating, however, because of the participation of the curb, the benefit ratio for reserve capacity

288

resulted in a larger adjusted rating compared with the interior girder. Overall, the AS method had the larger increase in the original rating.

As shown in Table 8.6, there was no major change in the measured section modulus as the bridge was loaded incrementally to yield which shows that the girders were able to maintain their bending resistance. However, this behavior applies only to the Marlin bridge units and may not occur for other non-composite bridges since the girder-slab interaction may not be the same as observed during the load testing reported herein. During a typical diagnostic test with a single vehicle, the loads applied are typically lower than the weight of the rating vehicle, which will require that the measured response be extrapolated to a larger load. The bending resistance used to establish an inventory rating must be known with confidence since it must endure sustained loading over long periods of time (e.g., between inspection intervals, which are typically every 2 years). This can be achieved by loading the bridge with two dump trucks positioned side by side. With this heavier loading, the section modulus of the girders can be ensured to remain at the rating load level. In addition, the two-truck loading will provide the means for determining load distribution factors for the girders representative of multiple lane loading.

8.3 SUMMARY

The response of the bridge units under the service load vehicles has been presented. Measured distribution factors for the three transverse positions of the test trucks compared relatively well with the theoretical distribution determined from a linear elastic finite element analysis. A better comparison was achieved in the positive moment region where the deck slab was primarily in compression. For negative moment, however, cracking of the deck led to larger discrepancies between the measured and theoretical distribution factors. Compared to the AASHTO Standard (1996) and LRFD (1998) empirical distribution factors, the measured distribution factors were consistently lower. The best approximation to the measured distribution factors was made with the LRFD moment distribution relationships assuming non-composite girder stiffness.

The experimental section properties (i.e., moment of inertia, elastic section modulus, and neutral axis position) showed evidence that the girders interacted with the deck slab the least amount when the service load vehicle was positioned adjacent to the girder where the interface shear stresses would be largest. Results showed that the girders experienced only a marginal change in bending stiffness and load distribution in the positive moment region as the trailer loads were increased up to first yield of the girders. The more significant changes in partial composite action of the girders occurred during the service load runs, as the vehicle moved closer to the girder. For instance, comparison of the neutral axis positions of the girders during the trailer loading and the dump truck loading showed that the neutral axis decreased significantly only as the transverse position

of the dump truck got closer to the girder in question. Under the trailer load cycles, the neutral axis position remained relatively constant in spite of the larger loads. From this observation, it appears that positioning the dump truck close to the girder maximized the resulting axial load in the tributary slab section above the girder (i.e., shear stresses at the girder-slab interface) causing the most amount of slip and thus, the lowest girder stiffness. Moving the truck off the girder reduced the shear stresses such that friction and mechanical interlock resulted in a larger amount of partial composite action.

The service load test results also showed that the level of interaction between the girders and the slab varied from girder to girder and that the curb participated with the slab as the tributary section above the exterior girder. In the negative moment region, the exterior girder showed evidence of partial composite action, which deteriorated significantly with increasing load. The interior girders all acted as non-composite sections. The service load test results also showed the stiffness of the girders to vary with the transverse position of the dump truck. This behavior complicates the use of linear elastic finite element models for computing theoretical distribution factors due to the changing stiffness of the girders of non-composite bridges.

Recommendations were made to implement the experimental distribution factors and girder stiffness properties into the AASHTO Allowable Stress (AS) and Load Factor (LF) rating methods. A benefit ratio was derived for each of these two methods, which accounts for the larger section modulus and improved distribution factors measured during a diagnostic load test. An example rating

analysis illustrated the increase in the rating factor afforded by load testing with larger improvements occurring in the AS method. Limitations were enforced for the AS method to account for the possibility of a break in the unintended girder-slab connection although not observed in the testing reported herein.

CHAPTER 9

CONCLUSIONS AND RECOMMENDATIONS

The experimental investigation of two steel girder bridge units built non-composite has been reported. The units were originally live load continuous over four spans but were altered to three spans by eliminating a support. This was done to increase the maximum span length and reduce the amount of load needed to yield the girders. The bridges were subjected to increasing static loads with a flatbed trailer loaded with concrete traffic barriers up to and beyond first yield of the steel girders. A unique feature of the tests was that dump trucks of constant weight were subjected to the bridges between trailer load increments to simulate normal traffic loads. These runs served as a continuous monitor of the influence of overloads on lateral load distribution and partial composite action. A benefit ratio was proposed for improving the original AASHTO Allowable Stress and Load Factor ratings by using the moment distribution factor and section modulus for the girders that were derived experimentally from the diagnostic load tests.

9.1   CONCLUSIONS

9.1.1   Load-Deformation Response during Trailer Load Cycles

Important conclusions regarding the load-deformation response of the tested bridge units included the following:

1. Girder behavior was nonlinear in the positive moment region starting at small loads. This response occurred before yielding of the girders and indicated that the bending resistance of the girders was slowly decreasing due to the deterioration of partial composite action.

2. Yielding initiated at the negative moment region where the girders were non-composite since the deck slab was in tension and most likely cracked. For positive flexure, inadvertent partial composite action increased the effective section moduli of the girders, thus reducing the measured strains.

3. The load causing first yield of the girders in the positive moment region was uncertain due to the nonlinear response caused by the loss of partial composite action. The uncertainty of the original dead load stress further complicated the identification of the start of inelastic behavior.

4. The exterior girder experienced smaller bending strains than the interior girders due to the flexural participation of the integral curb. There was also more partial composite action at this girder since it could not be loaded as directly and heavily as the interior girders.

9.1.2 Lateral Load Distribution

Major findings regarding lateral load distribution observed during the trailer load cycles and service load runs include the following:

Distribution Pattern during Trailer Load Cycles
1. Load distribution factors based on measured bottom flange strains gave an accurate indication of the amount of load distributed to the girders when

the effective section moduli of the girders were accounted for. If the bending resistance is ignored, the strains underestimate the load carried by the exterior girder and overestimate the load taken by the interior girders compared to factors determined from the measured girder moments.

2. The measured bridge moment for positive and negative flexure averaged 15% lower than the calculated bridge moment. Accounting for the effects of bearing restraint and using an elastic concrete modulus 20% higher than that given in the ACI (1995) Code for estimating the bridge deck stiffness reduced the margin of error to 9% in the positive moment region.

Distribution Pattern during Service Load Runs

1. The ratio of the measured to statical bridge moment for positive bending improved from 82% to 90% from the first to third load path. These ratios indicate that the procedures for estimating girder moments from measured strains were most accurate when the truck was positioned more concentric to the bridge width.

2. Positive moment distribution factors varied by less than 5% between runs. This small variation indicated that the large loads applied with the trailer and concrete barriers had a marginal effect on the lateral load distribution under normal traffic loading.

3. Assuming composite action, the finite element model overestimated the measured distribution factors for all girders by an average of 10%. The non-composite model underestimated the measured distribution factor for

the interior girders by an average of 14%. The discrepancies were larger in the negative moment region due to cracking of the bridge deck.

4. The measured bending stiffness varied from girder to girder and also between transverse positions of the dump truck. The fluctuating girder stiffness led to differences between the measured and finite element based distribution factors since the stiffness is more uniform between girders and also remains constant in the finite element model.

5. Distribution factors as given by AASHTO were conservative compared to those determined based on measured girder moments. For the exterior girder, the measured distribution factor averaged 23% lower than LRFD (1998) and 30% lower than the AASHTO Standard (1996). Measured distribution factors for interior girders averaged 17% and 30% lower than the LRFD (1998) factors assuming non-composite and composite action, respectively, and 56% lower than the AASHTO Standard (1996).

9.1.3 Unintended Girder-Slab Interaction

Major findings regarding partial composite action observed during the trailer load cycles and service load runs include the following.

Interaction during Trailer Load Cycles

1. Inadvertent partial composite action is primarily due to two factors; friction and mechanical interlock. The latter factor provides the more significant amount of shear transfer.

2. Aside from friction and mechanical interlock, the expansion joint detail also contributes to partial composite action. The experimentally derived moment of inertia and section modulus of the girders in the positive moment region were larger at the bridge unit with a detail consisting of an armored plate weld connected to the girder top flanges

3. The measured bending resistance (i.e., section modulus) of the girders differed by a smaller amount than the stiffness (i.e., moment of inertia) with respect to the composite section.

4. The curb contributed significantly to the bending stiffness and resistance of the exterior girder. Strain profiles measured over the depth of the curb and exterior girder were almost parallel with a strain discontinuity at the deck flange interface. With a larger stiffness, more load was distributed to the exterior girder thus decreasing the load to the interior girders.

5. Strain readings taken at the abutment end provided a qualitative measure of girder-slab interaction and bearing restraint. With the exception of one girder, the remaining girders all showed tensile strains on the top flange with magnitudes exceeding the bottom flange compression strains.

Interaction during Service Load Runs

1. Neutral axis positions in the positive moment region, derived from the dump truck strains, showed only a marginal downward shift following the heavy loads applied with the trailer and concrete barriers. The measured moment of inertia and section modulus also did not change much between

trailer loads indicating that the girders maintained their stiffness and resistance with no sudden and drastic loss of partial composite action.

2. In the negative moment region, the measured neutral axis positions for the interior girders indicated non-composite behavior. At one bridge unit, the exterior girder acted partially composite through the full range of loading.

3. Exterior girders had measured section properties similar to those of a full composite section due in part to the participation of the curbs. The interior girder response resembled non-composite action since these girders could be loaded more directly resulting in higher shear stresses.

4. The response of the girders depended on the lateral position of the dump truck. The bending stiffness and resistance increased as the truck got further away from the girder in question since the horizontal shear force at the girder-slab interface decreased. Measured section properties for all the girders were bounded full composite and non-composite behavior.

9.2   RECOMMENDATIONS

The proposed experimental bridge rating process consists of a hierarchy of steps of increasing complexity and effort until a satisfactory rating is achieved, some of which do not require load testing. A flowchart summarizing the steps is given in Figure 9.1. Rating factors are first computed for the exterior and interior girders using either the AASHTO Allowable Stress (AS) or Load Factor (LF) method. Initial load ratings should be based on the AASHTO design vehicle, AASHTO legal load, or Texas legal load causing the maximum bending moment.
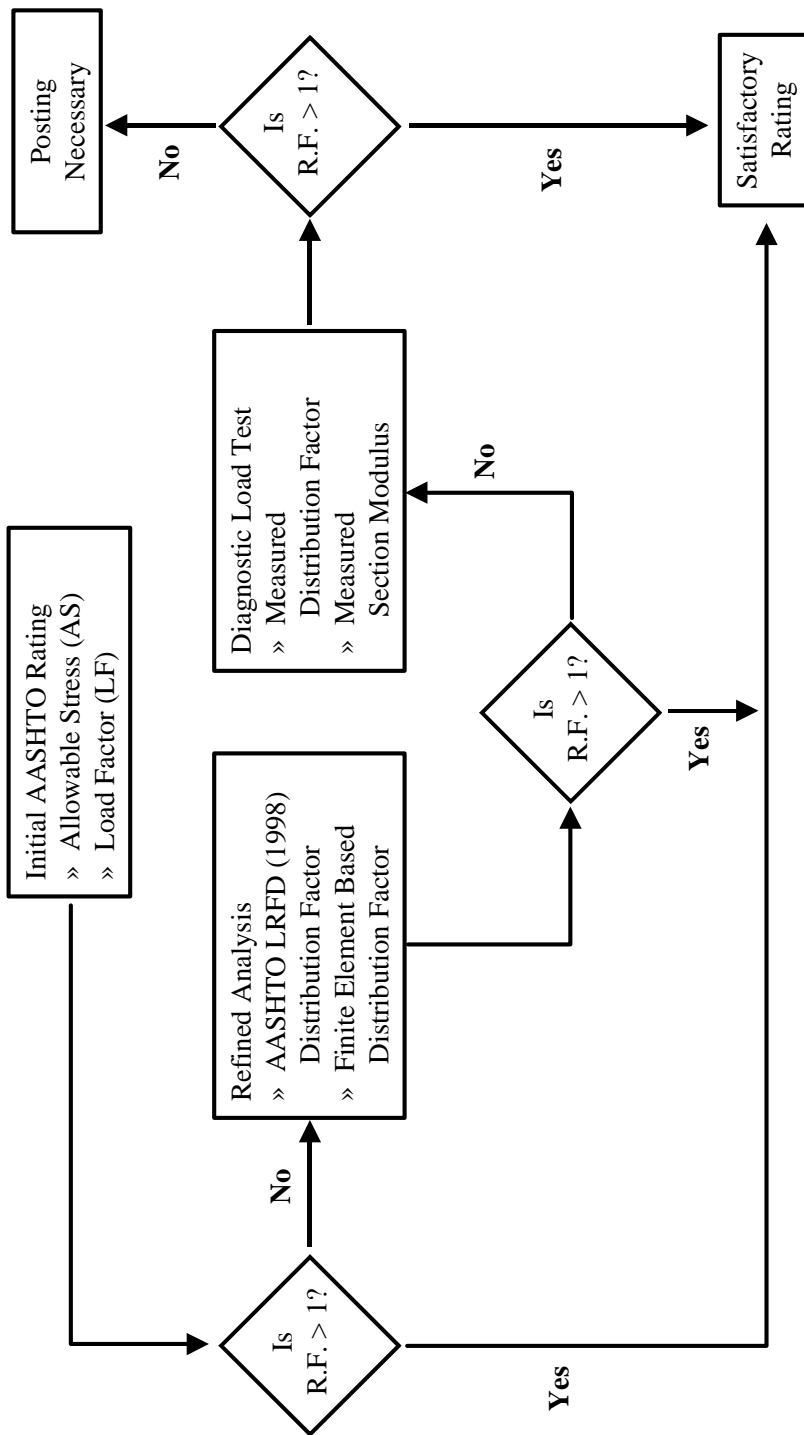
Figure 9.1 Flowchart of Experimental Bridge Rating Process.

Rating factors greater than one indicate that the bridge is safe to carry the rating vehicle, otherwise the rating must be improved to avoid posting the bridge.

The first adjustment that may be made to improve the original rating is to substitute the AASHTO LRFD (1998) for the Standard (1996) distribution factor and rerate the bridge. The lower LRFD (1998) distribution factor will result in smaller bending moments and thus, higher ratings. If the rating is still too low, further improvement may be made using the theoretical distribution factor from a composite finite element model. This type of analysis results in distribution factors slightly above the measured distribution factors but below the LRFD (1998) based factors assuming non-composite action. Distribution factors from a non-composite analytical model should not be used since measured distribution factors were underestimated as shown in Chapter 8.

Should the adjustments of the distribution factor discussed above fail to improve the load rating, the final option is to use the experimental findings from a diagnostic load test. For the test to be successful, a detailed load test plan must first be developed based on information gathered during a preliminary site visit and a thorough review of the design plans. The plan should outline the locations of strain gages and deflection transducers, the layout of the data acquisition system, the test truck positions and loading sequence, and the responsibilities of the test crew. The number and types of measurements should fit the configuration and capacity of the data acquisition system. Further details regarding the proper preparation for a load test are given in Appendix B.

<u>Instrumentation Requirements</u>

Since one advantage of load testing is related to load distribution, all girders should be instrumented over the cross-section of a bridge in order to estimate the total moment at the maximum positive and negative moment regions (if the bridge is continuous). Omitting any of the girders will underestimate the total bridge moment causing measured distribution factors to be overestimated. Strain gages should be installed at three positions over the depth of each girder according to the procedures given in Appendix B preferably on the top flange, the mid-web, and the bottom flange. At least two strain readings are needed to estimate the girder bending moments and section properties based on the procedures given in Chapter 7. Gages should also be installed on the curb to verify its interaction with the exterior girder.

Vertical deflection and slip measurements provide useful information for understanding bridge behavior but are otherwise unnecessary for improving the load rating. Strain measurements taken at support locations at the free ends of the girders should be used strictly as a qualitative tool for understanding the behavior of the bridge and not for making specific load-rating decisions. Due to the complex strain field that may exist the free ends of the girder, final load rating decisions should be made primarily based on the strain readings taken in the maximum moment regions as described earlier.

<u>Test Execution and Data Acquisition</u>

Because of the heavy loads required and traffic interruptions associated with proof testing, the recommended approach for evaluating suspect steel bridges is diagnostic load testing. The local bridge office can furnish a test truck with axle configurations typical of normal traffic. The test vehicle should be driven along the various transverse paths that maximize the bending moments in each girder. Measurements from the different paths can then be used to monitor the neutral axis of each girder for the different transverse truck positions. Other section properties such as moment of inertia and section modulus can also be determined experimentally for comparison with the theoretical properties for a non-composite and full composite girder section. Furthermore, the maximum distribution factor for each of the girders may be obtained for comparison with AASHTO and for possible use in improving the load rating along with the measured section modulus.

The rate at which data is written to the memory of the data logger should not be less than 10 Hz. This sampling rate is required to ensure that a continuous strain record is recorded as the service load vehicle is driven across the bridge at a speed of 2.2 m/s (5 mph). In addition, a 10 sample per second frequency allows sufficient time to perform the data integration required to keep the noise down to a level of 2 to 5 microstrain for the strain measurements. Appendix C provides a sample data collection program for use with the CR9000 data acquisition system that is applicable for 45 strain and 10 deflection measurements.

Post-Processing of Test Measurements

A significant effort should be made to refine the data collection programs in order to reduce the amount of strain data filtering that needs to be done following the load test to put the data in a suitable form for interpretation. Time saved in the post-processing can then be applied to the more important task of evaluating the measured bridge response. However, if filtering is necessary, a low pass Butterworth filter is recommended. The cutoff frequency should be set above the static frequency and the fundamental frequency to avoid eliminating signals representative of the "real" response of the bridge structure. The static frequency is taken as one over the duration of time for the service load vehicle to completely cross over the bridge. The first natural frequency may be determined from a dynamic analysis of the bridge or alternatively may be approximated with the simple relationship, $f_1 = 82L^{-0.9}$, developed by Paultre et al. (1992) where f_1 is the fundamental frequency (Hz) and L is the span length of the bridge (m).

Distribution factors should be evaluated using estimates of the bending moment in the girders, the procedure of which is given in Chapter 7. In addition to distribution factors, section properties should be derived using the girder strains with the test vehicle at the critical longitudinal and transverse locations resulting in the maximum bending moments.

Load Rating based on Measured Response

The benefits of load testing come from two sources: the measured bending resistance (i.e., reserve capacity benefit) and load distribution (i.e.,

303

distribution factor benefit) for the girders. The benefit formulations are given by Equations (8.7) through (8.9) for the AS method and Equations (8.14) through (8.16) for the LF method. For either method, it may be necessary to use only the distribution factor or the reserve capacity benefit ratio to increase the original load rating to an acceptable level. A combination of the two ratios is required when the initial rating is extremely low.

For both the AS and LF method, the distribution factor benefit ratio uses the measured girder distribution factor in place of the AASHTO Standard (1996) empirical factor. Applying this ratio will result in the same final inventory rating for both methods but a higher final operating rating for the LF method since the operating rating was initially larger for this method.

In the AS method, the reserve capacity benefit ratio improves the original rating by using a measured section modulus for the girders in place of the section modulus for just the steel girder as required by AASHTO. The measured section modulus for the girder, however, must be confirmed to be effective at the rating load level, otherwise the extra resistance due to partial composite action may not be considered. For the Marlin bridge units, the measured girder section modulus was maintained at loads exceeding the rating vehicle. This is usually not possible in diagnostic testing, thus the section modulus corresponding to the resistance of the bare girder and the tributary deck slab section (in the cracked condition) should be used. For the LF method, the flexural capacity of the girder section is based on the plastic capacity of just the girder plus the capacity of the tributary slab section (in the cracked condition). Hence, the LF method includes only a

small increase in reserve capacity since partial composite action of the girders is considered to be ineffective at the strength limit state.

If just the reserve capacity benefit ratio is used to improve the inventory rating, the AS method will have the higher final rating since the ratio is lower for the LF method. Both methods may have the same final operating ratings after applying the reserve capacity benefit ratios since the original AS rating is lower than the LF rating. However, as shown in the example rating analysis given in Chapter 8, the original operating ratings may be greater than unity and thus, may not need to be increased. Finally, larger increases in the original ratings based solely on reserve capacity are most likely at the exterior girder due to the participation of the curbs and the higher degree of partial composite action.

9.3   SUGGESTED RESEARCH AND DEVELOPMENT

Development of automated routines to convert the measured load test data into more meaningful properties of bridge behavior such as girder moments, section properties, and load distribution factors is needed. The routines could significantly reduce the time required to process the test data leaving more time for the more important task of evaluating the bridge behavior.

Improved data acquisition and instrumentation systems are needed to reduce the time spent in the field. Some progress has been made in wireless-based data acquisition systems, however, field evaluation of these systems has been limited. Improved methods are also needed for measuring vertical deflection of bridge girders using non-contact type instruments such as laser-based systems.

Lateral load distribution in negative moment regions must be studied further. Much work has been done regarding lateral load distribution, however, the work has focused on the positive moment region. Research is needed to determine appropriate expressions for evaluating girder bending moments and load distribution factors in the negative moment region where girder behavior is complicated by the cracking of the deck slab. In addition, the bending resistance and stiffness of the girders in the negative moment region must be studied, where the load rating is typically governed in continuous span bridges.

The results from the load tests reported herein showed that the girders maintained their original resistance and stiffness up to the load causing first yield. However, since testing was terminated well before the ultimate positive moment capacity of the bridge units, partial composite action of the girders could not be considered in the LF method where the bending resistance is based on the strength limit state. Further load testing of non-composite girder bridges is necessary to determine the nature of partial composite action of the girders at loads between yield and ultimate. Of particular interest is the point in which unintended interaction between the girders and the deck slab is completely lost. Finding from these tests would be beneficial to the LF rating method.

Because of the random nature of partial composite action observed from the testing reported herein, research on a retrofit design detail for connecting the girder top flanges to the deck slab may be warranted in situations where load testing may not be performed. Although friction and mechanical interlock does provide a means for partial composite action, the research reported herein does

not suggest complete reliability that the level will remain over the service life of the bridge. As a result, the inspection interval may need to decrease to adequately monitor the behavior of the bridge girders. With the definite connection provided by a retrofit design, the inspections can be left at the regular 2-year interval with the certainty that partial composite action will remain between inspections. The retrofit could be done strictly for interior girders which typically control the rating since the exterior girders are not loaded as heavily and also because these girders benefit from the participation of the curb. The definite connection between the girders and the slab will result in a girder section whose stiffness is known with reasonable accuracy. As a result, the response of the bridge may be approximated more accurately with finite element analysis. A retrofit would also result in a more uniform distribution of girder stiffness across the bridge cross-section.

REFERENCES

American Association of State Highway and Transportation Officials (AASHTO). (1994). *Manual for Condition Evaluation of Bridges*, Washington, D.C.

American Association of State Highway and Transportation Officials (AASHTO). (1996). *Standard Specifications for Highway Bridges*, 16th Edition, Washington, D.C.

American Association of State Highway and Transportation Officials (AASHTO). (1998). *LRFD Bridge Design Specifications*, 2nd Edition, Washington, D.C.

American Concrete Institute (ACI) Committee 318. (1995). *Building Code Requirements for Structural Concrete* (ACI 318-95) *and Commentary* (ACI 318R-95), American Concrete Institute, Detroit, MI.

Azizinamini, A., Shekar, Y., Barnhill, G., and Boothby, T. E. (1994). "Old Concrete Slab Bridges: Can They Carry Modern Traffic Loads?." *Concrete International*, Vol. 16, No. 2, pp. 64-69.

Azizinamini, A., Shekar, Y., Boothby, T. E., and Barnhill, G. (1994). "Old Concrete Slab Bridges. I: Experimental Investigation." *Journal of Structural Engineering*, Vol. 120, No. 11, pp. 3284-3304.

Azizinamini, A., Shekar, Y., Boothby, T. E., and Barnhill, G. (1994). "Old Concrete Slab Bridges. II: Analysis." *Journal of Structural Engineering*, Vol. 120, No. 11, pp. 3305-3319.

Bakht, B. and Csagoly, P. F. (1979). "Bridge Testing." *Technical Report No. 79-SSR-10*, The Research and Development Branch, Ontario Ministry of Transportation.

Bakht, B. and Csagoly, P. F. (1980). "Diagnostic Testing of a Bridge." *Journal of the Structural Division*, Vol. 106, No. ST7, pp. 1515-1529.

Bakht, B. and Jaeger, L. G. (1988). "Bearing Restraint in Slab-on-Girder Bridges." *Journal of Structural Engineering*, Vol. 114, No. 12, pp. 2724-2740.

Bakht, B. and Jaeger, L. G. (1990). "Bridge Testing – A Surprise Every Time." *Journal of Structural Engineering*, Vol. 116, No. 5, pp. 1370-1383.

Bakht, B. and Jaeger, L. G. (1992). "Ultimate Load-Test of Slab-on-Girder Bridge." *Journal of Structural Engineering*, Vol. 118, No. 6, pp. 1608-1624.

Bakht, B. (1988). "Actual Versus Assumed Behaviour of Girder Bridges." Proceedings of the 5th ASCE Specialty Conference (Probabilistic Methods in Civil Engineering), pp. 301-304.

Bakht, B. (1988). "Observed Behaviour of a New Medium Span Slab-on-Girder Bridge." *Technical Report No. SRR-88-02*, The Research and Development Branch, Ontario Ministry of Transportation.

Bakht, B. (1988). "Testing of an Old Short Span Slab-on-Girder Bridge." *Technical Report No. SRR-88-01*, The Research and Development Branch, Ontario Ministry of Transportation.

Bakht, B. (1987). "The Role of Bridge Testing in Evaluation." Proceedings of the US-European Workshop on Bridge Evaluation, Repair and Rehabilitation, pp. 209-218.

Bakht, B. (1988). "Ultimate Load Test of a Slab-on-Girder Bridge." *Technical Report No. SRR-88-03*, The Research and Development Branch, Ontario Ministry of Transportation.

Baldwin, J. W. (1965). "Field Tests of a Three-Span Continuous Highway Bridge." *Highway Research Record*, No. 76, pp. 140-167.

Barker, M. G. (1990). "Guide Specification Strength Capacity Rating of Existing Girder Bridges." *Transportation Research Record*, No. 1476, pp. 98-105.

Beal, D. B. and Chamberlin, W. P. (1982). "Effects of Concrete Deterioration on Bridge Response." *Transportation Research Record*, No. 853, pp. 43-47.

Beal, D. B. and Loftus, M. J. (1988). "Load Tests on Five Bridges." *Client Report 30*, Engineering Research and Development Bureau, New York State Department of Transportation.

Beal, D. B. (1992). "Destructive Testing of a Reinforced-Concrete T-Beam Bridge." *Research Report 100*, Engineering Research and Development Bureau, New York State Department of Transportation.

Beal, D. B. (1985). "Strength of Concrete T-Beam Bridges." symposia paper presented at *ACI Convention Strength Evaluation of Existing Concrete*

Bridges, ACI Committee 437 (Strength Evaluation of Existing Concrete Structures), pp. 143-164.

Boothby, T. E. and Craig, R. J. (1997). "Experimental Load Rating Study of a Historic Truss Bridge." *Journal of Bridge Engineering*, Vol. 2, No. 1, pp. 18-26.

Buckle, I. G., Dickson, A. R., and Phillips, M. H. (1985). "Ultimate Strength of Three Reinforced Concrete Highway Bridges." *Canadian Journal of Civil Engineering*, Vol. 12, No. 4, pp. 63-72.

Burdette, E. G. and Goodpasture, D. W. (1988). "Correlation of Bridge Load Capacity Estimates with Test Data." *NCHRP Report 306*, Transportation Research Board, National Research Council, Washington, D. C.

Burdette, E. G. and Goodpasture, D. W. (1973). "Tests of Four Highway Bridges to Failure." *Journal of the Structural Division*, Vol. 99, No. ST3, pp. 335-348.

Bussell, L. C. (1997). "Diagnostic Testing for Improved Load Rating of Reinforced Concrete Slab Bridges." Master's Thesis, University of Texas at Austin.

Chajes, M. J., Mertz, D. R., and Commander, B. (1997). "Experimental Load Rating of a Posted Bridge." *Journal of Bridge Engineering*, Vol. 2, No. 1, pp. 1-10.

Commander, B. C. (1989). "An Improved Method of Bridge Evaluation: Comparison of Field Test Results with Computer Analysis." Master's Thesis, University of Colorado at Boulder.

Commander, B. C., McMullen, M., and Mohseni, M. (1994). "An Integrated Approach to Load Rating." *Proceedings of the 11th Annual International Bridge Conference*, Engineers' Society of Western Pennsylvania, Paper No. IBC-94-63, pp. 1-7.

Commander, B., and Schulz, J. (1997). "A Field Verified Load Rating Method for Reinforced Concrete Slab Bridges." *Proceedings of Structures Congress XV (Building to Last)*.

Conner, G. H., Stallings, J. M., McDuffie, T. L., Campbell, J. R., Fulton, R. Y., Shelton, B. A., and Mullins, R. B. (1997). "Bridge Load Testing in Alabama." Transportation Research Board.

Craig, R. J., Gill, S. L., Everett, A. G., Vasquez, G. D., and Brooten, L. A. (1994). "Static and Dynamic Load Testing of 15 Chester County Bridges." *Proceedings of the 11th Annual International Bridge Conference*, Paper No. IBC-94-31, Engineers' Society of Western Pennsylvania, pp. 219-226.

Deatherage, J. H. (1987). "Investigation of Variables Affecting Beam-Slab Bridge Load Capacity." PhD Dissertation, University of Tennessee at Knoxville.

Denis, B., Karjuna, M., Fafard, M., Beaulieu, D., and Halchini, C. (1994). "Testing of a 55 Year Old Bridge in Canada." *Structural Engineering International*, pp. 29-33.

Edberg, W. M. (1994). "State-of-the-Art Survey in Experimental Load Rating of Bridges." Master's Thesis, University of Delaware.

Favre, R., Burdet, O., and Hassan, M. (1994). "Statistical Data Combined With Linear and Non-linear Analysis To Interpret Bridge Load Tests." *Proceedings of the 4th International Conference on Short and Medium Span Bridges (Developments in Short and Medium Span Bridge Engineering '94)*, pp. 1197-1208.

Favre, R., Hassan, M., and Markey, I. (1992). "Bridge Behaviour Drawn from Load Tests." *Proceedings of the 3rd International Workshop on Bridge Rehabilitation*, pp. 245-257.

Fu, C. C., Schelling, D. R., and Ayyub, B. M. (1992). "Evaluation of Truck Configurations based on Structural Performance of Bridges." *Journal of Advanced Transportation*, Vol. 26, No. 3, pp. 299-324.

Fu, C. F., Elhelbawey, M., Sahin, M. A., and Schelling, D. R. (1996). "Lateral Distribution Factor from Bridge Field Testing." *Journal of Structural Engineering*, Vol. 122, No. 9, pp. 1106-1109.

Fu. G., Pezze, F. P. III, and Alampalli, S. (1995). "Field Test of a Steel Bridge for Improved Rating." *Proceedings of Structures Congress XIII (Restructuring: America and Beyond,"* ASCE, Part 1 (of 2), pp. 903-906.

Fu. G., Pezze, F. P. III, and Alampalli, S. (1994). "Rating a Steel Multi-Stringer Bridge by Diagnostic Load Test." *Client Report 31*, Engineering Research and Development Bureau, New York State Department of Transportation.

364

Fu., G. and Tank, J. (1995). "Risk-Based Proof-Load Requirements for Bridge Evaluation." *Journal of Structural Engineering*, Vol. 121, No. 3, pp. 542-556.

Goble, G. G., Commander, B. C., and Schulz, J. X. (1990). "Simple Load Capacity Tests for Bridges to Determine Safe Posting Levels." *Final Report to the Pennsylvania Department of Transportation*, Report No. FHWA-PA-90-009+86-09.

Ghosn, M., Moses, F., and Gobieski, J. (1986). "Evaluation of Steel Bridges using In-Service Testing." *Transportation Research Record*, No. 1072, pp. 71-78.

Hassan, M., Burdet, O., and Favre, R. (1995). "Analysis/Evaluation of Bridge Behavior Under Static Load Testing Leading to Better Design and Judgment Criteria." *Proceedings of the Fourth International Bridge Engineering Conference*, pp. 296-303.

Hassan, M., Burdet, O., and Favre, R. (1993). "Interpretation of 200 Load Tests of Swiss Bridges." *Proceedings of the IABSE Colloquium (Remaining Structural Capacity)*, pp. 319-326.

Hays, C. O., Consolazio, G. R., Hoit, M. I., and Kakhandiki, A. (1994). "Bridge Rating of Girder-Slab Bridges using Automated Finite Element Technology." *Structures and Materials Research Report No. 94-1*, Engineering and Industrial Experiment Station, University of Florida, Gainesville, Florida.

Huria, V., Lee, K.-L., and Aktan, A. E. (1994). "Different Approaches to Rating Slab Bridges." *Journal of Structural Engineering*, Vol. 120, No. 10, pp. 3056-3062.

Imbsen, R. A., Liu, W. D., Schamber, R. A., and Nutt, R. V. (1987). "Strength Evaluation of Existing Reinforced Concrete Bridges." *NCHRP Report 292*, Transportation Research Board, National Research Council, Washington, D. C.

Jensen, V. P., Kluge, R. W., and Williams, C. B. (1943). "Highway Slab-Bridges with Curbs: Laboratory Tests and Proposed Design Method." *University of Illinois Engineering Experiment Station Bulletin*, Vol. 40, No. 346.

Jorgenson, J. L. and Larson, W. (1976). "Field Testing of a Reinforced Concrete Highway Bridge to Collapse." *Transportation Research Record*, No. 607, pp. 66-71.

Kim, S. and Nowak, A. S. (1997). "Load Distribution and Impact Factors for I-Girder Bridges." *Journal of Bridge Engineering*, Vol. 2, No. 3, pp. 97-104.

Kissane, R. J., Beal, D. B., and Sanford, J. A. (1980). "Load Rating Of Short-Span Highway Bridges." *Interim Report on Research Project 156-1*, Research Report 79 (US DOT/FHWA), Engineering Research and Development Bureau, New York State Department of Transportation.

Ladner, M. (1985). "In Situ Load Testing of Concrete Bridges in Switzerland." symposia paper presented at *ACI Convention Strength Evaluation of Existing Concrete Bridges*, ACI Committee 437 (Strength Evaluation of Existing Concrete Structures), pp. 59-79.

Lai, Leon L-Y. (1995). "Rating of an Open Spandrel Concrete Arch Bridge by Load Testing." *Proceedings of Structures Congress XIII (Restructuring: America and Beyond)*, Vol. 2 (of 2), pp. 1329-1332.

Lichtenstein, A. G. (1993). "Bridge Rating Through Nondestructive Load Testing." *Final Draft Report for NCHRP Project 12-28(13)A*, Transportation Research Board, National Research Council, Washington, D. C.

Mabsout, M. E., Tarhini, K. M., Frederick, G. R., and Kobrosly, M. (1997). "Influence of Sidewalks and Railings on Wheel Load Distribution in Steel Girder Bridges." *Journal of Bridge Engineering*, Vol. 2, No. 3, pp. 88-96.

Mabsout, M. E., Tarhini, K. M., Frederick, G. R., and Tayar, C. (1997). "Finite-Element Analysis of Steel Girder Highway Bridges." *Journal of Bridge Engineering*, Vol. 2, No. 3, pp. 83-87.

Mabsout, M. E., Tarhini, K. M., Frederick, G. R., and Kesserwan, A. (1998). "Effect of Continuity on Wheel Load Distribution in Steel Girder Bridges." *Journal of Bridge Engineering*, Vol. 3, No. 3, pp. 103-110.

Mabsout, M. E., Tarhini, K. M., Frederick, G. R., and Kesserwan, A. (1999). "Effect of Multilanes on Wheel Load Distribution in Steel Girder Bridges." *Journal of Bridge Engineering*, Vol. 4, No. 2, pp. 99-106.

Markey, I. (1991). "Load Testing of Swiss Bridges." *Steel Construction Today*, Vol. 5, No. 1, pp. 15-20.

MATLAB. (1997). *Using MATLAB (Version 5)*, The Mathworks, Inc., Natick, MA.

MATLAB. (1998). *Signal Processing Toolbox User's Guide*, The Mathworks, Inc., Natick, MA.

Matsis, P. (1999). "Diagnostic Load Tests of Two Prestressed Concrete Bridges." Master's Thesis, University of Texas at Austin.

Miller, R. A., Aktan, A. E., and Shahrooz, B. M. (1994). "Destructive Testing of a Decommissioned Concrete Slab Bridge." *Journal of Structural Engineering*, Vol. 120, No. 7, pp. 2176-2198.

Moses, F. and Verma, D. (1987). "Load Capacity Evaluation of Existing Bridges," *NCHRP Report 301*, Transportation Research Board, National Research Council, Washington, D. C.

Moses, F., Lebet, J. P., and Bez, R. (1994). "Applications of Field Testing to Bridge Evaluation." *Journal of Structural Engineering*, Vol. 120, No. 6, pp. 1745-1762.

Parsley, M. A. (1998). "Push-Out Behavior of Concrete-Filled Steel Tubes." Master's Thesis, University of Texas at Austin.

Pauw, A. (1960). "Static Modulus of Elasticity of Concrete as Affected by Density," *Proceedings of the ACI Journal*, Vol. 57, No. 6, pp. 679-687.

Pinjarkar, S. G. (1998). "An Overview of Current Worldwide Practices for Nondestructive Load Testing for Bridge Rating and Evaluation." *Proceedings of the 5th Annual International Bridge Conference*, Paper No. IBC-88-11, Engineers' Society of Western Pennsylvania, pp. 25-31.

Pinjarkar, S. G., Guedelhoefer, O. C., Smith, B. J., and Kritzler, R. W. (1990). "Nondestructive Load Testing for Bridge Evaluation and Rating." *Final Report for NCHRP Project 12-28(13)*, Transportation Research Board, National Research Council, Washington, D. C.

Rabbat, B. G. and Russell, H. G. (1985). "Friction Coefficient of Steel on Concrete or Grout," *Journal of Structural Engineering*, Vol. 111, No. 3, pp. 505-515.

Reid, J. S., Chajes, M. J., Mertz, D. R., and Reichelt, G. H. (1996). "Bridge Strength Evaluation based on Field Tests." *Proceedings of the 7th Specialty Conference on Probabilistic Mechanics and Structural Reliability*, Engineering Mechanics and Structural Divisions (ASCE), pp. 294-297.

Saraf, V., Sokolik, A. F., and Nowak, A. S. (1996). "Proof Load Testing of Highway Bridges." *Transportation Research Record*, No. 1541, pp. 51-57.

Scanlon, A. and Mikhailovsky, L. (1987). "Full-Scale Load Test of Three-Span Concrete Highway Bridge." *Canadian Journal of Civil Engineering*, Vol. 14, No. 1, pp. 19-23.

Schonwetter, P. (1999). "Field Testing and Load Rating of a Steel-Girder Highway Bridge." Master's Thesis, University of Texas at Austin.

Schulz, J. L. (1989). "Development of a Digital Strain Measurement System for Highway Bridge Testing." Master's Thesis, University of Colorado at Boulder.

Schulz, J. L., and Commander, B. C. (1995). "Efficient Field Testing for Load Rating Railroad Bridges." *Proceedings of SPIE – The International Society of Optical Engineering (Nondestructive Evaluation of Aging Railroads)*, Society of Photo-Optical Instrumentation Engineers, Vol. 2458, pp. 209-217.

Schulz, J. L., Commander, B., Goble, G. G., and Frangopol, D. M. (1995). "Efficient Field Testing and Load Rating of Short- and Medium-Span Bridges." *Structural Engineering Review*, Vol. 7, No. 3, pp. 181-194.

Schulz, J. X.., Goble, G. G., and O'Fallon, J. (1991). "Static Testing of Highway Bridges." paper submitted for publication in the *Transportation Research Record*.

Shahawy, M. A. (1995). "Nondestructive Strength Evaluation of Florida Bridges." Proceedings of SPIE – The International Society of Optical Engineering (Nondestructive Evaluation of Aging Bridges and Highways), Society of Photo-Optical Instrumentation Engineers, Vol. 2456, pp. 101-123.

Shahawy, M. E. and Garcia, A. M. (1990). "Structural Research and Testing in Florida," *Transportation Research Record*, No. 1275, pp. 76-80.

Shekar, Y. (1993). "Performance of Concrete Slab Bridges," Master's Thesis, University of Nebraska.

Smith, K. N. and Mikelsteins, I. (1988). "Load Distribution in Edge Stiffened Slab and Slab-on-Girder Bridge Decks." *Canadian Journal of Civil Engineering*, Vol. 15, No. 6, pp. 977-983.

Stallings, J. M. and Yoo, C. H. (1992). "Analysis of Slab-on-Girder Bridges." *Computers and Structures*, Vol. 45, pp. 875-880.

Stallings, J. M. and Yoo, C. H. (1993). "Tests and Ratings of Short-Span Steel Bridges." *Journal of Structural Engineering*, Vol. 119, No. 17, pp. 2150-2168.

Suetoh, S., Burdette, E. G., Goodpasture, D. W., and Deatherage, J. H. (1990). "Unintended Composite Action in Highway Bridges." *Transportation Research Record*, No. 1275, pp. 89-94.

Tharmabala, T. (1990). "Strength Evaluations of Bridges." *ASTM Special Technical Publication 1100 (Extending the Service Life of Bridges)*, American Society of Testing and Materials, pp. 53-69.

Tiedeman, J. L., Albrecht, P., and Cayes, L. R. (1993). "Behavior of Two-Span Continuous Bridge under Truck Axle Loading." *Journal of Structural Engineering*, Vol. 119, No. 4, pp. 1234-1250.

Velazquez, B. M. (1998). "Diagnostic Load Tests of a Reinforced Concrete Pan-Girder Bridge." Master's Thesis, University of Texas at Austin.

Yen, B. T. (1996). "Evaluation of Service Load Behavior of Small Bridges using Strain Measurement." *Proceedings of Structures Congress XIV (Building an International Community of Structural Engineers)*, Vol. 2, pp. 667-673.

Yoo, C. H. and Stallings, J. M. (1991). "Bridge Testing." *Final Report for Project Number ST 2019-12*, Auburn University Highway Research Center, The State of Alabama Highway Department.

Zokaie, T., Osterkamp, T. A., and Imbsen, R. A. (1991). "Distribution of Wheel Loads on Highway Bridges." *Report 12-26/1*, National Cooperative Highway Research Program, Transportation Research Board, Washington, D. C.

Zhou, Y. E. (1996). "Load Testing and Strength Evaluation of a Non-Composite Steel Plate Girder Bridge." *Proceedings of Structures Congress XIV (Building an International Community of Structural Engineers)*, Vol. 2, pp. 884-891.

VITA

David Villegas Jáuregui was born in Silver City, New Mexico on October 27, 1969, the son of David Ruiz Jáuregui and Alice Villegas Jáuregui. After graduating from Cobre High School, Bayard, New Mexico, he entered New Mexico State University in 1987 where he received the degrees of Bachelor of Science in Civil Engineering in 1992 and Master of Science in Civil Engineering in 1994. He then worked for one year as a graduate research assistant at the Los Alamos National Laboratory before entering the graduate program in Civil Engineering at the University of Texas at Austin in 1995. He is currently employed as a structural engineering professor in the CAGE (Civil, Agricultural, and Geological Engineering) Department at New Mexico State University in Las Cruces, New Mexico.

Permanent address: 5143 Micro Road, Unit 2
                       Las Cruces, NM 88011

This dissertation was typed by the author.